Development of TiC based wear resistance composite coating on AISI 304 steel by pulsed laser and TIG cladding process

Dissertation submitted in partial fulfillment

of the requirements of the degree of

Doctor of Philosophy

in

Mechanical Engineering

by

Chinmaya Kumar Sahoo

(Roll Number: 513ME1002)

based on research carried out

under the supervision of

Prof. Manoj Masanta

April, 2017

Department of Mechanical Engineering

National Institute of Technology Rourkela

Department of Mechanical Engineering
National Institute of Technology Rourkela

Certificate of Examination

April 10, 2017

Roll Number: *513ME1002*

Name: *Chinmaya Kumar Sahoo*

Title of Dissertation: Development of TiC based wear resistance composite coating on AISI 304 steel by pulsed laser and TIG cladding process

We the below signed, after checking the dissertation mentioned above and the official record book (s) of the student, hereby state our approval of the dissertation submitted in partial fulfilment of the requirements of the degree of *Doctor of Philosophy* in *Mechanical Engineering* at *National Institute of Technology Rourkela*. We are satisfied with the volume, quality, correctness, and originality of the work.

_____
Prof. Manoj Masanta
Supervisor

_____
Prof. Susanta Kumar Sahoo
Member, DSC

_____
Prof. Anindya Basu
Member, DSC

_____
Prof. Ashok Kumar Mondal
Member, DSC

_____
Prof. Siba Sankar Mohapatra
Chairperson, DSC

_____
Prof. Siba Sankar Mohapatra
Head of the Department

_____
Prof. G. L. Datta

Department of Mechanical Engineering
National Institute of Technology Rourkela

Dr. Manoj Masanta

Assistant Professor

April 10, 2017

Supervisor's Certificate

This is to certify that the work presented in the dissertation entitled *Development of TiC based wear resistance composite coating on AISI 304 steel by pulsed laser and TIG cladding process* submitted by *Chinmaya Kumar Sahoo*, Roll Number 513ME1002, is a record of original research carried out by him under my supervision and guidance in partial fulfilment of the requirements of the degree of *Doctor of Philosophy* in *Mechanical Engineering*. Neither this dissertation nor any part of it has been submitted earlier for any degree or diploma to any institute or university in India or abroad.

_____

Manoj Masanta

Assistant Professor

Dedication

I would like to dedicate
this dissertation
to
my parents and all my
teachers

Chinmaya Kumar Sahoo

Declaration of Originality

I, *Chinmaya Kumar Sahoo*, Roll Number *513ME1002* hereby declare that this dissertation entitled *Development of TiC based wear resistance composite coating on AISI 304 steel by pulsed laser and TIG cladding process* presents my original work carried out as a doctoral student of NIT Rourkela and, to the best of my knowledge, contains no material previously published or written by another person, nor any material presented by me for the award of any degree or diploma of NIT Rourkela or any other institution. Any contribution made to this research by others, with whom I have worked at NIT Rourkela or elsewhere, is explicitly acknowledged in the dissertation. Works of other authors cited in this dissertation have been duly acknowledged under the section "Reference". I have also submitted my original research records to the scrutiny committee for evaluation of my dissertation.

I am fully aware that in case of any non-compliance detected in future, the Senate of NIT Rourkela may withdraw the degree awarded to me on the basis of the present dissertation.

April 10, 2017
NIT Rourkela

Chinmaya Kumar Sahoo

Acknowledgement

At first, I would like to express my sincere gratitude to my research supervisor **Prof. Manoj Masanta** for his continuous support and encouragement to complete this research work. This work is polished and presentable due to his valuable suggestion, timely support, and conscientious effort.

I would like to thank **Prof. Siba Sankar Mohapatra**, HOD Mechanical for constant support and his valuable suggestions as DSC chairman. I am also thankful to **Prof. Anindya Basu** and **Prof. Ashok Kumar Mondal** of Metallurgical and Materials Engineering Department and **Prof. Susanta Kumar Sahoo** of Mechanical Department, for their valuable suggestion and critic evaluation of the research work. I am also grateful to all faculty member of the Department of Mechanical Engineering for their support and valuable advice.

I express my thanks to all technical staffs of the department of Mechanical Engineering and Central workshop for their help in my experimental work. I express special thanks to all staffs of Welding Shop for providing all necessary assistance in conducting TIG cladding experiment. I would like to thank **Mr. Subrat Pradhan** and **Mr. Ch Sivateja** of SEM lab for their help in utilizing SEM facility, **Mr. Kasinath Das Mohapatra** for wire-EDM, **Mr. Sushanta Kumar Sahu** and **Mr. Bikash Ranjan Moharana** for laser processing, **Mr. Arabinda Khuntia**, **Mr. Syamaghan Reddy**, and **Mr. Somnath Seth** of production lab for providing timely help. I also express my gratitude to the Department of Metallurgical and Materials Engineering for providing SEM, XRD, Micro-hardness, Optical microscope facility; Department of Ceramic Engineering for FESEM facility and Department of Chemistry for necessary chemicals and lab facilities. I would also like to acknowledge the financial support provided by DST for procurement of Micro-hardness tester and pin-on-disc wear tester and MHRD for providing scholarship during my Ph.D.

I thank to my co-researcher **Jageshwar Kumar Sahu**, **Tijo D**, **Lalit Soni**, **Kamalesh Kumar**, **Nitesh** for their help in conducting experiments and providing valuable

suggestions to improve the quality of the research work. I am also thankful to one and all who directly or indirectly, supported in my research work.

Apart from my research group, I express my heartfelt thanks to my parents, younger brother **Tanmaya** and wife **Monalisha** for their support and encouragement during my research days. Last but not the least, I thanks to the almighty Lord Jagannath for his blessings.

April 10, 2017
NIT Rourkela

Chinmaya Kumar Sahoo

Abstract

TiC is a preferred coating material for the components working under the extreme tribological condition, due to its high hardness, high melting temperature, and low density. In order to improve the hardness and wear resistance properties of stainless steel surface, TiC reinforced coating has been produced on AISI 304 stainless steel using pulsed Nd:YAG laser and Tungsten Inert Gas (TIG) cladding process. Further, to enhance the efficiency of TIG cladding process as well as to amend the tribological properties of TiC based coating, Ni (for better bonding) and CaF_2 (as a solid lubricant) have been incorporated in various phases of experiments. The produced composite coatings are then analyzed by using SEM, FESEM and XRD for microstructural evaluation and phase identification. Micro-hardness value of the produced TiC, TiC-Ni, and TiC-Ni-CaF_2 coating has been measured by Vickers micro-indentation tester and the tribological behavior of the produced coatings have been assessed by sliding abrasive wear test through pin-on-disc wear testing machine. The experimental analysis revealed that TiC reinforced composite coating produced by TIG heat source improved the micro-hardness and abrasive wear resistance significantly. Further, with the incorporation of Ni, bonding between the substrate and TiC reinforcement enhances, and consequently augmented the wear resistance of the coating. In addition, by employing CaF_2 with TiC and Ni, the coefficient of friction (COF) of the coating diminishes, which found become beneficial for the performance of the coating.

Keywords: Hard Coating; TiC-Steel; AISI 304 Steel; Pulsed Nd:YAG Laser; TIG cladding; Solid Lubricants; CaF_2

Contents

List of Figures

List of Tables

Abbreviations

BSE: Backscatter Electron

COF: Coefficient of Friction

CP: Commercially Pure

CVD: Chemical Vapour Deposition

DAS: Data Acquisition System

DMLS: Direct Metal Laser Sintering

EDS: Energy-dispersive X-ray spectroscopy

EPPD: Effective Peak Power Density

FESEM: Field Emission Scanning Electron Microscope

GTA: Gas Tungsten Arc

GTAW: Gas Tungsten Arc Welding

LENS: Laser Engineered Net Shaping

MMC: Metal Matrix Composite

PLD: Pulsed Laser Deposition

PPD: Peak Power Density

PTA: Plasma Transfer Arc

PVD: Physical Vapour Deposition

SAW: Submersed Arc Welding

SEM: Scanning Electron Microscope

SMAW: Shield Metal Arc Welding

TIG: Tungsten Inert Gas

XRD: X-ray Diffraction

Chapter 1

Introduction

Mechanical failure of machine components or elements leads to an enormous loss in the industry in term of economy and accidental hazard. Mechanical failure can be avoided by selecting the proper material and appropriate manufacturing process or by augmenting the lifespan of the components by various surface modification techniques i.e. surface hardening, shot peening or application of hard coating (Zikin et al., 2013). Hard coating methods like electroplating, PVD, CVD, thermal spraying, laser coating/cladding, weld cladding are successfully used to deposit a hard layer on the surface of a component. These coating methods with suitable coating materials enable to improve the tribological and corrosion resistance property of a material and enhance the life of a component. A coating should have characteristics like excellent bonding with the substrate, suitable layer thickness, and improved mechanical property like high hardness, wear resistance, toughness, and corrosion resistance, in combination with low coefficient of friction, resistance to thermal shock, and stability at high temperature (Jiang and Molian, 2001). These characteristics of the coating primarily depend on the properties of the coating material and the process involved. Further, the performance of the coating also influenced by the compatibility between the coating and substrate material in terms of mechanical, thermal and metallurgical properties. Therefore, selection of appropriate coating material and process to fabricate a reliable and defect-free coating with superior performance are the key challenges (Berger, 2015).

It is fairly acceptable that with the development of new superalloys, the performance of a component enhances due to their high strength to weight ratio, high corrosion resistance, and high-temperature resistance compared to the conventional structural materials. However, owing to relatively low hardness and wear resistance these newly developed superalloys are also not sufficient to perform in adverse environmental condition. On the other hand, refractory ceramics possesses high melting temperature, excellent hardness, and superior abrasive and adhesive wear resistance compared to the metal or alloy. Therefore, these ceramic particles are suitable candidate as a coating material for superior performance. Nevertheless, the low fracture toughness of the brittle ceramic cause failure in the coating by formation of cracks or delamination from the substrate surface. Brittle

ceramic particles combined with ductile metal can produce metal matrix composite (MMC) coating on the substrate surface that enable to provide superior hardness, wear resistance along with high toughness. The ceramic reinforced metal matrix composites are usually used for wear resistance components (Du et al., 2011). The MMC can withstand high tensile and compressive stress by distributing the applied load between the matrix and reinforced phases (Huang et al., 2003). The ceramic-reinforced MMC material exhibits superior performance characteristic at high-temperature application, due to high melting temperature of ceramic reinforcement (Emamian et al., 2012a). Nevertheless, making an entire component with reinforced ceramic become uneconomical, when the volume of the component become extremely large. Application of a hard coating layer or reinforcement of hard particles on the surface of the component can enhance its performance. Furthermore, it is well accepted that incorporation of solid lubricant in the coating may reduce the frictional force or coefficient of friction value of the surface during sliding wear and consequently reduces the wear rate of the component. Therefore, fabrication of a hard and wear resistance ceramic reinforced MMC coating in combination with solid lubricant is greatly needed. Furthermore, a suitable coating technique that enables to produce a reliable and defect-free coating at low cost is also indispensable. Tungsten inert gas (TIG) cladding or alloying is an emerging and low-cost coating method widely used for fabrication of hard-facing of metallic substrates, where an improved surface layer is produced by melting the powder or powder mixture preplaced on a substrate surface.

1.1 Hard and wear resistance coating processes

Hard and wear resistance coating usually fabricated on metallic substrate by using different type of coating or surface modification technique i.e. PVD, CVD, PLD, thermal spray coating, high energy beam methods like laser cladding/alloying, electron beam alloying, and weld deposition methods i.e. tungsten inert gas (TIG) cladding, shielded metal arc weld (SMAW) cladding, etc. Detail classification of different types of hard coating techniques is illustrated in Fig. 1.1. Among these processes, PVD, CVD, PLD are used for fabrication of thin coating. In contrast, to produce a thick coating, thermal spray, high energy beam methods like laser coating/electron beam coating and weld deposition methods are utilized (Pawlowski, 1999). A brief discussion on different type coating process used to deposit a thick layer of hard coating illustrated below.

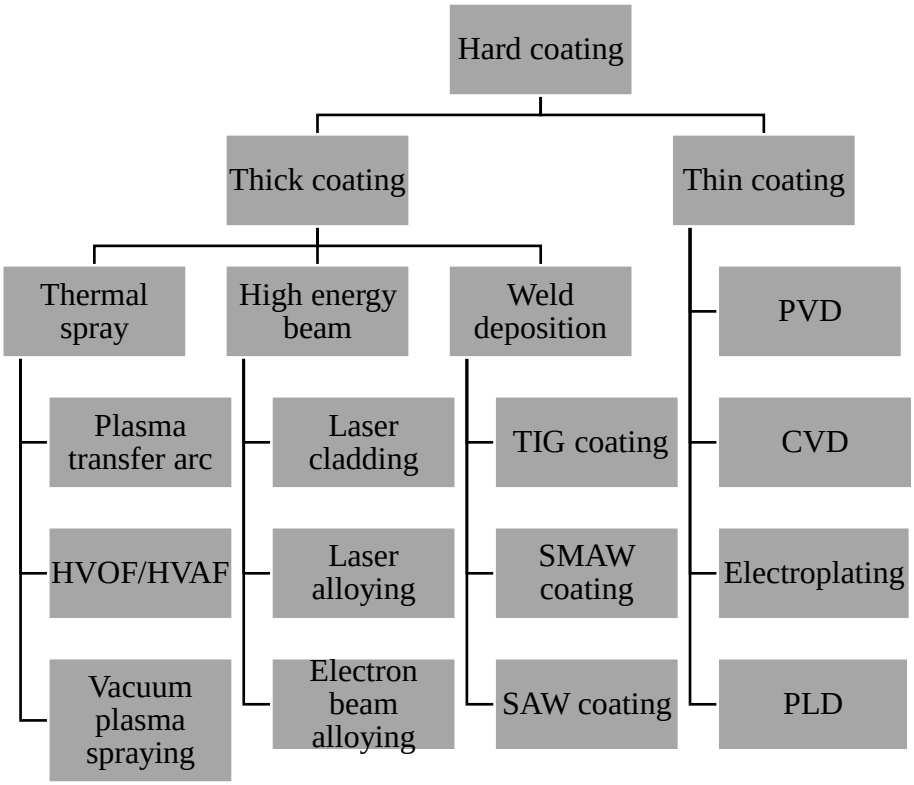

Fig. 1.1: Classification of hard coating methods

1.1.1 Thermal spray method

Among various thermal spray methods, plasma spray and high velocity oxy fuel (HVOF) are popular to deposit hard and wear resistance coating uniformly and at faster rate. In plasma spray coating, the plasma flame fully/partially melts the feed stock powder and spray at high velocity towards the substrate surface. The high velocity molten powder stick on the substrate surface and produce a uniform and thick coating layer (Pfender, 1988). In HVOF method, the combustion product from specially designed torch carries the feedstock powder at high velocity and impinge on the substrate surface to form a coating layer. The hard metal or ceramic powder deform (splat) due to high velocity impact of the powder on the substrate surface (Cetegen and Basu, 2009). The thermal spray methods are economical, reliable and repeatable and produce a coating with minimum distortion of substrate material. However, the produced coating by plasma spray method comprise high volume of porosity, low chemical homogeneity and suffering from weak bonding between the coating and substrate. These defects in the coating deteriorates the corrosion and wear resistance of the coating (Chen et al., 2014; Mateos et al., 2000; Singh et al., 2007).

1.1.2 High energy beam method

(i) Electron beam alloying/coating

High energy of the electron beam can be utilized for surface modification of various heat resistive material through surface melting or surface alloying. The electron beam melts the preplaced powder and substrate surface to produce a modified coating layer. The electron beam coating has successfully utilized to produce coating layer using hard ceramic materials (Dong et al., 2003). Nevertheless, application of electron beam alloying is limited due to high equipment cost, complex control system and requirement of vacuum during the coating process.

(ii) Laser coating

Laser coating method is one of the state of art method to produce a hard ceramic coating on the substrate. A defocused and moving laser beam act as a heat source to melt the feedstock (sprayed powder) or preplaced powder material and deposited on the substrate surface as a coating layer (Weng et al., 2014). The laser beam power and scan speed controlled in such a way that it only melt the preplaced or sprayed powder and the surface of the substrate material and produces a metallurgical bond between the coating material and the substrate with low dilution (mixing) of coating material (Nowotny et al., 2014). The laser coated surface possess superior surface property like wear resistance, corrosion resistance, hardness compared to the substrate material. For laser coating, both continuous and pulsed mode laser beam can be used. Fig. 1.2 shows the schematic diagram of laser coating process by co-axial powder blown method. Depending on the mechanism or mixing ratio the process is called laser coating/cladding or alloying.

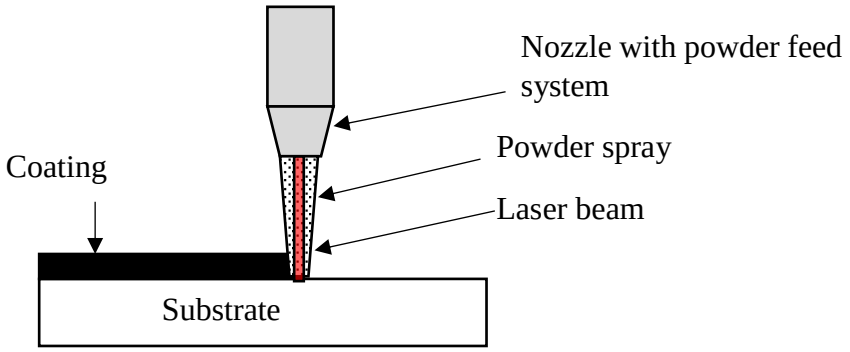

Fig. 1.2: Schematic diagram of laser coating by powder blow method

There are several advantages of the laser coating process those made it most popular coating technique to deposit various type of hard coating on versatile of substrate materials (Emamian et al., 2012a, 2012b; Jiang and Molian, 2001; Katipelli et al., 2000a). Some of the specific advantages of the laser coating process are listed below

- Laser coating/cladding can deposit a thick layer on the substrate surface.
- Due to occurrence of fusion in the coating material and substrate surface, a strong metallurgical bond obtained.
- In case of laser cladding, minimum dilution of the coating material with the substrate is possible, which enable to produce a unique coating as per the requirement.
- In laser coating process heat affected zone (HAZ) on the base material is minimum that maintains the base material properties.
- High cooling rate during solidification in laser coating process, induces fine grain microstructure, which improves the mechanical and metallurgical property of the coating.

Irrespective of the above advantages, application of laser coating process restricted in small scale industry due to the following drawbacks (Candel et al., 2010).

- High initial and running cost of laser setup.
- Non-uniform heat distribution in Nd:YAG and CO_2 laser.
- The absorptivity of laser beam is very less for metal that diminishes the efficiency of the process.
- Laser coating though powder blow method is highly complex, due to the involvement of a large number of processing parameters.

It is worth to mention that regardless of the above limitation laser coating or cladding have successfully used in various engineering application as follows (Emamian et al., 2012a; Jiang and Molian, 2001; Katipelli et al., 2000a; Nowotny et al., 2014):

- To repair worn-out surface of turbine blade and other mechanical component
- To improve the life of rolling mills, casting dies by depositing hard coating layer.
- To deposit wear resistance coating on large scale drill-bit rigs and other earth removal equipment used in mining industries.
- Corrosion resistance coating of large size hydraulic cylinder.

1.1.3 Weld deposition methods

(i) Shielded metal and gas metal arc deposition

In this method, shielded metal or gas metal arc welding setup is used, where the consumable electrode material deposited as a coating layer. The electrode material usually different from the substrate material and having superior mechanical properties. The electrode material melted due to the heat generation from arc and deposited on the substrate surface. A thick coating can be produced by depositing the molten electrode material overlapped after each track and layer by layer (Wang et al., 2008). The coating material can also be supply through continuous wire feeding like MIG welding. Shielded metal or gas metal arc deposition is an economical coating process, commonly used for repair work and to produce hard and wear resistance overlay coating for the components used in mining industry. However, uncontrolled heat supply causes high dilution of the coating material with substrate and sometime damage the substrate surface. Further, manufacturing of different type hard electrode or wire is highly challenging. Fig.1.3 demonstrate the schematic diagram of shield metal arc deposition process.

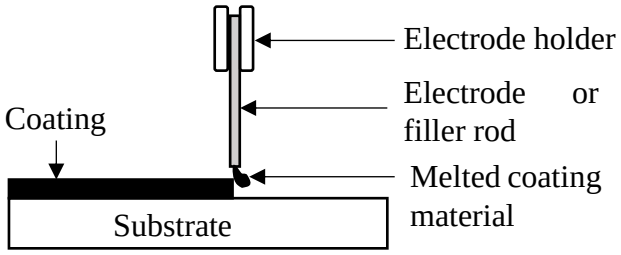

Fig. 1.3: Schematic diagram of shield metal arc deposition process

(ii) GTAW or TIG coating/cladding

GTAW or TIG welding is a fusion welding method usually used to join metallic plates. A non-consumable tungsten electrode used, and the arc is generated between the electrode and work piece, which melt the junction of the metallic plates to be join and after solidification a sound weld joint obtained. In TIG coating/cladding process, the arc is used as a heat source to melt the coating material as well as the substrate surface by moving it through a track on the substrate. The coating material applied either by powder preplacing on the substrate surface prior to the scanning of the arc or by blowing powder or feeding a wire during the scan of the arc. Fig 1.4 shows the schematic diagram of TIG cladding process. The TIG cladding is an economical coating process compared to the laser coating, plasma spraying

or other high-energy coating methods used to deposit hard and wear resistance coating. Employing the preplaced powder, TIG coating process successfully utilized to deposit a coating with hard ceramic particles i.e. TiC, WC, SiC or their composites. The ceramic reinforced composite coating produced by TIG cladding possesses high hardness and wear resistance. The performance of the coating depends on the TIG processing parameters like current, voltage, scan speed, gap between electrode and work surface, and coating materials. Both continuous and pulsed mode of power supply are used as heat source.

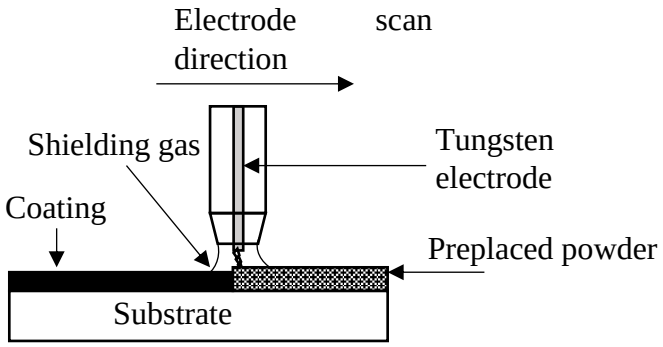

Fig. 1.4: Schematic diagram of TIG cladding process

Some of the basic advantages of TIG cladding process are illustrated below (Mridha et al., 2015; Patel et al., 2014)

- The process is highly economical compared to laser, plasma or HVOF coating due to low cost of the TIG welding set-up.
- By controlling the parameters either a thick coating of ceramic or ceramic reinforced metal matrix composite coating can be produced.
- Excellent adhesion between the coating and substrate material is possible due to strong metallurgical bonding.
- Different type of coating material in the form of powder can be employed to produce a hard, wear resistance and corrosion resistance coating surface.

Apart from the above advantages TIG cladding process has specific limitations as described below

- High heat input may damage the substrate material.
- High dilution of the coating material with substrate compared to laser coating process.
- Powder blown method sometimes interrupts the arc stability.
- Non-uniform heat distribution of TIG arc causes inhomogeneity in the coating.

1.2 Mechanism to incorporate the coating materials

To produce a thick layer, coating material usually deposited either by powder blown method or preplaced powder method. Apart from these, coating material sometimes also supplied through wire feeding mechanism. Different coating material feeding methods are briefly illustrated below

1.2.1 Powder blown method

In powder blown method, the substrate surface is melted by using either laser beam or TIG arc heat source and simultaneously fine powder of coating material (mainly ceramic particles or mixture of ceramic and metal powder) blown to the molten zone through a nozzle. An inert carrier gas is used to flow the powder and maintain its flow rate. During the coating process the blown powder partially or fully melted and deposited on the substrate surface to produce a thick coating layer. For laser cladding, sometimes a coaxial nozzle is used that provide very precise control on the melting and deposition of the powder. Fig. 1.5 illustrate the schematic diagram of the coating by powder blown method using laser beam as a heat source.

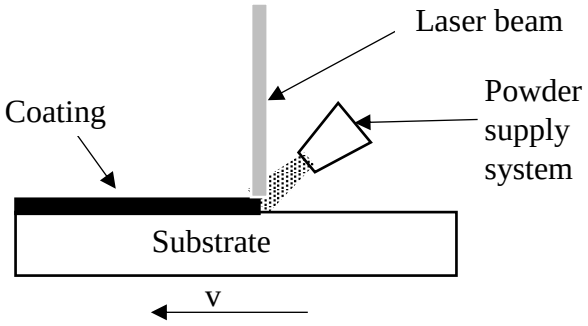

Fig. 1.5: Schematic diagram of powder blow method used in laser coating (Sahoo et al., 2015)

1.2.2 Wire feeding method

In this method, the coating material to be deposited supplied in the form of wire. The laser or TIG heat source melted the wire and deposited it on the substrate surface. Wire feeding method is highly efficient compared to powder spray and preplaced powder method, due to minimum loss of coating material. However, the precision alignment between the heat source and coating wire is necessary for any defect free coating. Fig. 1.6 shows the schematic diagram of the coating by wire feeding method utilizing laser beam as a heat source.

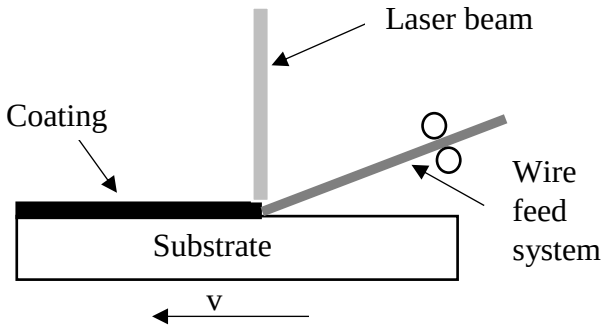

Fig. 1.6: Schematic diagram of wire feeding method using laser beam (Sahoo et al., 2015)

1.2.3 Preplaced powder method

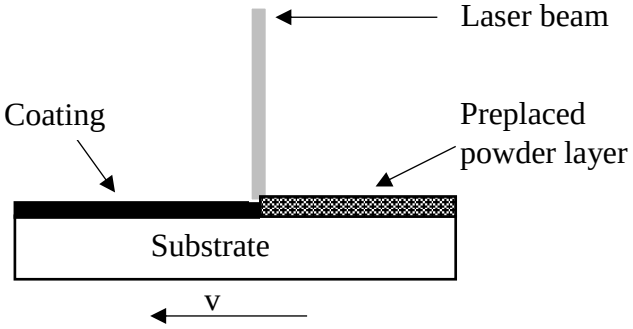

Fig. 1.7: Schematic diagram of coating by preplacing method using laser beam as heat source (Sahoo et al., 2015)

Preplaced powder method is a two steps process. In the first step, the powder or powder mixture to be coated is preplaced on the substrate surface. In the next step, the heat source i.e. laser beam or TIG arc scan over the preplaced powder layer. The high energy heat source melts the powder as well as a thin layer of the substrate to produce the coating. The powder pre-placement is one of the commonly applied methods due to its simplicity and requirement of low quantity powder for the coating. The preplacement of the coating material may be done in the form of dry powder, slurry, paste, strip, sheet, wire (Farnia et al., 2013a). The powder is usually mixed with an organic binder and applied on the substrate surface as paste. Sometimes, preplacement of the coating material also done by thermal spray method, and in next phase TIG arc or laser beam is used to re-melt the pre-deposited coating to produce a sound bond between the coating and substrate material (Ghadami et al., 2015; Mateos et al., 2000). Preplaced powder method is limited to produce a coating on a flat surface only and overlapping scan is required to make a large area coating surface (Farnia et al., 2013a; Paital et al., 2011). Fig. 1.7 represent the schematic diagram of the coating process by powder pre-placement method using laser beam as a heat source.

Basic parameters considered for the employment of coating powder in laser based and weld based coating process, which govern the performance of the final coating are illustrated in Fig. 1.8

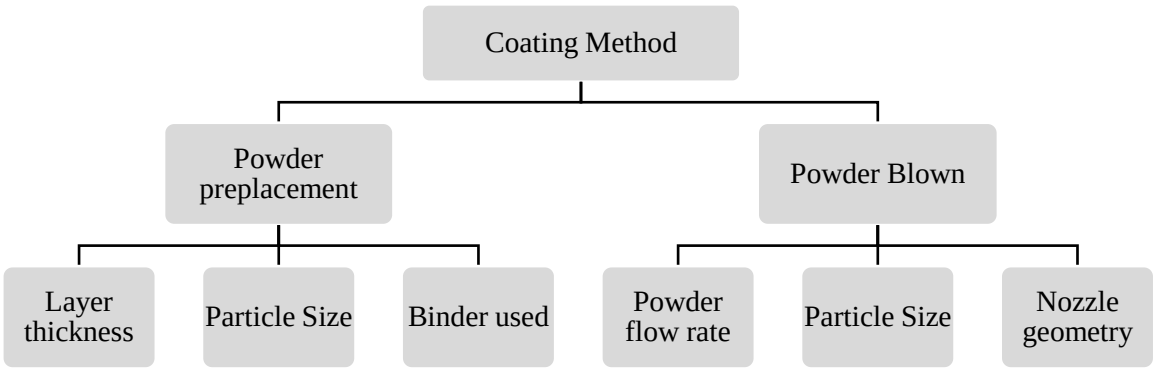

Fig. 1.8: Basic parameters for coating powder employment in laser and TIG cladding

1.3 Classification of hard coating based on coating structure

The thick coating process like thermal spray coating, laser coating, and weld deposition can be further classified based on the degree of mixing of the coating material with the substrate. It has been already described that thermal spray method like HVOF, plasma spray methods melt only the coating material and no dilution with the substrate. However, in laser coating or TIG coating/cladding process both the powder and substrate surface melted. Therefore, depending upon the degree of mixing of the coating and substrate material, and based on the characteristic of the coating material, the hard coating process can further categorize as surface alloying, dispersing or cladding. Fig. 1.9, show the schematics of surface alloying, dispersing and cladding.

In surface alloying, full dissolution of the coating material in substrate surface occurred. The coating material mixed with the substrate material in molten state and form an alloy. The produced alloy surface improve the surface property of the substrate. The alloyed layer may have different properties than the applied coating material or substrate. Fig. 1.9a shows that both coating material (y) and the surface of the substrate (x) melted and mixed in the melt pool. The solidified surface layer produces an alloy containing both the coating and substrate materials. In dispersion method, the substrate surface melted by laser beam or TIG arc heat source, and the coating material in the form of small particles dispersed in the molten surface. Commonly, hard ceramic particles like TiC, WC, Al_2O_3 are

used as dispersing element to produce a coating with superior mechanical properties than the substrate. After solidification, coating and substrate material remain unchanged and can be identified separately. Fig. 1.9b shows the schematic diagram of dispersion method. In the cladding process, the heat input controlled precisely to obtain minimum dilution of the coating material with the substrate surface. In this method, coating material produces a separate layer on the substrate surface. The properties of the clad layer are independent of the substrate material, whereas in alloying and dispersion method the substrate material has significant influence on the produced coating. Fig. 1.9c shows the schematic of cladding process.

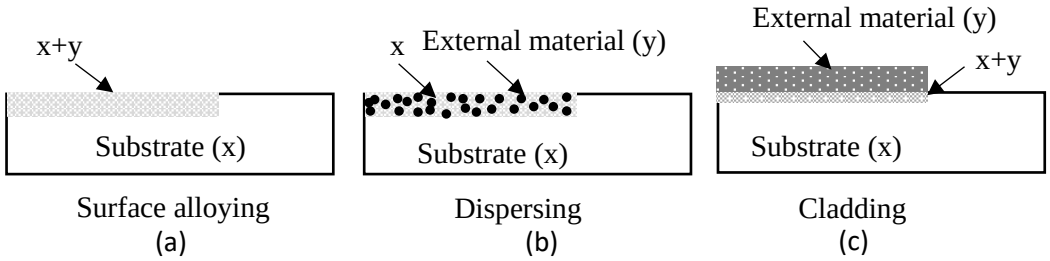

Fig. 1.9: Schematic diagram of alloying, dispersing and cladding process

1.4 Parameters of Laser and TIG coating/cladding process

In laser and TIG coating/cladding, structure and quality of the coating mostly depend on the rate of heat input, cooling rate, material properties. The heat input to the coating can be controlled by selecting appropriate processing parameters. Detail of parameters for laser and TIG coating process are described below.

1.4.1 Laser coating parameters

In laser coating process, a de-focused laser beam is scanned over the pre-deposited coating surface on the substrate material to obtain almost uniform heat distribution on the track profile. The laser beam with the interaction of preplaced coating surface produces heat, which completely or partially melts the coating layer and substrate surface to produce a strong coating on the substrate.

The parameters affecting the heat input in the processed zone mainly depends on the type of laser, wavelength of laser beam, laser power, beam diameter, scan speed, absorptivity of the coating material, and for pulse type laser, pulse duration, and frequency. Fig. 1.10 shows the laser processing parameters affecting the coating process.

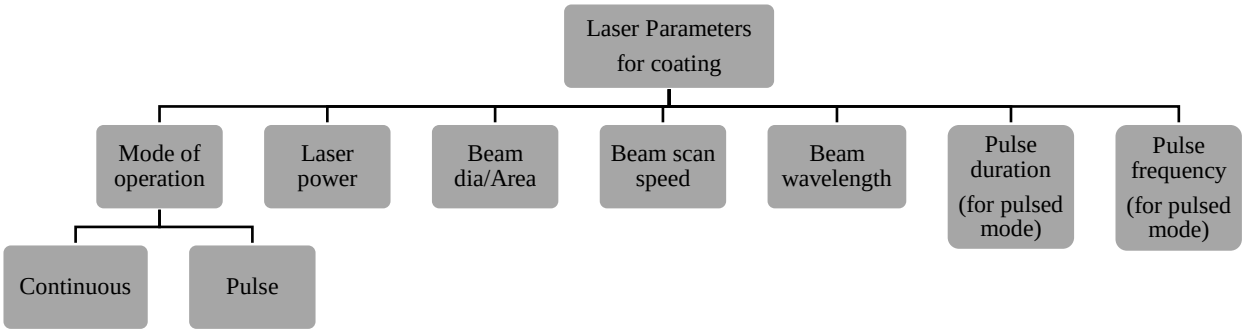

Fig. 1.10: Laser processing parameters affecting coating process

Heat supply by the laser beam during coating process depend on the mode of laser operation i.e. continuous or pulsed. In continuous mode of laser beam, energy per unit length can be calculated as

$$H = P/S \quad \ldots \text{Eqn (1.1)}$$

Where, H is energy per unit length; P and S are laser power and scan speed respectively (Hong et al., 2015). Power density or energy per unit area (laser power/beam area) also used as input parameter to represent the heat input.

(i) Pulse Laser coating

Although, continuous wave laser is extensively used for laser surface modification, owing to specific advantages of pulse laser such as high peak power controlled pulse duration, frequency, and pulse energy, the use of pulse laser for surface modification become an emerging area of research (Yan et al., 2010a).

However, there is a lack of study about employing the pulsed laser in surface modification, mainly due to its discontinuous behavior and lower processing capability. During pulse laser operation, laser beam energy is delivered through intermittent pulses, which can be controlled by pulse duration, frequency of pulses, and pulse energy. This allows more precise regulation of spatial and temporal modes of laser beam energy delivery, which could create different thermal condition, microstructures, and phases within the laser substrate interaction region, which is not possible for samples processed with a continuous laser (Farnia et al., 2013a). Again, due to short pulse width and high peak power, pulse laser could produce sufficient higher melting depth as well as substantially higher cooling rate in the melt pool than that of continuous laser processing. The laser power-off period between two pulses, allows the melt pool to solidify and the higher cooling rate could be obtained by pulsed laser processing and corresponding microstructure produced more

refined. Since hardness and other mechanical property of a particular material depend on the characteristic of the microstructure, therefore coated or alloyed zone produced by a pulsed laser should have superior mechanical property than that of produced by a continuous laser (Sun et al., 2005).

In pulsed laser, processing parameter like laser peak power, pulse duration, pulse frequency, scanning velocity are considered to calculate the heat input. Heat input per pulse and total heat input during the pulsed laser processing are described by peak power density and effective peak power density (EPPD) respectively (Ghaini et al., 2007; Lapsanska et al., 2010).

General observation states that laser input parameters have significant effect on the performance of the produced coating i.e. hardness and wear resistance. Owing to variation in the degree of mixing of the coating material with the substrate or due to difference in the melting and cooling rate, microstructure of the coating get altered. Consequently, the mechanical properties of the coating changed accordingly.

1.4.2 TIG coating/cladding parameters

In TIG coating/cladding process depending on the heat input, the degree of melting of the substrate decided and produces either a separate layer of coating material or a mixed metal matrix composite layer. Heat input during the TIG coating process can be control by regulating the electrode scan speed and input power i.e. voltage and current.
The heat input in the TIG process can be calculated by using equation 1.2.

$$H = \eta(V.I/S) \quad \ldots \text{Eqn. (1.2)}$$

Where V, I and S represent the voltage, current and scan speed respectively; η is heat absorption efficiency (Mridha et al., 2012a). The equation shows that the heat input is directly proportional to the current and voltage, and inversely proportional to arc scan speed. In addition, tool electrode gap, electrode diameter, gas flow rate, type of shielding gas are also affecting coating process and the properties performance of the produced coating. Patel et al. (2014) found that shielding gas has great influence on the temperature rise along the coating track. The melt pool or coating thickness also affected by the substrate temperature prior to coating (Mridha et al., 2015). Fig.1.11 shows the TIG processing parameters affecting the quality of the coating.

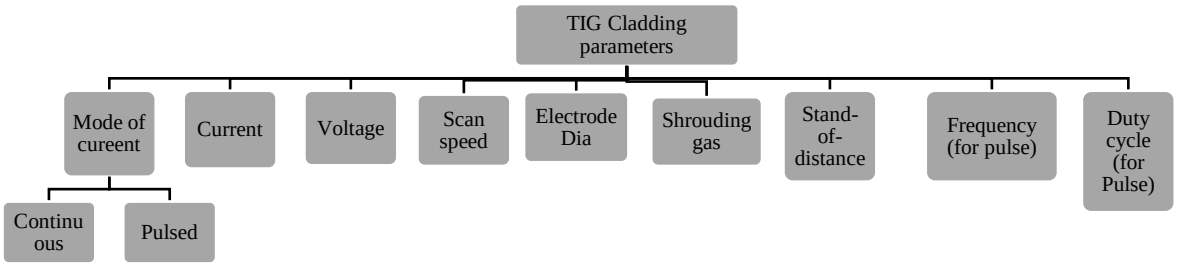

Fig. 1.11: TIG coating/cladding processing parameters affecting coating process

1.5 Substrate material (AISI 304 stainless steel)

Stainless steel is one of the primary choices for manufacturing of machine components, utensils, structural elements, due to its high strength, corrosion resistance (Akhtar and Guo, 2008). AISI 304 stainless steel have superior mechanical property and high corrosion resistance in adverse environment. Hence, AISI 304 stainless is widely used in structural applications, equipment associated with the chemical and nuclear power industries, food processing industry, petrochemical industry, condenser tubing, vapour lines tubing and heat exchangers (Majumdar et al., 2007; Singh et al., 2012; Majumdar and Manna, 1999). However, application of the austenite steel limited for the components those are directly involved in abrasive and adhesive wear environment i.e. mining and agricultural equipment chutes, rock excavator teeth, tool and dies in the manufacturing industry. The hardness of stainless steel can be improved by addition of carbon; however, reduction in ductility of steel may affect its overall performance (Ushashri and Masanta, 2015). Heat treatment process also not suitable for austenite steel to increase its surface hardness because during heat treatment the carbon and Cr in steel combined and formed chromium carbide ($Cr_{23}C_6$) along the grain boundary (McGuire, 2008). Lack of Cr in the steel consequently reduce the corrosion resistance of steel. Addition of hard ceramic particles like TiC, SiC, and WC on the austenitic steel surface may produce a composite clad layer that makes the steel component resistive against wear by improving its hardness. So far, different coating techniques were employed to deposit hard and wear resistance coating on various type of steel substrate (Masanta et al., 2011; Piasecki et al., 2016; Ramírez et al., 2015; Yang et al., 2014).

1.6 Ceramic reinforced composite coating

Ceramic particle reinforced metal matrix composites (MMCs) retaining high hardness, strength, stiffness and wear resistance compared to its matrix base, along with preeminent toughness than the monolithic ceramic or ceramic composites (Emamian et al. 2012b). However, it was revealed that fabrication of an entire MMC component sometimes uneconomical due to its manufacturing complexity and high cost of reinforced ceramic particles (Yan et al., 2012). It is worth to mention that a layer of ceramic particle reinforced MMC on the base material surface produced by high energy density deposition methods like laser cladding/alloying, thermal spraying, TIG melting/cladding can improve the surface properties of the component without affecting its bulk characteristics (Berger, 2015).

Hard ceramic materials like carbides (WC, TiC, SiC, VC, and Cr_3C_2), oxides (Al_2O_3, ZrO_2), borides (TiB_2, SiB_3, SiB_6) are widely utilized as reinforced or coating material to produce metal matrix composite (MMC). Among these, TiC is one of the eminent carbide used as reinforced particle in various type of metal matrix due to its high hardness, high melting temperature, and low density. TiC can retain its hardness at elevated temperature, which makes it most promising coating material for the high-temperature application (Rasool and Stack, 2014). TiC reinforced coating, further preferred in tribological application due to its low frictional coefficient, thermodynamic stability, high elastic modulus (Rajabi et al., 2015). Table 1.1 shows some of the physical properties of TiC along with other carbides normally used as reinforcement in MMC. It was reported that WC reinforced Co based MMC is most widely use coating material. However, its oxidation and corrosion resistance are lower than that of TiC (Candel et al., 2014).

Table 1.1: Properties of some metallic carbides used as hard and wear resistance coating (Ariely et al., 1991; Li et al., 2011; Groover, 2007)

Metallic-Carbides	**Hardness**	**Density (g/cm^3)**	**Melting temperature (^oC)**
TiC	3000 HV	4.93	3067
SiC	2600 HV	3.2	2700
WC	2600 HV	15.6	2870
VC	2800 HV	5.77	2810
Cr_2C_3	18.9 GPa	6.68	1895

1.6.1 TiC reinforced composite coating on AISI 304 steel surface

Poor wear resistance of AISI 304 steel surface can be improved by using hard TiC reinforced metal matrix composite coating. This type of MMC coating can be produced by using laser coating/cladding or TIG coating/cladding process. TiC possesses high hardness (3000 HV) compared to steel (200 HV) and has limited solubility with Fe (Ariely et al., 1991). Therefore, TiC reinforced particles can be reinforced in steel during the coating process without forming any intermetallic. TiC-steel MMC coating provides superior surface properties than the steel substrate. The effort of several research groups revealed that TiC reinforced coating on AISI 304 steel significantly improved the surface hardness, fretting and sliding wear resistance compared to the as received steel surface (Akhtar and Guo, 2008; Ayers and Tucker, 1980; Rasool et al., 2015; Ushashri and Masanta, 2015). Further, TiC-steel composite coating reduces the coefficient of friction and wear rate for a wide range of load and sliding speed (Peng, 2012). Moreover, TiC reinforced steel coating can be produced by both ex-situ and in-situ methods using high energy density heat sources like laser beam or TIG arc. The above discussion revealed that stainless steel is a suitable matrix material for TiC reinforced particles to improve its hardness and wear resistance.

1.6.2 Bonding material (Ni)

It is relevent to mention that major challenges associated with the fabrication of TiC reinforced steel composite coating is to attain proper interfacial bonding, as the solubility of TiC in steel is very low and frequently produces undesirable intermetallic compounds (Man et al. 2002). It is worth to mention that to obtain an appropriate bond between the substrate and the reinforced ceramic particles, interfacial materials like Ni and Co; those are retaining high wetting property with both TiC particles and steel matrix need to provide (Nowotny et al. 2014). It is well established that for thermal spray process, these interface materials produces a separate layer between the substrate and the ceramic coating with a minimum dilution (Pawlowski 1999). Table 1.2 illustrate the physical properties of Ni used as a bonding material between TiC and steel.

1.6.3 CaF_2 as Solid lubricant

It is well accepted that apart from the hard coating, employment of appropriate lubrication can also improve the lifetime of a component by reducing the frictional force between the moving parts. It has been observed that conventional liquid or semi-solid lubricants do not

work efficiently under vacuum, high load and extreme temperature condition (very high/low) (Liu et al., 2013). The solid lubricant is an alternate solution that effectively used in various components where the application of conventional lubricant is unjustified. Earlier, noble metal like gold and silver were commonly used as solid lubricants (Jin et al., 1999). However, the high cost of these metals is the major constraint in their application for regular use. Recent studies indicate that organic alkali fluorides (LiF_2, CaF_2, BaF_2), disulfides (MoS_2, WS_2), and some metal oxides (Zr_2O_3, Cr_2O_3, MoO_3) are good aspirants as solid lubricants (Liu et al., 2013). Among these, alkali fluorides are preferred due to their low density, low shear strength, stable thermos-physical and thermos-chemical properties at higher temperature in conjunction with their low cost and ease of availability (Xiao-feng et al., 2009).

CaF_2 is a well-known and widely used solid lubricant, normally utilized in self-lubricating ceramic composite and anti-wear applications. CaF_2 has a laminar structure with low shear strength, which prevent the adhesion wear and assist in tribo-chemical reaction to facilitate a reduction in wear. Additionally, it is chemically stable at high temperature and does not react with reinforced materials. Furthermore, due to low hardness and slip plane structure, CaF_2 easily soften to act as a lubricant. It is also used as fluxing medium and enhances fluidity of the melt-pool (Yan et al., 2012). CaF_2 can transform from brittle to ductile at higher temperature (600 ^oC) by forming low shear strength ductile phase (Wang et al., 2002). Table 1.2 demonstrate the physical properties of CaF_2.

Table 1.2: Physical properties of Ni and CaF_2[1] [2]

Properties	**Ni**	**CaF_2**
Melting point	1453 ^oC	1403 ^oC
Thermal expansion coefficient	13.4 $\times 10^{-6}$ ($^oC^{-1}$)	18.18 $\times 10^{-6}$ ($^oC^{-1}$)
Thermal conductivity	90.9 W/(m·K)	9.71 W/(m·K)
Density	8.9 g/cm³	3.18 g/cm^3
Crystalline structures	FCC	Hexagonal

[1] Calcium Fluoride (CaF_2), Fluorite or Fluorospar - Properties and Applications, accessed 24 October 2016, <http://www.azom.com/article.aspx?ArticleID=2352>.

[2] Nickel(Ni)- Properties, Applications, accessed 24 October 2016, <http://www.azom.com/properties.aspx?ArticleID=617 >.

1.7 Characterization of hard coating

Ceramic reinforced composite coating produced by high energy laser beam (laser cladding/alloying) and weld cladding method (TIG cladding/melting) have almost similar structure. The quality of the coating can be judged by considering the following aspects:

1.7.1 Coating profile or geometry of the coating

Coating profile is the geometry of the coating at the transverse cross-section for a single line scan. It indicates the extent of melting depth or deposited layer thickness and width of the melting for single line scan of laser beam or TIG arc. The geometry of the coating profile can be revealed from the macroscopic image of the coating at the cross-section.

1.7.2 Dilution with the substrate material

Microscopic images of the coating at the cross-section can be further utilized to identify the dilution of the coating material with the substrate. Characteristic of the coating property like hardness, wear resistance, corrosion resistance depends on the percentage of dilution of the coating material with the substrate. As already described, based on the dilution of coating material the coating can be classified as alloying, dispersing, and cladding.

1.7.3 Compounds or phases present in the coating

The coating properties may vary due to induction of high amount heat during the coating process. The employed heat may change the coating/substrate material properties by changing the material structure or due to formation of the new compounds. The compounds present in the final coating can be identified by X-ray diffraction analysis (XRD). The formation of new phases affect the hardness, corrosion resistance and wear resistance of the coating. Thus, identification of phases helps to evaluate the quality of the produced coating.

1.7.4 Microstructure of the coating

The microstructure of the coating produced by laser and TIG coating/cladding varied due induction of high heat and rapid solidification of molten material. The change in the microstructure of the coating can be identified through the high magnified SEM/FESEM images. The coating material may change its morphology during the coating process. The change in microstructure may affect the hardness and wear resistance properties of the coating.

1.7.5 Hardness of the coating

The hardness of any material is the resistance to plastic deformation against a hard indenter under a specific load. Micro-hardness values can be used to predict the coating structure i.e. distribution of the reinforced material. The variation in micro-hardness value can also be used to detect the quality of the coating. Vickers micro-hardness value is commonly used to measure the hardness value of hard coating surface within a localized zone. It is generally accepted that wear behavior of any coating largely depends on the hardness value of the coating.

1.7.6 Tribological behavior of the coating

Table 1.3: Various types of wear testing methods

Wear test rig/tester	Type of wear test	Test method
Pin-on-disc or Ball-on-disc	Adhesion, Abrasion, plastic deformation	Coated pin slide against any standard hard material disc or abrasive disc or abrasive paper or vice versa.
Block-on-ring	Adhesion	Coated block slid against a standard hard metal ring.
Fretting	Fretting wear	Standard tool oscillates with a small amplitude against the coating surface.
Erosion test	Erosion resistance of material against solid particles	Solid particles carried out by gas jet and impinge on the coating surface.
Wet-sand or rubber wheel abrasion test	Scratch resistance of material.	Abrasive particles rub against the coating surface.

Tribological behavior (wear resistance, COF) of any material assessed through various type of wear test i.e. adhesion, abrasion, fretting, and galling wear. Tribological behavior of a hard coating can be revealed through selection of appropriate wear test. The wear test confirms the reliability and sustainability of any coating under a specific load and environment condition prior to practical application. Table 1.3 shows the different wear testing mechanism and condition utilize to examine the tribological behavior of the coating. Among these, pin-on-disc is a standard wear test method, where a small diameter pin shaped

specimen slide (rotational) against a hard metallic or abrasive type plate or disc-shaped counter-body under a specific amount of normal load. Wear rate can be measured from the height or weight or volume loss after a specific time of test. In combination with the wear rate, the coefficient of friction (COF) can also be measured through the measurement of frictional force.

1.8 Coating defects

Selection of proper coating technique and process parameters are essential to produce a defect-free coating surface. Defects in the coating appear as porosity, crack inside the coating or coating-substrate interface, low bonding strength with the substrate, and high dilution of coating material.

Porosity may induce in the coating due to entrapment of gasses that generate during the process of high temperature or absorption of atmospheric gasses during the melting process. As molten pool during laser or TIG coating process solidify at an extremely fast rate, quick solidification of the coating layer causes entrapment of the gasses. Further, due to the incomplete melting of the coating materials, the inter-particle gap or agglomerated particles may induce porosity in the coating.

Formation of cracks in the coating, both in micro or macro level drastically deteriorate the performance of any hard and wear resistance coating. Cracks may appear in the coating substrate interface predominantly due to the mismatch in thermal and physical properties of the coating and substrate materials (Ouyang et al., 2016). Moreover, cracks on the surface or at the transverse cross-section may appear due to the generation of high thermal stresses during melting and solidification at an elevated rate (Gu et al., 2011; Li et al., 2015). During the coating process, high energy input induces microstructural stress, which may also lead to the generation of cracks in the coating (Li et al., 2015). The bonding strength between the coating and substrate depends on the diffusion or percentage dilution of the coating material on the substrate, which further governs by the thermos-mechanical properties of both the materials. It is worth to mention that the coating layer delaminates or peeled off owing to inadequate bonding strength between the coating and substrate.

In laser and TIG coating methods, when coating layer formed by incorporating hard ceramic particles, the applied heat control the dilution of the coating material in the substrate. By selecting suitable processing parameters, heat input during the coating process

can be regulated and consequently the dilution of the coating material. Dilution or percentage of coating material directly affect the performance of the produced coating in terms of its hardness and wear resistance. Therefore, it is essential to maintain an optimum value of dilution of the coating material. For laser or TIG cladding, a separate layer of the coating formed on the substrate with a minimum dilution of the coating material. High or low dilution of the coating material on the substrate govern the final coating properties i.e. coating strength, hardness, and wear resistance.

Chapter 2

Literature Review

To modify the surface properties of various substrate materials, TiC was applied to make a coating layer or reinforced on the substrate matrix. TiC is preferred as reinforced material due to its high hardness, high melting temperature, thermal stability, and low coefficient of friction. Numerous researches has been accomplished so far in this regard to enhance the surface hardness and wear resistance properties of different substrate materials by using TiC or TiC-reinforced composite coating.

2.1 TiC composite coating on Ti-6Al-4V

Ayers et al. (1980) deposited TiC/Ti-6Al-4V composite coating by laser melt ejection of TiC particles on Ti-6Al-4V surface. The coating exhibited improved surface hardness, reduced sliding wear and coefficient of friction compared to Ti-6Al-4V substrate. Sun et al. (2001) observed that TiC particles diluted in Ti-6Al-4V substrate, during laser melting process and precipitated as dendrite structure during solidification. It was also observed that with the increase in dilution of TiC in the substrate matrix, micro-hardness value of the modified layer reduces.

Candel et al. (2010) produced a TiC particle reinforced clad layer on the Ti-6Al-4V substrate by using a Nd:YAG laser with a coaxial powder feed mechanism. It was revealed that high-energy laser resulted in dissolution of the TiC particles and molten TiC particles solidified as dendrite structure within the Ti-6Al-4V alloy matrix. With the increase in TiC volume fraction in the coating, the micro-hardness and wear resistance of the coated surface also improved significantly. The authors (Candel et al., 2014) also studied the effect of laser parameter on failure mechanism of the coating. The presence of crack was witnessed in the coating due to non-uniform cooling of the coated surface at the clad substrate interference, track-overlapping zone or region where the volume fraction of TiC is reasonably low.

Wu et al. (2014) produced a wear resistance TiC composite coating using C powder on Ti–6Al–4V substrate by laser coating process. The presence of TiC particles was detected in the microstructure of the coating. It was found that the produced coating exhibited high micro-hardness value (up to 1400 $HV_{0.1}$) and high sliding wear resistance for

using Ti-C precursor. Further, the coefficient of friction (COF) of the TiC coating found lower (0.31) as compared to the COF of the substrate (0.5).

2.2 TiC composite coating on CP-Ti

Fouilland-Paille et al. (1996) produced Ti/TiC cermet coating on Ti foil by laser melting of preplaced carbon powder through an in-situ reaction. The coating exhibited superior hardness compared to the ex-situ TiC reinforced coating produced on the Ti surface. Courant et al. (2005) found that in-situ TiC particles produced by pulse laser irradiation improved the surface hardness of the Ti substrate (up to 650 $HV_{0.2}$) as compared to the untreated one (210 HV). Authors also revealed that the selection of laser processing parameters play an important role in TiC reinforced coating on Ti substrate. Hamedi et al. (2011) fabricated TiC reinforced coating on Ti substrate and observed that in-situ TiC formation depends on the pulse laser parameters. The TiC reinforced coating improve the micro-hardness value up to 1700 HV, which is ten times higher than the hardness value of pure Ti substrate. In addition, Chehrghani et al. (2012) from their study revealed that with the increase in heat input owing to augmentation in the mixing of preplaced graphite powder with molten Ti substrate, the rate of in-situ reaction to produce TiC enhances. Thus, fraction of TiC in the produced composite coating increases and consequently improved the hardness value of the coated layer.

Savalani et al. (2012) produced TiC-Ti reinforced composite coating on commercially pure (CP) Ti substrate using carbon nanotube (CNT) in Ti precursor. Experimental results indicate that with the increase in CNT quantity in the precursor, the hardness and wear resistance of the produced coating surface augmented due to the formation of denser TiC dendrites within Ti matrix. Li et al. (2014) also confirmed that the TiC composite coating produced by using Ti-CNT precursor mixture significantly improve the surface hardness and wear resistance of Ti substrate. It was also revealed that TiC reinforced coating augmented high temperature wear resistance up to 10 times (at 500 ^{o}C) than the pure Ti substrate.

Courant et al. (1999), Lu et al. (2000) and Saleh et al. (2010) through experimental analysis showed that in-situ TiC reinforced coating on Ti and Ti alloy improve the hardness and wear resistance of the produced coating significantly.

2.3 TiC-coating on stainless steel

The Fe-TiC composites are preferred due to their high wear resistance especially when applied on various graded steel substrate. Study on TiC reinforced composite coating on various grades of carbon steel, and stainless steel are illustrated below.

Ayers and Tucker (1980) produced TiC reinforced metal matrix composite (MMC) coating on AISI 304 stainless steel substrate by powder injected laser melting process. The TiC-steel composite layer improved the micro-hardness of the steel substrate from 152 HV to 200-250 HV. However, the formation of cracks within the carbide cluster due to thermal stress caused by rapid cooling was the major difficulty observed in the process. Axén and Gahr (1992) fabricated TiC–steel composite layer using preplaced TiC powder on 90MnCrV8 tool steel and subsequent laser surface melting process. Experimental results revealed that the composite coating fabricated with smaller size TiC particles (3 μm) exhibits harder and superior wear resistance surface as compared to the coating produced with larger size TiC particles (30 μm). Tassin et al. (1995) produced TiC reinforced AISI 316 L austenitic stainless steel surface by laser coating process. Sliding wear test of the coating performed against WC-Co demonstrated superior wear resistance of the TiC coating compared to the Cr_3C_2 coating on the steel surface.

Recently, Adebiyi et al. (2014) produced TiC reinforced alloyed surface on 12Cr martensitic stainless steel using laser cladding with powder feeding arrangement. The coating profile and its microstructure were related with the overlapping of tracks. It was revealed that high overlapping (75%) of the tracks resulted in microstructural change due to preheating and re-melting of the tracks. It was also found that TiC coating produced with high percentage of overlapping, exhibited harder and superior abrasive wear resistance. Ushashri and Masanta (2015) observed that pulse frequency has a vital role in the distribution of TiC reinforcement in steel substrate (AISI 304). It was revealed that micro-hardness of the coating varies between 650–1900 $HV_{0.1}$ depending on pulsed laser processing parameters. A high frequency laser pulse with constant peak power produced a high dilution of TiC in steel substrate. Dilution of TiC reinforcement in the substrate governs the hardness value of the coating.

2.4 TiC reinforced coating on medium carbon steel

Ariely et al. (1991) produced TiC alloyed layer on AISI 1045 steel surface by laser surface alloying and revealed that undissolved TiC particles as reinforcement in the steel matrix improve the surface hardness of the substrate significantly. The authors also found that the alloyed layer exhibited a limited solubility of TiC in the steel matrix as Ti and Fe does not produce any intermetallic compounds during laser alloying process. In recent years, Wang et al. (2008) produced in-situ TiC composite coating on AISI 1045 medium carbon steel using ferrotitanium alloy and graphite precursor by laser coating process. The block-on-ring wear test revealed that the produced Fe-TiC composite layer exhibited superior wear resistance and lower coefficient of friction compared to FeCrBSi coating and AISI 1045 substrate. Emamian et al. (2010, 2011) fabricated Fe–TiC composite coating on AISI 1030 medium carbon steel substrate using Ti, graphite and Fe precursor by laser surface alloying method. The study revealed that quality of the coating depends upon the laser processing parameters. The outcomes of the work established that the liquidus temperature of melt pool predominantly governed by the chemical composition of the precursor, which consequently alter the morphology of the coating i.e. dendritic, equiaxed, and spherical. Authors (Emamian et al., 2012b) also fabricated TiC reinforced composite layer on AISI 1030 substrate using Ti-C-Fe precursor by laser melting process. Authors studied the effect of Ti:C ratio on the morphology of TiC phase in the composite coating and found that higher carbon percentage resulted in a complete in-situ reaction that restricted the formation of Fe_2Ti brittle phase. The produced coating exhibited up to eight times higher hardness and 50-70 times better abrasive wear resistance compared to the substrate material.

TiC-Fe composite coating on low carbon steel substrate also deposited using ferrotitanium-graphite precursor through in-situ laser surface alloying (Du et al., 2011). It was established that Ti and C ratio is one of the important factor for in-situ TiC reinforced coating. Experimental results revealed that TiC reinforced coating improved the dry sliding wear resistance up to 15 times as compared to the steel substrate due to presence hard TiC reinforcement, which prevent severe plastic deformation of the surface during the wear test. Doubenskaia et al. (2013) formed steel-TiC composite layer on cast iron substrate by laser direct deposition method. The effect of various laser processing parameters like scan speed, laser power, and powder feed rate on the temperature distribution in the surface was studied. It was revealed that with the increase in laser power, as melt pool temperature increase, bead height and dilution depth also increases.

2.5 TiC reinforced coating on H13 die steel

Although H13 die steel is itself a hard material, however, to improve its hardness along with the erosion and corrosion resistance, TiC reinforcement was executed by various research groups. Pirzada et al. (2000) found that TiC reinforced laser surface coating on H13 die steel improved the corrosion and erosion resistance at high temperature (650 ^{o}C). Authors also found that fine TiC particles (0.3 µm) distributed uniformly in the coating and exhibited better static and dynamic corrosion-erosion resistance compared to the coating produced with coarse powder (2.0 µm). In addition, Jiang and Molian (2001) found that the laser coating produced using TiC on H13 steel improved the corrosion and erosion resistance of the substrate in combination with the hardness value.

2.6 TiC composite coating on Al-alloys

Various routes have also been considered to improve the surface quality of Al alloys by TiC reinforcement. TiC reinforced composite coating on various grades of Aluminium alloy (Al 2024, 5052 and 6061) was developed by laser surface modification technique (Ayers., 1984). It was revealed that a certain percentage of TiC reinforcement could be employed to produce a defect-free coating surface. Katipelli et al. (2000a) deposited TiC reinforced composite coating on 6061 Al alloy by laser surface alloying. The coating layer comprises of Al-Ti mixture, TiC particles and different intermetallic like $TiSi_2$, $TiAl_3$, which make a strong bond between the coating with the substrate. The coating showed significant improvement in the hardness and wear resistance (16 times) compared to the Al substrate. Similarly, Man et al. (2002) fabricated in-situ TiC reinforced MMC surface by preplacing Ti and SiC particles on Al6061 substrate by laser surface modification technique. It was revealed that crack free, porosity free uniformly dispersed TiC layer formed on the Aluminium substrate surface, which exhibited superior hardness (up to 650 $HV_{0.2}$) compared to as-received Al6061substrate (75 $HV_{0.2}$).

2.7 TiC composite coating on other alloys

Considering the advantages of TiC, it was also employed on various other materials to improve their surface properties. Chen and Wang (2003) deposited in-situ TiC composite on Ti–48Al–2Cr–2Nb substrate by laser melting process using preplaced carbon. Kim et al. (2014) formed TiC reinforced coating on AZ31 Magnesium alloy by laser surface melting of plasma deposited TiC coating layer. It was found that the TiC reinforced coating

improved both hardness (up to 700 $HV_{0.2}$) and corrosion resistance of the AZ31 Magnesium alloy significantly.

2.8 TiC composite coating with other compounds

It is accepted that use of multi-component composite instead of single /monolithic ceramic, the mechanical properties of the coating enhanced significantly by improving its fracture resistance. Further, the additional phases may aid different purpose and increases the utility of the coating for versatile application. In this section, a review on TiC coating deposited with other compounds on various substrate materials, to enhance their mechanical, metallurgical and tribological properties has been discussed.

In-situ TiC-Ti_5Si_3 composite coating was deposited on Ti–6Al–4V alloy by laser surface alloying with preplaced C and Si mixed powder on the substrate surface (Tian and Chen, 2007). It was revealed that the produced carbide layer improve the surface micro-hardness (up to 1500 $HV_{0.1}$), and wear resistance of titanium alloy significantly (more than four times). TiC-Ti-Al composite coating was deposited on γ-TiAl alloy substrate using a precursor containing nano-TiC, Ti and Al powder (Wang et al., 2009). Experimental results show that small particles shaped TiC morphology formed with low heat input, whereas dendritic structure of TiC obtained for higher heat input. Wear resistance of the coating improved up to 1.4 times compared to the substrate alloy.

In addition, TiC+Ti_3Al/TiAl clad layer was deposited on Ti–6Al–4V alloy by laser surface alloying using Al and TiC preplaced powder on the substrate (Li et al., 2010). Wear test results showed that the coating with 40 wt. %TiC exhibit lower COF (0.28) as compared to the coating containing 30 wt. % TiC (0.3) and substrate (0.5). However, a higher percentage of TiC content in the coating show detrimental effect on the wear resistance due to the formation of micro-cracks for brittle nature of TiC. TiC–$Al_{13}Fe_4$ composite layer deposited on Al–Si alloy substrate by laser surface alloying (Viswanathan et al., 2012) also found beneficial in terms of hardness and wear resistance as compared to Al–Si alloy substrate.

TiC/Ti-6Al-4V composite coating produced by laser coating process on Ti substrate show that hardness and wear resistance of the coating increases with the extent of TiC reinforcement (Sampedro et al., 2011). It was revealed that high amount TiC content in the coating improves the wear resistance and micro-hardness value of the coating significantly. However, the COF value augmented up to 0.7 compared to Ti-6Al-4V coating (0.5) for

using a higher percentage of TiC. Duraiselvam et al. (2007) produced TiC reinforced B_2–NiTi and Ti_3Al based intermetallic composite coating on Ti-6Al-4V alloy through laser melting process. It was found that TiC-Ti_3Al composite coating improved the hydro-abrasive erosion resistance up to 1.4 times as compared to the substrate material.

TiC- FeCrBSi composite coating on AISI 1045 steel (Wang et al., 2008) and TiC-NiCrBSi composite coating on Ti–6Al–4V (Sun et al., 2009) fabricated by laser surface alloying revealed that TiC reinforcement in the matrix alloy enhances the hardness, and wear resistance property of the composite significantly. In addition, COF value of the coating reduced significantly than the substrate surface or the matrix material used for the deposition of the coating.

2.9 TiC-Ni composite coating

From the above literature, it was revealed that TiC as reinforced particle either utilized the substrate material as a matrix or some other suitable metal or alloy was supplied to generate a TiC reinforced metal matrix composite coating. It is well accepted that, ductile matrix phase can restrict the crack propagation in the coating when the percentage of TiC is reasonably high in the composite system. In this regard, Ni and Co based matrix material are favorable owing to their superior corrosion resistance and compatibility with ceramic reinforcement (Nowotny et al., 2014). Literature revealed that TiC reinforced Fe, Ni or Co based composite coating successfully improved the surface properties of the substrate material. Recent study shows that Ni-based matrix materials are preferable due to high hardness, high wear and corrosion resistance (Cai et al., 2013). In addition, during high energy coating process, Ni produces hard phases, which further improve the surface properties of the coating. Being an interface material Ni is suitable for TiC reinforcement due to its excellent wetting behavior with TiC (Nowotny et al., 2014). Therefore, Ni and Ni-based alloys are superior choice as interface material to produce a coating on AISI 304 steel. Further, Ni has better solubility with Fe, which restrict the formation of cracks in the coating (Yi et al., 2013).

TiC–Ni alloy composite coating was deposited on 1045 steel substrate by preplaced laser cladding process (Pei and Zuo, 1998; Ouyang et al., 2000). From the experimental results TiC growth mechanism in the clad layer and bonding characteristic of the TiC within the matrix and the substrate was evaluated. TiCp reinforced Ni alloy composite coating was also synthesized by laser cladding process (Wu and Hong, 2001). The coating exhibited

superior wear resistance characteristic than the TiCp coating under similar test condition. Through the experimental analysis, authors revealed that the degree of wear for the composite coating depends primarily on the de-bonding and removal of TiCp reinforcement from the matrix. TiC-NiCr coating was also produced on SS304 and 12Cr–Ni steel by laser surface alloying, which show improved erosion resistance compared to Stellite 6 coating in sand blast erosion test (Kathuria, 2001). Yang et al. (2003) in their work produced in-situ TiC reinforced Ni alloy based composite layer on 45 carbon steel using Ti, graphite, and Ni–Cr–B–Si–C powders by laser melting process. The produced coating exhibited excellent interfacial bond with the substrate material due to the presence of Ni alloy.

Yang et al. (2004a) developed TiC particulate reinforced nickel-based composite coatings on carbon steel by laser cladding process. Compared to the carbon steel substrate (240 $HV_{0.2}$) high micro-hardness value obtained in the composite coating (920 $HV_{0.2}$) along with excellent bonding between the coating (TiC+Ni) and the substrate. Viswanathan et al. (2007) produced Ni-TiC composite coating on Al-Si alloy by laser surface alloying using preplaced Ni and TiC powder. The experimental results revealed that for using the low percentage of Ni, a separate composite layer formed, whereas with the increase in Ni content, dilution of Ni in the Al alloy enhances due to the higher density of Ni. The diluted Ni produces intermetallic phases, which further enhances the hardness value of the coating layer and provide a strong bond between the reinforcement and the matrix. A crack free Ni-based alloy-TiC coating with a hardness value of 1200 $HV_{0.2}$ was produced on medium carbon steel substrate (Yang et al., 2004b). It was revealed that the microstructure of the coating mainly composed of γ-Ni dendrites and dispersed TiC particles which significantly improved the mechanical properties of the coating. Duraiselvam et al. (2005) found that TiC-Ni alloy composite layer exhibits higher hardness (580-650 $HV_{0.2}$) compared to WC-Ni (430 to 505 $HV_{0.2}$) composite coating produced by laser cladding. However, TiC reinforced coating display low solid-liquid erosion resistance compared to WC reinforced coating layer, due to brittle nature of TiC particles.

To improve the cavitation erosion resistance of AISI 420 martensitic stainless steel, laser cladding was performed with Ni-Al and Ni-Al-TiC powder (Duraiselvam et al., 2006). Experimental results revealed that the coating produced with Ni-Al-TiC precursor, exhibited superior micro-hardness value (1000 $HV_{0.2}$), and improved cavity erosion resistance due to the formation of Ni-based intermetallics like NiAl or Ni_3Al in the coating.

Cui et al. (2007) fabricated a hard, wear resistance composite layer with preplaced Ni-Ti-C powder by laser coating process. The clad layer exhibited hardness values up to 59.5 HRC and wear resistance up to 4.5 times higher than the substrate material. Dong and Wang (2009) fabricated (33Ti–49Ni–18Si+20%TiC) composite layer on TA15 titanium alloy by laser cladding process. The composite layer improved the dry sliding wear resistance of the TA15 substrate approximately 170 times. Liu et al. (2012) deposited TiC-Ni composite coating on Ti-6Al-4V substrate using Ni-C preplaced powder by laser surface alloying. The produced TiC-Ni coating retain high hardness (~840HV) and wear resistance with a low coefficient of friction (0.23) compared to titanium alloy substrate.

Apart from the composite coating, favorable effect of Ni was also witnessed in the bulk composite fabricated by laser sintering route. Lu et al. (2000) fabricated Cu–Ti–C and Cu–Ni–Ti–C composites by selective laser melting process. It was revealed that addition of Ni powder in Cu–Ti–C precursor improved the microstructure and surface quality of the produced parts due to the improvement in melting and wettability of Cu with TiC. Li et al. (2009) produced Ni/TiC metal matrix composite by direct laser fabrication (DLF) method using Ni-Ti-C as initial powder mixture. The analysis of experimental results revealed that wear resistance and micro-hardness value of the produced composite gradually enhances with the increase in TiC content. In-situ TiC-Ni composite was also produced by laser engineered net shaping (LENS) process using nickel, titanium, and carbon (graphite) powder mixture (Gopagoni et al., 2011). The results indicate that the produced TiC-Ni composite exhibited higher micro-hardness (370 VHN) compared to pure Ni (165 VHN). Steady-state COF of the TiC–Ni composite was also found lower (∼0.5) than that of pure Ni deposition (∼0.75).

2.10 Ni-WC composite coating

Besides TiC-Ni composite coating, the beneficial effect of Ni was also employed in other ceramics to attain a stronger bond between the coating and substrate materials. In this regard, effect of Ni on WC-Ni composite coating was studied by various research groups. Tosun (2014) deposited crack free Ni-WC composite coating on AISI 1010 steel using TIG welding heat source. Li et al. (2015) deposited a Ni–30%WC composite coating on Ti-6Al-4V alloy by laser cladding and subsequent heat treatment process. It was witnessed that the clad layer consisted equiaxed WC particles, accompanied with TiC particles and the matrix zone consisting α-Ti with some intermetallic like Ti_2Ni and TiNi. It was revealed that due

to the presence of these intermetallic phases in combination with the hard TiC and WC particles the mechanical properties and wear resistance of the coating enhances significantly.

2.11 Ni-based composite coating by other methods

As binding material Ni was also used in various thermal spray coating. TiC-Ni-Mo composite coating was deposited on austenitic stainless steel by plasma transferred arc (PTA) process using TiC–NiMo and NiCrBSi as a precursor (Zikin et al., 2013). It is well accepted that with the addition of Ni, the produced coating show less porosity and superior bonding between carbide phases and matrix material. The composite coating also exhibited superior abrasive wear resistance as compared to WC/W_2C reinforced coating under high stress condition. In order to improve the bonding characteristic of TiC with steel substrate, hard and wear resistance TiC-NiTi composite coating was deposited on 34CrMo4 carbon steel by plasma spray and HVOF process (Isalgue et al., 2013). TiC-(Fe,Ni) MMC composite with different percentage of TiC was fabricated by direct metal laser sintering (DMLS) process (Gåård et al., 2006). It was found that with the increase in Ni percentage as binding material, the tendency of crack and porosity formation reduces significantly.

2.12 CaF_2 as Solid lubricant

Literature revealed that TiC reinforced Ni or Fe based MMC coating was successfully produced by various researcher utilizing laser cladding and TIG cladding methods. In the following section literature related to the use of solid lubricant specifically, CaF_2 with the hard and wear resistant coating produced by various high energy methods i.e. laser coating, plasma spraying and TIG or GTAW coating has been discussed. CaF_2 is a well-known and widely used solid lubricant, normally utilized in self-lubricating ceramic composite and anti-wear applications. Experimental analysis of various research groups indicates that incorporation of CaF_2 in the composite can improve its tribological properties even at room temperature by reducing the coefficient of friction (Muthuraja and Senthilvelan., 2015; Liu et al., 2009).

Jeng and Soong (1993) utilized Ag and BaF_2-CaF_2 solid lubricants with Cr_3C_2-NiAl powder to fabricate a wear resistance layer by laser cladding process on AISI 1020 low carbon steel. Wear test results revealed reduction in COF value from 0.38 (Cr_3C_2-NiAl composite) to 0.23 for Ag/BaF_2-CaF_2 coating. It was also found that addition of solid

lubricant (Ag and BaF_2-CaF_2) enhances the wear resistance properties of Cr_3C_2-NiAl coating at high load and high-temperature condition. Further, microstructure and tribological behavior of low-pressure plasma-sprayed ZrO_2-CaF_2 composite coating deposited on AISI 304 stainless steel depicted that CaF_2 effectively act as a solid lubricant at 600 ^oC and reduces the coefficient of friction significantly (Ouyang et al., 2001). The authors (Ouyang et al., 2005) also synthesized self-lubricating $ZrO_2(Y_2O_3)$ matrix composites with different percentage of CaF_2 and Ag as solid lubricants.

Wang et al. (2002) fabricated self-lubricated, wear-resistant CaF_2-Al_2O_3 composite coating on Al_2O_3 substrates by laser cladding process. The experimental results established that the addition of CaF_2 reduces COF value of the coating (from 0.6 to 0.48) and enhances the wear resistance (29 times) compared to only Al_2O_3 coating. The microstructure of the coating revealed that, CaF_2 present as isolated spherical particles with Al_2O_3 primary phase. Jianxin et al. (2006) developed Al_2O_3/TiC ceramic cutting tool with the addition of CaF_2 solid lubricant by the hot-pressing method. Significant reduction in COF value at the tool-chip interface was observed during dry machining of hardened steel and cast iron with Al_2O_3/TiC/CaF_2 ceramic cutting tool as compared to Al_2O_3/TiC tool. The authors (Jianxin et al., 2007) also found that due to the addition of CaF_2 (up to 10 vol.%) in the Al_2O_3/TiC composite a CaF_2 self-tribofilm form between the sliding couple and reduced the coefficient of friction value from 0.47 to 0.27. However, it was also found that additions of CaF_2 with Al_2O_3/TiC causes reduction in flexural strength, fracture toughness, and hardness value of Al_2O_3/TiC composite. The authors also reported that regulated amount of CaF_2 with hard reinforced ceramic materials like TiC, Al_2O_3, Cr_3C_2 improve the tribological properties of the composite significantly (Jianxin et al., 2007).

Furthermore, NiCr-Cr_3C_2-CaF_2 self-lubricant composite coating was deposited on TiAl alloy by laser coating process using preplaced powder mixture (W.-G. Liu et al., 2009). It was found that the wear resistance of the substrate material improved up to 5 and 24 times for NiCr-Cr_3C_2 and NiCr-Cr_3C_2-CaF_2 coating respectively. The Ni-Cr-C-CaF_2 composite coating produced on γ-TiAl substrate by laser cladding process revealed that fine isolated spherical CaF_2 particles uniformly dispersed in Ni-Cr-Al-Ti matrix (Liu et al., 2009). The experimental results indicated that micro-hardness value of the composite coating is approximately two times greater (HV 650) than the TiAl substrate. The authors also (Liu et al., 2013) fabricated self-lubricating and wear-resistant NiCr/Cr_3C_2–WS_2–CaF_2 composite coating by laser cladding process on austenitic stainless steel. The coating exhibited

excellent tribological behavior at 300 ^{o}C temperature and 5 N normal load. Due to the presence of solid lubricants (WS_2, CaF_2), frictional coefficient of the coating found significantly lower (0.29) than the base material (0.37) under similar test condition. Yan et al. (2012, 2013) through different experimentation revealed that with the accumulation of CaF_2 in Ni-Cr/TiB_2 MMC coating and Co-based alloy/TiC/CaF_2 self-lubricating composite coatings on Cr-Zr-Cu alloy substrate by laser cladding process, exhibited superior wear resistance and lower COF than the substrate materials.

In addition, Muthuraja and Senthilvelan (2015) fabricated Co based WC-CaF_2 composite by powder metallurgy route. The study revealed that limiting quantity of CaF_2 improves the wear resistance of the composite by reducing the frictional force or COF value. The lowest COF value (0.24) obtained for composite formed with 5 wt.% CaF_2 as compared to the composite produced without addition of CaF_2 (0.4) when sliding test performed against WC–6%Co disc.

2.13 Pulse Laser coating

Although continuous wave laser is used extensively for laser surface modification, there is a lack of study about employing pulsed laser in this emerging area of research, mainly due to its discontinuous behavior and lower processing capability (Yan et al., 2010a). However, specific characteristic of pulse laser sometimes beneficial for better control of the process. Therefore, few research groups initiated to employ the pulse laser for surface modification purpose.

Das et al. (1994) investigated the surface alloying of commercially pure aluminium with nickel using a pulsed Nd-YAG laser. It was observed that, distribution of the alloying element in the alloyed layer is uniform for a relatively low initial layer thickness. Surface modification of commercial Titanium was performed by means of laser gas nitriding (melting of titanium and reaction with nitrogen gas) and carburizing (melting and reaction with pre-deposited carbon powder), using pulsed Nd:YAG laser (Covelli et al., 1996; Ettaqi, 1998). The modified layer improve the mechanical properties of the component significantly. Laser cladding of WC/Ni layers on H13 tool steel substrate and Al-Al_2O_3 powder on AZ91D magnesium alloy were performed to improve the surface property of the base material with a low power pulsed Nd:YAG laser using pre-placed powder technique (Huang et al., 2003; Liu et al., 2006).

Pulsed Nd:YAG laser was used for laser surface alloying of electro-less plated Ni–P coatings on Al-356 aluminium alloy (Gordani et al., 2008). It was found that laser surface treatment produces a relatively smooth, crack-free and hard surface layer. Furthermore, surface carburizing of Ti-6Al-4V alloy by laser melting was investigated experimentally using a pulse Nd:YAG laser (Saleh et al., 2010). Results show that the produced carburized layers are macroscopically homogeneous and have gradient features.

In addition, Yan et al. (2010a) fabricated multi-carbide reinforced metal matrix composite (MMC) layer on ductile iron by laser surface alloying (LSA) using both continuous wave CO_2 laser and pulsed Nd:YAG laser. It was revealed that the hardness of the alloying layer produced by Nd:YAG laser is almost uniform, whereas hardness of alloying layer by CO_2 laser decreases continuously as the depth from the surface increase. The authors (Yan et al., 2010b) also investigated the deposition of Co-based alloy coating on copper by pulsed Nd:YAG laser cladding process. In order to improve the corrosion behaviour of low carbon steel, integrated layer of iron-aluminides was formed on the surface of a low carbon steel by hot dipping of the steel in a molten aluminium pool and subsequent laser surface processing using a pulsed Nd:YAG laser (Abdolahi et al., 2011).

During laser alloying of high-chromium ferritic alloys on mild steel substrate with a low power pulse Nd:YAG laser, it was observed that, with the increase in pulse duration, penetration depth and alloying element content in the alloyed zone increases due to lower evaporation loss resulting from reduction in peak power density (Goswami et al., 1995). Effects of laser parameters on the microstructure and micro-hardness value of the laser alloyed Ni and Cr on AA 6061 aluminium alloy using a low power pulsed Nd:YAG laser was evaluated by Fu et al. (1998). The hardness of the coating was found maximum at low laser power due to less dilution of the hard phases in aluminium substrate, however, the probability of crack and pore formation augmented in the coating with the increasing laser power and overlapping ratio. A novel composite coating of zirconium nanoparticles on austenite stainless steel surface was synthesized by laser alloying using a pulsed Nd:YAG laser (Wu and Hong, 2000). Sun et al. (2005) study the effects of laser pulse energy, pulse frequency, and spot overlap along with powder flow rate on the clad layer geometry i.e. height, dilution and heat-affected zone (HAZ) during laser cladding of stellite-6 on stainless steel by pulsed Nd:YAG laser. It was found that both the clad height and penetration of clad material into the substrate increases with the pulse energy, spot overlap, and pulse frequency.

In addition, Courant et al. (2005) in their study during the carburization of titanium surface by pulsed Nd:YAG laser revealed that, melt zone or carburized layer thickness mainly depends on the laser pulse duration and pulse frequency. Du et al. (2008) analyzed the effect of repetition rate and pulse width during the development of wear, and corrosion resistant TiB_2 based coating with the help of pulsed Nd:YAG laser for using TiB_2 and iron–aluminide preplaced powder on steel substrate. Vaziri et al. (2009) investigated that, beam spot size and peak power density of a pulsed Nd:YAG laser have a strong influence on the depth of alloyed layer, microstructure and surface hardness during laser surface alloying of Al with Ni.

Tariq et al. (2009) explained the importance of pulse laser parameters i.e. peak power and pulse width for the development of crystalline-amorphous composite layer during the surface modification of Zr-based amorphous alloy using a pulse type Nd:YAG laser. Hamedi et al. (2011) correlated pulsed laser parameters i.e. pulse duration and overlapping factor with microstructure and micro-hardness of the in-situ synthesized TiC composite coating on Titanium substrate. It was observed that at high pulse duration and low process speed, TiC content in coating zone increases due to the higher dissolution of carbon into the molten Ti with higher heat input and positive influence of the Marangoni flow in the melt zone. Chehrghani et al. (2012) during carbonization of Titanium surface using pulse Nd: YAG laser, revealed that higher pulse duration and overlapping factor leads to high heat input into the substrate surface and increase the micro-hardness value significantly. With higher overlapping factor (90%), diffusion of deposited carbon in the melt pool become much higher than the lower overlapping factor (50%), which enhanced the formation of TiC inside the melt zone.

Recently, pulse laser parameters i.e. laser power, pulse width, frequency and scanning speed were optimized for (Ti,W)C reinforced Ni-30Cu alloy composite coating on a copper substrate by laser surface cladding using a pulse Nd:YAG laser (Yan et al., 2012). During deposition of TaC on Stellite 6 alloy by using low power Nd:YAG pulsed laser, Farnia et al. (2012) revealed that, higher overlapping of the laser pulses resulted in a formation of inter-run porosity and lower overlapping leads to excessive hills and valleys on the surface. The authors (Farnia et al., 2012, 2013b) also revealed that the energy density, interaction time (pulse duration) and overlapping factor are most significant parameters which affect the clad profile in preplaced Stellite-6 and Co-based cladding fabricated by pulsed Nd:YAG laser. Recently, Vora et al. (2013) studied the effect of pulse laser

parameters on dilution of molybdenum in aluminum substrate during laser surface alloying and observed that the dilution increases with the increase in laser power, and decreases with the increase in scanning speed. Computational results also indicated that the melt pool width, depth, and dilution were increases with the increasing laser energy density.

2.14 TIG coating/cladding

Heat generated through gas tungsten arc (GTA) or tungsten inert gas (TIG) welding arc have been used by a large number of researchers to deposit a hard ceramic coating on the various substrate material.

In this regard, Mirdha and Ng (1999) produced hard and defect-free ceramic reinforced composite coating on commercially pure (CP) titanium surface using Ti and SiC precursor by TIG cladding process. The composite coating consisted in-situ TiC, Ti_5Si_3, unreacted SiC and Titanium phases that resulted in a hard surface (1600 HV). The study also revealed that selection of proper TIG processing parameters is important to obtain a defect-free coating. Using the TIG arc heat source, author (Mridha., 2005) also deposited a hard (up to 2000 HV) TiN layer on CP-Ti surface by melting the Ti surface under nitrogen environment. Results show the successful formation of TiN in the melt surface. However, the presence of defect like porous structure at the melt pool edges, and irregularity in the melt pool also observed. The research group also fabricated titanium aluminide intermetallic alloy coating on titanium surface by TIG arc scanning on the preplaced layer of Ti (53 wt.%)-Al (47 wt.%) powder mixture (Mridha et al., 2001). The coated layer improved the hardness up to four times (~ 600 HV) than the Ti substrate.

TiC reinforced Fe-based composite coating was produced on AISI 1045 steel by GTAW process using FeCrBSi alloy, graphite, and ferrotitanium powders as a precursor (Xinhong et al., 2006). Using a 1.2 mm thick preplaced powder layer, defect free coating was formed, which exhibit gradient distribution of hardness value in the coating layer. With an extension of the work, for the same coating, Wang et al. (2006a) established that the TIG processing parameters (current, scan speed) and thickness of preplaced coating layer affected the hardness and coating quality significantly. The produced TiC-Fe coating reduced the coefficient of friction (from 0.78 to 0.28) and improved the wear resistance significantly. The authors (Wang et al., 2006b) also fabricated TiC-Fe based composite coating by gas tungsten arc (GTA) melting process on AISI 1045 steel using FeTi alloy and graphite precursor. It was found that TiC particles were homogeneously distributed in the

melt zone and different morphology of TiC particles like cubic, fine needle-shaped and dendrite structure was present in the coating zone. The composite coating improved the hardness (up to 1400 HV) and wear resistance (up to 4 times) of the steel substrate significantly. Similar type of coating was also deposited on AISI 1020 steel substrate by overlapping of GTA melting process (Wang et al., 2007). The authors found the variation in the TiC morphology and hardness value of the coating in the overlapping zone. The wear resistance of TiC-Fe composite coating improved (4 to 6 times) and the coefficient of friction of the coating reduced to 0.6 as compared to the steel substrate (0.85). Wang et al. (2008) also deposited Fe–Ti–V–Mo–C hard-facing alloy layer on AISI 1020 steel substrate by using shield manual arc welding (SMAW) process. The coating improved the wear resistance and lower the coefficient of friction compared to EDRCrMoWV-A3-15 hard facing alloy coating.

In recent years, Mridha and Dyuti (2011) attempted to produce TiN reinforced coating by melting the preplaced Ti powder on plain carbon steel surface using TIG arc heat source under nitrogen environment. The analysis of experimental results revealed that the solidified surface consisting hard phases like TiN, Ti_2N, and $TiN_{.88}$, which enhances the coating hardness up to 2000 HV. In a different study, the effect of processing voltage (constant current) on the melt pool geometry i.e. width and thickness were studied for TiC reinforced coating on AISI 4340 alloy steel deposited by TIG arc melting process (Mridha et al., 2012b). It was revealed that depending on the heat input and cooling rate TiC reinforced coating microstructure consisting un-melted, partially melted and dendritic TiC particles. The coating exhibited micro-hardness values up to 1200 HV. The authors (Mridha et al., 2012a) also studied the effect of energy input and TiC powder content on the coating geometry, microstructure, and hardness value. From the aforementioned study, the research group established that, with the increase in energy input, the coating (melt pool) depth and width enhances owing to dilution of coating materials at higher temperature. It was also found that the coating exhibited higher hardness value for applying lower heat input and higher TiC content. Recently, Mridha et al. (2015) fabricated TiC coated surface by overlapping the tracks of TIG arc heat source and obtained 1 mm thick coating, which is free from any defects like cracks and pores. They observed that overlapping (50 %) of tracks cause re-melting of the tracks, which resulted in precipitation of melted TiC into cubic, globular or dendritic structure

Considering the beneficial effect of TIG coating, TiC-composite coating was also deposited on AISI 1020 steel surface by TIG coating process (Peng, 2012). An in-depth study on the effect of processing parameter on hardness and wear resistance of the coating was reported. It was found that the composite coating is almost crack and porosity free and the hardness value of the coating improved significantly (up to HRB 81) compared to the steel substrate (HRB 6.6). The authors (Peng et al., 2013) also revealed that TiC reinforced composite coating exhibited a low coefficient of friction and high wear resistance (about six times) compared to the AISI 1020 carbon steel substrate. The micro-hardness value of the coating was found upto 800 HV at the top surface and gradually decreases towards the coating-substrate interface. In continuation of the work, the authors (Peng, 2014) also studied the effect of TiC powder content in the wear behavior of the produced TiC-steel composite coating. It was revealed that the wear resistance of the coating enhanced with the increase in TiC content. The coating produced with 100 % TiC as precursor produced highly dense dendritic microstructure, which prevents the plastic flow of the coated layer during wear test.

In addition to above works, very recently Rasool and Stack (2014) successfully deposited TiC coating on 303 stainless steel using TIG arc scanning method. The produced TiC coating improved the surface hardness of the steel substrate significantly. Sliding wear test performed against alumina ball showed that with the incorporation of TiC coating, the wear resistance of the substrate surface enhanced expressively. The authors (Rasool et al. 2015) also produced TiC/Ti composite coating on Ti substrate with preplaced TiC powder and using TIG arc as a heat source. The dry sliding wear of the coating against harden steel disc showed that the wear mechanism of the composite coating depends on the sliding speed and applied normal load during the wear test. The worn composite surface exhibits micro polishing, adhesive wear, and mild abrasion.

Apart from the single phase ceramic coating, Wang et al. (2011) deposited a multi-component TiB_2–TiC–Al_2O_3 composite coating utilizing TIG cladding process using Al, B_4C, TiO_2 precursor mixture on AISI 1020 stainless steel. The composite coating significantly improved the wear resistance (upto 18 times) of the substrate surface due to the presence of hard TiB_2, TiC and Al_2O_3 compounds and suitable bonding of these particles with the substrate. Ghadami et al. (2015) fabricated WC-Co coating on a mild steel substrate by scanning the TIG arc heat source over the plasma sprayed WC-Co pre-coated layer. It was observed that the re-melted layer exhibits high hardness and wear resistance compared

to the plasma sprayed layer. The improvement in the coating property attained due to the reduction in porosity and formation of a metallurgical bond between the substrate and coating layer. Utilizing the gas tungsten arc (GTA) cladding process very recently, Fe–TiC–Al_2O_3 composite coating was deposited on 1045 steel with TiO_2–4Al–3C precursor (Sharifitabar et al., 2016). It was observed that high heat of the arc melt and dissolve the precursor materials in the weld pool, and during solidification TiC and Al_2O_3 particles precipitates in the matrix. The coating exhibited hardness value up to 830 HV and three times higher wear resistance than the substrate surface when wear test was performed against 600 mesh SiC emery paper.

Patel et al. (2014) studied the effect of shielding gas (Ar or Ar-He mixture) used for the surface treatment of micro-alloy steel substrate using TIG welding torch as a heat source. It was revealed that with the addition of SiC particles, the hardness of the melt pool improved significantly (up to 1200 HV). The experimental analysis revealed that use of Ar-(20%)He shielding gas produces high temperature, which results in better melt pool.

2.15 Self-lubricating coating by TIG cladding

Although, in laser coating technique, application of solid lubricant is reasonably familiar, however, it is not so common in the case of TIG coating process for composite coating. Very limited works in this regard were reported so far. Peng and Kang (2014) deposited TiC-Nano-diamond clad layer on AISI 1020 steel surface by TIG cladding process, where nano-diamond act as lubricating film during the wear test. It was reported that hard TiC with nano-diamond improved the coating surface hardness, and enhanced the wear resistance by reducing the plastic deformation of the coating. Dendrite structure of TiC reinforcement and uniformly distributed nano-diamond particles in the coating improved the wear resistance and reduced the COF as compared to both TiC coating and steel substrate. Authors (Peng and Kang, 2015) also fabricated TiC-BN composite coating on AISI 1020 steel surface by TIG cladding process. Here, BN act as a solid lubricant and reduces the COF and consequently improve the wear resistance of the coating.

Apart from these hard carbide coating, TIG cladding has been used to deposit different hard facing materials to improve the surface properties of various substrates. Table 2.1 shows the hard facing of various steel surface with different material by TIG coating method.

Table 2.1: Different coating material used to improve surface property by TIG coating process

Sl No	Author	Substrate	Coating material	Remark
1	Cheng et al. (2003)a	AISI 316 stainless steel	NiTi wire	Improved the hardness (700 HV) and cavitation erosion resistance.
2	Cheng et al. (2003)b	AISI 316 stainless steel	NiTi wire	Pores are observed in the coating and lower corrosion resistance compared to steel substrate.
3	Lin and Cho (2008)	AISI 1050	NiCrAlCoW and NiCrAlCoSi	NiCrAlCoW clad layer showed better wear resistance compared to NiCrAlCoSi
4	Lin and Cho (2009)	AISI 1050	NiCrAlCoCu and NiCrAlCoMo	NiCrAlCoMo clad layer showed higher hardness and wear resistance compared to NiCrAlCoCu clad layer and substrate.
5	Chang et al. (2009)	ASTM A36 steel plates	Fe–40Cr–xC hardfacing	4.05wt% Carbon content produced harder $(Cr, Fe)_7C_3$ carbides, which improve hardness up to 1250 $HV_{0.2}$.
6	Chen et al. (2009)a	Low-carbon steel	Al0.5–Fe2–Co–Ni–Cr–Mo–Si	Better mechanical properties
7	Chen et al (2009)b	Low-carbon steel	Mo–Cr–Fe–Ni–Co	Increase in Mo concentration in the precursor, the coating hardness also improved (210 to 465 HV)
8	Chen et al. (2008)	Low carbon steel	Ni, Co, Cr, Mo, and Al	Hardness (up to 800 HV) and wear resistance improved
9	Çelik et al. (2011)	AISI 8620 steel	SiC and C	Hard and wear resistance coating surface.
10	Buytoz et al. (2005)b	AISI 4340 steel	Fe–Cr–C alloy	Hardness improved upto 861 HV. Precursor content and heat input is important criteria for the coating.
11	Buytoz (2006)a	AISI 4340 steel	Fe–Cr–C	Hardness of the coating improved up to 750 HV, due to formation of hard M7C3 carbides.

12	Buytoz et al. (2005)a	AISI 4340 steel	WC	Improved the hardness and wear resistance. The quality of clad layer depend on the heat supply during the coating process.
13	Buytoz (2006)b	SAE 1020 steel	SiC	Coating microstructure depend upon heat input, powder content, and processing speed. M_7C_3 and SiC phases present in the coating.
14	Buytoz and Ulutan (2006)	AISI 304	SiC	SiC particles completely dissolved during TIG coating. Formation of M7C3 type carbides improved the hardness up to 1210 HV
15	Hsieh et al. (2014)	low carbon steel (SS400)	Fe-6Cr-1.9C-0.7Si-0.7Mn-xTi alloy	Increase in Ti content in precursor increases the TiC precipitation, which help in improvement in hardness.
16	Amirsadeghi and Sohi (2008)	Austempered ductile iron	ferrochromium or ferromolybdenum powder	Surface melting of substrate improves the hardness (HV 895) and wear resistance (37 %). Chromium or Molybdenum alloying improved the substrate had ness and wear resistance 66 and 60 % respectively.
17	Jeshvaghani et al. (2014)	Ductile iron	Inconel 617 alloy (3 mm dia wire)	Improved the hardness (three times than substrate) and wear resistance.
18	Eroğlu and Özdemir (2002)	SAE 1020 steel	Graphite or High-carbon-ferro-chromium or Chromium	High-carbon-ferro-chromium surface alloying with SAE 1020 steel substrate showed high hardness and wear resistance.
19	Hajihashemi et al. (2015)	St52 carbon steel	Fe-Cr-C or Fe-Cr-C-W alloy	Fe-Cr-C-W alloy coating on steel surface formed hard and wear resistance surface due to formation of in-situ WC.
20	Islak et al. (2011)	AISI 304	FeW and SiC	Improvement in hardness and wear resistance.

21	Islak et al. (2012)	AISI 1060	FeW and B_4C	Coating improved the hardness upto 1095 HV
22	Eghlimi et al. (2014)	HSLA steel	ER2594N SDSS	The coating produced using constant current show high corrosion resistance compared to pulsed current.
23	Lin et al. (2014)	Ti–6Al–4V	TiN powder or melted in N_2 environment	TiN coating produced using N_2 gas shielding produced hard and wear resistance coating.

2.16 Research gap and objectives

From the review of these literature, it is revealed that the research work on laser surface alloying or cladding using pulsed laser mainly concentrated on the formation of hard, wear resistance and corrosion resistance coating on various substrate surface. Very few works related to study on the effect of pulse laser parameters i.e. laser peak power, pulse duration or laser pulse on time, pulse frequency, and pulse to pulse overlapping or overlapping factor on melting depth of the substrate material and corresponding dilution of pre-deposited material during laser surface modification has been reported.

In pre-placed laser surface modification technique, a homogeneous mixture of preplaced powder on the substrate surface deposited up to a reasonable depth to enhance the surface properties of the base material. AISI 304 steel has excellent corrosion resistance and good oxidation resistance properties in a wide variety of environment along with superior mechanical properties. However, due to low hardness (200 HV), its wear resistance property is very poor (Laroudie et al., 1995). TiC-steel metal matrix composites show excellent hardness along with high toughness (Parashivamurthy et al., 2001). Laser surface modification can be used to produce TiC-steel MMC coating on the surface of AISI 304 steel substrate, which enables to increase the hardness and wear resistance of the substrate material. As melting temperature of TiC is (~ 3067 $^{\circ}$C) much higher than the evaporation temperature of steel (~2000 $^{\circ}$C), it is very important to select proper laser processing parameters so that TiC particles can uniformly distribute in the molten pool without causing any defect.

Although, GTA/TIG cladding is widely used for hard-facing of structural steel, however controlling the dilution of the substrate material in the deposited layer is quite challenging. Since dilution is the key issue for ensuring the functionality and reliability of the component, an optimum processing condition must be regulated for assured percentage of dilution (Chakraborty et al., 2014). It was revealed from the literature that, with the increase in welding current, dilution of the substrate into the coating material increases, whereas hardness of the coating decreases (Chen et al., 2009b, 2008; Madadi et al., 2012). However, for a single scan of the TIG arc over the preplaced powder, the geometry of the melt pool (depth and width of coating) as well as the microstructural variation due to melting and solidification of the coating material for changing the current and scan speed were hardly discussed for TIG cladding/alloying process. Depending on the dilution of the substrate with the coating material, this process can be classified as either TIG cladding (deposited material produce a layer after solidification with minimum dilution to substrate) or TIG alloying (deposited material completely mixed with the substrate material producing a new alloy layer). However, the distinction of these methods is difficult, since the mechanism of both the process is comparable. In the present study for simplicity, the process has been described as TIG cladding.

From the literature, it is also revealed that the effect of Ni addition in the TiC composite coating is familiar by laser cladding process. However, no such studies on TiC-Ni coating through TIG cladding process has been reported till date. The literature also depicted that, CaF_2 was successfully used as a solid lubricant in different type of coating produced by laser cladding, plasma spraying, or in bulk component fabricated by various sintering routes. However, there is a lack in the study, on the use of solid lubricant (especially CaF_2) by Tungsten Inert Gas (TIG) cladding process. Since TIG cladding is an economical process for producing a hard and wear resistance overlay coating, it is relevant to study the effect of incorporation of CaF_2 with the TiC-Ni coating produced by TIG cladding process.

With these motivations, for the present investigation following major objectives have been established

2.16.1 Objectives

1. Investigation on the feasibility of a hard and wear resistance TiC reinforced steel MMC coating on AISI 304 stainless steel substrate using low power pulse Nd:YAG laser.
2. Evaluation of the coating cross-sectional geometry and study the effects of pulse laser parameters on the geometry, morphology of the coating, microstructure, and mechanical properties i.e., hardness and wear behavior of the produced coating.
3. Development of TiC or TiC-steel composite coating on AISI 304 stainless steel substrate by TIG cladding or alloying method using TIG welding arc as a heat source.
4. Study the effects of TIG welding parameters mainly processing current and scanning speed on the geometry, morphology, microstructure, and mechanical properties, i.e., hardness and wear behavior of the produced coating. Correlation between the microstructure and mechanical characteristic of the coating. A detail study on the abrasive wear behavior of the produced coating.
5. Development of TiC-Ni composite coating on AISI 304 stainless steel substrate to enhance the bonding strength between TiC coating and steel substrate by TIG cladding process. By incorporating Ni, an attempt has also made to enhance the heat input in the melting zone due to metallization effect of Ni during the scanning of the arc.
6. Study the effects of TIG welding parameters (TIG current and arc scan speed) as well as the effect of Ni incorporation on the geometry, morphology, microstructure, and mechanical properties i.e. hardness and wear behavior of the produced TiC-Ni composite coating.
7. Development of TiC-Ni-CaF_2 composite coating on AISI 304 stainless steel substrate to by TIG cladding process, to reduce the coefficient of friction of the coating.
8. Study the effect of TIG processing current and the CaF_2 content in the coating on the geometry, morphology, microstructure, hardness and wear behaviour of the TiC-Ni-CaF_2 composite coating on AISI 304 stainless steel.

9. Comparison of the performances of TiC coating produces by laser and TIG cladding method.
10. Comparison of the performances of TiC, TiC-Ni and TiC-Ni-CaF_2 coating produced by TIG cladding process

Chapter 3

Experimental planning and procedure

3.1 Experimental Planning

For the present study total work has been divided into four phases. Details of the work plan are as follows:

1. Development of TiC reinforced composite coating on AISI 304 stainless steel by laser coating process using pulse Nd:YAG laser

(i) Evaluation of coating geometry at the cross-section of the coating for single line scan of laser beam.

(ii) Measurement of micro-hardness value of the produced TiC coating from the top surface using Vickers micro-indentation tester.

(iii) Study the effect of pulse laser parameters on the geometry, microstructure and micro-hardness value of the developed composite coating.

(iv) Study the tribological behavior of the developed coating by sliding abrasive wear test using a pin-on-disc wear test rig.

2. Development of TiC/TiC-steel composite coating on AISI 304 steel by Tungsten Inert Gas (TIG) Cladding process

(i) Evaluation of coating geometry (depth or height, width) at the cross-section of the coating for single line scan of TIG arc.

(ii) Measurement of micro-hardness value of the coating at the cross-section.

(iii) Study the effect of TIG processing parameters i.e. current and scan speed on the coating geometry, microstructure and micro-hardness value of the developed TiC/TiC-steel composite coating.

(iv) In-depth analysis of the tribological behavior of the produced coating through sliding abrasive wear test against alumina disc and sliding adhesion test against harden steel to attain the coefficient of friction of the coating.

3. Deposition of TiC-Ni coating on AISI304 steel by Tungsten Inert Gas (TIG) cladding process

(i) Study the effect of TIG processing parameters on microstructure and micro-hardness of the composite coating.

(ii) Study of the tribological behavior of the developed coating for different processing condition

4. Effect of CaF_2 content as solid-lubricant on microstructure and tribological behaviour of TiC-Ni-CaF_2 composite coating produced by TIG cladding process

(i) Study the effect of CaF_2 percentage and processing current on the coating geometry, microstructure and micro-hardness of the composite coating.

(ii) Study of the wear behavior and variation in coefficient of friction for the developed TiC-Ni-CaF_2 composite coating produced with different percentage of CaF_2 in the precursor.

3.2 Substrate material

Table 3.1: Composition of AISI 304 stainless steel

Fe	**C**	**Si**	**Mn**	**P**	**S**	**Ni**	**Cr**	**Mo**
Balance	0.067	0.753	1.731	0.045	0.031	8.554	18.97	0.224

Table 3.2: Properties of AISI 304 stainless steel

Properties	**Value**
Density	8.0 g/cm^3
Elastic modulus	193 GPa
Thermal conductivity	16.2 W/m.k at 100^{o}C 21.5 W/m.k at 500^{o}C
Thermal expansion coefficient	17.2 ×10^{-6}/ ^{o}C
Tensile strength	515 MPa
Yield strength	204 MPa

For the entire work in different phases, commercial AISI 304 stainless has been selected as workpiece material. Detail composition and properties of the AISI 304 stainless steel are shown in Table 3.1 and 3.2. For laser coating and TIG cladding process steel plate of

50 × 30 × 5 and 100 × 50 × 8 mm^3 were selected respectively. (R_a value at the top surface in the range 0.18- 0.25)

3.3 Precursor powder use for coating

In different phases of experiment TiC, Ni, CaF_2 powders has been used as precursor material. Detail of these precursor powders is shown in Table 3.3. Fig. 3.1 shows the SEM images of TiC, Ni, and CaF_2 powders.

Table 3.3: Specification of TiC, Ni, CaF_2 powders

Powder	Size	Purity	Make
TiC	~2–5 µm	99.5%	Alfa Aesar
Ni	~74 µm	99.5%	Loba Cheme
CaF_2	~10 µm	97%	Alfa Aesar

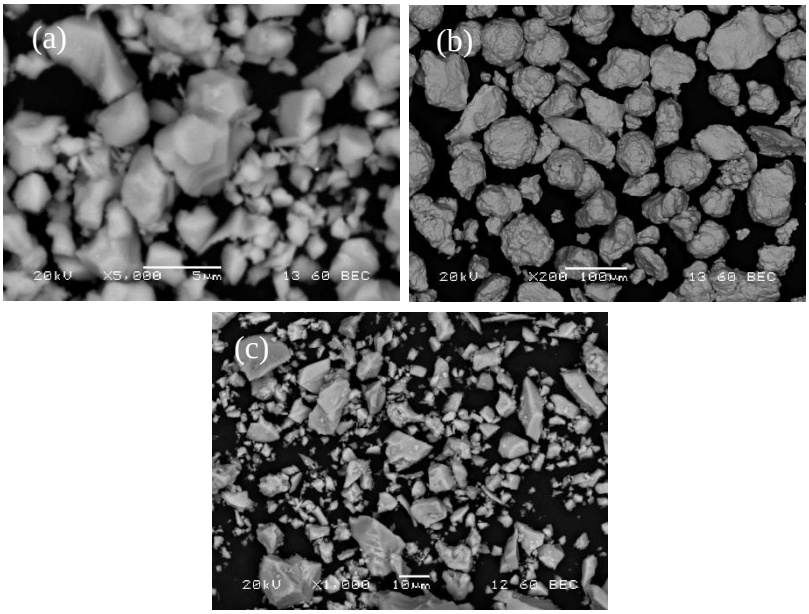

Fig. 3.1: SEM images of (a) TiC, (b) Ni, (c) CaF_2 powders

3.4 Experimental procedure

Although in different phases of the experiment, the procedure of experiment is varying, the actual sequence of experiment has been described in individual chapters corresponding to the experiments. Here, detail of individual methods used in different phases of experiments has been discussed.

3.4.1 Substrate preparation

AISI 304 stainless steel plates as per required dimension (100 mm × 50mm× 5mm for laser coating, and 100 mm × 50mm× 8mm for TIG cladding) were cut, ground with a surface grinder and the surface to be coated was polished with emery paper. The polished samples were then cleaned with ethyl alcohol and acetone sequentially to remove any surface contamination.

3.4.2 Preplacement of powder mixture

In this stage, the precursor powders were selected as per the required coating. Table 3.4 shows three different precursor mixture used in different phases of experiments to produce TiC reinforced composite coating. After selecting the powders as per required composition, the powders were mixed with acetone and polyurethane-based adhesive to make a semi-liquid solution. The semi-liquid solution was then dispersed on the already prepared substrate surface to form a layer of preplaced powder on the steel surface. The preplaced steel surface was then cured in room temperature. A Vernier caliper was used to measure the preplaced powder thickness.

Table 3.4: Precursor mixture for producing TiC reinforced composite layer on AISI 304 steel

Sl. No.	**Type of coating**	**Process**	**Precursor used**	**Preplaced layer thickness**
1	TiC composite coating	Laser coating	TiC	150±10 μm
2	TiC composite coating	TIG cladding	TiC	400±20 μm
3	TiC-Ni composite coating	TIG cladding	TiC, Ni	350 ± 20 μm
4	TiC-Ni-CaF_2 composite coating	TIG cladding	TiC, Ni, CaF_2	350±20 μm

3.4.3 Scanning of heat source for coating

(i) Laser beam scanning

For laser coating a pulsed Nd:YAG laser (ALPHA LASER, GERMANY/ALT-200) with maximum average power of 200 W, maximum pulse frequency of 20 Hz and pulse duration in the range 0.5–20 ms was used for laser irradiation. Fig. 3.2 shows the image of pulse Nd:YAG laser system and Table 3.5 shows its detail specification. Laser beam diameter at

focused position on the substrate is fixed as 1.5 mm. Laser scanning was performed on TiC pre-deposited steel substrate by moving the pulse laser beam with varying peak power, pulse duration, pulse frequency and scan speed to produce a single line coating track for each combination of parameter setting. Argon protective atmosphere was used to avoid oxidation of the substrate layer during laser processing of samples. Fig. 3.3 shows the schematic diagram of laser surface modification process using pulse laser.

Fig. 3.2: Pulse Nd:YAG laser system for laser coating process

Table 3.5: Specification of pulsed Nd:YAG laser system

Laser parameters	**Value**
Maximum average power	200 W
Maximum pulse frequency	20 Hz
Pulse duration	0.5–20 ms
Focused laser beam diameter	0.2–2 mm
Peak pulse power	10 kW

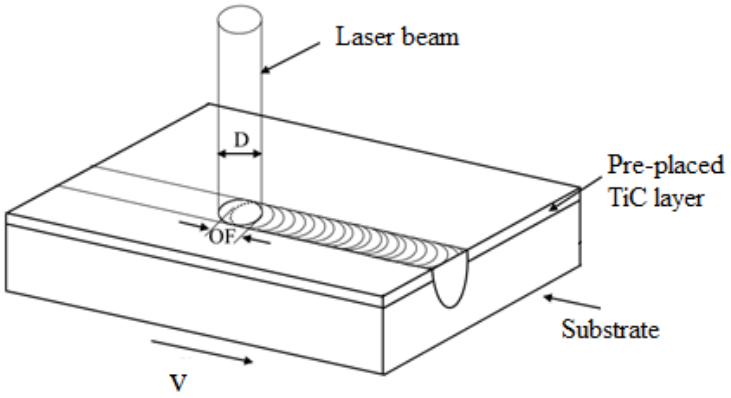

Fig. 3.3: Schematic diagram of laser surface modification process using pulse laser

(ii) TIG coating

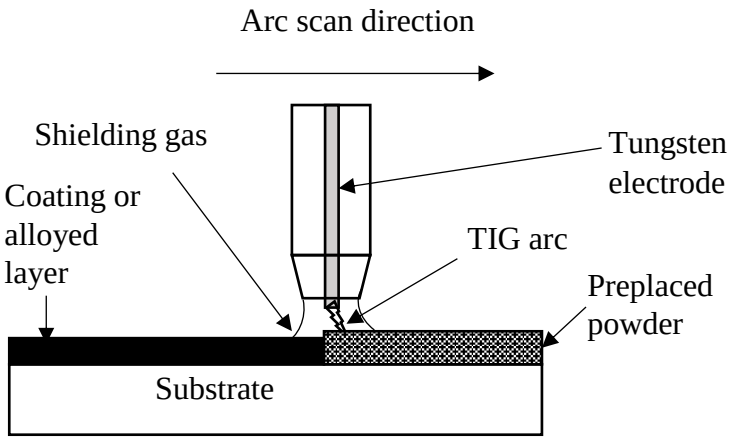

Fig. 3.4: Schematic diagram of TIG cladding process

For the second, third and fourth phase of experiments, to produce TiC, TiC-Ni and TiC-Ni-CaF_2 coating respectively by TIG cladding process, a TIG welding machine (Fronius A-4600, Magicwave 2200) accompanied with a welding torch containing 2.4 mm diameter tungsten electrode was used. The TIG welding torch was attached to a speed controlled linear moving trolley to obtain variable scan speed. Processing parameters i.e. welding current and scan speeds were controlled to obtain specific current and speed combination as per the requirement for the individual experiment. Details of processing conditions are indicated in Table 3.4. On each pre-coated steel substrate, single line scan of TIG arc was executed as per the experimental planning. The schematic diagram of the TIG cladding process is illustrated in Fig. 3.4. Before TIG arc scanning, a dummy steel plate of 100 × 30 × 8 mm^3 was placed in front of the pre-coated substrate for easy initiation of the arc and to avoid the effect of high initial arc current on the coating track. Further, to avoid any effect of pre-heating because of the previous coating track, 6 mm gap between two consecutive tracks was maintained. Adequate time for cooling was secured after each scan for all set of experiments. Fig. 3.5 shows the TIG welding setup used for present TIG cladding process.

Heat input per unit length, H (J/m) during the arc scan was calculated by using equation

$$H = \eta.(V.I/S.1000) \quad \ldots \text{Eq. 3.1}$$

Where η is the efficiency of heat absorption which is considered to be 48% for TIG cladding (Mridha et al., 2015), V, I and S are Voltage (V), welding current (A) and scan speed (mm/s) respectively.

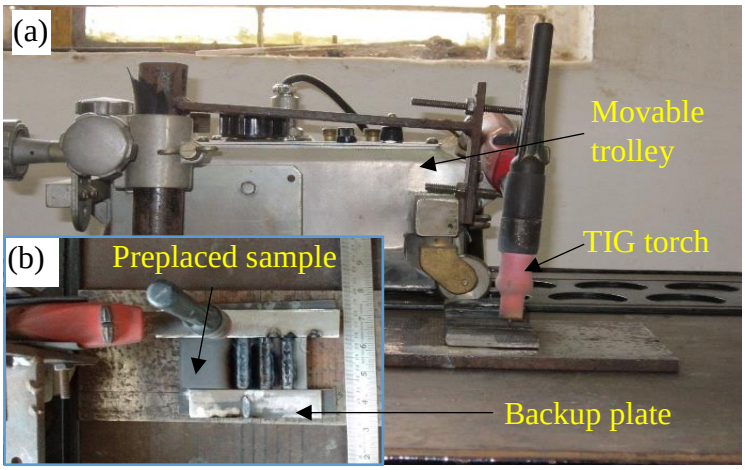

Fig. 3.5: Images of (a) TIG torch fitted with linear moving trolley (b) top view of experimental setup for TIG cladding process

Table 3.6: TIG processing conditions

Electrode	Thoriated Tungsten (2.4 mm dia)
Electrode–work piece distance	3 mm
Polarity	DCEN
Arc Voltage	12-15 V
Shielding gas	Argon (10 l/min)

3.4.4 Sample preparation for metallurgical analysis

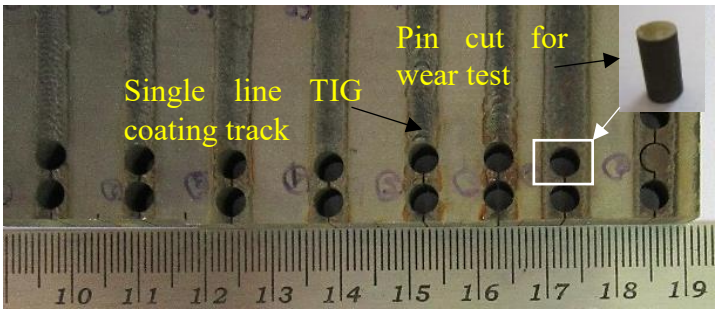

Fig. 3.6: Single track coating and pin cut by wire-EDM for wear test

After performing the laser coating or TIG cladding, the processed samples were cut as per the required dimension for different test. For microstructural analysis and micro-hardness test samples were cut at perpendicular to the scan direction so that cross-section of the coating layer becomes exposed. The cut specimens were then polished to analyze the microstructure of the produced coating layer by SEM. The metallographic polishing was done with different graded SiC paper sequentially followed by polishing with 1 μm diamond solution. For XRD analysis 10×10 mm^2 samples were cut from each track so that a sufficient

area of the top surface of the coating available for the XRD analysis. For wear test, 3 mm diameter pin was extracted from each coated track by wire- EDM. Fig. 3.6 shows the image of pin cut from single track coating using wire-EDM.

3.4.5 Microstructure and phase analysis

SEM images were taken with SEM (JEOL JSM-6084LV) for low magnification images and FESEM (Nova NanoSEM-FEI) for the high magnification images both secondary (SE) and backscatter electron (BSE) mode. The composition of the coating layers was analyzed by EDS attached with the FESEM.

3.4.6 XRD analysis

The compound phases present in the coated surface were identified from the X-ray diffraction (XRD) pattern obtained from BRUKER D8 ADVANCE diffractometer, using cobalt target (λ= 1.79026 Å) considering scan range of 20–100°, step size of 0.02° and scan rate of 10^{o} per min.

3.4.7 Micro-hardness measurement

For the first phase of experiment (laser coating), hardness of the coating was measured from the top surface of the coating and for TIG cladding hardness was measured at the cross-section of the coating. The hardness value was measured by a Vickers' micro-indentation hardness tester (LECO LM248AT and LECO LM810 in different phases of the experiment) with 50 g (0.49 N) load and10 s dwell time. Average micro-hardness value of the coating assessed from 8 to10 measurement taken at the coating cross-section or surface randomly.

3.4.8 Tribological test

Tribological properties of the produced coatings was evaluated using a pin-on-disc type wear test rig (ASTM G99, Make: Magnum) against SiC abrasive paper (220 grade), alumina abrasive disc and hardened die steel (58 HRC) separately for the assessment of wear rate and measurement of coefficient of friction (COF) in different phases. Here, alumina disc (45 mm diameter) was used as counter-body to assess the abrasive wear behavior of the coating, whereas hardened die steel disc was used to quantify the COF value of the coating. In addition, for TiC-steel coating produced by TIG cladding process, the coated pin was tested against 220 grade SiC abrasive paper. Detail of wear test condition for each phase of experiment has been illustrated in the corresponding chapters. Prior to wear test, the coated

pins were polished with 600 grade SiC paper to acquire a flat coating surface and remove the protuberance formed at the edge of the track during the arc scanning. Fig. 3.7 shows the schematic diagram of the pin-on-disc type sliding wear test setup used in different phase of experiments. During the sliding abrasive wear test variation of wear (height loss) with respect to time was attained through data acquisition system integrated with the pin-on-disc test rig. In addition, a vernier calliper with a least count of 0.01 mm was also used to measure the height loss of the coated pin after the wear test. During the test against hardened die steel disc, COF value was recorded through data acquisition system and plotted against test time. Average value of steady state COF was considered as COF value of the respective coating under specified test condition. Fig. 3.8 shows the images of the pin-on-disc wear test rig used in the various phase of the experiment.

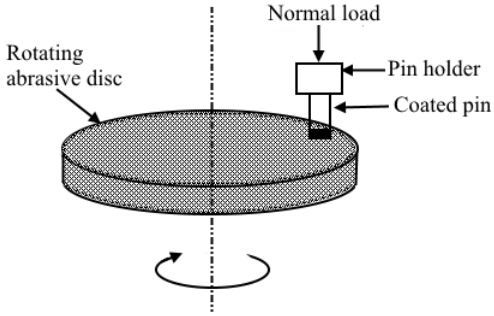

Fig. 3.7: Schematic diagram of the pin-on-disc experimental setup

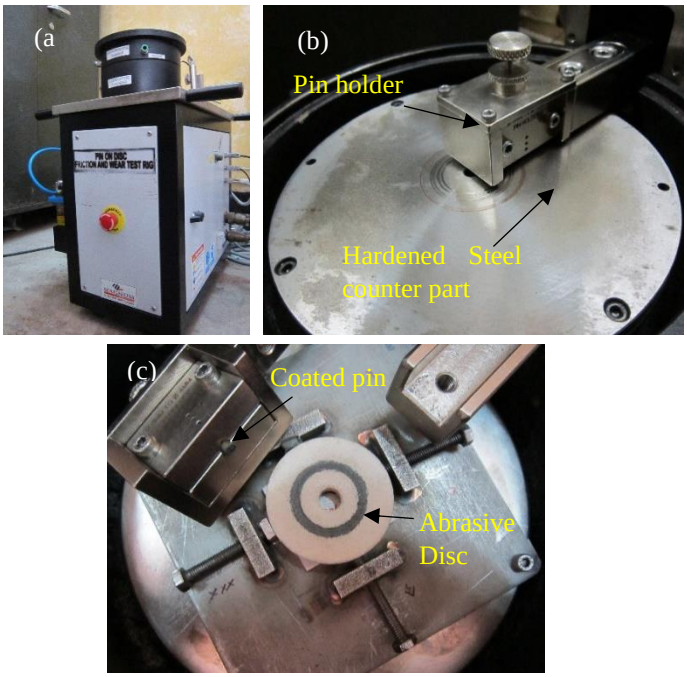

Fig. 3.8: (a) Pin on Disc wear test rig, (b) abrasion wear test of coated pin against Al2O3 abrasive disc, (b) adhesion wear test of coated pin against hardened steel counter part

Fig. 3.9 illustrate the steps followed in the present experiments for laser or TIG cladding through the flow chart.

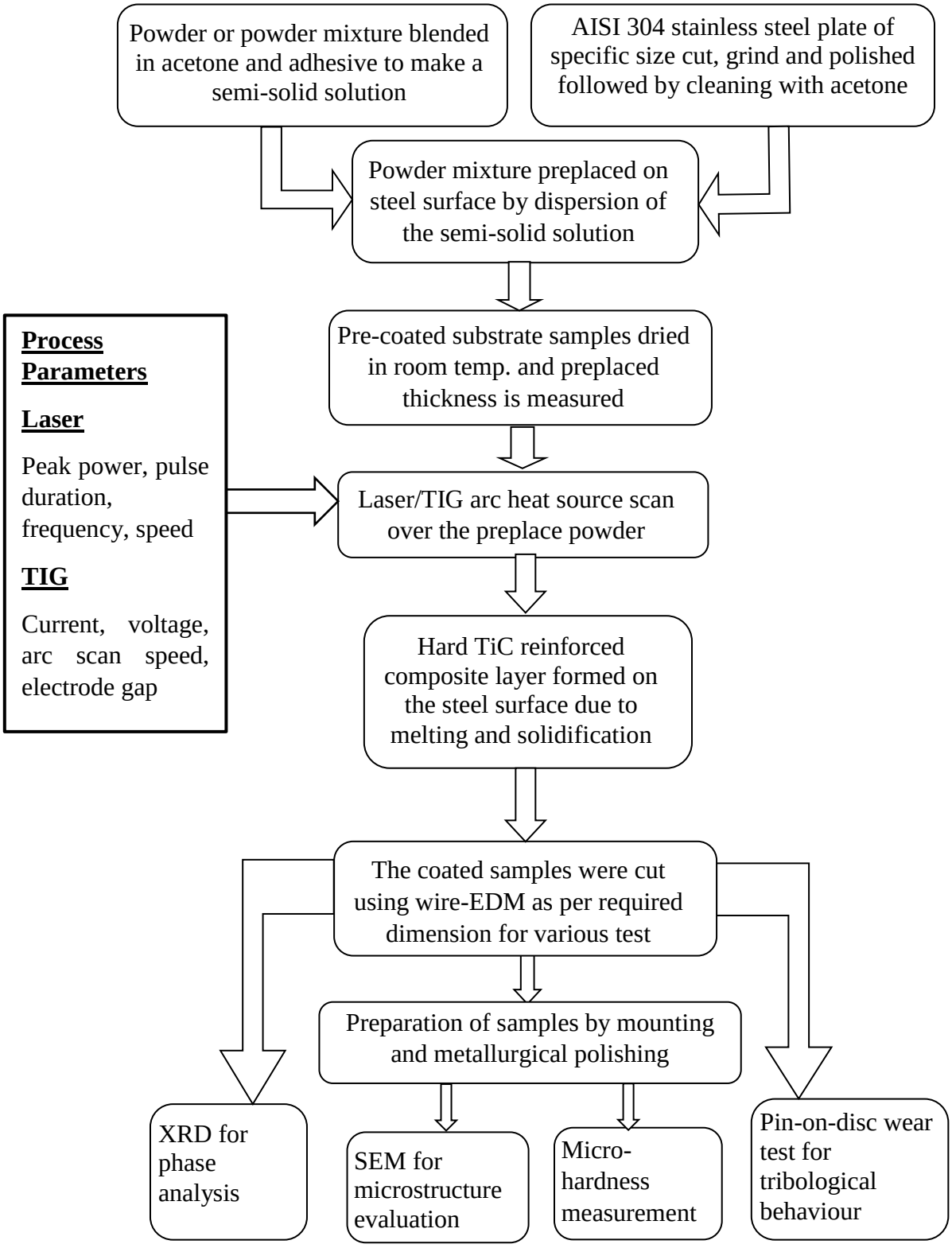

Fig. 3.9: Flow chart of laser or TIG cladding

Chapter 4

TiC reinforced composite coating on AISI 304 steel by pulsed laser coating process

In this chapter, investigation on the TiC reinforced steel composite coating produced by laser scanning over the preplaced TiC powder on AISI 304 steel substrate, using a pulsed Nd:YAG laser has been discussed. It was revealed that depending on the pulse laser parameters, TiC either deposited or dispersed on the surface of the steel substrate. Depth and width of laser processed TiC-steel composite layer have been measured from the SEM images at the transverse cross section of the laser scanned samples. The hardness value of the laser processed composite layer has been measured through Vickers micro-hardness tester. Effect of pulsed laser parameters like peak power, pulse duration, overlapping factor (corresponding to scan speed and frequency) on micro-hardness, composite layer profile (depth and width) and microstructure of the laser processed TiC-steel composite layer has been studied. From the experimental analysis, it is revealed that laser peak power and overlapping factor have significant effect on the TiC-Steel composite layer profile and hardness value.

Keywords: Pulse Nd:YAG laser; TiC-steel composite; Laser coating; Pulse laser parameters; Overlapping factor; Micro-hardness

4.1 Introduction

In laser surface cladding/alloying commonly known as laser coating, high-power laser beam is used as a heat source to melt a hard layer of ceramic particles preplaced on a metallic substrate. After solidification a new layer of ceramic particulate reinforced metal matrix composites (MMC) formed on the metallic surface (Agarwal and Dahotre, 1999; Cheng et al., 2001). Although continuous wave laser is extensively used for laser coating process, there is lack of study about the use of pulse laser in this emerging area of research (Yan et al., 2010a).

Specific advantages of pulse laser beam like precise regulation of spatial and temporal modes of laser beam energy, short pulse width and high peak power and power-

off period between two pulses (allows the melt pool to solidify at higher cooling rate and produces more refined microstructure) may produces a coated or alloyed zone with superior mechanical property (Farnia et al., 2013a; Sun et al., 2005).

From the literature review, it was revealed that works regarding laser surface alloying or cladding using pulse laser mainly concentrated on the formation of a hard, wear resistance and corrosion resistance alloy/coating on various substrate materials. The effects of pulse laser parameters on melting depth of the substrate material and corresponding dilution of pre-deposited material during pulsed laser surface modification/alloying process was hardly discussed. In preplaced laser surface modification technique, a homogeneous mixture of preplaced powder on the substrate surface (like MMC) could be formed up to a reasonable depth to enhance the surface properties of the base material. TiC-steel metal matrix composites show excellent hardness along with high toughness (Parashivamurthy et al., 2001). Therefore, laser surface modification technique can be used to form a TiC-steel MMC on the surface of AISI 304 steel substrate, which enables to increase the hardness and wear resistance of the substrate material. In the present work, an attempt has been made to produce TiC reinforced MMC coating on AISI 304 steel using a pulsed Nd:YAG laser by preplaced laser coating process. A wide range of pulse laser parameters has been employed to study the effect of each parameter on the produced surface. Depending on the parameters it is found that the pre-deposited TiC particles either formed a layer over steel surface or produced a TiC reinforced steel MMC coating layer.

4.2 Experimental procedure

At first, AISI 304 stainless steel substrate plates of size 50 × 30 × 5 mm^3 were ground by a surface grinder to get a flat and smooth surface and then cleaned with ethyl alcohol and acetone respectively to remove any surface contamination. TiC powder (particle size of 2–5 μm) was mixed with acetone and a specific amount of organic binder in a beaker and stirred with a glass rod to make a semi-solid solution. The semi-solid mixture was then dispersed over the clean steel surface uniformly and dried at room temperature to get a preplaced layer of TiC with an approximate thickness of 150±10 μm.

A pulsed Nd:YAG laser (ALPHA LASER, GERMANY/ALT-200) as per the specification detailed in Chapter-3 was used for laser irradiation. Laser beam diameter at focused position on the substrate is fixed as 1.5 mm. Laser scanning performed on TiC pre-deposited steel substrate, by moving the pulse laser beam with varying peak power, pulse

duration, pulse frequency and scan speed to produce a single line coating track for each combination of parameter setting as detailed in Table-4.1. Argon protective atmosphere was used to avoid oxidation of substrate layer during laser processing of samples. The schematic diagram of laser coating process using pulse laser has been already illustrated in Fig.3.3 (Chapter-3). In each pre-coated sample, several numbers of tracks were scanned, and the distance between two conjugative tracks kept 3 mm to avoid any preheating effect. Total 42 numbers of tracks were made to evaluate the effect of peak power, pulse duration and overlapping factor on the TiC coated laser processed zone.

Pulse to pulse overlapping of laser spot during laser material processing is an important factor to form a continuous scan on the substrate. Various research groups suggested different equation to calculate overlapping factor (OF). As overlapping factor is not a laser input parameter, it is useful to calculate scan velocity for a required overlapping factor and evaluate the effect of it on produced coating. Eqn. (4.1) shows the relation between overlapping factor, beam diameter, pulse frequency and scan velocity which has been applied for pulse laser welding, machining and surface modification by different research groups (Hu and Yao, 2008; Paul et al., 2007; Samant and Dahotre, 2010; Thawari et al., 2005).

$$v = f \times D \times (1 - OF) \quad \text{… Eqn. 4.1}$$

From which overlapping factor can be calculated as $OF = 1 - [v/(f \times D)]$, Where D = laser beam diameter (mm), f = laser pulse frequency (s^{-1})

However, during pulse laser processing due to change in peak power and pulse duration, laser spot diameter on the substrate also changes. Therefore, actual overlapping factor more precisely depends on scan velocity, pulse duration and spot size on substrate. Eqn. (4.2) shows the actual overlapping factor used by some research groups during pulse laser welding or cladding process by considering pulse duration, scan velocity and spot size on substrate (Farnia et al., 2013b; Ghaini et al., 2007; Lapsanska et al., 2010; Sabbaghzadeh et al., 2008).

$$OF_{actual} = \left(1 - \frac{v/f}{D_s + v.t}\right) \times 100 \quad \text{… Eqn. 4.2}$$

Where D_s = spot diameter on substrate, t = pulse duration.

Table 4.1: Experimental condition for laser coating of TiC on AISI 304 steel

Exp. No.	Peak power (kW)	Pulse duration (ms)	Pulse freq. (Hz)	Scan speed (mm/s)	OF (%)	Actual OF (%)	Spot dia. (mm)	EPPD (kW/mm^2)	Peak power density (W/mm^2)	Avg. power (W)	Energy per pulse (J)
1	1	9	18	10.8	60	57.47	1.31	2.35	565	162	9
2	1	9	18	8.1	70	68.85	1.37	2.74	565	162	9
3	1	9	18	5.4	80	78.46	1.34	3.86	565	162	9
4	1	10	15	9	60	58.65	1.36	2.25	565	150	10
5	1	10	15	6.7	70	70.38	1.45	2.55	565	150	10
6	1	10	15	4.5	80	80.32	1.48	3.45	565	150	10
7	1	12	14	8.4	60	60.66	1.42	2.12	565	168	12
8	1	12	14	6.3	70	71.82	1.52	2.41	565	168	12
9	1	12	14	4.2	80	81.55	1.58	3.21	565	168	12
10	1.5	10	11	6.6	60	60.50	1.45	3.09	848	165	15
11	1.5	10	11	4.9	70	73.09	1.62	3.34	848	165	15
12	1.5	10	11	3.3	80	82.56	1.69	4.44	848	165	15
13	1.5	12	9	5.4	60	59.33	1.41	3.22	848	162	18
14	1.5	12	9	4.0	70	72.62	1.59	3.41	848	162	18
15	1.5	12	9	2.7	80	82.31	1.66	4.51	848	162	18
16	1.5	14	8	4.8	60	59.78	1.42	3.17	848	168	21
17	1.5	14	8	3.6	70	71.57	1.53	3.58	848	168	21
18	1.5	14	8	2.4	80	81.28	1.57	4.83	848	168	21
19	2	10	8	4.8	60	61.53	1.51	3.92	1131	160	20
20	2	10	8	3.6	70	73.39	1.65	4.35	1131	160	20
21	2	10	8	2.4	80	82.78	1.72	5.80	1131	160	20
22	2	14	6	3.6	60	62.57	1.55	3.79	1131	168	28
23	2	14	6	2.7	70	73.66	1.67	4.30	1131	168	28
24	2	14	6	1.8	80	83.19	1.76	5.64	1131	168	28
25	2	12	7	4.2	60	62.80	1.56	3.76	1131	168	24
26	2	12	7	3.1	70	72.80	1.62	4.47	1131	168	24
27	2	12	7	2.1	80	82.05	1.65	6.09	1131	168	24
28	2.5	8	8	4.8	60	61.96	1.54	4.79	1414	160	20
29	2.5	8	8	3.6	70	73.34	1.66	5.42	1414	160	20
30	2.5	8	8	2.4	80	83.25	1.77	7.00	1414	160	20
31	2.5	11	6	3.6	60	61.44	1.52	4.88	1414	165	27.5
32	2.5	11	6	2.7	70	71.97	1.58	5.77	1414	165	27.5
33	2.5	11	6	1.8	80	83.21	1.77	7.02	1414	165	27.5
34	3	9	6	3.6	60	61.72	1.53	5.77	1697	162	27
35	3	9	6	2.7	70	72.81	1.63	6.64	1697	162	27
36	3	9	6	1.8	80	81.79	1.63	9.23	1697	162	27
37	3	8	7	4.2	60	62.53	1.57	5.61	1697	168	24
38	3	8	7	3.1	70	73.10	1.65	6.55	1697	168	24
39	3	8	7	2.1	80	83.30	1.78	8.36	1697	168	24
40	3.5	8	6	3.6	60	62.35	1.56	6.56	1980	168	28
41	3.5	8	6	2.7	70	73.29	1.66	7.56	1980	168	28
42	3.5	8	6	1.8	80	83.65	1.82	9.50	1980	168	28

It is found that, to calculate the actual overlapping factor, spot diameter on the substrate (which is not an input parameter of laser system) need to measure after each experiment. However, Eqn. 4.1 gives a simple relation between laser beam diameter (which is an input parameter of laser system) and overlapping factor. In this work, Eqn. 4.1 has

been used to calculate required overlapping factor by changing scan velocity and its effect on produced coating has been studied. Considering same scan velocity, frequency, and spot diameter on substrate (measured after experiments) and using Eqn. 4.2 actual overlapping factor was also calculated. Maximum ± 3.65 % variation in overlapping factor was observed between the overlapping factors calculated using Eqn. 4.1 and Eqn. 4.2, for all set of experiments. For this study, laser peak power varies from 1 to 3.5 kW; pulse duration considered 8 to 14 ms and overlapping factor taken as 60%, 70%, 80% and corresponding scan speed calculated as per Eqn. 4.1. The combination of pulse duration and pulse frequency selected in such a way that average power should not reach the limit of Nd:YAG laser system used and maintain within a range (for the present study between 150-168 W). Due to pulse nature of beam, peak power density (PPD) and effective peak power density (EPPD) (Ghaini et al., 2007; Lapsanska et al., 2010) have been calculated to find out the heat input per pulse and total heat input during laser processing through Eqn. (4.3) and Eqn. (4.4) respectively.

$$\mathrm{PPD} = \text{Peak power}/\text{Area of beam at focal position} \quad \text{...Eqn. 4.3}$$

$$\mathrm{EPPD} = \text{Peak power} \times (\mathrm{F})/\text{Area of Spot on work piece} \quad \text{...Eqn. 4.4}$$

Where F is the cumulative overlapping index, $\mathrm{F} = 1 + \mathrm{n}\{1 - (\mathrm{n} + 1)\mathrm{v}/(2\mathrm{fDs})\}$, and $\mathrm{n} = [\mathrm{Ds.f}/\mathrm{v}]$

After laser processing, the specimen were cut at the transverse cross-section of laser scan direction by wire-EDM and polished sequentially with 220, 600, 1200 grit size SiC polishing paper. Final polishing was done with diamond paste suspension. Scanning Electron Microscope (Make: JEOL-648OLV) with Back Scattered Electron (BSE) mode was used to study the TiC coated composite layer and its microstructure, and energy dispersion X-ray spectroscopy (EDS) was used to identify the elements present in the laser processed zone. Prior to hardness measurement of the coated track, the top surface of the specimen were polished with 1200 grit paper to remove any unbounded layer of TiC from the surface and make it smooth so that proper indentation could be done. The micro-hardness of the laser processed composite surface was taken with 50g load at 10s dwell time using a Vickers micro-hardness tester (LECO-LM248AT). Average hardness value for each sample processed with different laser processing parameters was obtained from 8-10 hardness reading taken randomly on the top surface of the TiC coated AISI 304 steel substrate.

In order to assess the wear behavior of the produced TiC coating on AISI 304 steel substrate, a wider area coating was accomplished by side-by-side overlapping of single line tracks for selected samples. In this way, by maintaining 20 % overlapping between two consecutive tracks, a wider area (6 mm width) of coating formed on the steel substrate. For the present study, wider area coating was performed with laser peak power of 1.5 kW, pulse duration of 12 ms and pulse to pulse overlapping factor of 60, 70 and 80 %. After getting the wider coated area, for wear test 3 mm diameter pin was extracted from each sample with the help of wire-EDM.

Sliding abrasive wear test of the coated pins was performed by sliding the pins against Al_2O_3 abrasive disc rotating on a pin-on-disc type friction and wear test rig as per ASTM G99 standard (Make: Magnum). Schematic diagram of the abrasive wear test setup has been illustrated in Fig. 3.8 (Chapter-3). Conditions used for this pin-on-disc type sliding abrasive wear test are stated in Table 4.2. Height loss of the pin during wear test was monitored through a data acquisition system equipped with the test rig. Height loss of the coated pins after the test was also measured with the help of a vernier caliper to attain the actual height loss. To assess the wear behavior, the worn out surfaces of the coated pins were analyzed by SEM and EDS.

Table 4.2: Condition for pin-on-disc type sliding abrasive wear test

Sample	3 mm diameter TiC coated pin
Normal load	10 N
Disc rotation speed	300 rpm
Track radius	10 mm
Sliding velocity	314 mm/s
Test duration	5 minutes
Counter-body	Al_2O_3 abrasive wheel

4.3 Result and discussion

4.3.1 Coating morphology

SEM images of the cross-section of laser processed samples are used for study the morphology of TiC coated or reinforced zone, and to measure the TiC-steel composite layer depth and width on the surface of AISI 304 steel substrate. SEM images are taken in BSE

mode so that distributions of TiC particles in steel matrix are clearly visible. Fig. 4.1 and Fig. 4.3-4.5 show the SEM images at the cross section of laser processed zone with different pulse duration and overlapping factor for peak power of 1, 1.5, 2 and 3 kW respectively. From EDS analysis (Fig. 4.2) of laser coated zone corresponding to the marked region of Fig. 4.1(b), it is clearly seen that dark region on the surface contains a high amount of titanium and carbon and the lighter zone is rich in iron. This indicates that dark region on the surface is TiC, which deposited on bright shaded steel surface after laser irradiation. Therefore, it may be concluded that in SEM image, the dark black portion is un-melted and agglomerated TiC particles deposited or reinforced on steel substrate during laser irradiation; light gray shaded portions are molten and re-solidified TiC particles uniformly distributed inside steel matrix, and bright portion is steel substrate. From Fig. 4.1 and Fig. 4.3, it is clearly observed that, at low peak power i.e. 1 and 1.5 kW, a bulk amount of TiC deposited on the steel surface, but this deposition is not uniform in terms of thickness and concentration. Due to low heat input at lower peak power, preplaced TiC particles are melted partially and distributed randomly on the steel substrate. As a result, some bulk layer of TiC, which is not dispersed inside the steel substrate, deposited over the surface region and relatively thin layer of TiC on steel substrate formed.

From the SEM images (Fig.4.4, 4.5) of the cross-section of laser processed track with higher peak power (2 and 3 kW) it is clearly observed that TiC distributed inside the molten steel surface more uniformly and depth of TiC reinforced steel zone is much higher than the TiC deposited layer with relatively low peak power. Effect of peak power on melt pool structure can be observed from Fig. 4.6 (a-d), where SEM images for the cross-section of composite layer processed with 80% overlapping factor and different peak power of 1, 1.5, 2 and 3 kW are shown. From the images, it is clearly seen that TiC-steel composite layer depth increases with the increase in peak power when other parameters are almost unchanged. Again, distribution of TiC also found more uniform for the sample processed with higher peak power. As laser peak power increase, peak power density on the surface of the TiC preplaced steel substrate also increases. Therefore, melt pool temperature at the center of the Gaussian beam distribution reaches a higher value compared to the outer region that creates a steep temperature gradient. Since surface tension is dependent on temperature, the TiC particles along with molten steel flow within the melt pool (Marangoni flow). This results in an increase in convective flow, which causes stirring of melt pool and

homogenizes the TiC-steel mixture and increases overall composite layer depth (Hamedi et al., 2011; Ion, 2005).

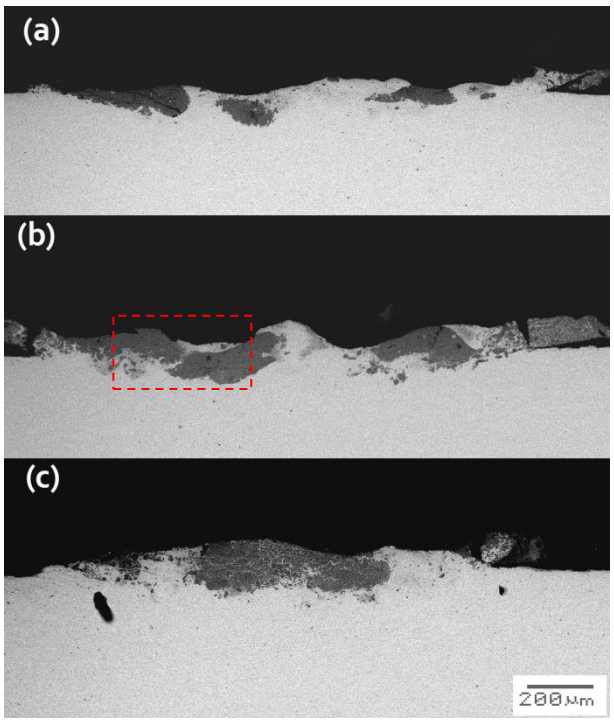

Fig. 4.1: SEM images at the cross-section of TiC-steel composite layer produced by pulse Nd:YAG laser with peak power = 1 kW, pulse duration = 10 ms with overlapping factor of (a) 60% (b) 70% and (c) 80%

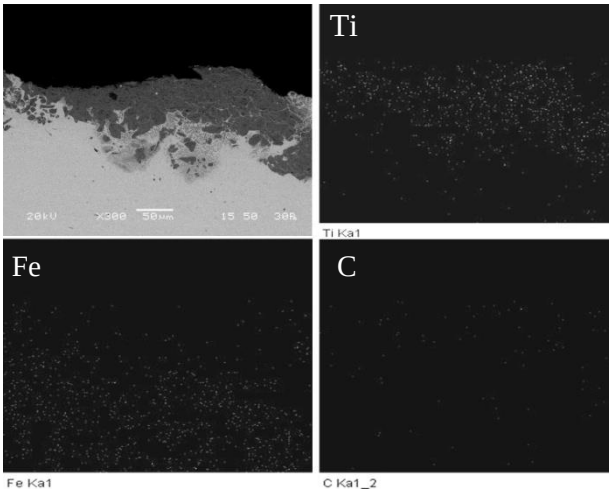

Fig. 4.2: EDS elemental mapping of laser coated zone corresponding to Fig. 4.1(b)

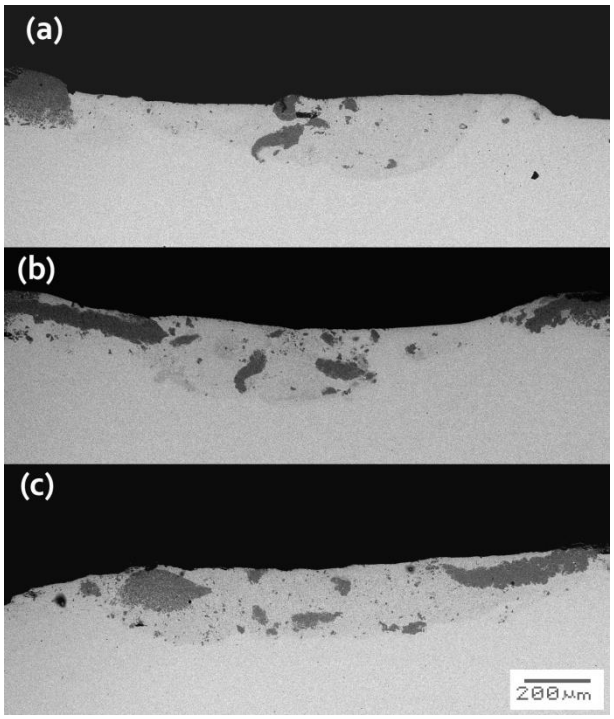

Fig. 4.3: SEM images at the cross-section of TiC-steel composite layer produced by pulse Nd:YAG laser with peak power = 1.5 kW, pulse duration = 12 ms with overlapping factor of (a) 60% (b) 70% (c) 80%

From the SEM images (Fig. 4.1, 4.3, 4.4 and 4.5), the effect of laser pulse overlapping factor on the distribution of TiC particles inside the steel substrate for a particular peak power and pulse duration condition could be observed. In low power range (peak power = 1 kW and 1.5 kW) and low overlapping condition (60%), maximum depth of penetration of TiC on the molten substrate or coating thickness is very less and a major portion of TiC deposited non-uniformly on the upper surface of the substrate. As overlapping factor increases, distribution of TiC on steel surface found relatively uniform and depth of TiC-steel composite layer on steel substrate increases. At low overlapping condition, effective peak power density in the laser processed zone is relatively less, therefore preplaced TiC powder melted and deposited over the surface substrate. However, with the increase in overlapping factor (from 60 to 80%) as effective peak power density increases, the deposited bulk TiC particles on the substrate surface further melted and re-distributed over the melt pool. Effect of overlapping factor more clearly visible for the samples processed with higher peak power. From Fig. 4.4 and 4.5, it is clearly observed that with the increase in overlapping factor, the depth of TiC-steel composite layer and uniformity of TiC distribution on the steel surface enhances. Effect of pulse duration on TiC distribution in steel layer can be observed from SEM images as shown in Fig. 4.7. Here, the cross-section of samples processed with laser peak power of 2 kW and 80% overlapping

factor with a pulse duration of 10, 12 and 14 ms are shown. The images indicate that TiC-steel composite layer depth increases with increase in pulse duration.

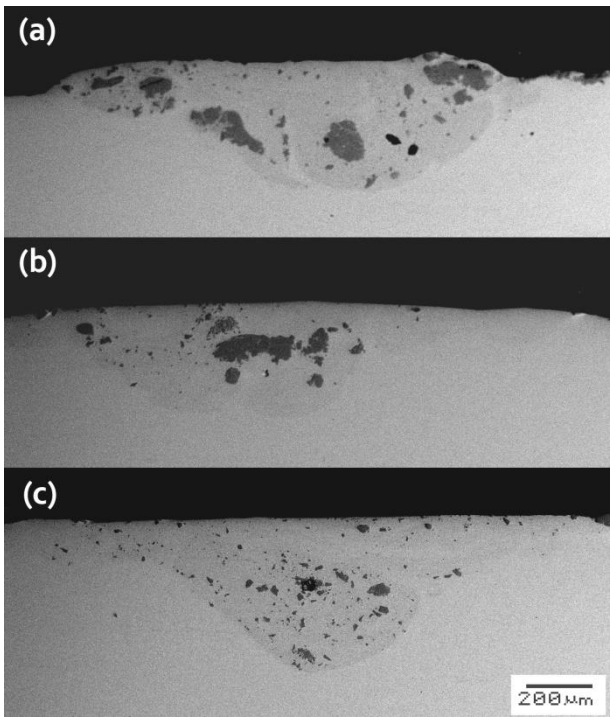

Fig. 4.4: SEM images at the cross-section of TiC-steel composite layer produced by pulse Nd:YAG laser with peak power =2 kW, pulse duration = 12 ms with overlapping factor of (a) 60% (b) 70% (c) 80%

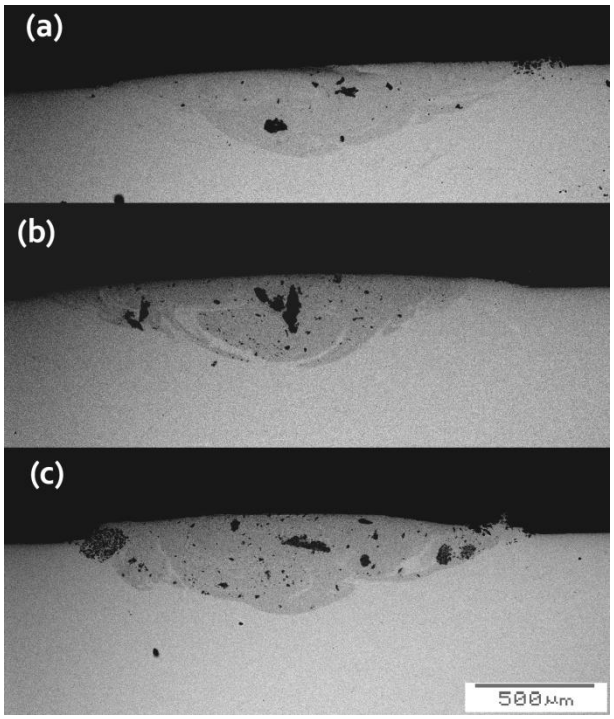

Fig. 4.5: SEM images at the cross-section of TiC-steel composite layer produced by pulse Nd:YAG laser with peak power = 3 kW, pulse duration = 9 ms with overlapping factor of (a) 60% (b) 70% (c) 80%

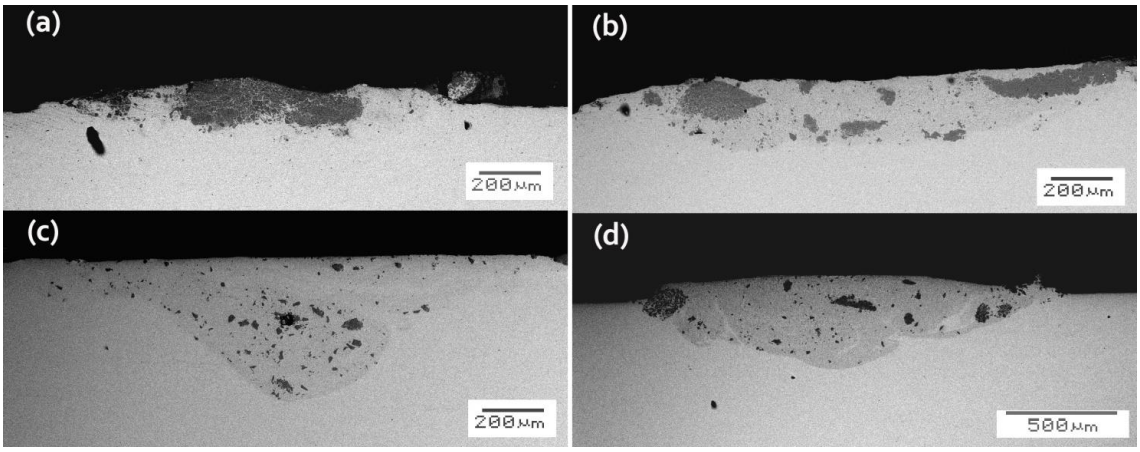

Fig. 4.6: SEM images at the cross-section of TiC-steel composite layer produced by pulse Nd:YAG laser with overlapping factor of 80% and (a) peak power = 1 kW, pulse duration =10ms (b) peak power = 1.5 kW, pulse duration = 12 ms (c) peak power = 2 kW, pulse duration= 12 ms (d) peak power = 3 kW, pulse duration = 9 ms

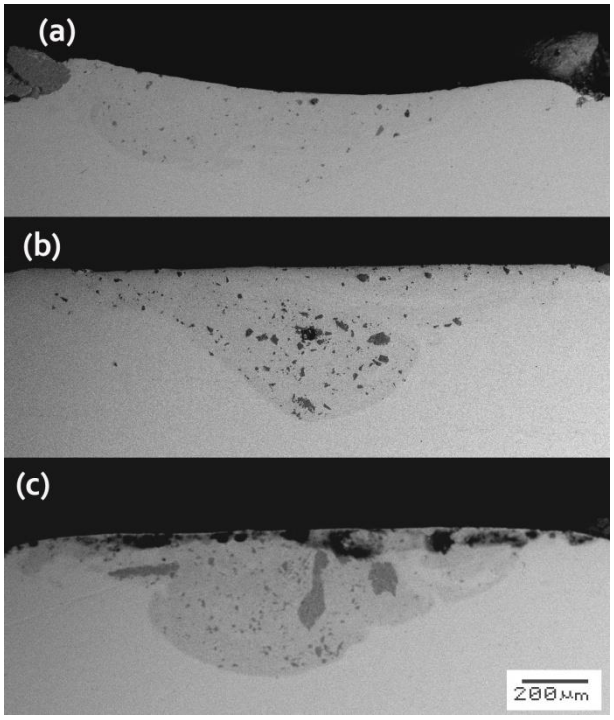

Fig. 4.7: SEM images at the cross-section of TiC-steel composite layer produced by pulse Nd:YAG laser with peak power = 2 kW, overlapping factor = 80%, pulse duration (a) 10 ms (b) 12 ms and (c) 14 ms

4.3.2 TiC-steel composite layer profile

For the present study, TiC-steel composite layer depth or maximum penetration depth of TiC particles in the steel substrate and maximum width of the composite layer was measured. The objective of this study is to find out the effect of pulse laser parameters on TiC-steel composite layer depth and distribution of TiC particles inside the steel substrate.

Professional image analysis software (ImageJ) was used to measure maximum composite layer depth and width of TiC inside steel substrate.

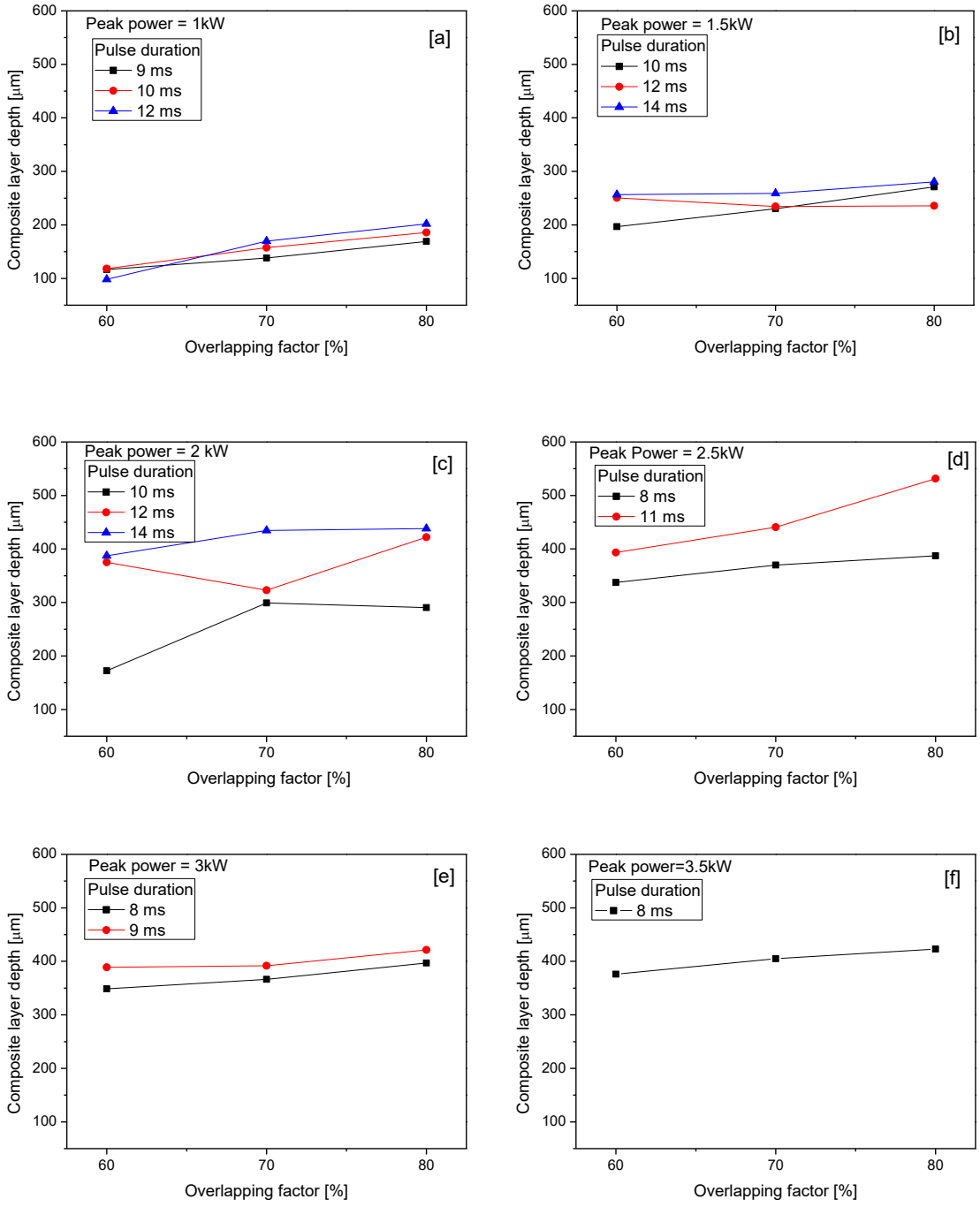

Fig. 4.8: Maximum depth of TiC-steel composite layer on steel substrate against different overlapping factor for different laser peak power and pulse duration condition processed with pulse Nd:YAG laser

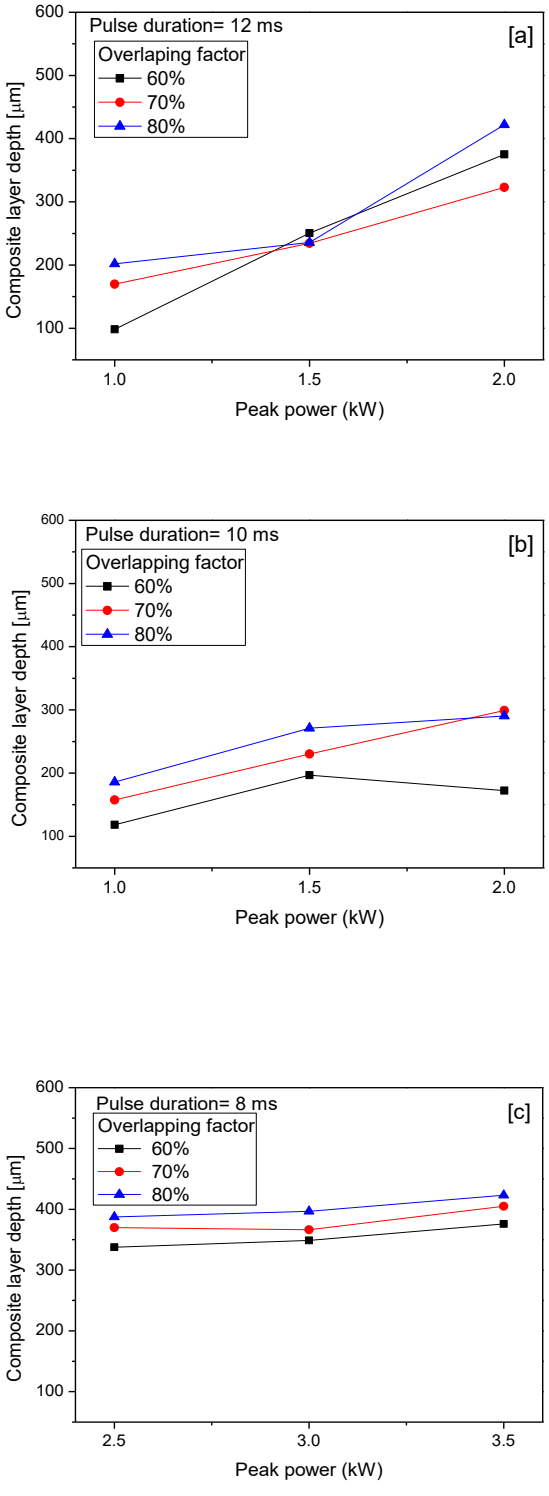

Fig. 4.9: Maximum depth of TiC-steel composite layer on steel substrate against laser peak power for different overlapping factor and pulse duration condition processed with pulse Nd:YAG laser

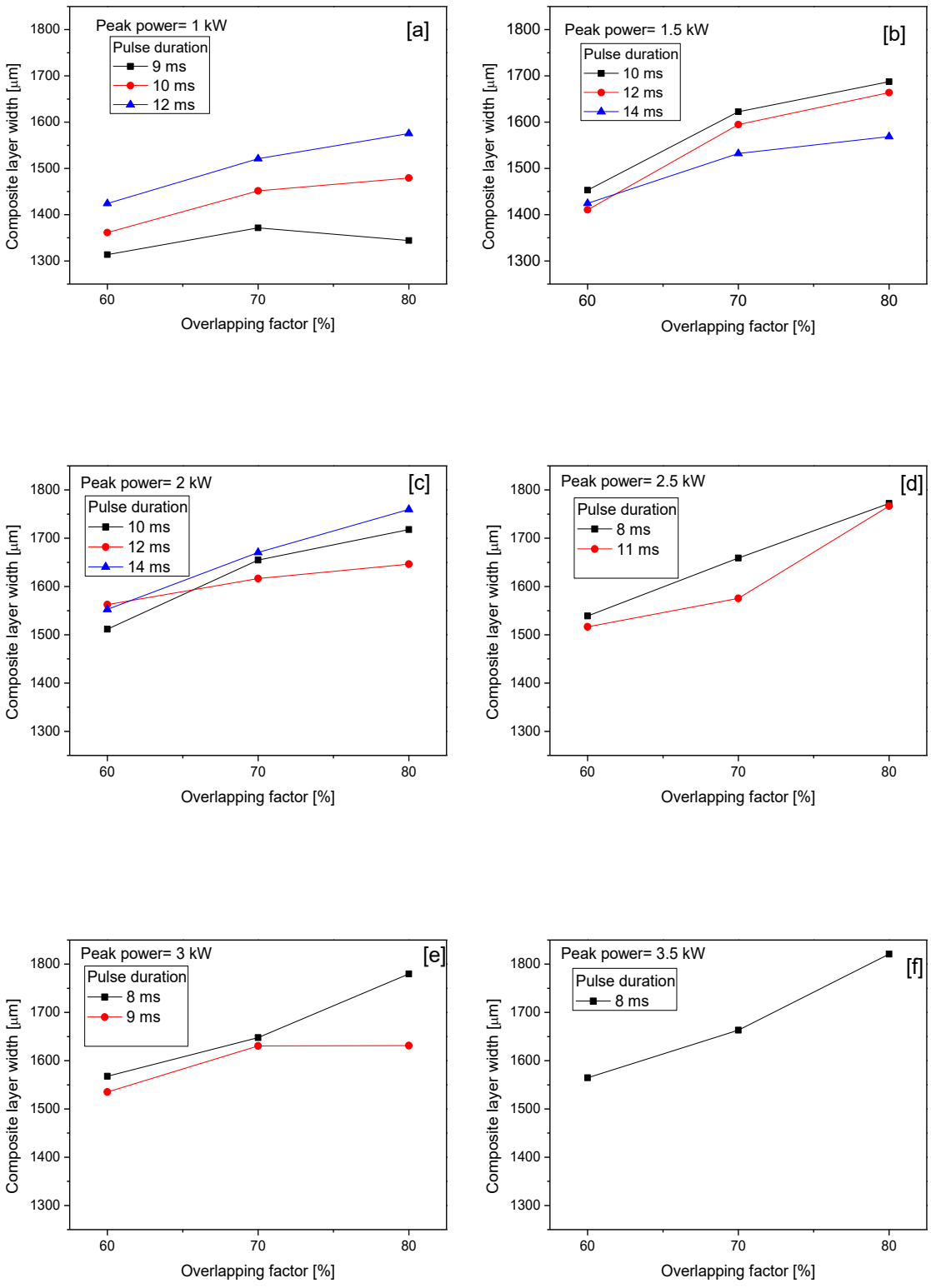

Fig. 4.10: Maximum width of TiC-steel composite layer on steel substrate against different overlapping factor for different laser peak power and pulse duration condition processed with pulse Nd:YAG laser

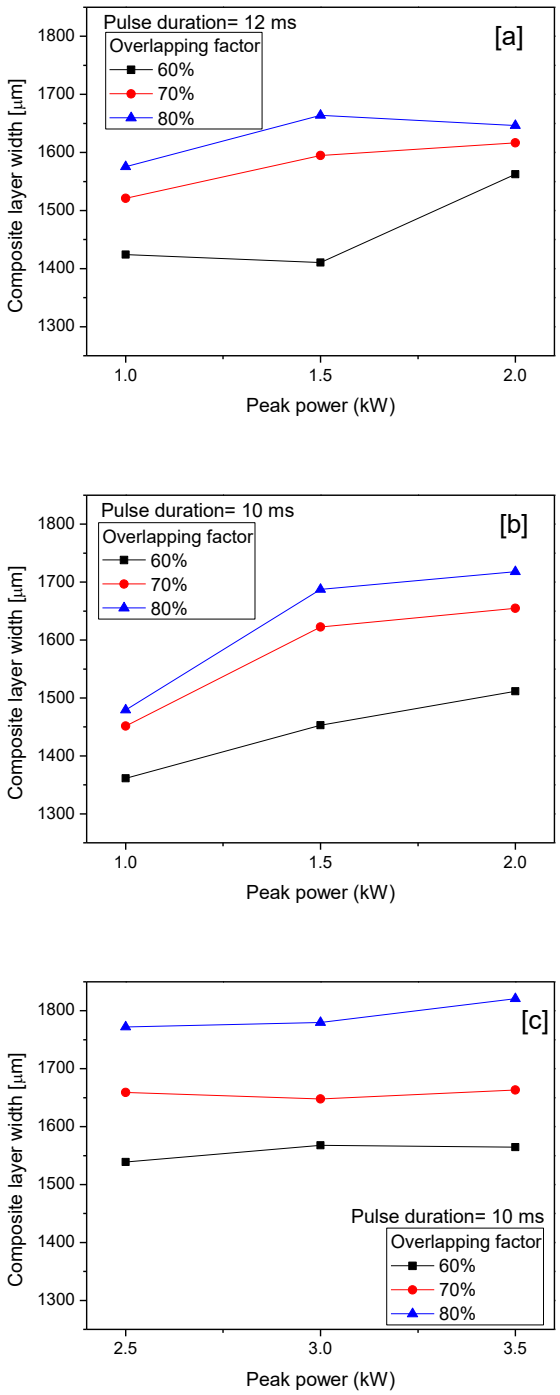

Fig. 4.11: Maximum width of TiC-steel composite layer on steel substrate against laser peak power for different overlapping factor and pulse duration condition processed with pulse Nd:YAG laser

The measured composite layer depth and width for all the samples processed at different laser processing condition as detailed in Table-4.1 are plotted against the overlapping factor for each of the laser peak power conditions. Fig. 4.8(a-f) show the effect of overlapping factor on the composite layer depth for different laser pulse duration and processed with peak power of 1, 1.5, 2, 2.5, 3 and 3.5 kW respectively.

From Fig. 4.8(a-f), it is clearly seen that TiC-composite layer depth is much lower (in the range of 100 to 200 μm) for the sample prepared with laser peak power of 1 kW, a pulse duration of 12 ms and different overlapping factor. This composite layer depth gradually increases with the increase of laser peak power. At relatively low peak power (1 and 1.5 kW) due to lower power density, melt pool temperature is relatively less and preplaced TiC particles not melted and distributed properly inside the steel substrate. Therefore, some bulk layer of TiC over the steel surface deposited and relatively lower layer depth of the TiC-steel composite layer on steel substrate obtained. At high peak power, due to higher peak power density, temperature and corresponding melting depth of TiC coated steel substrate also increase. Detail discussion for higher composite layer depth at high peak power condition has already discussed in the previous sub-section.

From these graphs [Fig. 4.8(a-f)], it is also observed that with the increase in overlapping factor, composite layer depth also increases for the sample processed with a particular laser peak power and pulse duration condition. Fig 4.9 (a) shows that for samples processed with 1 kW peak power and 10 ms pulse duration, when overlapping factor increases from 60 to 80%, maximum depth of the composite layer also increases from 118 μm to 185 μm. A similar phenomenon also observed for the samples processed with higher peak power i.e. 1.5 to 3.5 kW and different pulse duration. The variation in depth of TiC-steel composite layer due to overlapping factor clearly visible for the sample processed with 2.5 kW peak power and 11 ms pulse duration (Fig 4.9 (d)), where composite layer depth increases from 393 μm to 531 μm for changing the overlapping factor from 60 to 80%. For the samples processed with 3 and 3.5 kW, this composite layer depth increases slightly with the increase in overlapping factor. Composite layer depth found higher (more than 400 μm) for the laser tracks processed with 2.5 kW peak power, 11 ms pulse duration and 3.5 kW peak power, 8 ms pulse duration with 60-80% overlapping factor. In these conditions, peak power density is reasonably high, which induces high heat input and subsequently higher melting depth of TiC coated steel substrate. As overlapping factor increase, effective peak power density in the laser processed zone also increases, which causes higher depth of TiC-steel composite layer. It is well accepted that when a single spot laser beam irradiated on the TiC coated substrate, due to high peak power density at the centre of the beam spot, some portion of TiC powder melted and heat is transferred to the substrate by conduction heat flow, that again melt the base material below the preplaced TiC layer. Thus, a mixture of molten TiC and steel substrate flow towards the bottom side and edges of the melt pool

(Marangoni flow). In other word, an increase in overlapping factor increases the effective peak power density to the laser processed zone, which enhances the composite layer depth due to more number of pulses within a fixed operating length. Effect of both peak power and overlapping factor can be observed clearly from the graphs illustrated in Fig. 4.9. From these graphs, it is found that effect of the peak power is more significant than the effect of overlapping factor on the depth of TiC-steel composite layer. This effect can be seen qualitatively in the distribution of TiC throughout the molten pool.

A careful observation of the plots (Fig. 4.8(a-e)) also revealed that, for a particular laser peak power and overlapping factor, maximum depth of composite layer increases with the increase in laser pulse duration; and this phenomenon is more prominent for the sample processed at the higher overlapping condition. For example, Fig. 4.8(d) shows that for sample processed with 2.5 kW peak power and 80% overlapping factor, maximum depth of TiC-steel composite layer increases from approximately 387 micron to 531 micron when pulse duration changes from 8 ms to 11 ms. A similar effect can also be seen from the TiC particles distribution in SEM images (Fig. 4.7) for the sample processed with laser peak power of 2 kW and 80% overlapping factor with a pulse duration of 10, 12 and 14 ms respectively. The images indicate that TiC-steel composite layer depth increases with the increase in pulse duration within the operating range. Pulse duration is the interaction time of the laser beam with the material for each pulse. As pulse duration increase, the interaction time also increases; Therefore, for a particular peak power condition, overall heat input increases and as it work for a relatively longer time, and consequently melting depth of TiC coated steel substrate also enhances. Again, due to larger interaction time, the peak temperature of the molten pool became lower and corresponding cooling rate decreases. Thus, the high value of pulse duration augmented the penetration depth of TiC inside the steel surface through declining the solidification rate of TiC reinforced molten pool and smoothening the convective flow inside the melt pool. Pulse duration also contributes an important role in achieving uniform distributed TiC-steel composite layer in combination with peak power and overlapping factor. Only for peak power of 1.5 kW and 14 ms pulse duration condition, TiC-steel composite layer depth decreases, which may be due to some localized defect in the substrate or error in the laser processing.

Fig. 4.10 (a-f) show the variation of the maximum width of the composite layer for different laser processing condition. From the graphs, it is observed that for the variation in laser parameters, the maximum width of the composite layer varies in the range of 1.3 to

1.8 mm. It is also observed that this value increases with the increase in overlapping factor when peak power and pulse duration are fixed for lower peak power condition. For peak power of 1 kW with different overlapping factor and 1.5 kW with 60% overlapping factor, the maximum width of the composite layer found below 1.5 mm. However, for higher peak power condition, this width value is larger or equivalent to 1.5 mm. Again from Fig. 4.11 (a-c), where the width of the composite layer is plotted against applied peak power for different overlapping factor and pulse duration condition, it is observed that, for relatively lower peak power (1 to 2 kW), the width of the composite layer increases with the increase in peak power. However, for higher peak power (2.5 to 3.5 kW), change of width is almost negligible for an increase in peak power when the overlapping factor is constant.

4.3.3 Micro-hardness

Average micro-hardness value with a standard deviation of TiC coated AISI 304 steel substrate plotted against overlapping factor for different pulse duration, and laser peak power of 1, 1.5, 2, 2.5, 3 and 3.5 kW are shown in Fig. 4.12(a-f) respectively. From the graphs, it is clearly observed that average micro-hardness value of laser processed composite layer largely depends on the applied peak power. Average micro-hardness value found reasonably high (in the range of 800-1200 $HV_{0.05}$) for samples processed with relatively low peak power i.e. 1 and 1.5 kW for different pulse duration and overlapping condition (Fig. 4.12(a-b)). Fig. 4.12(c-f) show that average micro-hardness values for the samples processed with 2 and 2.5 kW are in the range of 500- 800 $HV_{0.05}$ and 400-600 $HV_{0.05}$ respectively. However, the hardness value for the sample processed with 3 and 3.5 kW are found in the range of 380-680 $HV_{0.05}$ and 550-600 $HV_{0.05}$ respectively. Therefore, it is revealed that the average micro-hardness value of the coated zone reduces as peak power increases for different pulse duration condition. Careful observation of the graphs also revealed that, for most of the cases, average micro-hardness value of the coated zone slightly increases with the increase in overlapping factor. However, no specific effect of the pulse duration on the average micro-hardness value has been observed. From all the graphs, it is also found that the standard deviation for hardness value is reasonably high for sample processed with low peak power i.e. 1 and 1.5 kW, but these standard deviation values are reducing as the applied peak power increases.

Effect of peak power on the average micro-hardness value of the TiC coated zone could be clearly visible from Fig. 4.13(a-c) for a specific pulse duration and different overlapping condition. From the graphs, it is revealed that when the laser peak power range

is relatively low i.e. 1-2 kW, the average hardness value of the composite layer reduces with the increase in laser peak power. However, for higher peak power range (2.5-3.5 kW) it is surprisingly found that with the increase in laser power, average micro-hardness value of the composite layer increases.

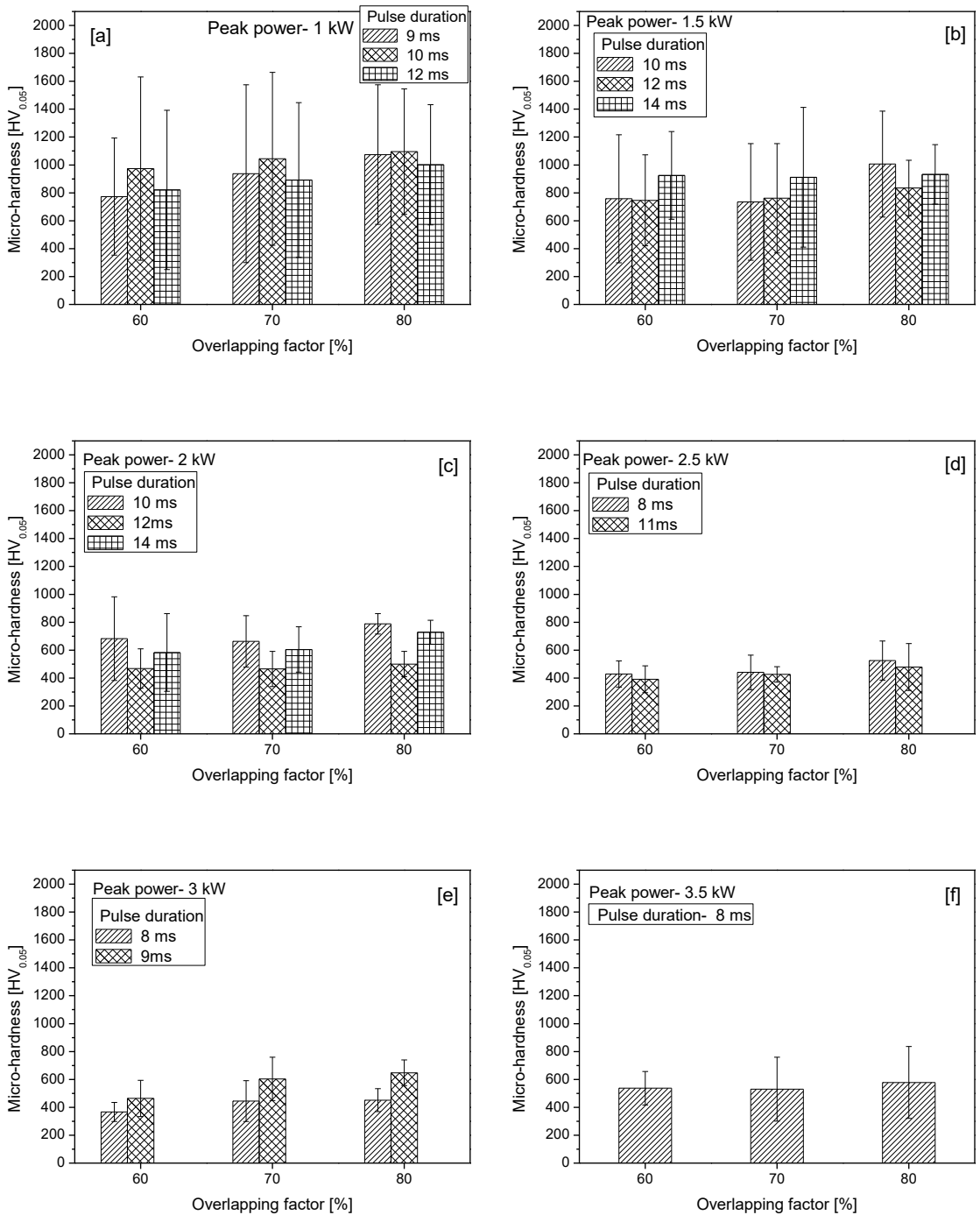

Fig. 4.12: Average micro-hardness value of TiC-steel composite layer produced by pulsed Nd:YAG laser at different overlapping factor, pulse duration and peak power condition

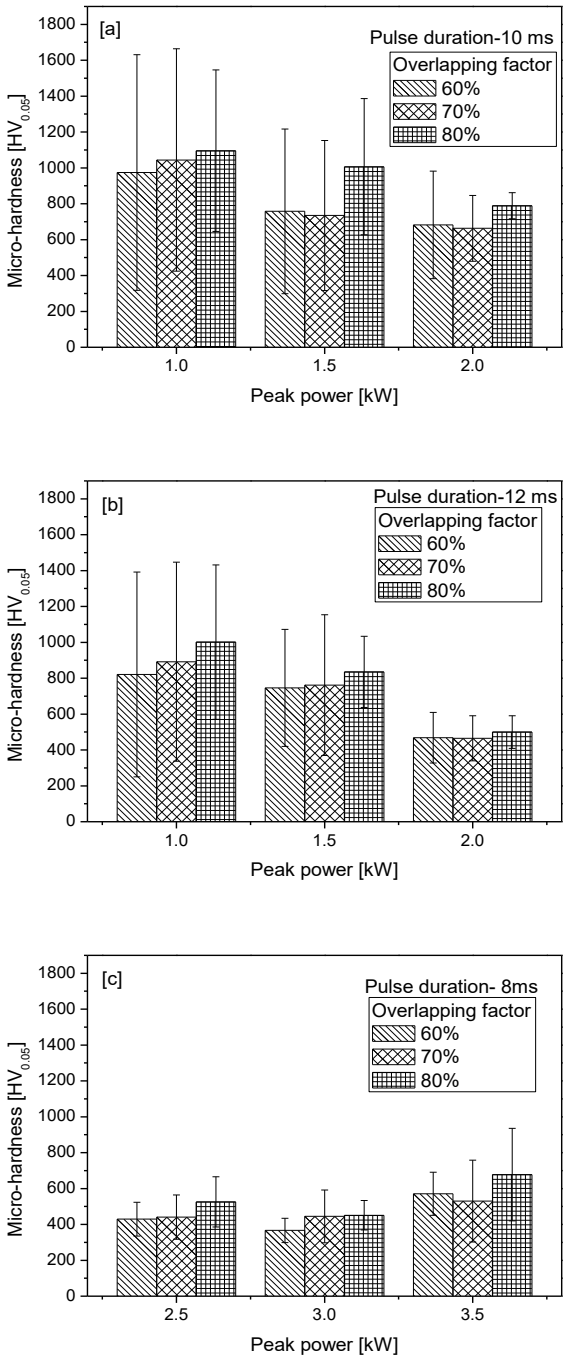

Fig. 4.13: Average micro-hardness value of TiC-steel composite layer produced by pulsed Nd:YAG laser at different peak power condition for different pulse duration and overlapping factor

Average micro-hardness value of the laser coated surface mainly governs by the distribution of the TiC particles in the steel surface and microstructure of the coated region. For the sample processed with a lower peak power (1 and 1.5 kW), the average value of surface micro-hardness found reasonably high with a wide range of variation. This is mainly because, at lower peak power due to relatively low power density, melting of preplaced TiC particles are incomplete and dispersed non-uniformly on the substrate surface and after

solidification deposited at the outmost surface of the steel substrate. These un-melted TiC particles increase the average hardness of the composite layer when hardness value measured from the top surface. At the same time, some portion of the steel substrate spread over the bulk TiC layer. Hence, a relatively non-uniform and thin layer of TiC on steel substrate was produced, which exhibited hardness value in a wider range (high value for bulk TiC and low value for re-solidified steel surface). As peak power increases, melting depth of the pre-deposited steel layer also increases and due to convective flow of the molten metal, TiC particles distributed inside the steel surface for a larger depth, which dilutes the TiC particles in the steel matrix. As a result, the overall hardness value of the composite layer reduces.

Furthermore, as the overlapping factor increases, TiC particles distributed uniformly in the molten pool, but within a small depth. Therefore, the average hardness value of the laser coated sample augmented, but standard deviation reduces. From the SEM images, for instance in Fig. 4.5, it is observed that with the increase in overlapping factor, agglomeration of TiC particles reduces and distributed all over the melt pool. However, from the plots (Fig. 4.12(a - f)) no specific effect of pulse duration on micro-hardness value of the laser coated samples was observed.

4.3.4 Sliding abrasive wear test

Fig. 4.14(a) shows the sliding abrasive wear (as height loss) of TiC coated pins prepared by laser coating method with different pulse overlapping factor (60, 70 and 80%) and as received AISI 304 steel substrate. The plot indicates that the abrasive wear in term of height loss of the laser coated pins are significantly lower than the height loss of AISI 304 steel substrate under similar test condition. It can also be observed from the plot that the wear (height loss) of the coated pins decreases with the increase in overlapping factor from 60 to 70 %. However, with further increase in overlapping factor the height loss of the pin found increased marginally. Fig. 4.14 (b) show the height loss against time monitored through data acquisition system during the wear test of TiC coated pins produced with different overlapping factor. The plot shows almost similar wear characteristic but with a larger value than the wear of TiC coated pin measured by Vernier caliper. Here, the graph demonstrates the combined wear or height loss of both coated pin and alumina abrasive disc, which was directly obtained through data acquisition system and plotted against test time.

It is worth pointing out that sliding abrasive wear behavior of the coating depends on the hardness value, morphology (distribution of TiC particles) and the depth of the coating. From the SEM images (Fig. 4.3), it was found that for the sample processed with low overlapping factor (60%), maximum depth of TiC reinforcement on the molten substrate or coating thickness is comparatively low and large portion of TiC deposited at the upper surface of the substrate only. As overlapping factor increases, distribution of TiC on steel surface become relatively uniform, as well as, the depth of TiC-steel composite layer enhances. Thus, for low overlapped samples (60%), during sliding abrasive wear test, after a certain time period, TiC layer removed out and exposure of steel substrate occurred. However, for higher overlapped samples (70 and 80%), as the coating depth is larger, within the test period, coating layer removed partially, and overall wear or height loss of the coating reduced.

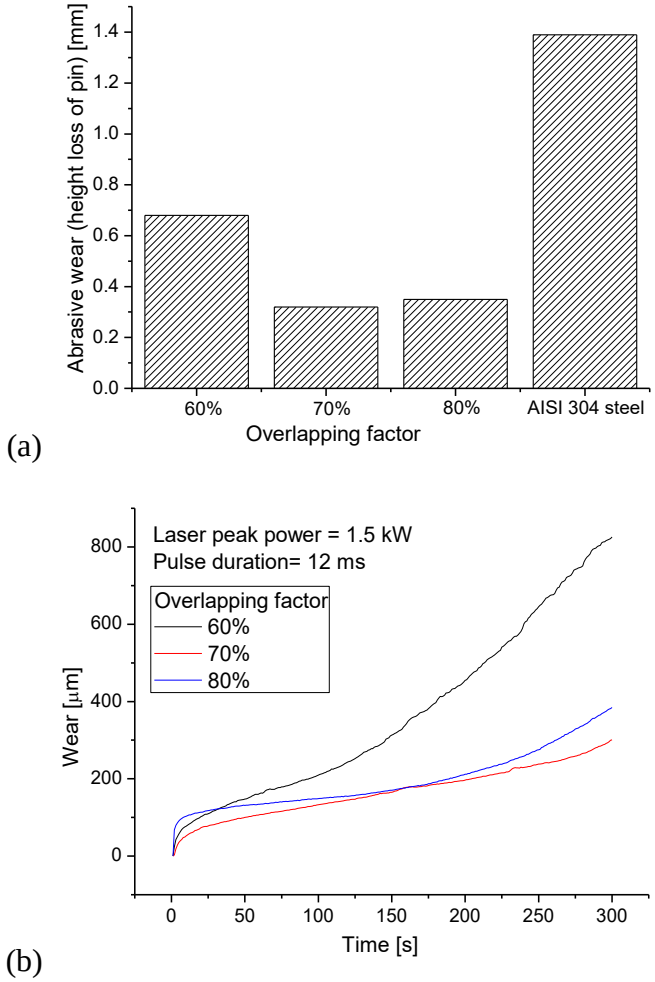

Fig. 4.14: (a) Abrasive wear or height loss of pin (b)wear behavior (height loss of pin against time) during wear test of the laser coated samples produced with peak power of 1.5 kW, pulse duration of 12 ms and overlapping factor of 60, 70, and 80%

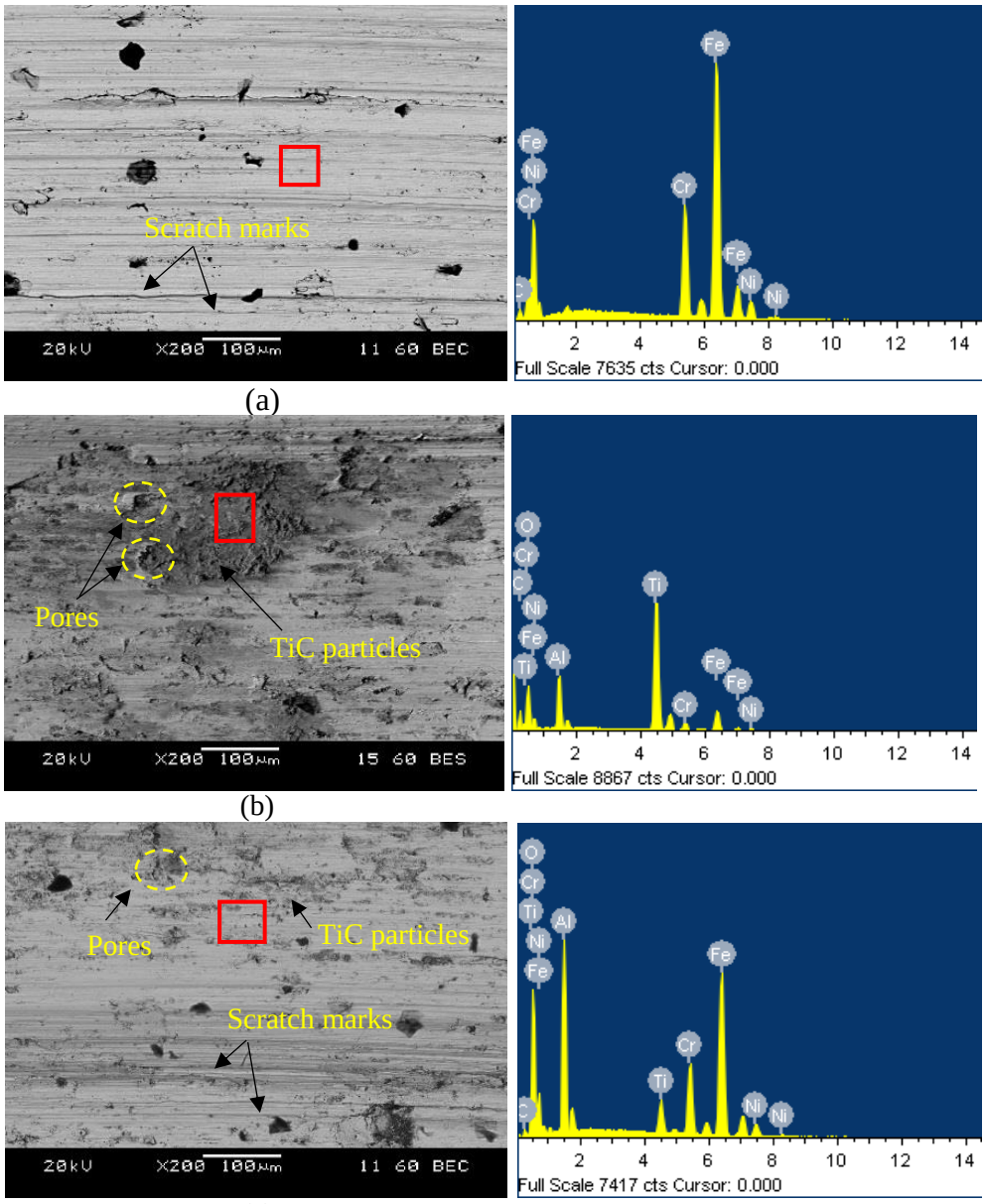

Fig. 4.15: SEM micrograph of the worn surface of TiC coated pin produced by laser coating process with peak power 1.5 kW, pulse duration 12 ms and pulse to pulse overlapping factor of (a) 60%, (b) 70% and (c) 80%

Table 4.3: EDS analysis for the selected region corresponding to Fig. 4.15

Sample with OF	Element (Wt.%)						
	C	Ti	O	Al	Cr	Fe	Ni
60%	6.19				18.37	67.60	7.84
70%	14.27	30.34	36.64	6.06	2.35	9.18	1.16
80%	4.71	3.69	24.95	14.27	10.78	37.39	4.21

Fig. 4.15 (a–c) shows the SEM images and corresponding EDS analysis of the worn out surface of TiC coated pins (processed with 60, 70 and 80% pulse overlapping factor) after the wear test. The images clearly indicate that for the sample processed with 60% overlapping factor, entire TiC layer removed after the wear test and steel surface exposed. However, for the sample processed with 70% overlapping factor, the existence of TiC (dark zone) on the worn out surface clearly observed. Similarly, for 80% overlapped sample, trace of TiC also detected on the worn out surface. EDS elemental analysis of the selected region of the SEM images are illustrated in Table 4.3. From the table it is clearly evident that for 60% overlapped sample, on the worn out surface, there is no existence of Ti. However, for higher overlapping factor (70 and 80%), Ti exist on the surface, which represent the presence of TiC on the worn out surface after the wear test.

In addition, on the worn surface of coated pin produced at 60% overlapping factor, severe scratch marks are visible, which form due to the plastic deformation of the steel substrate against the alumina abrasive. In contrast, for the coated pin produced with 70% overlapping factor, some tiny voids or pores as marked in the figure can be seen, those were induced mainly because of the pull out of TiC particles during the abrasive wear test against alumina disc. Minor scratch mark can also be detected on the worn surface; those are produced perhaps due to the abrasion effect of Al_2O_3 particles from the abrasive disc. For the coated pin produced with 80% overlapping factor, in combination with pores scratch marks also visible. However, the intensity of these scratches is relatively less than the scratches induced in the sample produced with 60% overlapping factor.

4.3.5 Coefficient of friction

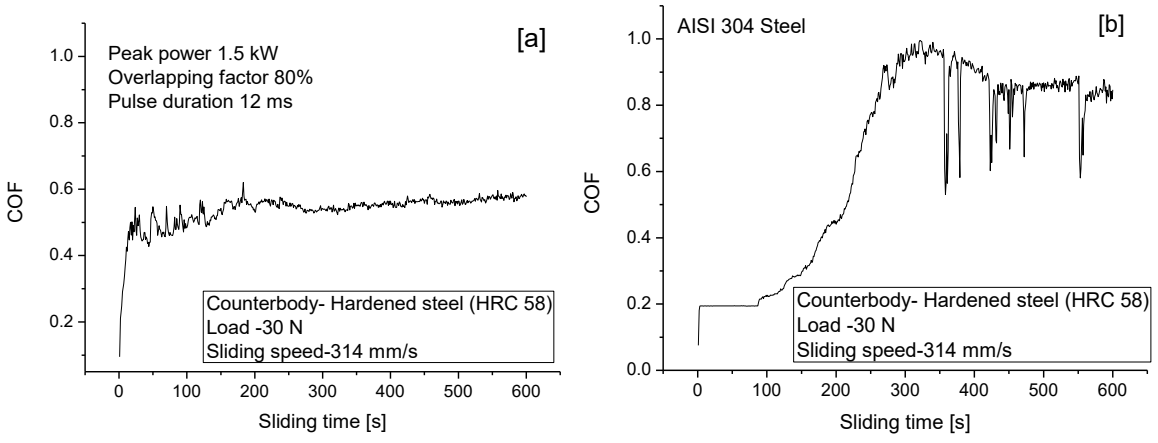

Fig. 4.16: Variation in coefficient of friction (against hardened steel, HRC 58) of (a) TiC coating produced at peak power of 1.5 kW, pulse duration of 12 ms and overlapping factor of 80% (b) AISI 304 steel

To assess the coefficient of friction (COF) value of the TiC coating by laser coating process sample produced with 1.5 kW laser power, 12 ms pulse duration, and 80% overlapping factor was considered. Sliding wear test of the aforesaid coated pin sample was carried out against a rotating hardened steel (HRC 58) disc, under 30 N normal load and sliding speed of 314 mm/s. A pin cut from the as received AISI 304 steel also tested under a similar test condition, to attain its COF value against hardened steel (HRC 58). Fig. 4.16 shows the variation of COF against the time of test for the TiC coated pin and as received AISI 304 steel pin. The plots clearly indicate that for TiC coating, the steady state COF value is approximately 0.6; however, the steady-state COF of bare steel is much higher under similar test condition.

4.4 Outcomes

A hard layer of TiC deposited or reinforced on AISI 304 steel substrate after laser irradiation over TiC preplaced steel surface using a pulsed Nd:YAG laser, depending on the laser processing parameters. From the experimental analysis following conclusion can be drawn

- Pulse laser parameter i.e. peak power and overlapping factor have great influence on the formation of TiC-steel composite layer.
- The increase in overlapping factor shows an improvement in the distribution of TiC particles inside steel substrate and increases the laser processed composite layer depth and width. 80% overlapping factor show a superior TiC distribution inside steel surface as compare to 60 and 70% overlapping factor.
- The lower range of peak power (1-1.5 kW) shows a relatively low composite layer depth and width, where TiC agglomerated and deposited over steel substrate. Whereas at higher peak power range (2 kW and above) TiC particles partially melted and distributed on the surface of the steel substrate. At high peak power and higher overlapping condition, homogeneous structure of TiC inside the steel surface formed due to melting and re-solidification.
- Higher pulse duration inside steel surface improves the TiC distribution and increases the composite layer depth.
- The average surface hardness of AISI 304 steel substrate (220 $HV_{0.05}$) improves to 400-1200 $HV_{0.05}$ depending on laser processing parameters after laser surface coating with TiC. Average micro-hardness value of the composite layer is considerably high for using

lower peak power with less uniformity in the hardness value. However, at higher peak power, relatively low but uniform hardness value obtained.

- Sliding abrasive wear resistance of TiC coating has improved significantly than the as received AISI 304 steel substrate. High sliding abrasive wear resistance observed in the samples processed with higher overlapping factor (70 and 80 %). The TiC coated pin show relatively lower COF value compared to steel pin.
- Proper combination of peak power, overlapping factor and pulse duration is required to create a defect-free and uniform coating using pulse laser.

Chapter 5

TiC/TiC-steel composite coating by Tungsten Inert Gas (TIG) cladding process

In this chapter, TiC/TiC–steel composite layer was produced on AISI 304 steel substrate by Tungsten Inert Gas (TIG) cladding process to improve its hardness and wear resistance properties. Effect of processing current and scan speed on the coating geometry and corresponding microstructure has been investigated from the SEM images. Pin-on-disc type sliding abrasive wear test has been performed to assess the tribological behavior of the coating. At low current and high scan speed, a distinguished layer of TiC deposited on the substrate that exhibits significantly higher hardness and high wear resistance than the steel substrate. Conversely, at high current and low scan speed produced TiC–steel composite layer exhibits relatively low hardness and low wear resistance. The wear resistance improved five to fifty times depending on the coating microstructure.

Keywords: Micro-hardness; Abrasive wear; TIG cladding; Microstructure

5.1 Introduction

So far, different coating technics were employed to deposit hard and wear resistant coatings on various graded steel substrate to improve their hardness and wear resistance (Piasecki et al., 2016). Laser alloying/cladding, and weld cladding (Jankauskas et al., 2015; Lin et al., 2013) are high-energy coating processes which received considerable attention due to their rapidness, applicability in versatile material and specific metallurgical advantages. In spite of specific advantages, the application of laser surface modification is inadequate in the manufacturing sector, due to its technological complexity, and high equipment cost (Mridha and Baker, 2015). TIG melting/cladding is a low-cost alternative to depositing a thick coating layer, due to its convenience to use, and low setup/running cost. In tungsten inert arc (TIG) cladding/alloying process ceramic or metallic powder or powder mixture preplaced on a substrate surface melted and after solidification produces an improved surface layer (Ghadami et al., 2015; Rasool and Stack, 2014; Sohi et al., 2012). Melting of the preplaced powder on the work-piece surface ensued due to the arc generated between the tungsten electrode and the surface, enabling metallurgical bonding between the coating

material and the substrate. Rapid solidification produces fine-grained microstructures, which may also improve the surface mechanical properties of the coating layer (Mridha et al., 2001). Numerous works have been reported on gas tungsten arc (GTA) or tungsten inert gas (TIG) cladding/alloying process to improve the surface properties of different substrate materials.

Although, TIG cladding widely used for hard-facing of structural steel, however controlling the dilution of the substrate material in the deposited layer is quite challenging. Since dilution is the key issue for ensuring the functionality and reliability of the component, an optimum processing condition must be regulated for assured percentage of dilution (Chakraborty et al., 2014). It has been revealed from the literature that, with an increase in welding current, dilution of the substrate into the coating material increases, whereas hardness of the coating decreases (Chen et al., 2009, 2008; Madadi et al., 2012). However, for a single scan of the arc over the preplaced powder, the geometry of the melt pool (depth and width of coating) as well as the microstructural variation due to melting and solidification of the coating material for changing the current and scan speed was hardly discussed for TIG cladding/alloying process.

In this study, TiC or TiC-steel composite layer has been deposited on AISI 304 austenitic stainless steel by TIG cladding process. Coating layer depth and corresponding microstructure were evaluated by FESEM and EDS analysis. The composition of the coating layer was assessed by XRD analysis, and hardness was measured by Vickers micro-indentation hardness tester. Sliding abrasive wear of the coating was studied by pin-on-disc type sliding abrasive wear test, and wear behavior was correlated with the microstructure and the hardness value obtained on the coated surface.

5.2 Experimental procedure

For this phase of experiments, AISI 304 stainless steel plates of dimension 100 mm×50 mm×8 mm, were cut, ground with a surface grinder and the surface to be coated was polished with 220-grade emery paper. The polished samples were then cleaned with alcohol and acetone sequentially to remove any surface contamination. Commercially pure TiC powder as detailed in Chapter-3 was mixed with acetone and an organic binder to make a semi-solid solution. The paste-like solution of TiC was then dispersed uniformly over the already prepared clean steel surface and dried at room temperature so that after evaporation of the acetone a solid layer of TiC remain on the substrate surface. Thus, a preplaced layer

of 400±20 µm was deposited on the steel substrate by controlling the amount of dispersed powder solution.

After preplacing the TiC powder layer on steel substrate, the coating was carried out using a Tungsten inert gas welding setup as specified in Chapter-3. Fig. 5.1 shows the schematic diagram of the TIG cladding process using TiC as preplaced powder. A tungsten-thoriated electrode of 2.4 mm diameter was used, and the electrode-workpiece gap was fixed at 3 mm to produce a stable arc. Argon gas was supplied as the inert gas, with a flow rate of 10 l/min. Table-5.1 illustrate the detail of parameters used for the present experiments. The operating current and the arc scan speed were varying as per the experimental planning presented in Table-5.2. Heat input per unit length (H), during the arc scan, was calculated by using Eqn. 3.1 as described in Chapter-3. The heat input for each condition with different welding current and arc scan speed combination employed in this experiment are presented in Table-5.2. After scanning the TIG arc over the pre-deposited substrate and consequent melting and solidification of preplaced powder, the processed samples were cut as per required dimension using wire-EDM. The cut specimens were then polished to analyze the microstructure of the produced coating layer by SEM. The metallographic polishing was done with SiC paper followed by 1 µm diamond solution. Photomicrographs of the cross-section of the coating were taken with SEM (JEOL JSM-6084LV) for low magnification images and FESEM (Nova NanoSEM-FEI) for the high magnification images in backscatter electron (BSE) mode. The composition of the coating layers was analyzed by EDS attached with the FESEM. The compound phases present in the coated surface were identified by the X-ray diffraction (XRD) pattern obtained from BRUKER D8 ADVANCE diffractometer, using cobalt target (λ= 1.79026 Å). The hardness value at the cross-section of the coated layer was measured by a Vickers' micro-indentation hardness tester (LECO-LM248AT) with 50 g (0.49 N) indentation load and dwell time of 10 s. Sliding abrasive wear test of the coated samples was performed using a pin-on-disc friction and wear test rig (ASTM G99 standard, Make: Magnum) as detailed in Chapter-3. From each coated track, a 3 mm diameter pin was cut with the help of wire electro discharge machine. The prepared pins were then slid against 220 grade SiC paper with a sliding velocity of 314.15 mm/s and normal load of 30 N. Prior to wear test, the coated pins were polished with 600 grade SiC paper to acquire a flat coating surface and to remove the protuberance formed at the edge of the track during the arc scanning. Fig. 5.2 shows the schematic diagram of the pin-on-disc experimental setup. The details of sliding abrasive wear test condition are depicted in

Table-5.3. Abrasive wear of the coated samples was measured in terms of average height loss of the pin after the test, using a digital vernier caliper with a least count of 0.01 mm.

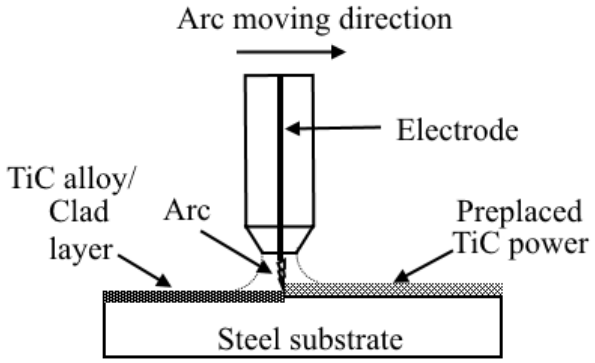

Fig. 5.1: Schematic diagram of Tungsten Inert Gas (TIG) cladding process

Table 5.1: Experimental condition for TIG cladding process

Parameters	**Condition**
Current	60, 80, 100 A
Voltage	15 V
Shielding gas	Argon
Current type	DC Straight polarity
Gas flow rate	10 l/min
Electrode diameter	2.4 mm
Electrode-workpiece distance	3 mm

Table 5.2: Detail experimental condition for Tungsten Inert Gas cladding process

Exp. No.	**Applied current (A)**	**Scan speed (mm/s)**	**Heat Input (J/m)**
1	60	4.1	105.36×10^{-3}
2	60	5.3	81.51×10^{-3}
3	60	6.5	66.46×10^{-3}
4	80	4.1	140.48×10^{-3}
5	80	5.3	108.68×10^{-3}
6	80	6.5	88.61×10^{-3}
7	100	4.1	175.61×10^{-3}
8	100	5.3	135.85×10^{-3}
9	100	6.5	110.77×10^{-3}

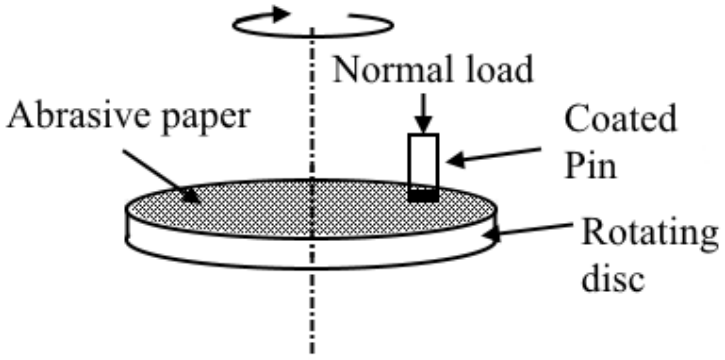

Fig. 5.2: Schematic diagram of the pin-on-disc experimental setup

Table 5.3: Sliding abrasive wear test condition by pin-on-disc wear test rig

Parameters	**Condition**
Pin diameter	3.0 mm
Normal load	30 N
Disc speed	300 rpm
Track radius	10 mm
Sliding velocity	314 mm/s
Test duration	10 minutes
Abrasive medium	220 grade SiC paper

5.3 Result and discussion

5.3.1 Coating morphology

Fig. 5.3 to 5.5 illustrate the SEM images taken at the cross section of the coating track processed at different current and scan speed condition by TIG cladding process. From the SEM images, the dimension of the coating layer, such as coating depth and width was measured (as shown in Fig. 5.3a). The SEM images revealed that TiC powder was either deposited on the top surface or dispersed on the upper surface of the steel substrate depending on the processing current and scan speed. Thus, the dimension of the coating zone primarily depends on the heat input during arc scanning. Maximum depth and width of the coating layer were measured for all the samples and plotted against scan speed for the different current condition as shown in Fig. 5.6 and 5.7.

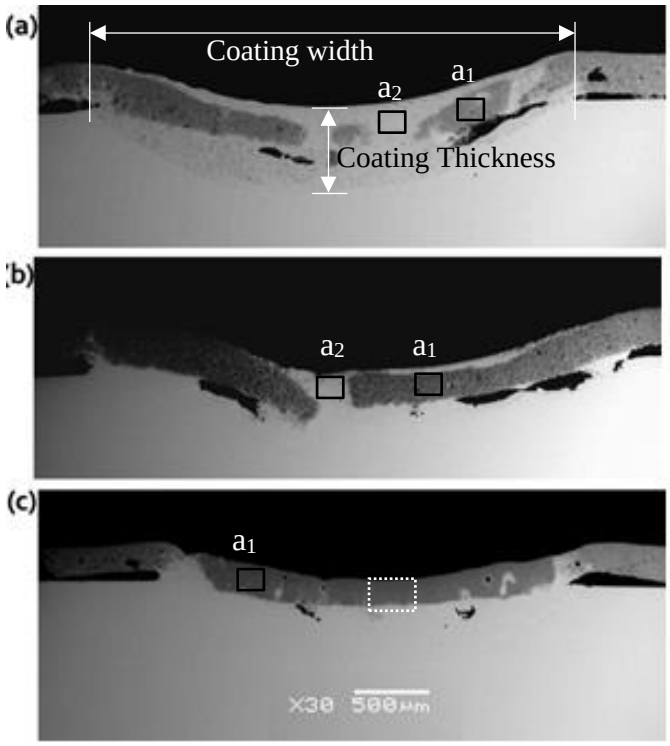

Fig. 5.3: SEM images of the cross-section of TiC coating produced by TIG cladding method with 60 A current, and scan speed of (a) 4.1 mm/s, (b) 5.3 mm/s and (c) 6.5 mm/s

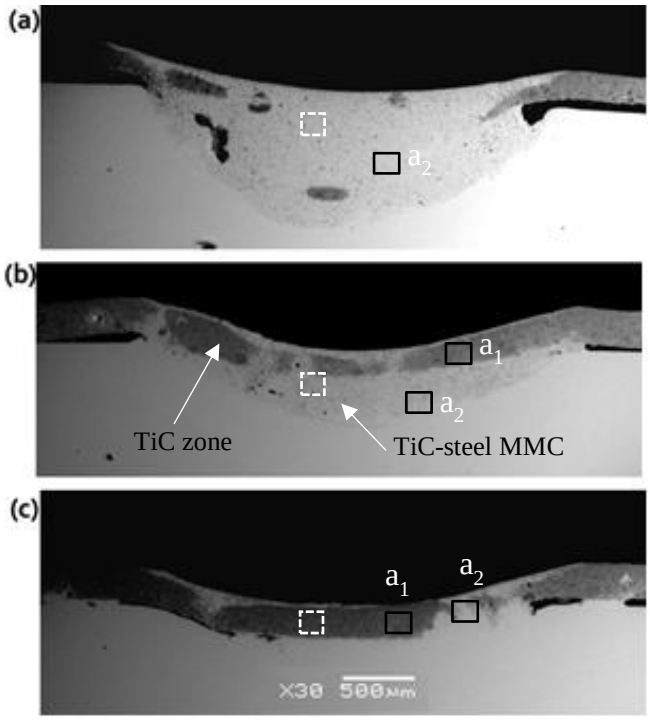

Fig. 5.4: SEM images of the cross-section of TiC coating produced by TIG cladding method with 80 A current, and scan speed of (a) 4.1 mm/s, (b) 5.3 mm/s and (c) 6.5 mm/s

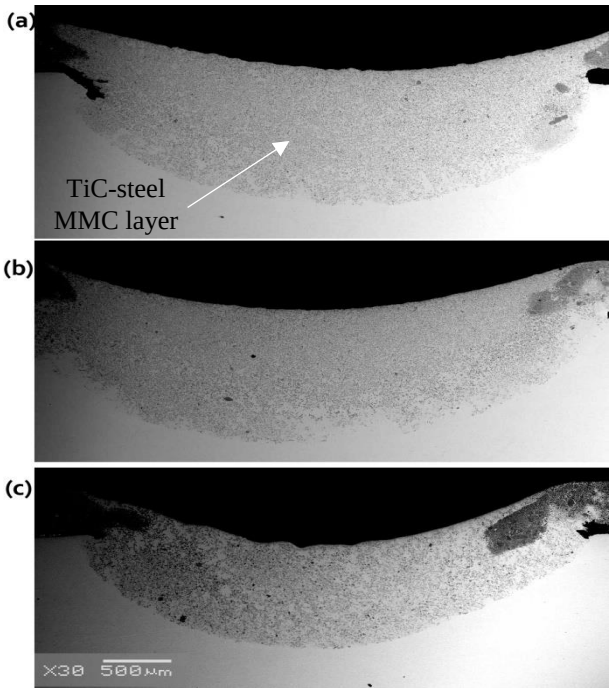

Fig. 5.5: SEM images of the cross-section of TiC coating produced by TIG cladding method with 100 A current, and scan speed of (a) 4.1 mm/s, (b) 5.3 mm/s and (c) 6.5 mm/s

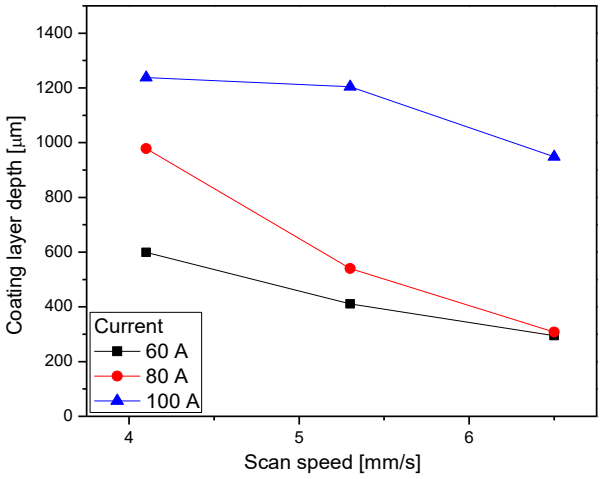

Fig. 5.6: Variation of coating layer depth against arc scanning speed for different processing current

The graph (Fig. 5.6) revealed that the maximum coating depth largely depends on the applied current. At lower current (60 A), coating layer depth was relatively low (250-600 µm), and this value increased for the sample processed with higher processing current. For using 100 A current, coating depth was found in the range of 900-1200 µm and the maximum layer depth obtained for the sample prepared at 100 A current and 4.1 mm/s scan

speed. The graph also revealed that with increasing scan speed, the coating depth decreases. With an increase in applied current, energy transfer to the TiC coated substrate also increases that resulted in an enhancement of melting depth of TiC coated steel. Further, for using 60 A current, mixing of TiC with the steel substrate is very less, that leads to reduced coating layer depth. In the case of arc scanning with 100 A current, TiC mixed with the steel substrate and produced a TiC–steel composite zone of larger depth.

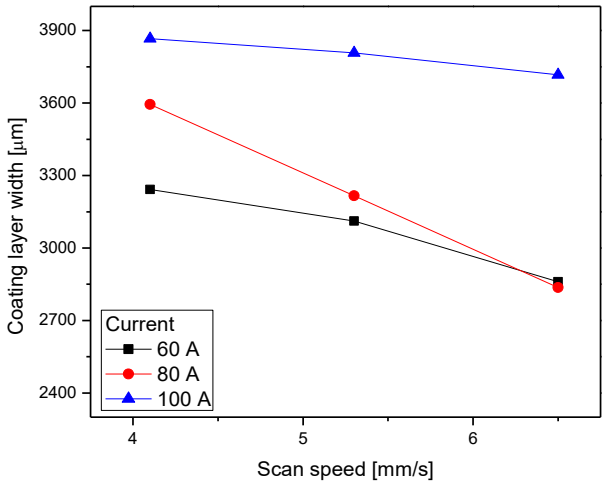

Fig. 5.7: Variation of coating layer width against arc scan speed for different TIG current

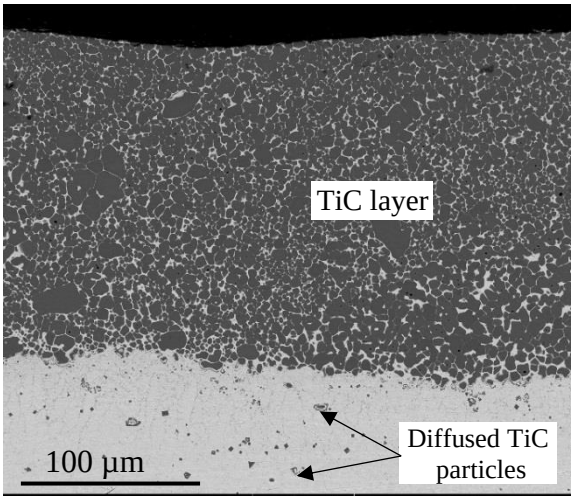

Fig. 5.8: Magnified FESEM image of the TiC coating processed with 60 A current and 6.5 mm/s arc scan speed, corresponding to Fig. 5.3c

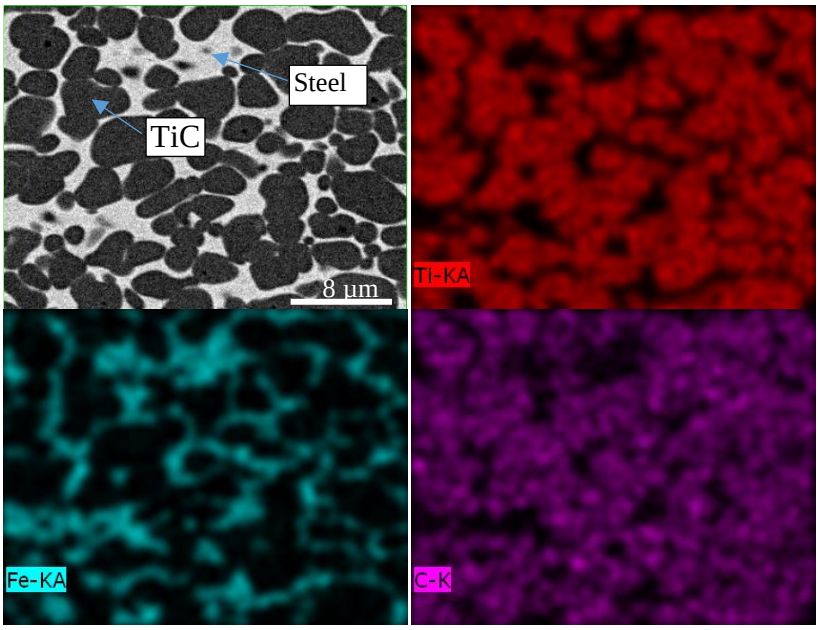

Fig. 5.9: EDS elemental mapping of the dark zone of the coating layer corresponding to SEM image shown in Fig. 5.8

Fig. 5.7 shows the variation of maximum coating width at the top surface against the arc scan speed. Here, the arc scanning for all the experiments was performed with 2.4 mm diameter electrode, and by maintaining a constant distance between the electrode and TiC preplaced steel workpiece. However, the graph illustrates that the coating layer width varies in the range of 2.8 to 4 mm. This attributed to the change in heat input into the TiC coated steel workpiece for the variation in current and arc scan speed. The graph also indicated that the width is higher for higher current and declines with the increase in scan speed.

For using low or intermediate current, relatively low heat input is not sufficient for mixing the TiC powder inside the steel substrate. Further, due to inadequate heating, the convective flow of molten metal restricted and trapped the blown Ar gas used for shielding the arc. These may causes formation of large voids specifically at the coating-substrate interface. Interface crack mainly observed for the coating produced at 60 A current or near the edges of the coating track produced at 80 A current. In these conditions, the supplied heat may be insufficient to make a strong bond between the coated TiC layer and steel substrate. Further during cooling, due to the difference in the coefficient of thermal expansion between TiC (8.5×10^{-6} °C^{-1}) and AISI 304 steel (1.7×10^{-5} °C^{-1}) and generation of residual stress a gap or interfacial crack formed at the coating and substrate interface. Candel et al. (2014), described that in laser cladding process during the development of TiC composite coating on Ti alloy, interfacial crack form as a result of the development of thermal stresses owing to mismatch in thermal and physical properties between two phases.

Fig. 5.3(a-c) show the SEM images at the cross-section of the TiC coated AISI 304 steel substrate after TIG cladding with 60 A current and different scan speed. The image indicates that at low current, and high scan speed (6.5 mm/s) condition, pre-deposited TiC powder melted, which after solidification produced a highly dense TiC reinforced steel matrix coating on the steel substrate. The image also indicated that, at relatively lower scan speed (4.1 mm/s, 5.3 mm/s), along with the formation of TiC layer, an MMC zone containing a mixture of TiC and steel substrate formed beneath the TiC layer. Careful observation of the images revealed that due to the higher energy intensity of the arc at the center, the middle portion of the track melted more and the TiC particles dissolved into the melt pool of the substrate to form an MMC structure. However, at the edges of the track comparatively low heat intensity restrict the total mixing of TiC powder with the substrate surface. For using of 60 A current, overall heat input on the preplaced TiC layer is relatively less, which further reduced at higher scan speed. Thus, at low current and high scan speed (60 A and 6.5 mm/s) combination, preplaced TiC powder melted and produced a clad layer with a negligible dilution of iron from the base material. Further, due to the low density of TiC, at low heat input condition convective flow of molten layer is inadequate to dispense the TiC particles inside the melt pool. As scan speed reduced to 5.3 and 4.1 mm/s, the heat input in the processed zone increased as illustrated in Table 5.2. With relatively higher heat input, melting depth of TiC layer as well as the upper layer of the substrate augmented that causes mixing of TiC powder particles with the substrate matrix. In addition, some amount of TiC diffused into the steel substrate at higher temperature and produces a MMC type coating of TiC and steel.

It is also apparent from the SEM images (Fig.5.3-5.5) that, these coatings are free from any cracks. However, some void or pores present at the interface between the coating and the substrate, and at the edges of the molten track where the temperature during the arc scanning is relatively less. Magnified FESEM image of the TiC coating processed by TIG cladding process with 60 A current and 6.5 mm/s scan speed (corresponding to the marked region of Fig. 5.3c) is shown in Fig. 5.8. The image clearly shows a highly dense TiC layer on the steel substrate without any crack or gap at the coating-substrate interface. The image also indicates that TiC particle diffused inside the steel substrate to some extent. No crack or pores can be observed in the coating, which indicate that a solid uniform coating is possible by TIG cladding process at suitable processing condition.

Fig. 5.9 illustrates the high magnified FESEM image taken in BSE mode and corresponding EDS elemental mapping of the dark zone of the clad layer produced with 60 A current and 6.5 mm/s scan speed. The magnified image confirmed that this dark zone consist highly concentrated black particles with a relatively less amount of white matrix. The EDS elemental mapping reveals that these dark particles are rich in titanium and carbon whereas, white matrix zone is rich in iron. Therefore, it can be concluded that these black particles are TiC, embedded in the iron matrix of the substrate and produced a highly concentrated layer of TiC. During the scanning of the arc, due to heating and corresponding melting of TiC particles, the surface of the substrate material also heated and tried to evaporate, and fraction of which mixed with the TiC layer. Thus, bonding between the TiC particles ensued with a very low dilution of the steel substrate.

Fig. 5.10 (a-c) show the high magnified FESEM image corresponding to Fig. 5.3 (a-c). From the micrograph (Fig. 5.10a), it is seen that the dark layer on the steel substrate consists of globular shape TiC particles and corresponding EDS analysis revealed that the percentage of TiC is reasonably high in this layer. Table-5.4 illustrate the detail of EDS analysis for the whole region of high magnified images corresponding to Fig. 5.10, 5.11 and 5.12, i.e. for the coating produced with different current and arc scan speed condition. For using 60 A current, relatively low heat input causes melting of TiC powder layer and very thin layer of the steel substrate. This low heat input is not sufficient for mixing the TiC powder inside the steel substrate and confining the convective flow of molten metal. At maximum scan speed (6.5 mm/s), the amount of iron in the dark region is almost negligible. When scan speed is relatively low, (4.1 and 5.3 mm/s), along with this dark layer, a gray shaded zone also form (Fig. 5.10b and 5.10c) that contains a relatively low amount of TiC dispersed in the steel matrix. EDS analysis shows that the percentage of iron and other constituent of stainless steel increases in the dark layer with the reduction of the scan speed. At low scan speed, with relatively higher heat input, partial melting of substrate augmented, and TiC mixed with the substrate and produced a gray shaded MMC zone. Careful observation of the microstructure of the clad layer produced with 60 A current revealed that, spherical shape and partially melted TiC produced (Fig. 5.10a) at the clad layer after solidification of the melt pool. Mridha et al. (2015) in their work demonstrated that, due to relatively low heat input and faster cooling rate, localized Marangoni forces causes preferential dissolution of irregularly shaped TiC particulates that resulted in globular precipitated particles in the coating layer.

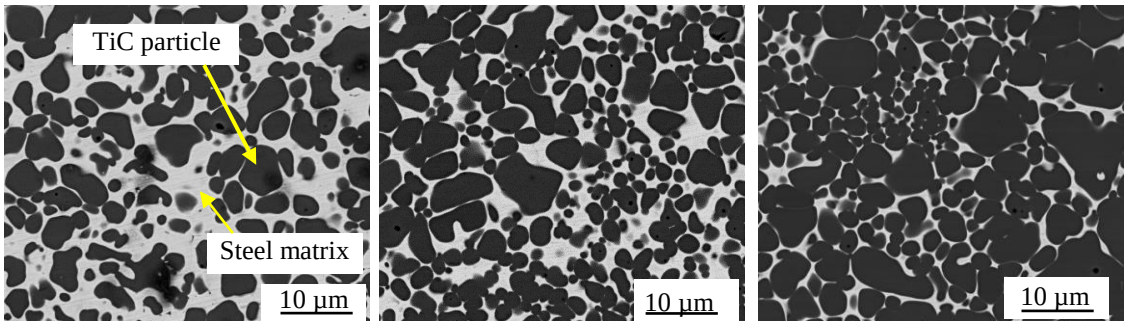

Fig. 5.10: High magnified FESEM micrograph of the coating prepared with 60 A current and scan speed of (a) 4.1 mm/s, (b) 5.3 mm/s and (c) 6.5 mm/s

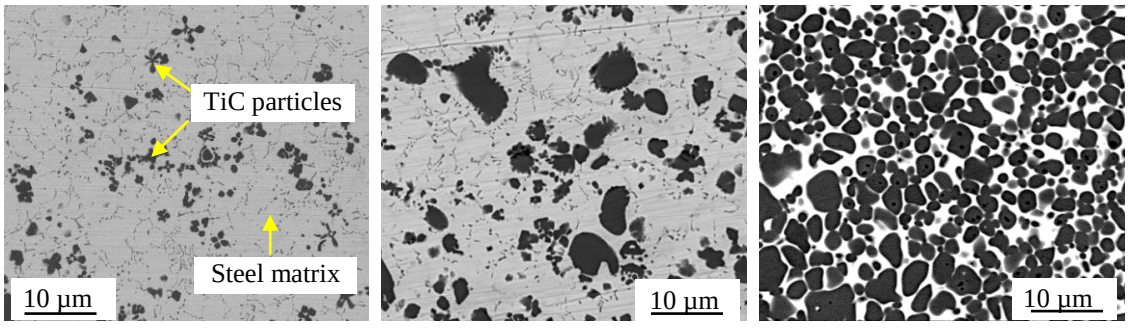

Fig. 5.11: High magnified FESEM micrograph of the coating prepared with 80 A current and scan speed of (a) 4.1 mm/s, (b) 5.3 mm/s and (c) 6.5 mm/s

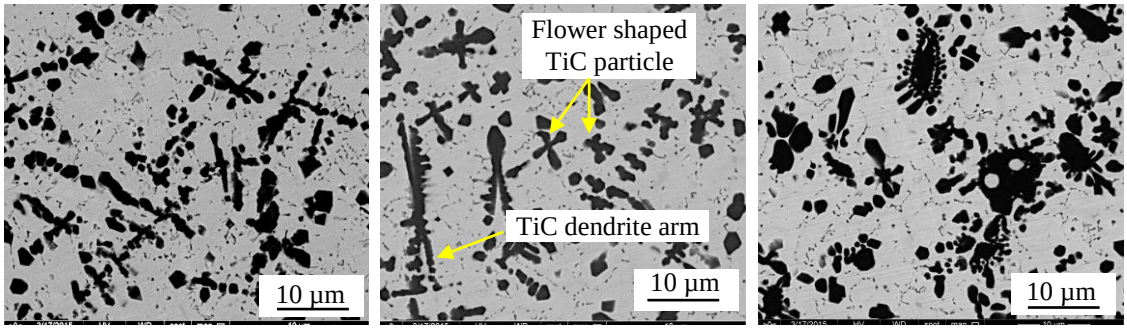

Fig. 5.12: High magnified FESEM micrograph of the coating prepared with 100 A current and scan speed of (a) 4.1 mm/s, (b) 5.3 mm/s and (c) 6.5 mm/s

Fig. 5.4 (a-c) show the SEM images at the cross-section of TIG coated samples processed with 80 A current and different scan speeds. Depending on the scan speed, these layers are consist of either an MMC of TiC–steel or a mixed layer containing TiC–steel MMC and highly dense TiC layer. At low scan speed, a layer of TiC reinforced steel composite produced at the top surface of the substrate. However, for using higher scan speed, a non-uniform mixed layer containing dense TiC region and TiC–steel MMC zone produced. This may be attributed to the fact that, with a high heat input at low scan speed,

the convective flow of molten TiC inside the molten steel surface occurred, resulting in TiC particles distributed uniformly on the steel surface. However, samples processed with higher scan speed (5.3 and 6.5 mm/s), did not acquire adequate energy for complete melting of TiC powder layer, and the upper surface of the steel substrate. Thus, the subsequent convective flow of molten layer restricted, that leads to the formation of a non-uniform dark layer of TiC along with the gray shaded region of TiC–steel composite. Fig. 5.11(a-c) shows the high magnification FESEM images corresponding to the marked zone of Fig. 5.4 (a-c), where TiC mixed with steel substrate. Since, for using 80 A current at different scan speed, TiC–steel layers are not uniform in the melt pool (coating layer), it is hard to compare the microstructure and EDS analysis at high magnification.

Fig. 5.5 (a-c) show SEM images at the cross-section of the TiC coated samples processed with 100 A current and different scan speeds. The images revealed that, at high welding current, a gray shaded layer of uniformly dispersed TiC–steel composite produced at the substrate surface. High heat input due to higher welding current causes melting of pre-placed TiC powder layer as well as the upper layer of steel substrate and produced uniformly distributed TiC–steel metal matrix composite after solidification. At relatively low scan speed (4.1 mm/s), due to maximum heat input almost the entire preplaced TiC powder melted and diffused into the steel substrate due to the sturdy convective flow of the molten pool. This causes TiC to mix uniformly and dispersed at the upper layer of steel substrate during solidification. However, at relatively high scan speed, some amount of TiC powder was not melted properly and remains agglomerated or present as bulk, especially at the edges of the melt pool (Fig. 5.5b and 5.5c).

Table 5.4: EDS analysis showing wt.% of elements present in the entire region of FESEM images corresponding to Fig.5.10-5.12

Current	**60 A**			**80 A**			**100 A**		
Scan speed (mm/s)	4.1	5.3	6.5	4.1	5.3	6.5	4.1	5.3	6.5
Elements	wt.%								
Ti	74.21	78.42	78.49	2.14	5.35	75.53	44.11	28.79	21.89
C	19.86	19.44	20.25	7.89	13.89	18.2	14.34	18.84	18.06
Fe	3.72	1.51	0.78	68.37	62.43	4.10	31.69	39.41	46.39
Cr	1.57	0.43	0.39	12.90	10.35	1.63	6.80	7.74	9.00
Mn	0.64	0.20	0.08	8.71	5.35	0.54	3.06	5.49	4.67

Fig. 5.12(a-c) show the high magnified FESEM images of the coatings shown in Fig. 5.5(a-c). From these images, it is revealed that the coating layer is mainly consisting of a dark dendritic structure of TiC and white steel matrix. At relatively high current (100 A), due to high heat input and corresponding slow cooling rate, TiC particles entirely melted within steel matrix and during solidification nucleation start and grow into dendrite structure. EDS analysis (Table-5.4) indicate that the percentage of Ti and C (which represent the amount of TiC in the coating) is higher for the sample processed at low scan speed, and with the increase in scan speed extent of TiC reduces in the composite layer. Higher heat input during the coating process produces a thermal shock on the preplaced TiC particles, which may cause cracking of the TiC particulates and intrusion within the molten steel (Mridha et al., 2015). The Marangoni convective flow of the molten material, agitates and accelerates the cracked particulates into the melt pool adjacent to the arc source and moves them towards the bottom part of the melt pool. Thus, dissolution of reinforcing material with the substrate increases. At higher scan speed, inside the melt pool, some amount of TiC particles remain un-melted, those may be appeared at the edges or agglomerated inside the melt pool. Consequently, an overall reduction in the percentage of TiC at the remaining part of the coating was witnessed.

A careful observation of the micrograph (Fig. 5.12a) revealed that, at relatively low scan speed (4.1 mm/s), eqi-armed TiC dendrites form in the steel melt pool. Low scan speed contributes higher heat input on the melt pool with relatively slow cooling rate, which causes TiC dendrites to grow into a larger structure. However, increase in scan speed (5.3 mm/s) resulted in overall low heat input and subsequently higher cooling rate, which hinders the growth of TiC dendrites within the melt pool and solidified as block shaped or flower-shaped structure (Fig. 5.12b). At highest scan speed (6.5 mm/s), melting and nucleation of few TiC particles occurred, however, due to low heat input TiC particles are partially melted and solidified rapidly (Fig. 5.12c). Thus, larger black particles surrounded by smaller blocky particles formed in the melting zone. Wang et al. (2001) in their work on laser surface alloying of titanium aluminide alloy, showed that TiC solidified into the dendritic structure at the lower cooling rate. However, with the increase in solidification rate, the growth morphologies of TiC became flower shape or radially branching colonies.

Comparing the high magnified FESEM images of the coating layer produced with different TIG current (Fig. 5.10 and 5.12), it is obvious that, at low current (60 A) TiC assorted with very small amount of iron and during solidification produces spherical shape

structure. However, at higher current (100 A), TiC particles melted along with the steel substrate, dissipated inside the melt pool and solidified as dendritic, block or flower shape structure.

5.3.2 XRD analysis

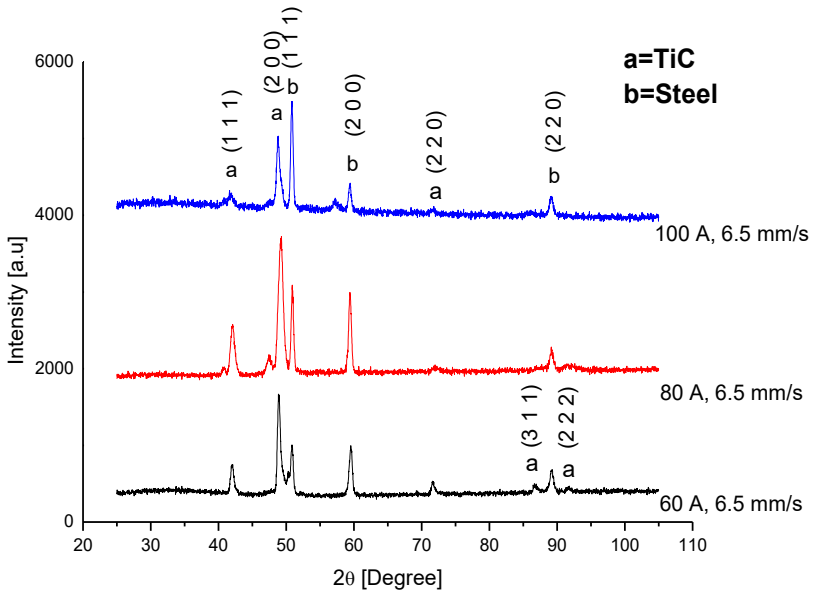

Fig. 5.13: XRD pattern of TiC coating on AISI 304 stainless steel substrate processed by TIG cladding with scan speed of 6.5 mm/s and different current

Fig. 5.13 represents the XRD pattern of the coated AISI 304 stainless steel surface processed with 6.5 mm/s scan speed and different current setting. The plot indicates that TiC and steel are the major phases present in the coating surfaces processed at the various current condition. No significant peak of other intermetallic compounds was witnessed from the plot, which indicates that no reaction occurred between TiC and AISI 304 austenitic steel during the TIG cladding process. Careful observation of the XRD pattern revealed that intensity of TiC peak is higher for the sample processed with 60 A current, than those of the samples treated with 80 and 100 A current, and the intensity of the peaks for steel increases with the increase in processing current. The semi-quantitative analysis performed based on the peak intensity of the individual phases indicate that the relative percentage of TiC for the samples processed with 60, 80 and 100 A current are 53.61, 47.45 and 33.96 % respectively. Thus, it is clear that amount of TiC on the coating surface reduces with the increase in processing current during the coating process. The reduction in the quantity of TiC with the increase in current is consequent with the result of EDS analysis as depicted in Table. 5.4. Gibbs free energy of formation of TiC is lower compared to Ti-Fe or Ti-Ni

(Li et al., 2015; Zhong et al., 2011). Therefore, the probability of formation of any intermetallic compound like Ti-Fe or Ti-Ni is very low in the considered TiC-steel system. During TIG cladding, TiC precipitates from the melt pool at the time of solidification which restricts the formation of any other compounds of Ti or diffusion of carbon from TiC to the steel substrate (Verezub et al., 2009).

5.3.3 Micro-hardness

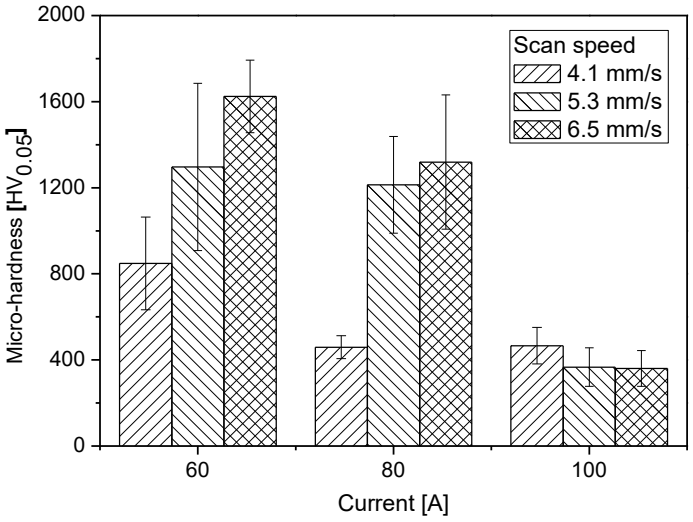

Fig. 5.14: Average micro-hardness of the coating produced at different current and scan speed

Micro-hardness values of the TiC coating were measured at the cross section by Vickers micro-indentation hardness tester. Average value of the micro-hardness was calculated from 10 readings taken randomly at the coating cross-section and plotted against the used scan speed for different samples as shown in Fig. 5.14. The graph indicates a large variation in the hardness value when current changes from 60 to 100 A. The graph also revealed that the hardness value for the samples processed with 60 and 80 A current, exhibits high average hardness i.e. in the range of 800 to 1600 $HV_{0.05}$. However, samples processed with 100 A current, which produced almost uniform metal matrix composite structure exhibit relatively lower hardness value, i.e. in the range of 360 to 470 $HV_{0.05}$.

As already described, at lower current (60 A), due to low heat input, a dense TiC layer with a negligible dilution of steel substrate formed (Fig. 5.3). High concentration of hard TiC particles is the key reason for the higher hardness of the coating produced at 60 A current. As current increases to 80 A, owing to relatively larger heat, TiC particles partially diluted and produces a mix type structure that contains hard TiC zone, as well as softer TiC-

steel MMC zone (Fig. 5.4). As a result, the average hardness value of the coating reduces for the increase in current from 60 to 80 A. Again, for using 100 A current, high heat input causes melting of pre-placed TiC powder as well as the upper layer of steel substrate that leads to the formation of TiC-steel MMC structure on the entire coating surface (Fig. 5.5). Higher percentage of softer steel matrix present in the coating zone leads to a relatively low hardness of the coating produced at 100 A current. Uniform distribution of TiC in the steel matrix causes a uniform micro-hardness value on the coating layer. On the other side, variation in the hardness value is significantly higher for using 60 and 80 A current that is mainly due to the non-uniform structure of the surface layer (TiC layer + TiC–steel MMC layer). It is also observed from the graph that, for using lower welding current (60 and 80 A), when a mixed type structure is formed, average hardness value increased with the increase in scan speed. However, for high current (100 A), when uniform MMC type layer is produced, average micro-hardness value decreases with the increase in scan speed. It is revealed from the EDS analysis of the microstructure that, for the samples processed at 100 A current, with the increase in scan speed, weight percentage of Ti decreased, or TiC concentration on the coating layer became lower. Since hard TiC is the key reason for the higher hardness of the coating, it is postulated that for 100 A current average micro-hardness value declined with the increase in arc scan speed. Again EDS analysis describes that for lower current setting, the percentage of Ti in the coating layer increases with the increase in scan speed, which resulted in superior hardness. At low scan speed (4.1 mm/s) due to higher heat input, the entire TiC powder layer melted and mixed in steel substrate within a specified depth, and during cooling produces dendrite structure that causes a relatively higher percentage of TiC in the coating layer. However, at relatively higher scan speed, the entire preplaced TiC powder did not melt properly to blend with the steel substrate, and the percentage of TiC at the uniformly solidified zone is less than that of sample processed with low scan speed. This phenomenon has been confirmed from the EDS analysis. Further, local micro-hardness value at different type of structure (as marked in Fig. 5.3 and 5.4) of the coatings produced at different condition has been measured as depicted in Table-5.5. From the table, it is worth pointing out that hardness value at the dark zones (marked as 'a_1') consisting highly dense TiC particles is significantly higher than the hardness value of the light shaded MMC zone (marked as 'a_2'). The calculated average hardness value found lower than the dark zone and higher than the MMC zone. The variation of hardness value found larger for the coating layer comprising an inhomogeneous structure than the layer consisting a uniform structure.

Table 5.5: Local hardness value for the selected coating consisting non-uniform morphology

Fig. No.	**Selected Area**	**Hardness Value ($HV_{0.05}$)**
5.3a	a_1	1281, 1220, 815
	a_2	707, 516, 587
5.3b	a_1	1652, 1424, 1283
	a_2	342, 452
5.3c	a_1	1825, 1630, 1511
5.4a	a_2	374, 358, 406
5.4b	a_1	760, 1431,1345
	a_2	352, 415, 398
5.4c	a_1	1632, 1469, 1552
	a_2	365, 487

5.3.4 Sliding abrasive wear test

Fig. 5.15 shows the variation of abrasive wear in terms of height loss of the pin prepared from the coated samples processed at different current and scan speed condition, during pin-on-disc sliding abrasive wear test. The graph indicates that the abrasive wear (height loss) of the samples is varying from approximately 0.01 to 0.11 mm depending on the current and arc scan speed. At similar wear test condition abrasive wear or height loss of as received AISI 304 steel pin was found approximately 0.5 mm. This indicates that the produced TiC or TiC–steel composite coating exhibits five to fifty times (depending on the processing condition) higher abrasion resistance than the substrate material. It is also comprehended from the graph that, wear loss is comparatively low for the coating produced with 60 A current, and maximum for the coating processed with 80 A current. The sample produced with 100 A current exhibited relatively lower abrasive wear than those of the coating produced with 80 A, but higher than the coating produced with 60 A current. Further, the graph also indicates that for 60 and 80 A current, wear loss is minimum for 6.5 mm/s scan speed, and increased for the sample processed with lower arc scan speed. For the coating produced with 100 A current, no specific trend of wear against scan speed was observed. Due to the formation of highly dense TiC layer at 60 A current, hardness of the coating become very high, that make the coating extreme resistance to abrasive wear against SiC abrasive paper.

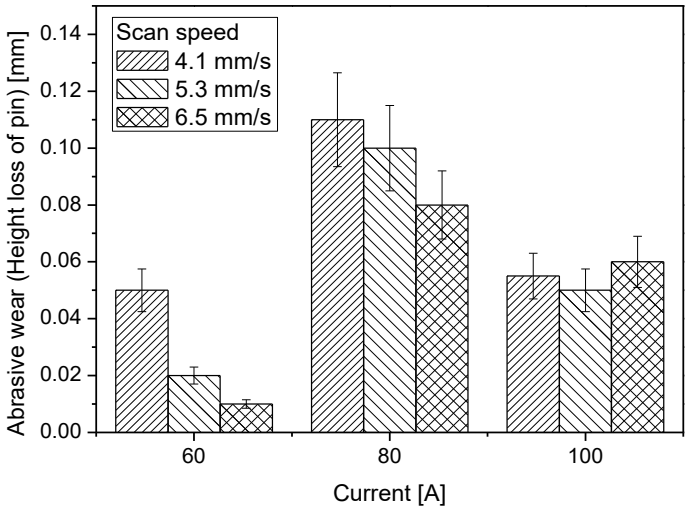

Fig. 5.15: Variation of abrasive wear (height loss) for the TIG coated samples processes at different current and scan speed condition, after sliding wear test

Fig. 5.16(a-c) show the wear behavior or height loss, at the time of test for the TiC coated samples processed with different scan speed and current of 60, 80 and 100 A respectively. The graph (Fig. 5.16a) for the samples processed with 60 A current indicate almost uniform and steady height loss with time. However, for the sample processed with 80 A current, wear rate is found relatively higher than those of the sample processed with 60 A current, and the variations of height loss against time are also uneven. For the samples processed at 80 A current, it is revealed from the microstructure analysis that, the coating structure is not uniform throughout the track width and depth, and TiC particles are not bonded uniformly with the steel substrate. Thus, during wear test, for using SiC abrasive paper as counter-body and 30 N load on pin type sample, along with the abrasive wear of the coating, TiC particles those are not bonded properly with the steel matrix were plowing out. Further, due to non-uniformity of the coating, the region where TiC concentration is very less, wear rate became faster, which causes an overall escalation in height loss of the coated samples. In Fig. 5.16b, abrupt augmentation in wear rate is clearly perceptible for the samples processed with 80 A current. However, uniform variation in the height loss with time can be observed for the sample processed with 100 A current and different scan speed in Fig. 5.16c. The uniform metal matrix composite microstructure of the coated samples processed with 100 A current indicate higher wear loss than the dense TiC layers, those were made with 60 A current. However, because of steady removal of the MMC coating due to sliding abrasive wear a lower value of wear compared to the samples processed with 80 A current was witnessed.

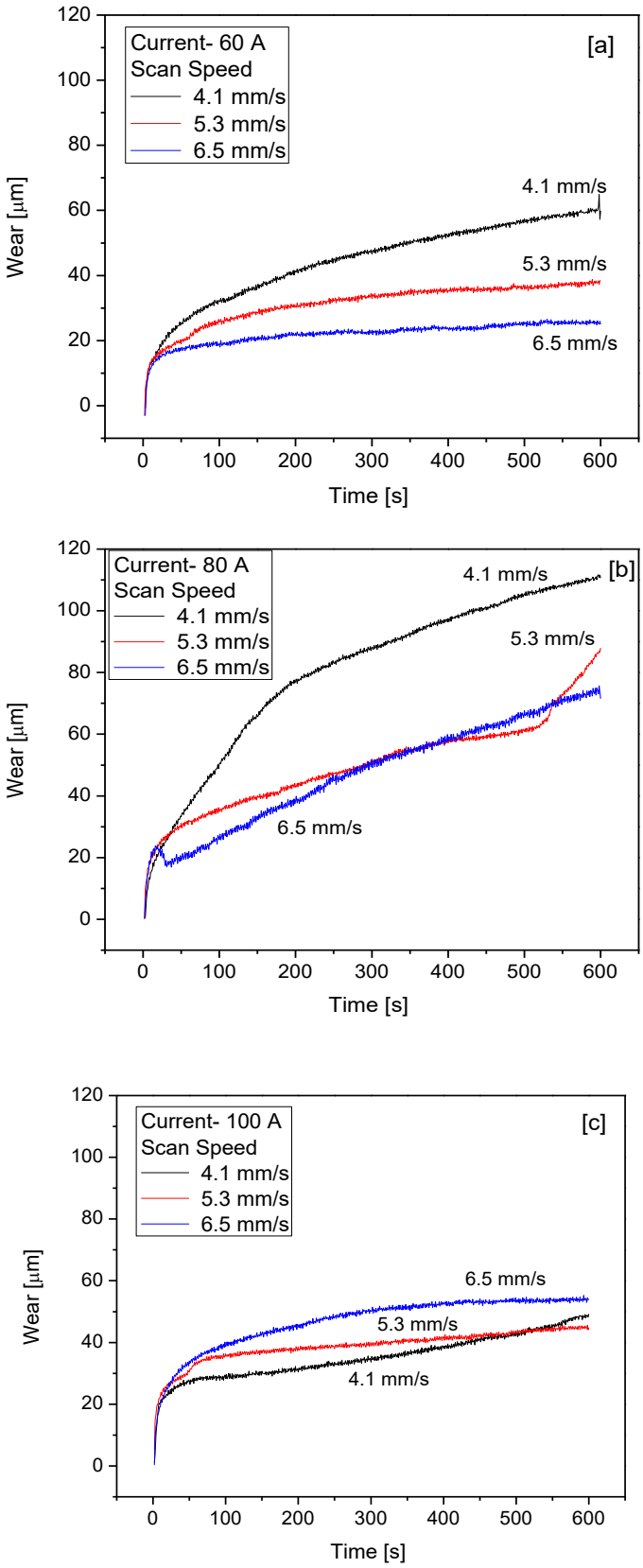

Fig. 5.16: Sliding abrasive wear behavior or height loss against the time elapsed during wear test of the TIG coated samples processed with current of (a) 60 A, (b) 80 A and (c) 100 A and different scan speeds

Careful observation of the graph (Fig. 5.15) points out that the coating produced at 80 A current shows higher hardness value compared to the coating produced at 100 A current. However, wear rate for the coating produced at 80 A current found higher than the wear rate of the coating produced at 100 A current. It is worth pointing out that wear resistance of the coating depends not only on the hardness value but also on the structure of the coating, uniformity in the microstructure, and bonding strength of the coating with the substrate. From the SEM images (Fig. 5.4) it was found that coating produced at 80 A current exhibits inhomogeneous structure, consisting hard TiC layer as well as relatively soft MMC structure. Higher wear rate for the samples processed with 80 A current attribute to non-uniform distribution of TiC particles in the coating and improper bonding of the coating material or non-uniform layer formation on the substrate surface. These type of structure may cause the bulk removal of material at high load and sliding speed condition and causes higher wear rate. Conversely, the morphology of the coating produced at 100 A current (Fig. 5.5) shows almost uniform structure, where TiC particles distributed uniformly in the matrix. The hardness value of this structure is relatively less due to the presence of softer matrix material. However, uniform distribution of TiC particles and stronger bond between the particles and steel matrix made these coatings relatively higher wear resistant compared to coating produced with 80 A current.

SEM images of the coated surface (produced with a scan speed of 6.5 mm/s and different current) after sliding abrasive wear test are shown in Fig. 5.17. The micrographs demonstrated that for the coating with 60 A, highly dense TiC particles are embedded in the white steel matrix. Due to the high hardness of these TiC particles, abrasion wear against SiC paper is very less and no scratch mark on the coated surface after wear test was observed. However, some TiC particles have been removed out from the matrix due to plowing action. As shown earlier, in the case of the coating produced with 80 A current, a mixed type zone containing MMC structure as well as highly dense TiC region formed. Consequently, removal of this coating was executed by abrasive wear as well as plowing of TiC particles. On the soft white matrix, scratch by SiC particle or by expelled TiC particles from the coating can be seen. On the other side, for the coating with 80 and 100 A current, intensity of dark TiC particles is relatively less, and scratch marks due to the impression of SiC abrasive are clearly visible.

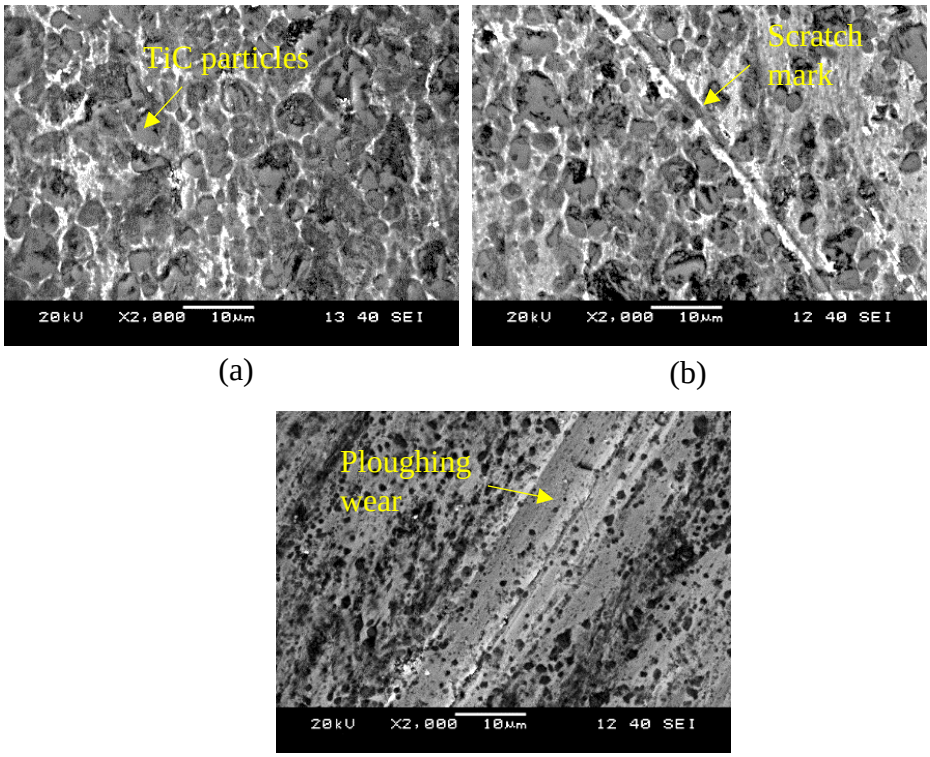

Fig. 5.17: SEM images of the coated surface after sliding abrasive wear test, produced with scan speed of 6.5 mm/s and current of (a) 60 A, (b) 80 A and (c) 100 A

5.3.5 Coefficient of friction

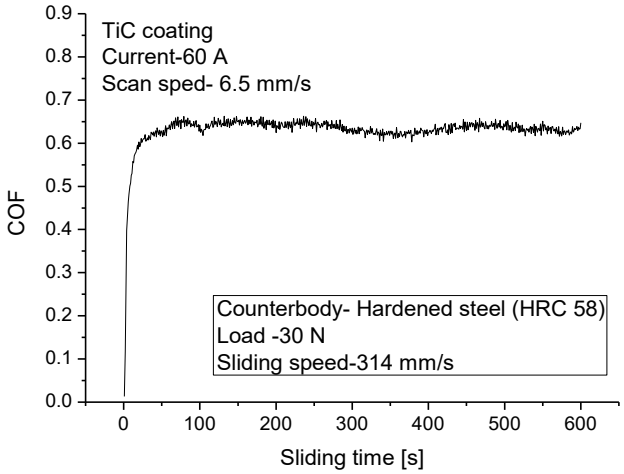

Fig. 5.18: Coefficient of friction (against hardened steel, HRC 58) of TiC coating produced by TIG cladding process with 60 A current and 6.5 mm/s scan speed

In order to measure the coefficient of friction (COF) value of the TiC coating produced by TIG cladding process, a specific sample was considered in which density of TiC in the coating layer is very high. Therefore, the sample produced with 60 A current and 6.5 mm/s

scan speed was selected. Coated pin of the selected sample was slide against hardened steel (HRC 58) disc with a sliding speed of 314 mm/s, under 30 N normal load.

Fig. 5.18 shows the variation of COF of the TiC coated pin against hardened steel disc. The plots clearly indicate that the steady state COF value for the TiC coated sample produced by TIG cladding process is approximately 0.65. However, comparing the COF value of the bare AISI 304 steel, as described in Chapter-4, it is clearly seen that COF value of TiC coating significantly reduces as compared to the COF of the as received steel under similar test condition.

5.4 Outcomes

TiC or TiC–steel composite coating has been successfully applied on AISI 304 steel by using TIG cladding process. Depending on the applied current and scan speed, TiC either deposited on the steel substrate as a dense layer with very low dilution steel or formed a TiC particle reinforced steel matrix composite layer.

From the coating layer geometry, it can be concluded that the melt pool depth and width decreases with the reduction of heat input during the arc scanning. At low current (60 A) and high scan speed (6.5 mm/s), owing to low heat input partially melted dense TiC layer produced over the steel substrate. In contrast at high current (100 A), as a result of high heat input, TiC powder melted and diffused into the steel substrate due to the sturdy convective flow of the molten pool. This leads TiC to mix uniformly and dispersed at the upper layer of steel substrate during solidification. At intermediate current (80 A), and low current (60 A) higher speed (4.1 and 5.3 mm/s) combination, the heat input becomes insufficient for mixing the TiC powder inside the steel substrate and confining the convective flow of molten metal. Hence, a mix type structure consisting dense TiC layer and TiC-steel MMC structure formed. Furthermore, due to inadequate heating, the convective flow of molten metal restricted and trapped the blown Ar gas used for shielding the arc, which leads to the formation of large voids specifically at the coating-substrate interface.

The micro-hardness value of the TiC coating produced with lower current (60 A) and high scan speed extended up to 1600 $HV_{0.05}$. Nevertheless, for the sample processed with high current and slow scan speed due to dilution of TiC in the steel matrix, a reduced hardness value observed. Additionally, because of non-uniform coating morphology, the variation of hardness value found larger for the coating comprising an inhomogeneous structure.

Sliding abrasive wear test of the TIG cladded TiC coating shows five to fifty times improvement in the wear resistance than the as received AISI 304 steel substrate. Owing to the high concentration of TiC and corresponding high hardness value of the coating, abrasive wear of the coating accomplished in low current and high scan speed combination found very low. Conversely, coating processed with high heat input (high current and low scan speed combination), the abrasive wear become extreme due to the removal of softer steel matrix at a higher rate. In addition, COF of the coating against hardened die steel (HRC 58) found 0.65, which is lower than the AISI 304 steel under similar test condition.

Chapter 6

Deposition of TiC-Ni composite coating on AISI 304 steel by TIG cladding process

In this phase of the experiment, TiC–Ni composite coating was produced by preplacing a powder mixture of TiC and Ni on AISI 304 steel substrate and subsequent TIG melting process. A hard and wear resistance composite coating with improved bonding between the TiC particles and the steel matrix was obtained due to the incorporation of Ni powder. The X-ray diffraction (XRD) analysis revealed the presence of TiC and some intermetallic of Ni and Ti in the coating; those are responsible for the superior interfacial bonding and consequently higher wear resistance of the coating. The microstructure of the coating analyzed through FESEM micrographs revealed that the applied current has a significant influence on the microstructure and corresponding mechanical properties of the coating. Based on the heat input, dilution of TiC on Ni-steel matrix regulate the micro-hardness and corresponding wear properties of the coating. Pin-on-disc type sliding abrasive wear test performed against alumina abrasive disc shows that the TiC-Ni coating exhibit up to seventy times better wear resistance than the AISI 304 steel substrate.

Keywords: TiC-Ni composite; TIG cladding; Micro-hardness; Abrasive wear; Wear resistance

6.1 Introduction

Ceramic particle reinforced metal matrix composites (MMCs) retaining high hardness, strength, stiffness and wear resistance compared to its matrix base, along with preeminent toughness than the monolithic ceramic or ceramic composites (Emamian et al., 2012a). Berger (2015) described that a layer of ceramic particle reinforced MMC on the base material surface produced by high energy density deposition methods like laser cladding/alloying, or TIG melting/cladding can improve the surface properties of the component without affecting its bulk characteristics. So far, laser cladding/alloying have extensively used, to create a thick coating of TiC or TiC reinforced composite on various substrate materials containing enriched mechanical properties (Hong et al., 2015; Sahoo and Masanta, 2015). It was revealed that TiC reinforced coating produced by TIG

cladding/alloying process exhibited significant improvement in the hardness and wear resistance than the steel substrates (Wang et al., 2006a; Mridha and Baker, 2015; Rasool et al., 2015). However, it was also found that major challenge associated with the fabrication of TiC reinforced steel composite coating is to attain proper interfacial bonding, as the solubility of TiC in steel is extremely low and frequently produces undesirable intermetallic compounds (Man et al., 2002). From the recent works, it is revealed that, to obtain an appropriate bond between the substrate and the reinforced ceramic particles, interfacial materials like Ni and Co, those are retaining high wetting property with both TiC particles and steel matrix need to provide (Nowotny et al. 2014; Desale et al., 2009). Several attempts have been made so far to enhance the strength of the ceramic reinforced MMC coating by incorporating Ni as binding material using different high energy density process (Liu et al., 2012; Viswanathan et al., 2007; Li et al., 2009). From the literature, it is revealed that the effect of Ni addition in the TiC composite coating is common by laser cladding process. Nevertheless, no such studies on TiC-Ni coating produced by TIG cladding process, has been reported till date.

Therefore, with an objective to develop a hard and wear resistance coating with a strong interfacial bond between substrate and coating material and enhanced mechanical properties, in the present work, TiC-Ni composite coating has been produced on AISI 304 steel substrate using the TIG arc heat source. Effect of TIG current and arc scan speed on the microstructure of the produced composite coating has been analyzed in depth. To investigate the mechanical behavior of the produced TiC-Ni composite coating, micro-hardness value was measured and sliding abrasive wear test was carried out against Al_2O_3 grinding disc. A comparative study between TiC coating and TiC-Ni coating prepared in similar condition has also been accomplished to reveal the effect of Ni addition with TiC powder.

6.2 Experimental procedure

For this phase of experiment, the surface of AISI 304 stainless steel plate of 100×45×8 mm^3 was prepared by polishing and cleaning as described in Chapter-3. Commercially pure Ni and TiC powders as per the specification tabulated in Table 3.2 in equal weight ratio mixed thoroughly with a specific amount of acetone and a polyurethane based organic binder to prepare a semi-solid solution. This semi-solid solution was then dispersed on the steel surface uniformly and dried at room temperature to evaporate the acetone and cure the

binder. To deposit a predefined thickness, the volume of the powder require to cover a specific area (here, 100 mm × 45 mm × 0.35 mm) was calculated and accordingly the amount of powder was mixed with the acetone and polyurethane based organic binder. Thus, TiC-Ni preplaced layer of approximately 350±20 μm thickness was obtained on the steel surface.

Processing parameters i.e. welding current and scan speeds were varied to obtain an optimum condition that enables to produce a feasible coating layer having sufficient bond with the substrate. Detail of the processing conditions is indicated in Table 6.1. On each pre-coated steel substrate, single line scan of TIG arc was executed as per the experimental planning demonstrated in Table 6.2. The schematic diagram of the TIG cladding process to produce TiC-Ni coating is illustrated in Fig. 6.1. The figure shows that due to the scanning of arc over the pre-deposited TiC-Ni powder layer, composite coating forms on the steel substrate.

After performing the TIG cladding, the coated samples were cleaned and cut by wire EDM for further analysis. The cross-section of the coated samples was metallographically polished as detailed in Chapter-3 to analyze the microstructure of the coating and to measure the micro-hardness value at the cross-section of the coating. For this phase of the experiment, micro-hardness value was measured using LECO micro-hardness tester (LECO-LM810) with 50 gf load and 10-second dwell time. To assess the wear rate and tribological behavior of the produced coating, 3 mm diameter pin was extracted from each TiC-Ni coated track by wire cut EDM. These coated pins were then slid against fine grade Al_2O_3 abrasive disc rotating on a pin-on-disc type friction and wear test rig as per ASTM G99 standard (Make: Magnum). Schematic diagram of the sliding abrasive wear test setup is illustrated in Fig. 6.2. Conditions used for this pin-on-disc type sliding abrasive wear test are mentioned in Table 6.3. During wear test, combined height loss of the pin and abrasive disc against the test time was monitored through a data acquisition system. Further, after wear test, height loss of the coated pin was measured by using a vernier caliper to obtain the actual height loss of the pin. After the sliding abrasive wear test, the worn out surfaces of TiC-Ni coatings were analyzed through scanning electron microscopy (JEOL, JSM-6084LV) to assess its wear behavior. The X-ray diffraction (XRD) patterns of the TiC-Ni coating surfaces were obtained from BRUKER D8 ADVANCE diffractometer, using cobalt target (λ= 1.79026 Å).

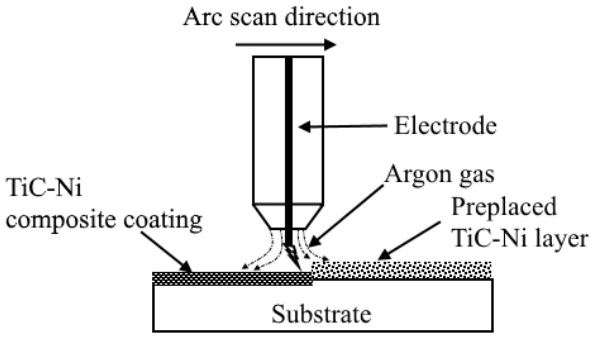

Fig. 6.1: Schematic diagram of TIG cladding process

Table 6.1: TIG processing conditions

Electrode	Thoriated Tungsten (2.4 mm dia)
Electrode–work piece distance	3 mm
Polarity	DCEN
Arc Voltage	12-15 V
Shielding gas	Argon (10 l/min)

Table 6.2: Experimental table for TIG cladding

Sl. No	**Current (A)**	**Speed (mm/s)**
1	40	5.3
2	40	6.5
3	50	5.3
4	50	6.5
5	60	5.3
6	60	6.5
7	80	5.3
8	80	6.5

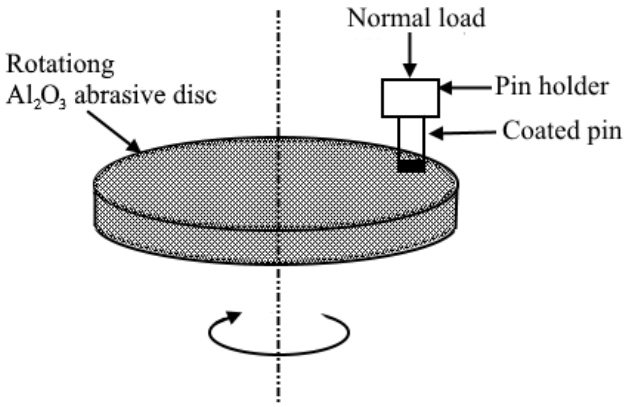

Fig. 6.2: Schematic diagram of pin-on-disc sliding abrasive wear test set-up

Table 6.3: Operating condition for Pin-on-disc type sliding abrasive wear test

Pin diameter	3 mm
Normal load	10 N
Disc rotation speed	300 rpm
Track radius	10 mm
Sliding velocity	314 mm/s
Test duration	5 minutes
Abrasive medium	Al_2O_3 abrasive disc

6.3 Results and discussion

6.3.1 Microstructural analysis

Fig.6.3 and Fig.6.4 show the FESEM images at the cross-section of the TiC-Ni composite layer produced on AISI 304 steel substrate by TIG cladding process for different current setting (i.e. 40, 50, 60, and 80 A) and arc scan speed of 5.3 and 6.5 mm/s respectively. Corresponding high magnified FESEM images of the selected region are also shown in Fig. 6.5 and Fig. 6.6. The images revealed that a thick and almost uniform layer of dark particles reinforced in a white shaded matrix formed on the steel substrate for using 40 to 60 A current at both scan speed condition. However, at relatively higher current (60 A), the intensity of the dark particles are found detrimental with a non-uniform distribution of the particles. It is evident that TiC particles are diluted in the steel substrate and distributed to a larger depth when the coating was produced at higher current (80 A). It is worth pointing out that the heat input in TIG cladding process depends on the applied current as per the Eqn. 3.1 suggested by Mridha and Baker (2015).

In TIG cladding process, the pre-deposited TiC-Ni layer melted and a convective flow of molten layer followed, that resulted in melting of a thin layer of substrate surface along with the TiC-Ni powder layer. Thus, a dense and uniform layer of TiC along with Ni and distinguishable amount of steel matrix produced on the steel substrate. It can also be noted that at lower current (40 to 60 A), the heat input during TIG cladding process is reasonably less, which may lead to partial melting of the TiC powder in conjunction with the complete melting of Ni powder. Thus, the produced coating shows large size TiC particles within the matrix. In contrast, the coating processed with higher current (80 A), induces higher heat in the processed region, resulted in full melting of TiC particles. During solidification, these molten TiC particles are fragmented into a smaller size and distributed in the matrix of steel-Ni solid solution. Owing to excess heat, these tiny TiC particles are

diffused into the steel substrate to a larger depth. This phenomenon is more clearly observed for the coating produced with lower scan speed, where input heat energy is relatively higher than those of coating produced at higher scan speed.

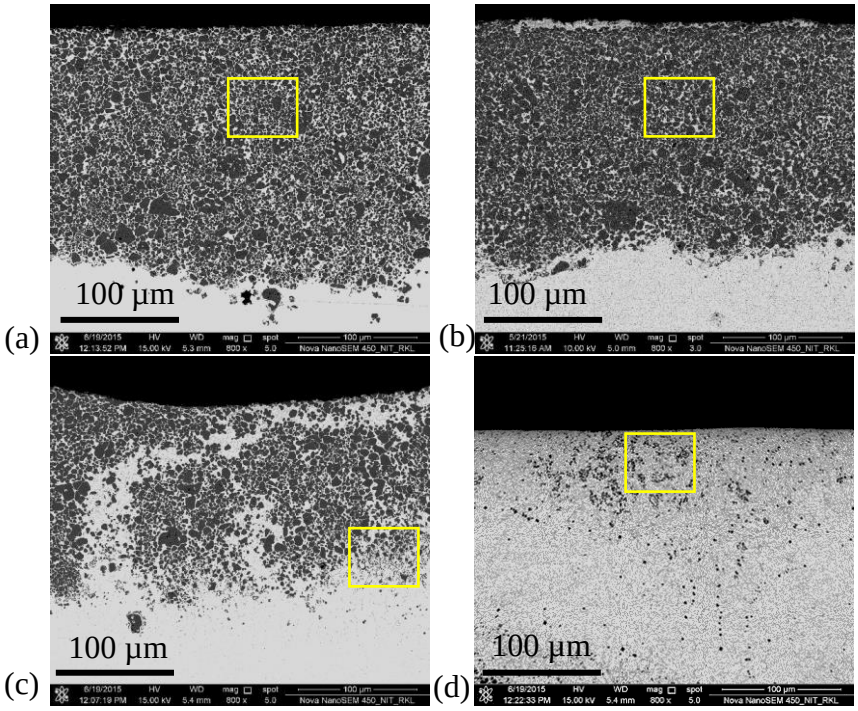

Fig. 6.3: FESEM micrographs at the cross-section of TiC-Ni coated AISI 304 steel sample produced by TIG cladding process with scan speed of 5.3 mm/s and current (a) 40 A, (b) 50 A, (c) 60 A, (d) 80 A

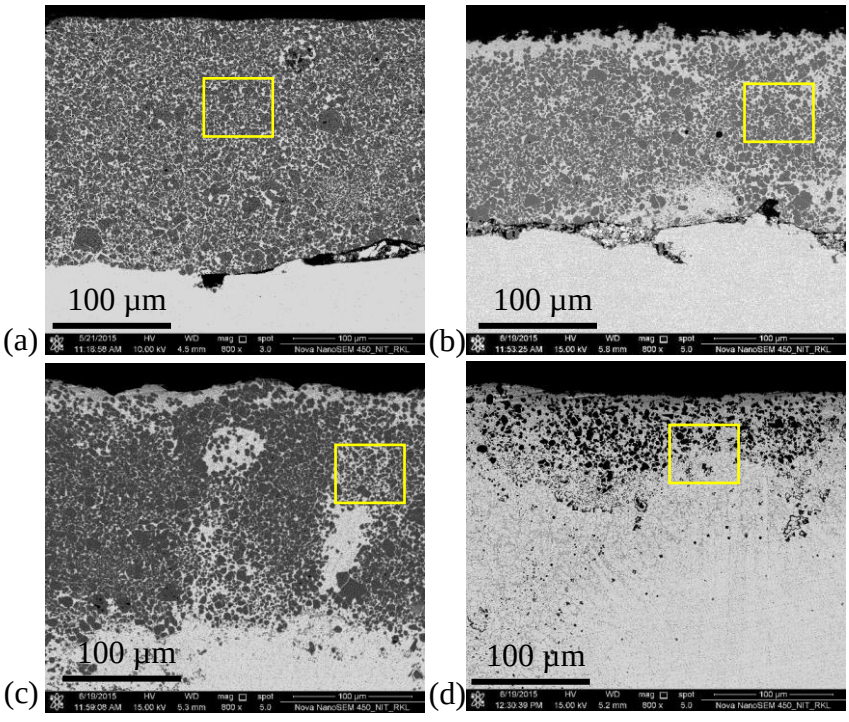

Fig. 6.4: FESEM micrographs at the cross-section of TiC-Ni coated AISI 304 steel sample produced by TIG cladding process with scan speed of 6.5 mm/s and current (a) 40 A, (b) 50 A, (c) 60 A, (d) 80 A

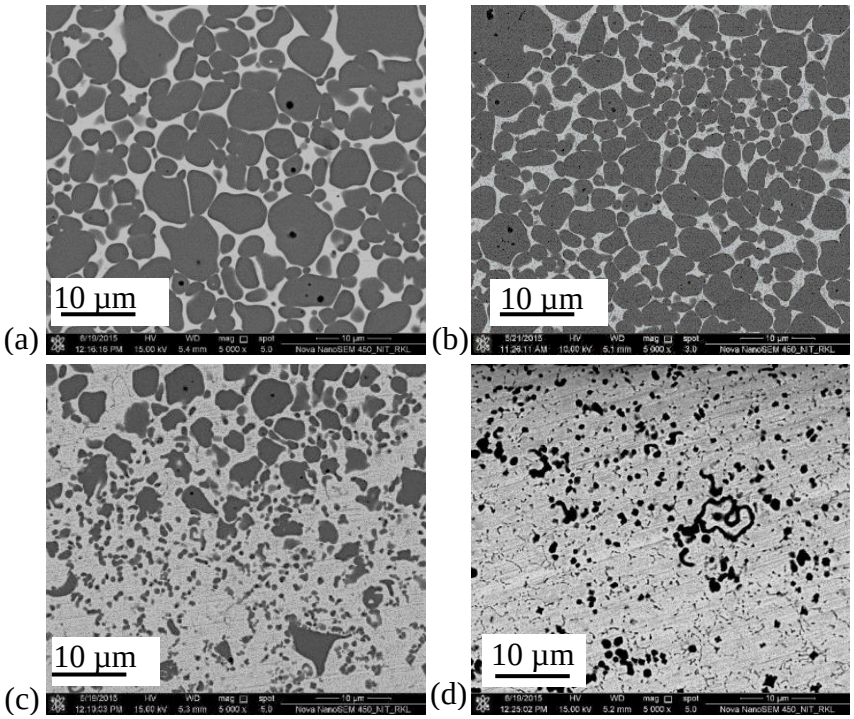

Fig. 6.5: High-magnified FESEM images corresponding to marked portion of Fig. 6.3 i.e. TiC-Ni coating prepared by TIG cladding process with scan speed of 5.3 mm/s and current (a) 40 A, (b) 50 A, (c) 60 A, (d) 80 A

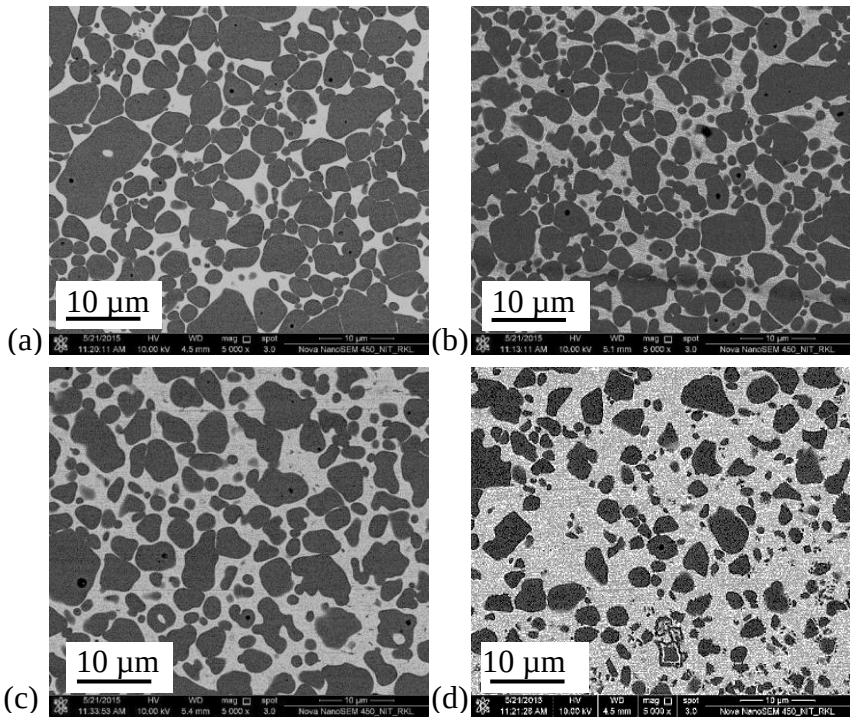

Fig. 6.6: High-magnified FESEM images corresponding to marked portion of Fig. 6.4 i.e. TiC-Ni coating prepared by TIG cladding process with scan speed of 6.5 mm/s and current (a) 40 A, (b) 50 A, (c) 60 A, (d) 80 A

Detail EDS analysis of the coating produced with 50 A current and 6.5 mm/s scan speed as shown in Fig. 6.7 revealed that the dark layer of the coating is primarily concentrated with Ti and C, along with the traceable amount of iron. Conversely, the substrate region (below the dark coating layer) was found rich in iron and chromium; and a low concentration of Ni was detected in both coating and the substrate region.

EDS mapping of the high magnified coating zone (Fig.6.8) corresponding to Fig. 6.4a revealed that the dark particles those are dispersed in the coating layer are composed of highly concentrated Ti and C along with the traceable amount of Ni; whereas, the white matrix region is composed of Fe, Cr, and Ni. Thus, it may be concluded that the dark particles are TiC, those are reinforced in the steel matrix mixed with the additional Ni powder. In the present coating process, Ni powder was added with an expectation to attain TiC-Ni metal matrix composite layer. However, the EDS analysis revealed that Ni is distributed uniformly all over the coating surface. This may be attributed to the result of partial dilution of Ni within TiC particles or formation of Ti-Ni intermetallic that mixed with the steel matrix. Further, due to the higher density of Ni, it is possible that some amount of molten Ni precipitated or diffused in the steel substrate at elevated temperature. Hence, the distinction of additional Ni, with the Ni present in the steel substrate is difficult. It was reported in the earlier literature that, the diffusion coefficient of Ni in iron at 1230 ^{o}C during sintering is very high. Thus, Ni and γ-Fe are miscible in any proportion at high temperature. Yi et al. (2013) in their work showed that this phenomenon resulted in complete diffusion of Ni in the iron matrix and consequently the Ni phase in the composite virtually absent. Further, the solid solubility of Ni in α-Fe is much higher, which may also cause absent of Ni phase in the composite at room temperature.

From the SEM image (Fig. 6.5), it is also observed that for the coating produced at higher scan speed (6.5 mm/s) and low current (40 and 50 A), an interfacial gap between the coating and substrate was formed. Heat input for the coating produced in this low current and high scan speed combination is relatively lower, which may not be sufficient to melt the surface of the base material. As a result, the bond between the coating and the substrate surface become inadequate, which leads to the formation of an interfacial gap between the coating and substrate. Further, owing to mismatch in thermal and mechanical properties of the coating and substrate material, the crack may also appear at the coating-substrate interface. It is expected that, due to high scan speed, the cooling rate of the melt pool become very high, that induces residual stress in the coating layer and leads to form interfacial

cracks. Formation of interfacial crack was reported earlier by Katipelli et al. (2000a) for producing TiC coating on Al substrate by laser surface modification. Since at low current and high scan speed, the cooling rate of the molten coating material is very high, the consequence may be considered comparable to the laser coating process, which usually generates residual stress on the coating and corresponding crack formation observed at the coating-substrate interface.

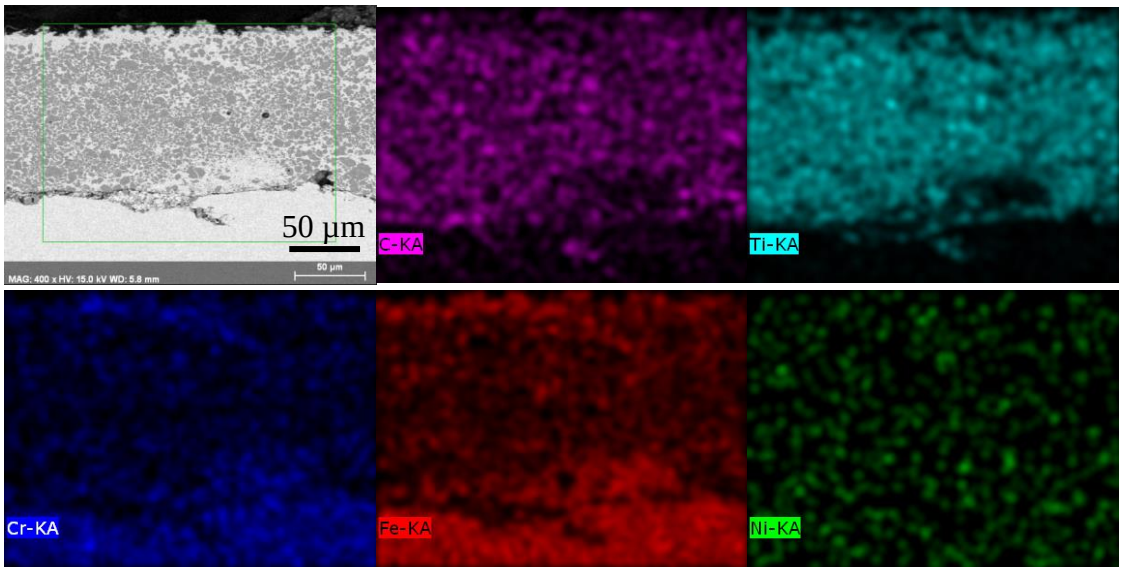

Fig. 6.7: EDS elemental mapping of the TiC-Ni coating produced with 50 A current and 6.5 mm/s scan speed by TIG cladding process

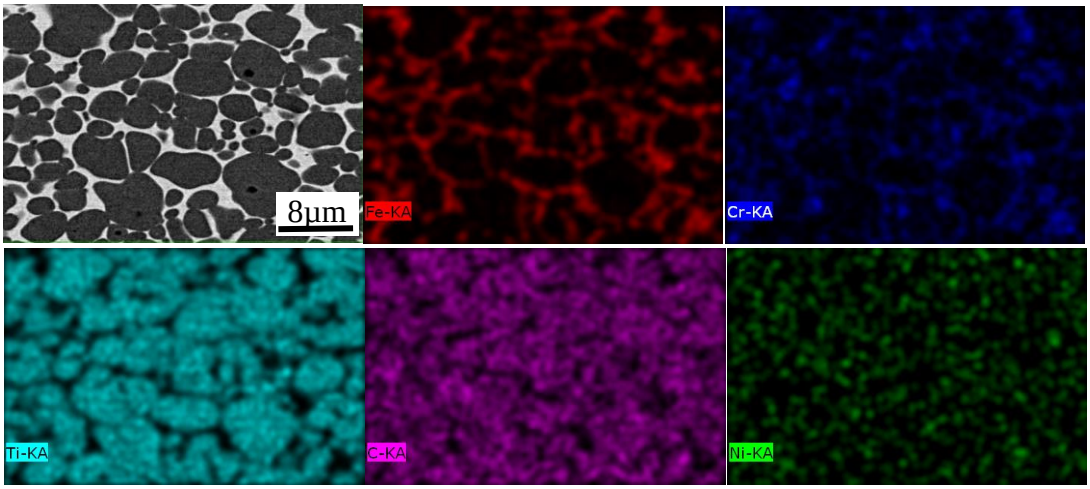

Fig. 6.8: EDS elemental mapping of the dark zone of the coating produced at 40 A current and 5.3 mm/s scan speed (corresponding to Fig. 6.5a)

Morphology of the TiC particles in the coating layer, which may affect the coating properties, largely governs by the amount of heat supplied during the coating process. High magnified FESEM images (Fig. 6.5 and 6.6) of the coating produced with low heat supply condition i.e. 40-50 A current for both scan speed condition and 60 A current, 6.5 mm/s

scan speed show highly dense spherical shaped TiC particles dispersed in the matrix. As discussed earlier, low heat input in this condition, restrict the complete melting of TiC particles. Due to partial melting, sharp edges of TiC particles melted and transformed into spherical shaped. The molten part of the TiC particles after solidification produced smaller spherical shaped structure and dispersed in the coated layer. The coating layer created at higher heat input condition i.e. 60 A current at low scan speed (5.3 mm/s) and 80 A current, undergoes melting and re-solidification of TiC particles in the steel-Ni matrix. Thus, the fine nucleated particles shaped are distributed uniformly in the matrix.

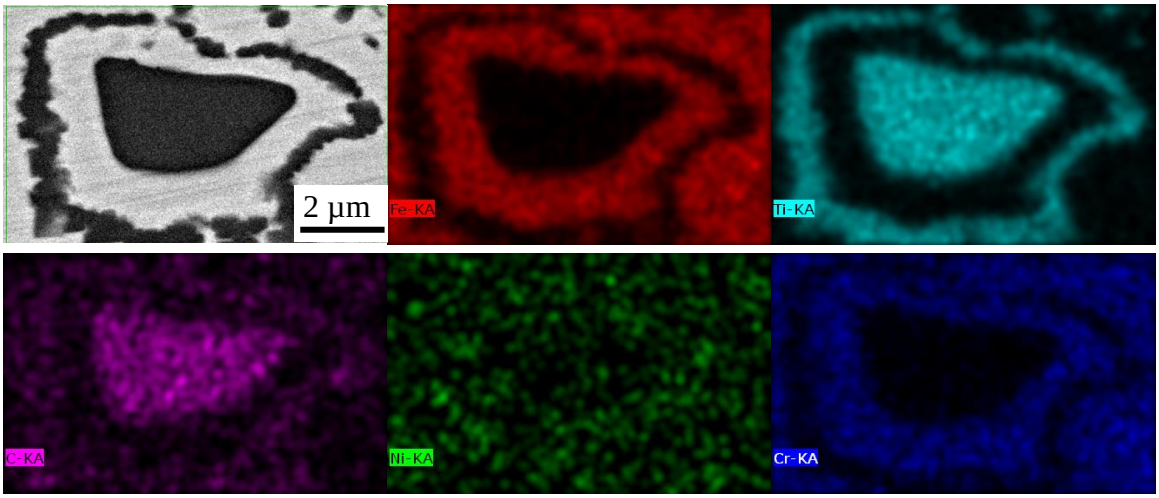

Fig. 6.9: High magnified FESEM image and corresponding EDS mapping of TiC-Ni coating produced by TIG cladding process with 80 A current and 5.3 mm/s scan speed

High magnified image (Fig. 6.9) of the coated zone processed with 80 A current and 5.3 mm/s scan speed demonstrate the nucleation of TiC inside the steel-Ni matrix. The image shows a cluster of re-solidified TiC particles those have formed a thread-like structure surrounding the main TiC particle. The EDS analysis revealed that the dark particles and thread-like structure are rich in Ti and carbon, and matrix part is a mixture of Fe, Cr, and Ni. The traceable amount of Ni observed inside the TiC particles. Here the edges of the TiC particles melted and mixed in the steel-Ni matrix. During solidification, nucleation of the molten TiC occurred and produced the thin tiny structure. At high temperature, TiC is partially soluble in Ni, which may responsible for the amalgamation of the nucleated TiC particles and produces a thread like structure. A similar phenomenon of variation of TiC morphology during solidification for laser surface alloying process was observed by Chen and Wang (2003) in their study.

From the aforementioned discussion, it is worth to point out that TIG processing parameters i.e. current and scan speed have a significant effect on the morphology of TiC-

Ni composite coating. It is evident that at low processing current highly dense uniformly distributed TiC reinforced composite coating formed. However, with the increase in processing current, owing to larger heat input, an MMC type coating with lower percentage TiC particle reinforcement has been formed. However, the effect of scan speed on the coating morphology found insignificant within the domain of present experimental condition.

6.3.2 Micro-hardness

Average micro-hardness value of the produced TiC-Ni composite coating was calculated from ten reading measured at the cross-section of each coating produced by TIG cladding process with different parametric condition. The average micro-hardness value of the coated samples plotted against the applied current for different scan speed condition are depicted in Fig. 6.10. The graph revealed that TiC-Ni composite coatings processed with 40-60 A current exhibit average micro-hardness value in the range of 800–1300 $HV_{0.05}$. However, for the coating processed with 80 A current, the hardness value obtained in the range of 430–550 $HV_{0.05}$. The plot also indicates that the average micro-hardness value of the TiC-Ni composite coating decreases with the increase in applied current during TIG cladding process for both 5.3 and 6.5 mm/s of scan speed. It is also revealed from the graph that, the coating produced at higher scan speed (6.5 mm/s) shows relatively higher micro-hardness value with large variation (high standard deviation) than those of the coating produced with low scan speed (5.3 mm/s) for using same current setting.

Micro-hardness value of the produced TiC-Ni composite coating measured at the cross-section predominantly depends on the melt pool profile, concentration and distribution of TiC particles in the steel matrix, the size of the TiC particles in the coating, and morphology of the composite structure. The hardness value of pure TiC particle is close to 3000 HV, whereas hardness value of AISI 304 stainless steel is approximately 220 HV (Sahoo and Masanta., 2015). Thus, high density of TiC inside the coating produced at relatively low current condition is responsible for excellent micro-hardness value of the coating layer.

It is worth pointing out from the microstructure analysis that due to low heat input, TiC-Ni composite coating produced at lower current range (40–60 A), contain highly dense TiC particles in the matrix. It is observed from the SEM images (Fig. 6.5 and Fig. 6.6) that, with the increase in current, the extent of soft matrix zone also augmented, which reduces

the average hardness value of the coating. The SEM image of the coating produced with 80 A current, clearly indicates that the proportion of TiC in the steel matrix is very low, that resulted in a lower average hardness value of the coating.

The above discussion revealed that with the increase in processing current from 40 A to 80 A, the average hardness value of the TiC-Ni composite coating diminishes from 1300 $HV_{0.05}$ to 430 $HV_{0.05}$. However, with the increase in scan speed (from 5.3 to 6.5 mm/s), enhancement in the micro-hardness value observed for all the TiC-Ni composite coating produced at different current setting by TIG cladding process.

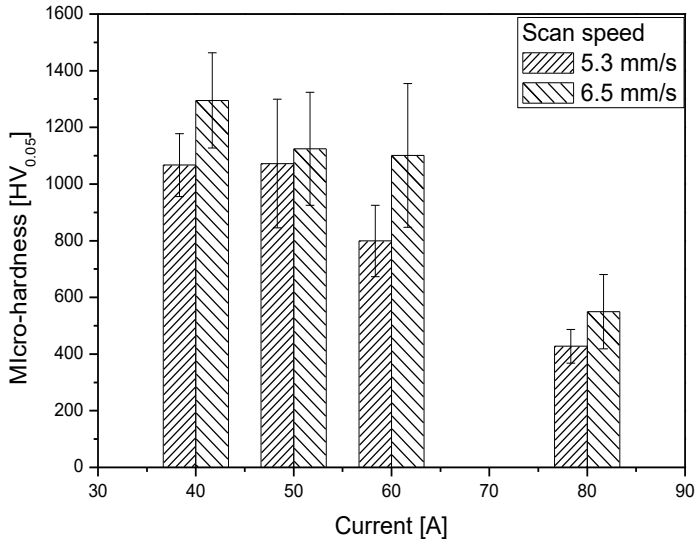

Fig. 6.10: Average micro-hardness value of TiC-Ni coating produced by TIG cladding process with different current and scan speed

6.3.3 Sliding abrasive wear

An assessment of wear behavior of the developed TiC-Ni composite coating was performed by pin-on-disc type sliding abrasive wear test, where the pin of 3 mm diameter coated sample was slid against alumina (Al_2O_3) abrasive disc, and the value of wear was measured from the height loss of the pin during the test. Fig. 6.11 shows the wear (as height loss) of TiC-Ni composite coated pin, prepared from the coated samples processed with different current, and scan speed. The graph indicates that the abrasive wear in term of height loss of the TiC-Ni coated AISI 304 steel substrate pin are in the range of 0.02 to 0.11 mm, depending on the processing condition, which is reasonably less than the uncoated AISI 304 steel pin. It is worth pointing out that for uncoated steel pin, height loss after wear test in similar condition was found 1.39 mm. It can also be observed from the graph that the wear (height loss) of the coated pins increases with the increase in applied TIG current. Sample

processed with 80 A current and 5.3 mm/s scan speed, exhibits maximum abrasive wear of 0.11 mm while lowest wear (0.02 mm) was observed for the sample processed with 40 A current and 5.3 mm/s scan speed. The graph also revealed that abrasive wear or height loss is higher for the coating processed with 5.3 mm/s than those of the coating processed with 6.5 mm/s, except for the sample processed with 40 A current.

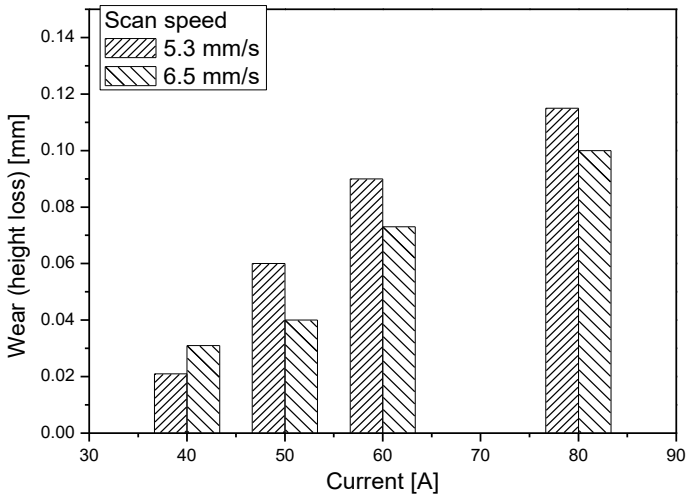

Fig. 6.11: Variation of sliding abrasive wear of TiC-Ni composite coating specimen processed at different TIG current and processing speed against Al_2O_3 abrasive disc

Fig. 6.12(a & b) show the wear behavior (in term of height loss against time during the wear test) of TiC-Ni composite coated samples produced with different current and scan speed of 5.3 mm/s and 6.5 mm/s respectively. The plots indicate almost similar wear characteristic for the TiC-Ni composite coating produced at the different current condition. Careful observation of the graph revealed that, at the initiation of the test, the rate of the height loss is quite rapid, and after a certain time, the height loss becomes smooth and steady. Here the graph demonstrates the combined wear or height loss of both coated pin and alumina abrasive disc, which was directly obtained by data acquisition system and plotted against test time.

Owing to high initial frictional force between the TiC-Ni coated surface and Al_2O_3 abrasive disc, along with the removal of the coating surface, some loosely bonded abrasive particles from the Al_2O_3 disc also removed, which reflected as high initial wear through the online data acquisition system. It is clearly seen from the graph that, the coated samples processed at low current, exhibit overall lower wear than those of the samples produced at higher current. At lower current, because of low heat input, only pre-coated TiC, and Ni powder melted and produced a hard TiC-Ni composite surface. In contrast, higher current

creates larger melt pool depth that dilutes the TiC and Ni with the base material, resulted in lower surface hardness (already discussed in the previous section).

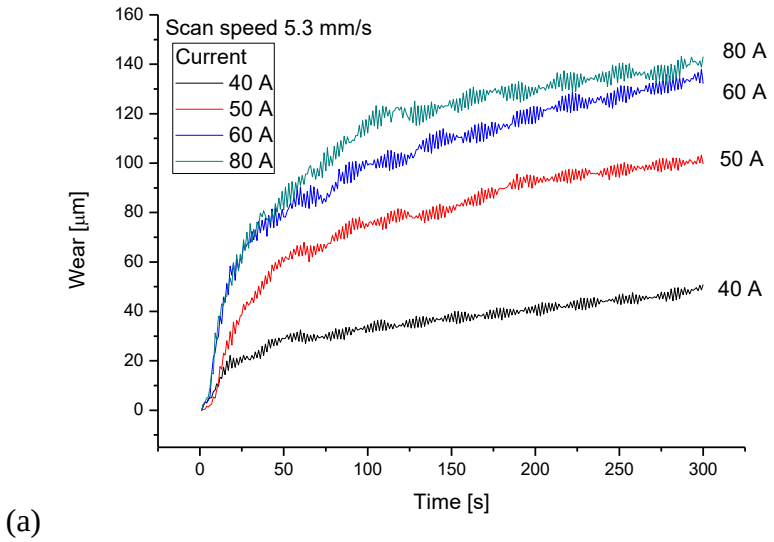

(a)

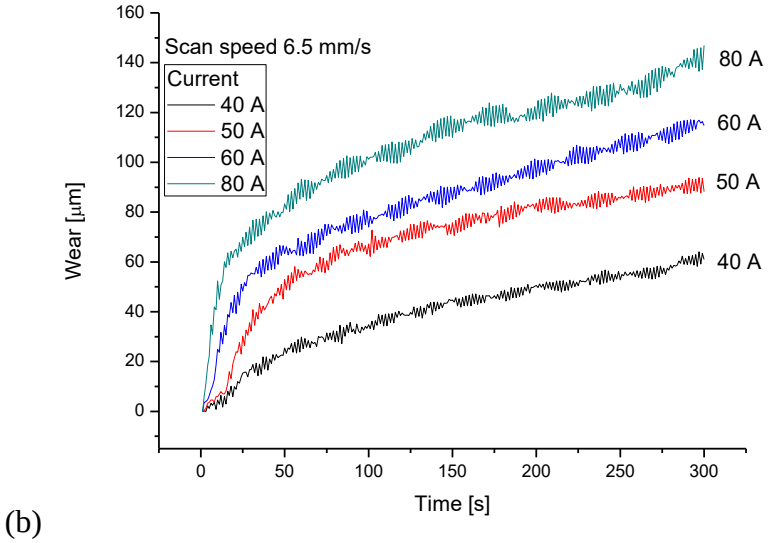

(b)

Fig. 6.12: Sliding abrasive wear behavior (height loss against time) of TiC-Ni coated steel samples produced by TIG cladding process with different current and arc scan speed of (a) 5.3 mm/s and (b) 6.5 mm/s

Comparison of Fig. 6.11 and 6.12 revealed that the value of abrasive wear (height loss) acquired from the direct data acquisition system (DAS) is a little bit larger than the actual height loss of the coated sample measured with Vernier caliper. As already discussed, at the initiation of the wear test, some loosely bonded abrasive particles removed out from the abrasive disc, the overall wear or height loss obtained from the DAS is the combination of actual wear of the coated pin and wear of the abrasive disc. It is observed from the plots that, the trend of wear for different samples processed at different condition is comparable in both types of measurement,. Thus, from the above discussion, it is worth to point out that

abrasive wear of the TiC-Ni composite coating gradually enhances with the increase in processing current from 40 to 80 A. However, with increasing scan speed, the abrasive wear or height loss reduces for different current condition.

6.3.4 XRD analysis

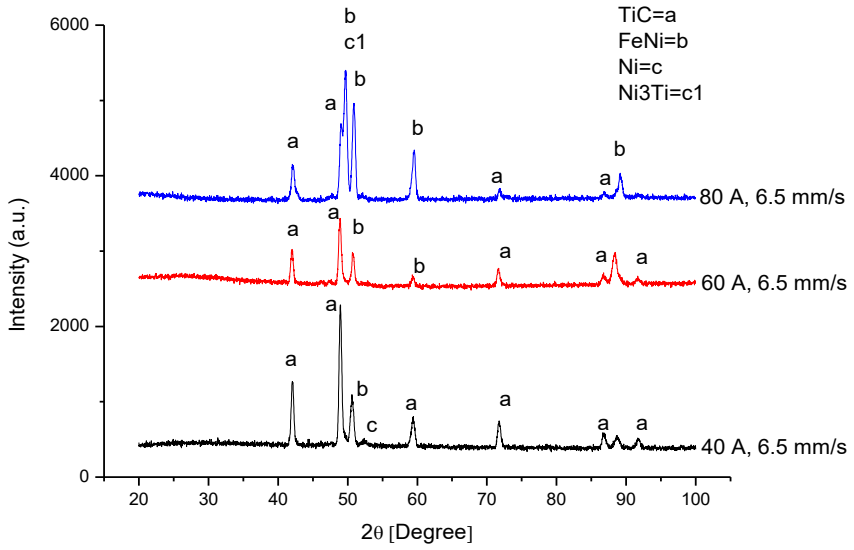

Fig. 6.13: XRD pattern of TiC-Ni composite coating surface produced on AISI 304 steel by different TIG current (40, 60 and 80 A) and scan speed of 6.5 mm/s

Fig. 6.13 represents the XRD patterns of TiC-Ni composite coating produced on AISI 304 steel by TIG cladding process, with 6.5 mm/s scan speed and current of 40, 60, and 80 A. From the analysis of the XRD patterns, peaks of TiC have been identified for all processing condition. Apart from TiC, peak of Fe-Ni which represent the AISI 304 steel also observed. It is interesting to note that the relative intensity of TiC peak reduces and the intensity of Fe-Ni peak increases for increasing the processing current.

Careful observation of the pattern also shows the presence of Ni (at $2\theta = 52.60^{o}$) in the coated surface processed with 40 A current. However, no absolute peak of Ni was identified in the XRD patterns attained for the samples processed at relatively higher current (60 and 80 A). It is worth pointing out that at high current condition, due to higher heat input, Ni dissolved in γ-Fe during the melting process (**Yi et al., 2013**). However, at low current, due to lower intensity of the produced arc, the fractional amount of Ni powder unable to dissolved in Fe matrix. Further, it can also observe from the XRD patterns that in the coating surfaces processed with 80 A current some peak of intermetallic compounds like Ni_3Ti is present. The possibility of TiC phase formation during solidification process is

fairly high in the coating due to low Gibbs free energy of TiC compared to other phases like Ti-Fe, Ti-Ni phases. Nevertheless, for applying high current (80 A), due to the generation of higher heat, a large melt pool was created and TiC particles distributed more uniformly in the melt pool. Although the melting temperature of TiC is very high (~3000 ^{o}C), dissociation of TiC into Ti and C occurred for applying high current (80 A). In the course of solidification, the presence of high quantity of Ni in the melt pool causes the formation of Ni_3Ti. Candel et al. (2014) and Chong et al. (2002) through their analysis demonstrated the possibility of formation of these intermetallic phases.

A semi quantity analysis accomplished through the relative peak height intensity illustrated that the relative percentage of TiC in the coating surface for the samples processed with 6.5 mm/s scan speed and current of 40, 60 and 80 A are 81.27, 64.93, and 28.53 % respectively. The higher quantity of TiC in the coating processed with 40 A current was acquired due to the appearance of highly dense TiC powders in the coated surface. As discussed earlier, with the increasing current at similar scan speed condition, during TIG cladding process, dilution of TiC in the Fe-Ni matrix augmented and the density of TiC particles in the coating layer diminishes, that resulted in a lower percentage of TiC in the coating.

6.3.5 Comparison between TiC and TiC-Ni coating

To explore the effect of Ni incorporation with TiC on the mechanical behavior of the TiC-Ni composite coating produced by TIG cladding process, the micro-hardness and wear behavior of the coating has been compared with the unadulterated TiC coating produced by the similar method (Sahoo et al., 2016). Fig. 6.14 (a, b) shows the hardness value of TiC and TiC-Ni composite coating produced by TIG cladding process at different current for scan speed of 5.3 and 6.5 mm/s respectively. Here, the hardness values are shown for the TiC coating produced with 60, 80 and 100 A current, whereas for TiC-Ni coating the hardness values considered for the samples produced with 40, 50, 60 and 80 A current. During the experimentation, it was observed that at 40 and 50 A current, owing to lower heat input, for using only TiC, the produced coatings were not properly bonded to the steel substrate and delaminated from the substrate surface. However, for the addition of Ni with the TiC powder, thanks to metallization and better arc formation, at relatively lower current (40 and 50 A), TiC-Ni coating able to deposit on the steel substrate with the strong interfacial bond. Concurrently, owing to higher heat input, TiC-Ni coating produced with

100 A current became over melted, and the produced coated surface was found inappropriate for the further study. Hence, in this section, only the selected coatings were analyzed for the comparison of mechanical characteristic, i.e. hardness and wear behavior.

Comparing the hardness value of TiC and TiC-Ni coating as depicted in Fig. 6.14a, it is obvious that the hardness values of the TiC-Ni composite coating are reasonably less than the TiC coating produced at similar condition (i.e. 60 and 80 A). However, for both type of coating, hardness value degraded for increasing the processing current. Further, comparing Fig. 6.14a and Fig. 6.14b, it is also revealed that for both types of coating, hardness value is relatively larger for using higher scan speed (6.5 mm/s) than those of the coating produced at lower scan speed (5.3 mm/s). Even though incorporation of Ni in the TiC-Ni coating reduces the hardness value of the coating, it offers certain advantages during the formation of TiC-Ni coating by TIG cladding method. The reduction in hardness value of TiC-Ni coating produced at similar current condition (60 A) ensued due to the dilution of TiC in the steel-Ni matrix. However, TiC-Ni coating produced with 40 and 50 A current show comparatively higher hardness value than pure TiC coating produced at 60 A current. It is postulated that addition of Ni with the preplaced TiC powder reduces the arc voltage discrepancy during arc scanning. As thermal and electrical conductivity of Ni is higher than that of TiC powder, incorporation of Ni in the preplaced powder mixture, alter the conductivity of the preplaced layer, that resulted in a continuous and smooth arc. Further, the addition of Ni diminishes the total heat requirement for the melting of the preplaced TiC-Ni layer, since melting temperature of Ni (1453 ^{o}C) is less than the melting temperature of TiC (3140 ^{o}C) (Viswanathan et al., 2012**)**. Thus, with lower heat input, a coating layer of TiC-Ni is likely to form at relatively low current, while Ni powder was added with TiC. It is also observed that for using the similar processing condition, the addition of Ni causes uniform distribution of TiC particles in the steel during the melting process.

Sliding abrasive wear of pure TiC coating and TiC-Ni coating was performed against Al_2O_3 abrasive disc and a comparison of wear as height loss has been reported. Fig. 6.15(a, b) show the variation of abrasive wear for TiC and TiC-Ni composite coated AISI 304 steel sample produced by TIG cladding process at different current for arc scan speed of 5.3 mm/s and 6.5 mm/s respectively. The graph revealed that for similar processing condition (60 and 80 A current) TiC composite coatings exhibit lower abrasive wear (height loss) compared to TiC-Ni composite coating (except the coating processed with 80 A and 6.5 mm/s).

However, wear resistance of TiC-Ni coatings produced with 40 and 50 A current found superior or almost equivalent to the TiC coating produced with 60 A current.

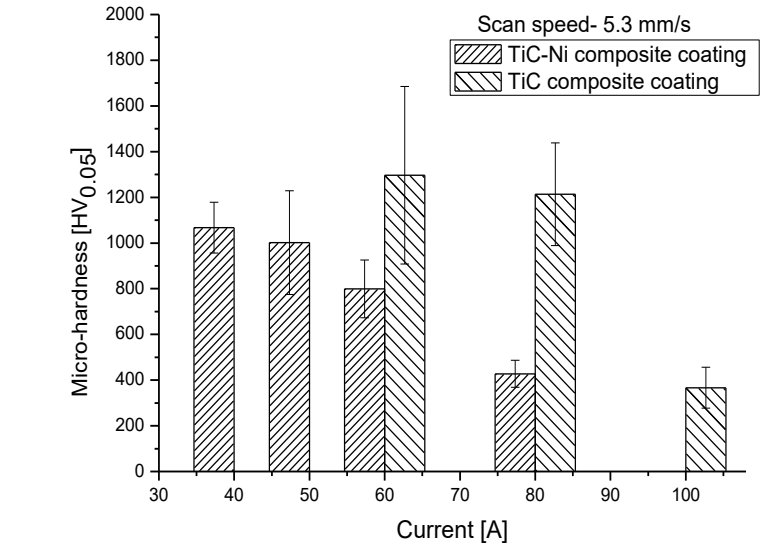

(a)

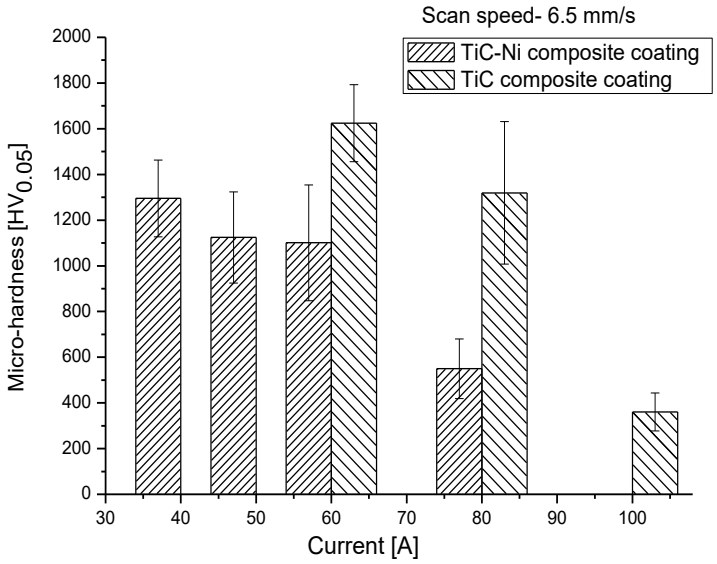

(b)

Fig. 6.14: Variation of micro-hardness value of TiC-Ni and TiC coating produced by TIG cladding process at different current for scan speed of (a) 5.3 mm/s and (b) 6.5 mm/s

It is worth pointing out that, the wear resistance of the coating predominantly govern by its hardness value. Highly concentrated TiC particle reinforcement in the TiC-Ni coating produced at relatively low current (40 and 50 A) exhibit high hardness in the coating which is the key aspect for low wear of the TiC-Ni coating. However, in the same processing condition, pure TiC coating was unable to produce because of inadequate heat energy at low

current. In contrast, due to the addition of Ni powder, thermal and electrical conductivity of the pre-deposited mixture enhanced and consequently at low current (40 and 50 A) TiC-Ni composite coating able to produce successfully. Hence, the addition of Ni with TiC augmented the wear resistance of the produced coating that is possible to yield at low processing current.

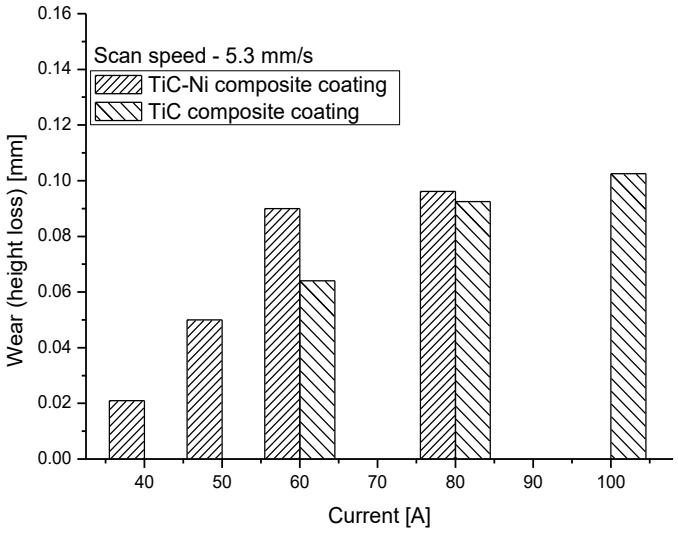

(a)

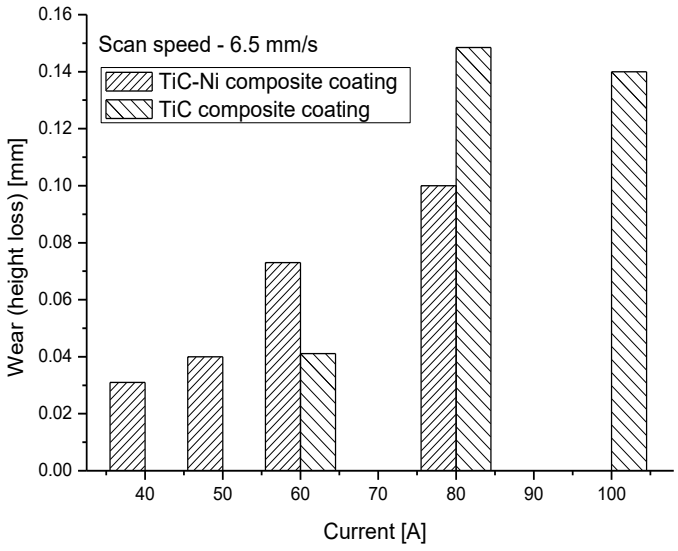

(b)

Fig. 6.15: Variation of abrasive wear (height loss) of TiC-Ni and TiC coating produced by TIG coating process at different current for scan speed of (a) 5.3 mm/s and (b) 6.5 mm/s

The graph also revealed that at relatively higher current (80 A), even though the TiC coating exhibit higher hardness value than TiC-Ni coating, the abrasive wear (height loss) found higher for TiC coating than TiC-Ni coating (for scan speed of 6.5 mm/s as shown in Fig. 6.15b) or almost equivalent (for scan speed of 5.3 mm/s as shown in Fig. 6.15a). This

is perhaps due to a superior bonding between the TiC particles with steel-Ni matrix than those of bonding between TiC and steel matrix.

6.3.6 Worn-out coating morphology

From the earlier discussion, it is revealed that microstructural characteristic and mechanical properties of the coating produced with TiC-Ni and pure TiC powder at similar processing condition are not identical; hence it is unjustified to relate their wear behavior directly. Rather, TiC-Ni coating produced with 40 A current and TiC coating produced at 60 A, at similar scan speed, show identical microstructure and almost equivalent mechanical properties i.e. micro-hardness and sliding abrasive wear behavior. For both the cases a highly dense TiC coating produced on steel substrate, although for using TiC-Ni, the coating was produced with relatively lower current. Therefore, to understand the wear mechanism of pure TiC and TiC-Ni coating with identical properties, worn out surfaces of TiC coating produced at 60 A current and TiC-Ni coating produced at 40 A current were studied under SEM.

Fig. 6.16(a-b) shows the SEM images of the TiC-Ni coating surface (processed at 40 A current and 6.5 mm/s scan speed), after the wear test. Fig. 6.16a shows that after the sliding abrasive wear test, TiC-Ni coated surface become smooth due to continuous sliding against alumina abrasive disc. No crack or large scale removal of the coating material was observed on the worn surface after the test. However, in the magnified image of the worn surface, some tiny voids or pores as marked in the figure can be seen, those were induced mainly because of the pull out of TiC particles from the Ni-steel matrix during the sliding abrasive wear test against alumina disc. Minor scratch mark can also be detected on the worn surface; those are yielded perhaps due to the abrasion effect of Al_2O_3 particles from the abrasive disc or due to pull out TiC particles from the coated surface. The high density of TiC in the coating resist the abrasion of the coating and causes very low wear, which resulted in a smooth worn surface. It is worth pointing out that, retaining high hardness, when TiC particles bonded with metallic Fe-Ni matrix, abrasive wear, as well as plowing of TiC particles restricted that diminishes the overall wear of the coating.

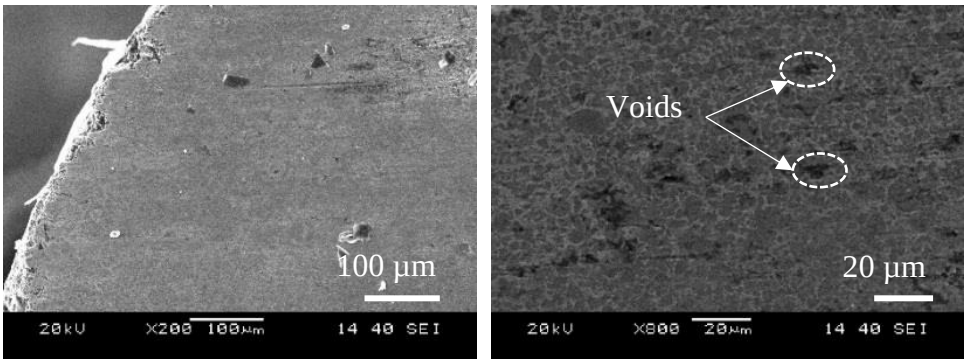

(a) (b)

Fig. 6.16: SEM micrograph showing the worn surface (at different magnification) of TiC-Ni coating processed at 40 A and 6.5 mm/s

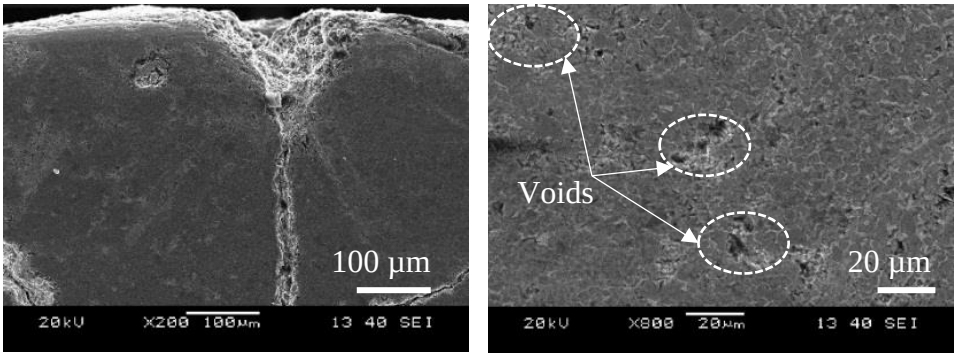

(a) (b)

Fig. 6.17: SEM micrograph showing the worn surface (at different magnification) of TiC coating processed at 60 A, 6.5 mm/s

Fig. 6.17 (a-b) shows the SEM images of TiC coated surface processed at 60 A current and 6.5 mm/s scan speed after the wear test. From the images, it is observed that due to abrasive wear against the alumina disc a smooth surface formed; however the amount of pores or voids produces due to dislodging of TiC particle from the coating surface is considerably higher than those observed on the worn surface of TiC-Ni coating (Fig. 6.16b). This may attribute to the inferior bonding of TiC particles with only steel matrix (when Ni was not added in the precursor powder mixture), which leads to easy removal of TiC particles from the coating surface during sliding abrasive wear test. Further, low magnified image of the worn out surface of pure TiC coating (Fig. 6.17a) revealed that, for using only TiC, a large size crack propagated at the edge of the pin. This is perhaps due to the formation of dense, brittle TiC on the coating zone that may get fractured owing to the concentration of stress during the sliding abrasive wear test against alumina disc at high normal load. Nevertheless, in spite of dense TiC reinforcement in the TiC-Ni coating, crack formation on the coating surface was constrained after the wear test. The addition of Ni with TiC powder enhances the ductility of the composite coating, which resulted in restriction of crack

formation on the coating surface during the wear test at high load. Further, TiC-Ni coating produced at relatively lower current (40 A) than the pure TiC coating (60 A) causes an overall low heat input in the TiC-Ni coating. Therefore, it is quite possible that the residual stress developed on pure TiC coating become much higher than the coating produced with TiC-Ni, and during the wear test, the initiation of the crack formation augmented for TiC coating.

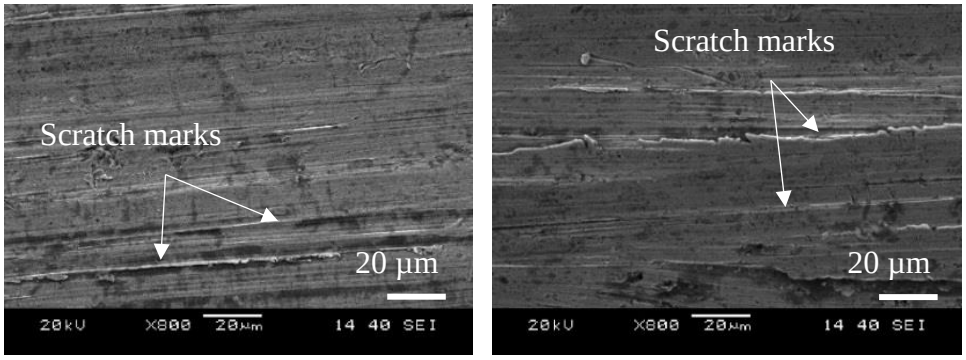

(a) (b)

Fig. 6.18: SEM micrograph of the worn surface of (a) TiC-Ni coating produced with 80 A current and 6.5 mm/s scan speed (b) TiC coating 100 A current and 6.5 mm/s scan speed

In the case of TiC coating, the TiC particles peeled off from the matrix during the abrasive wear, due to the weak bonding of TiC with the steel matrix. Further, these peeled off TiC particles produces grooves on the coating surface during the sliding against the soft coating matrix. The addition of Ni precursor in the coating assists in forming a superior bonding between the steel substrate and the coating material and perhaps restrict these type three-body abrasive wear.

On the other hand, to comprehend and compare the wear behavior of low-intensity TiC particle reinforced TiC-Ni and TiC coating produced on the steel substrate, SEM images of the worn surface were analyzed. Fig. 6.18 shows the SEM micrographs of the worn surfaces of TiC-Ni coating processed at 80 A current and 6.5 mm/s scan speed and TiC coating produced at 100 A current and 6.5 mm/s scan speed. Because of low concentration of TiC, occurrence of a high degree of abrasive wear witnessed through the dense scratch marks on the worn surfaces of both types of samples. However, careful observation of the images revealed that the intensity of abrasion or scratch marks on the TiC coating is relatively higher than the abrasion mark observed in the TiC-Ni coating. Due to the low concentration of hard TiC particle, an overall hardness value of the coating is

relatively less for both type of coating that reduces the wear resistance property of the coating surfaces.

Further, owing to the non-uniform distribution of TiC particles in the coating produced at higher current, an augmentation in the removal of the metal matrix zone of the coating occurred and in specific region plastic flow of the softer matrix material become predominant. Consequently, a significant amount of wear scratches appears on the coating surface. In contrast, for using Ni powder with TiC in the TiC-Ni coating, due to the formation of a stronger bond between the TiC particles and steel-Ni matrix, abrasion of the coating material become lower. Thus, relatively low wear was observed for TiC-Ni composite coating compared to the pure TiC coating.

6.3.7 Coefficient of friction

In order to measure the coefficient of friction (COF) value of the TiC-Ni coating produced by TIG cladding process, for the present phase of experiment sample produced with 40 A current and 6.5 mm/s scan speed was selected. Similar to previous experiments, COF of the TiC-Ni coated pin was measured by sliding the pin against hardened steel (HRC 58) disc with a sliding speed of 314 mm/s, under 30 N normal load.

Fig. 6.19 shows the variation of COF of the TiC-Ni coated pin against hardened steel disc. From the plot, it is evident that the steady state COF value of the selected TiC-Ni coating is approximately 0.65, which is marginally higher than the COF value of TiC coating produced by TIG cladding with 60 A current and 6.5 mm/s scan speed.

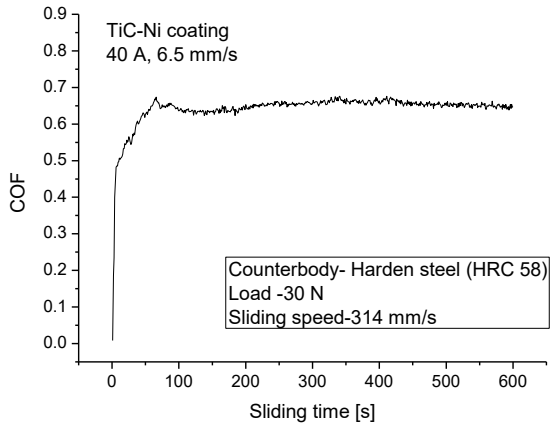

Fig. 6.19: Coefficient of friction (against hardened steel, HRC 58) of TiC-Ni coating produced by TIG cladding process with 40 A current and 6.5 mm/s scan speed

6.4 Outcomes

A hard and wear resistance TiC-Ni composite coating successfully deposited on AISI 304 stainless steel substrate by TIG cladding process.

TiC-Ni metal matrix composite layer made a strong interfacial bond between the coating and substrate surface owing to the incorporation of Ni with TiC preplaced powder.

The experimental results revealed that TiC-Ni coating is possible to produce at relatively lower heat input (lower current) which exhibits comparatively higher hardness value than pure TiC coating. As the thermal and electrical conductivity of Ni is superior to TiC powder, incorporation of Ni in the preplaced powder mixture alter the electrical conductivity of the preplaced layer, that resulted in a continuous and smooth arc. Furthermore, the addition of Ni diminishes the total heat requirement for the melting of preplaced TiC-Ni layer.

The average micro-hardness value of TiC-Ni coating improved up to 1300 $HV_{0.05}$. The hardness value of TiC coating found superior to TiC-Ni coating deposited under similar processing condition; however, the enhanced bonding between the TiC particles with steel-Ni matrix compared to the bonding between TiC and steel matrix leads to a higher abrasive wear resistance in TiC-Ni coating than TiC coating.

Sliding abrasive wear resistance of TiC-Ni coating improved up to 70 times than the as received AISI 304 steel substrate and significantly higher than the TiC coating. High sliding abrasive wear resistance observed in the low diluted coating, and the wear resistance decreases with the dilution of TiC reinforcement in the steel-Ni matrix. COF value of TiC-Ni coating found marginally higher than the COF value of TiC coating of similar type morphology.

TiC morphology in the TiC-Ni coating essentially depends on the TIG processing parameters i.e. current and scan speed that consequently affect the mechanical properties of the coating.

Chapter 7

Effect of CaF_2 content on TiC-Ni-CaF_2 composite coating produced by TIG cladding process

In this phase of work, TiC-Ni-CaF_2 self-lubricating composite coating has been deposited on AISI 304 steel substrate by TIG cladding process using powder mixture of TiC, Ni, and CaF_2. Effect of CaF_2 percentage in the precursor has been emphasized for the metallurgical and mechanical characteristic of the produced coating. SEM and EDS analysis of the coating revealed that processing current and CaF_2 percentage in the precursor have a significant influence on the microstructure and corresponding mechanical properties of the coating. Based on the heat input, which is the synergic effect of processing current and CaF_2 content, dilution of the coating material in steel matrix altered and consequently the micro-hardness and corresponding wear properties of the coating varied. Sliding abrasive wear test performed against alumina abrasive disc show that wear rate of the composite coating expressively governed by the processing condition of the coating. Further, to assess the coefficient of friction (COF) of the coating, sliding wear test have been performed against hardened steel disc, which clearly exhibits that with the increase in CaF_2 percentage in the precursor, COF significantly reduced.

Keywords: TiC-composite; CaF_2; Solid lubricant; TIG cladding; Micro-hardness; Abrasive wear; Coefficient of friction

7.1 Introduction

Earlier, TiC reinforced Co, Ni or Fe-based MMC coating was successfully fabricated by various researcher utilizing laser cladding and TIG cladding methods and significant improvement in the surface hardness and wear resistance of the coating has been reported. Nevertheless, frictional force or COF value of these MMC coatings found reasonably high due to the presence of a metallic binder. It is anticipated that tribological properties of MMC coatings can be improved with the assimilation of CaF_2, in consequence of its specific properties as described in Chapter-3.

Among the various solid lubricants, organic alkali fluorides (LiF_2, CaF_2, BaF_2) are favourable owing to their low density, low shear strength, stable thermo-physical and thermo-chemical properties at a higher temperature in combination with their low cost (Liu et al., 2013). Recent studies revealed that CaF_2 is a widely used solid lubricant, utilized in self-lubricating ceramic composites for the anti-wear and anti-frictional application (Yan et al., 2013). Furthermore, CaF_2 also used as flux material and enhances the fluidity of melt-pool when employed in laser coating process (Yan et al., 2012). Experimental analysis of various research groups revealed that incorporation of CaF_2, significantly enhanced the tribology properties of the composite or composite coating even at room temperature by reducing the frictional force against metallic counterpart (Wang et al., 2002; Liu et al., 2009; Cai et al., 2013; Muthuraja and Senthilvelan, 2015).

Review of the literature depicted that reduction in coefficient of friction attained in composite coatings produced by laser cladding, plasma-spraying route, or in the bulk composite component fabricated by different sintering methods after incorporating CaF_2 as a solid lubricant. However, hardly any effort was made so far to produce a hard and wear resistance composite coating by incorporating solid lubricant, especially CaF_2 via TIG cladding route. Furthermore, analysis of the effect of CaF_2 percentage in the composite coating on its mechanical and tribological properties is also rare. Very recently, TiC-BN composite coating has been produced on AISI 1020 steel by TIG cladding process, where BN act as a solid lubricant (Peng and Kang, 2015). As an economical method to produce a hard and wear resistance overlay coating, it is relevant to study the effect of CaF_2 in the TiC-Ni-CaF_2 coating produced by TIG cladding process.

In this phase of work TiC-Ni-CaF_2 composite coating has been produced on AISI 304 steel substrate by TIG cladding process. It is expected that with the incorporation of CaF_2 in TiC-Ni composite system, along with the reduction in COF value, owing to fluxing effect coating layer could be deposited on the substrate with relatively low heat input. The effect of different percentage of CaF_2 on the formation of the coating as well as their mechanical and tribological properties has also been analyzed. The macrostructure of the coating morphology, as well as the performance of the coating produced at various TIG current condition, and with different percentage of CaF_2 has been analyzed in terms of wear resistance and frictional resistance.

7.2 Experimental procedure

The current research work utilized ground AISI 304 stainless steel plates of 100×45×8 mm^3 as substrate material to deposit TiC-Ni-CaF_2 composite coating by TIG cladding process. At first, the surfaces of steel plates were prepared by polishing and cleaning as detailed in Chapter-3. TiC, Ni, and CaF_2 powders specification of which already detailed in Table 3.3 were used as precursors mixture to create a preplaced layer on the AISI 304 stainless steel substrate. TiC and Ni powder mixed in 1:1 weight ratio, and then 5, 10, 15 and 20 wt.% CaF_2 powder added with TiC-Ni powder mixture separately to make precursor containing a different percentage of CaF_2. These precursor powders were then mixed with a polyurithin based organic binder and a specific quantity of acetone to make a semi-solid solution. The paste-like solution then dispersed uniformly on the prepared substrate and dried at room temperature for curing the binder. The thickness of the preplaced layer was maintained by using the appropriate amount of powder mixture required to cover the surface of the substrate. Thus, approximately 350±20 μm thick preplaced layer was produced on the substrate surface.

Fronius A-4600 (Magic Wave 2200) welding machine attached with a TIG torch was used for the present experimentation. Detail of the set-up already was illustrated in Chapter-3. Table.7.1 indicates the processing condition for deposition of TiC-Ni-CaF_2 coating on AISI 304 steel substrate using preplaced TiC/Ni/CaF_2 powder mixture. For the present work, the scan speed of the heat source kept fixed at 6.5 mm/s and TIG welding current considered as 60, 80 and 100 A for each type of preplaced mixture. The TIG heat source or arc was scanned over the preplaced steel substrate that resulted in melting of the powder mixture and a thin layer of the substrate underneath the coating layer. Fig. 7.1 shows the schematic diagram of TIG cladding process for present TiC-Ni-CaF_2 coating by powder preplacement method. After performing the TIG cladding, the samples were cut in the transverse direction of arc scanning by using wire-EDM for further analysis. The cross section of the samples was metallurgically polished with different graded SiC emery paper followed by final polishing with diamond paste (average size: 1 μm) suspended polishing cloth. The SEM (JEOL, JSM-6084LV) analysis at the cross section of coating was performed in BSE mode to reveal the coating profile and its microstructure. Micro-hardness value of the coating was measured using a Vickers micro-indentation tester (LECO-LM810) with 50 gf load. Average micro-hardness value of the coating assessed from the ten measurements taken at the coating cross-section randomly. X-ray diffraction (XRD)

technique was employed to evaluate the compounds present in the produced coating surface for all the samples processed at different condition. XRD was performed with the help of BRUKER D8 ADVANCE diffractometer using cobalt target (λ= 1.79026 Å) considering scan range of 20–100°, step size of 0.02° and a scan rate of 10^{o} per min.

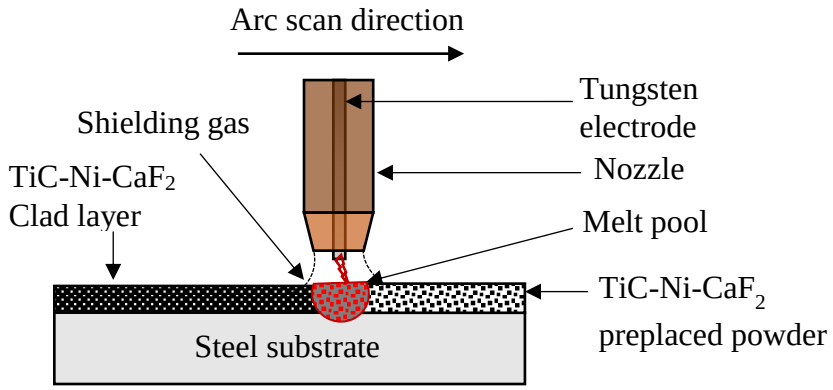

Fig. 7.1: Schematic diagram of TIG cladding process

Table 7.1: Experimental condition to produce TiC-Ni-CaF_2 coating on AISI 304 steel by TIG cladding

Exp. No.	**CaF_2 (wt.%)**	**Current (A)**	**Scan Speed (mm/s)**	**Voltage (V) (average)**	**Heat input (J/mm)**
1	5	60	6.5	15	66.461
2	5	80	6.5	15	88.615
3	5	100	6.5	15	110.769
4	10	60	6.5	15	66.461
5	10	80	6.5	15	88.615
6	10	100	6.5	15	110.769
7	15	60	6.5	15	66.461
8	15	80	6.5	15	88.615
9	15	100	6.5	15	110.769
10	20	60	6.5	15	66.461
11	20	80	6.5	15	88.615
12	20	100	6.5	15	110.769

Tribological properties of the produced TiC-Ni-CaF_2 composite coating was evaluated using a pin-on- disc type tribometer (ASTM G99 standard Make: Magnum) against alumina abrasive disc and hardened die steel (58 HRC) separately. Here, alumina disc of 45 mm diameter was used as counter-body to assess the sliding abrasive wear

behavior of the coating, whereas hardened steel plate was used to quantify the COF value of the coating. Pins of 3 mm diameter were cut from the TiC-Ni-CaF_2 coated steel plates using wire-EDM to use as a test sample. Detail of the sliding abrasive wear test conditions and test condition for measurement of COF are illustrated in Table 7.2 and Table 7.3 respectively. During the wear test variation of wear (height loss) with respect to time was attained through data acquisition system integrated with the pin-on-disc test rig. Also, a vernier caliper was also used to measure the height loss of the coated pin after the wear test. During the test against hardened die steel plate, COF value was recorded through data acquisition system and plotted against test time. Average value of steady state COF was considered as COF value of the respective coating under specified test condition

Table 7.2: Condition for pin-on-disc type sliding abrasive wear test

Sample	3 mm dia coated pin
Normal load	10 N
Disc rotation speed	300 rpm
Track radius	10 mm
Sliding velocity	314 mm/s
Test duration	5 minutes
Counter-body	Al_2O_3 abrasive wheel

Table 7.3: Sliding test condition for measurement of COF

Sample	3 mm diameter coated pin
Counter-body	Hardened steel disc (58 HRC)
Load	30 N
Sliding velocity	314 mm/s
Time	10 minute

7.3 Results and discussion

The present investigation describes the influence of CaF_2 percentage in TiC-Ni-CaF_2 composite coating produced by TIG cladding process on different metallurgical and mechanical aspects such as coating morphology, compound phases present, micro-hardness, and tribological behavior of the coating. The detail discussion as follows:

7.3.1 Coating profile

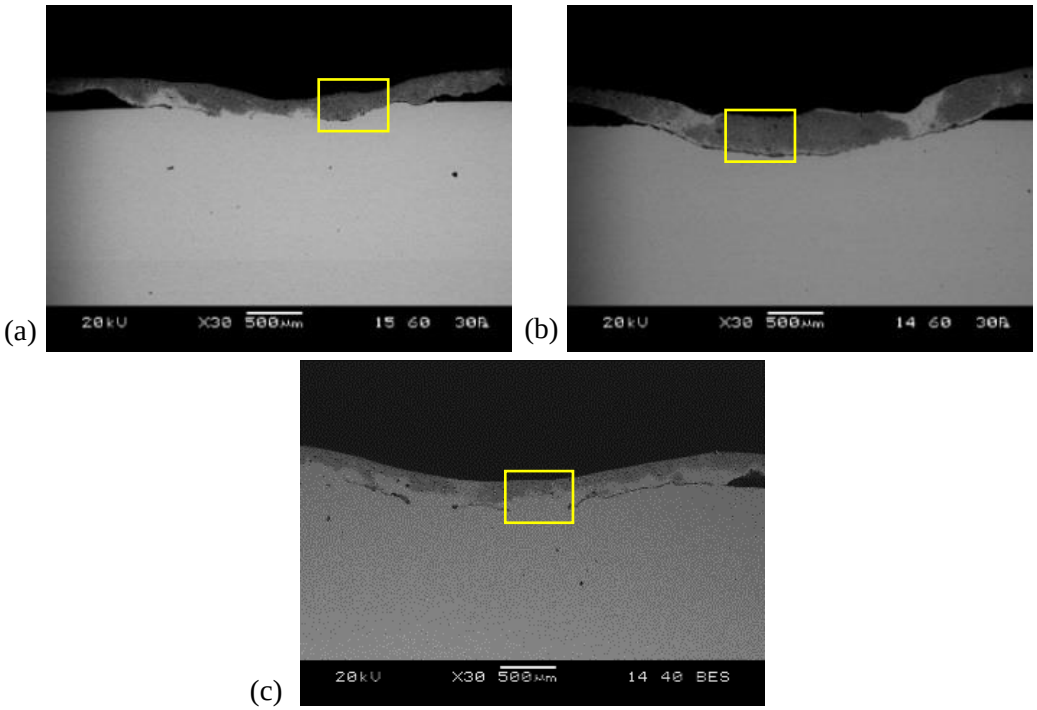

Fig. 7.2: SEM images of the cross-section of TiC-Ni-CaF_2 composite coating produced by TIG cladding process using 5wt.% CaF2 in the precursor and welding current of (a) 60 A (b) 80 A and (c) 100 A

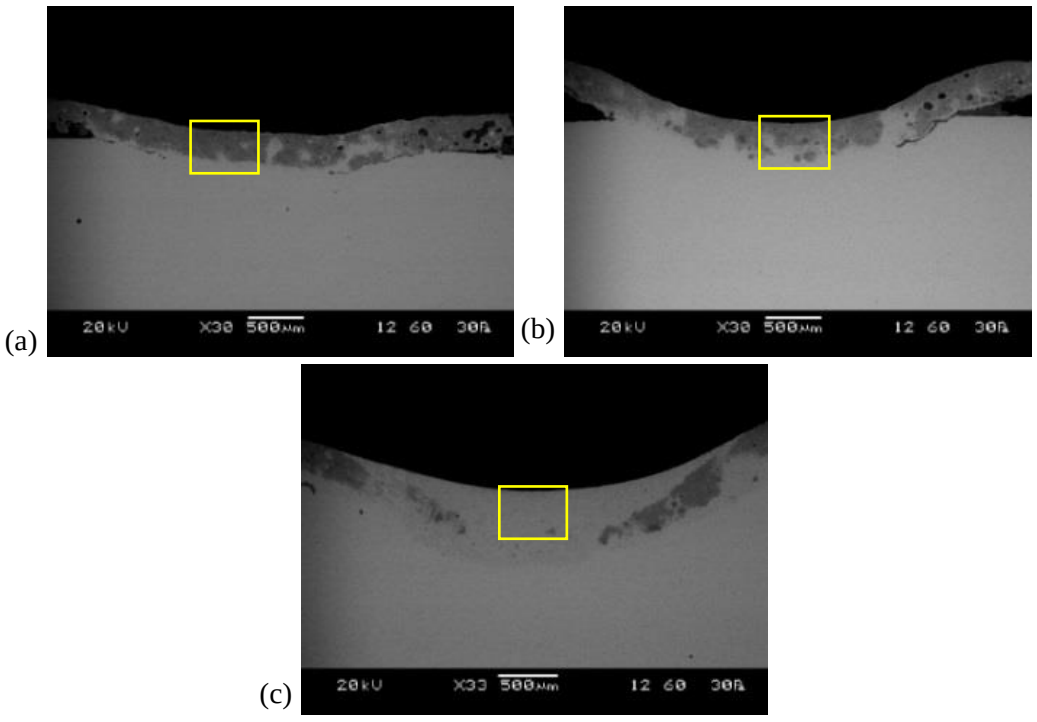

Fig. 7.3: SEM images of the cross-section of TiC-Ni-CaF_2 composite coating produced by TIG cladding process using 10wt.% CaF_2 in the precursor and welding current of (a) 60 A (b) 80 A and (c) 100 A

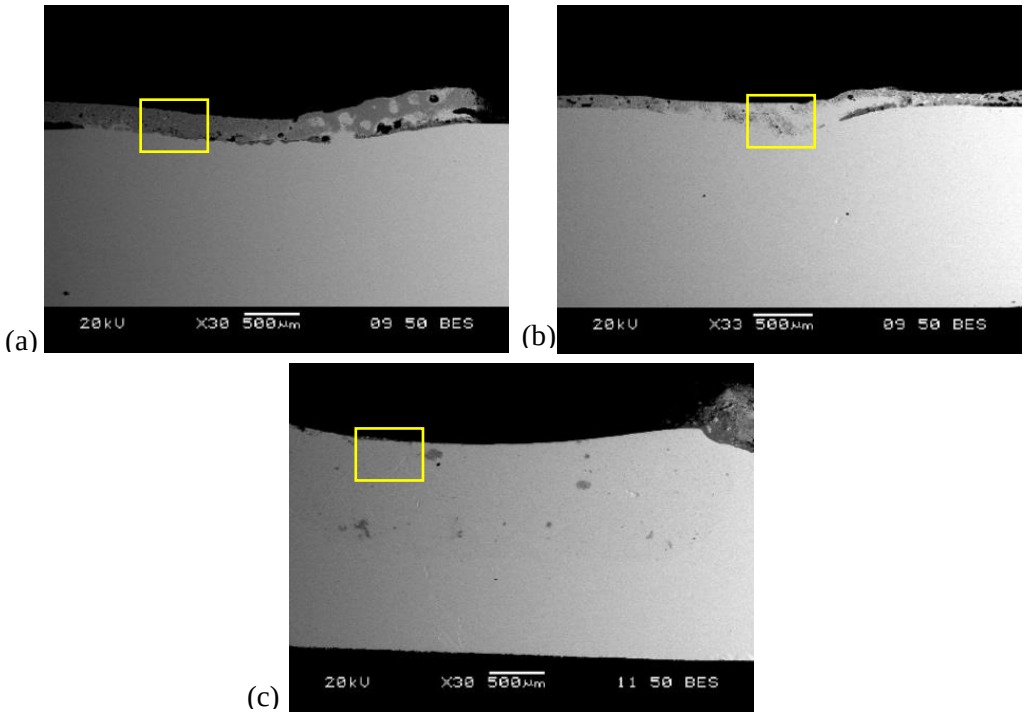

Fig. 7.4: SEM images of the cross-section of TiC-Ni-CaF_2 composite coating produced by TIG cladding process using 15wt.% CaF2 in the precursor and welding current of (a) 60 A (b) 80 A and (c) 100 A

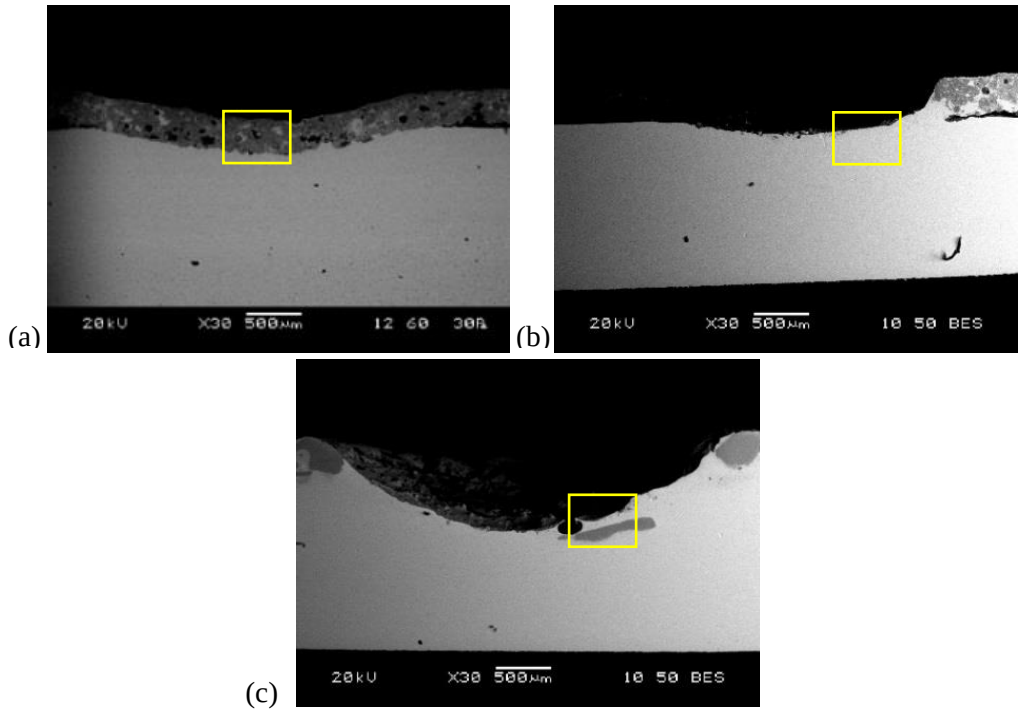

Fig. 7.5: SEM images of the cross-section of TiC-Ni-CaF_2 composite coating produced by TIG cladding process using 20wt.% CaF_2 in the precursor and welding current of (a) 60 A (b) 80 A and (c) 100 A

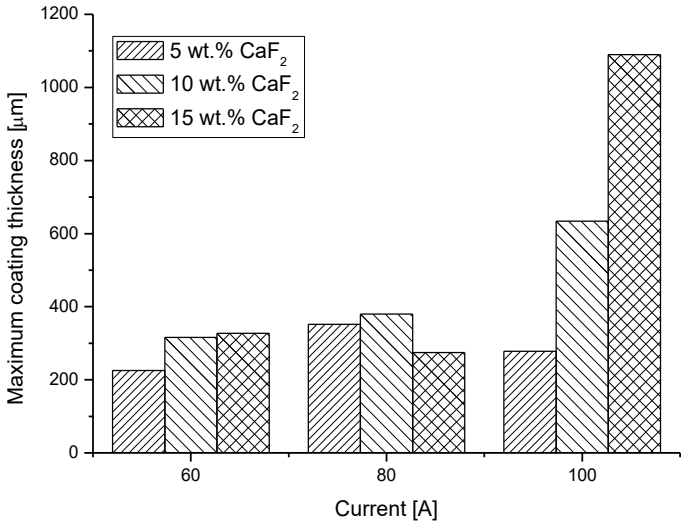

(a)

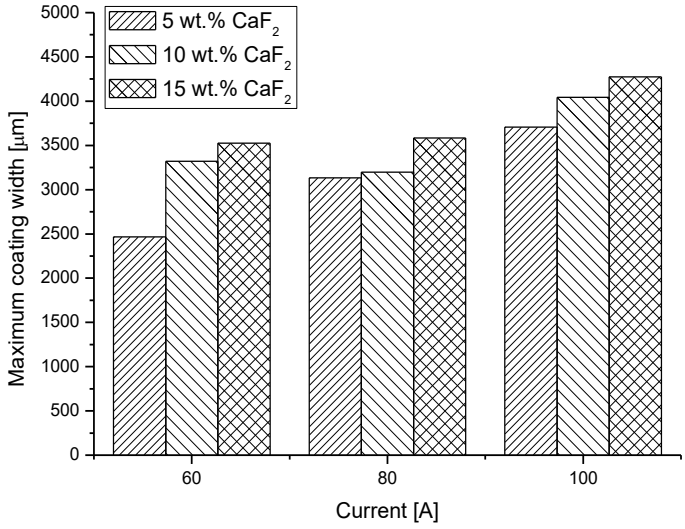

(b)

Fig. 7.6: Variation of (a) maximum coating thickness and (b) width of the TiC-Ni-CaF_2 coating produced by TIG cladding for single line scan with different current and CaF_2 percentage in the precursor

Fig.7.2 to Fig.7.5 illustrate the SEM images of the cross-section of TiC-Ni-CaF_2 composite coating produced on AISI 304 steel substrate with different current (60, 80 and 100 A) and using precursor containing 5, 10, 15 and 20 wt.% CaF_2 respectively. The images clearly depict the formation of either a thick and dark coating layer over the substrate or a gray shaded mix type layer on the upper surface of steel substrate for using the different percentage of CaF_2 in the precursor and processed with the variable current.

The SEM images indicate that for applying lower current (60 A) during TIG cladding process, an uniform layer of composite coating formed on the steel substrate

irrespective of the CaF_2 percentage used in the precursor. However, similar uniform and a dark coating formed for using 80 A current, when the amount of CaF_2 used in the precursor was limited to 5 and 10 %. It is evident that, for using a higher percentage of CaF_2 (10 and 15%), at relatively higher current (100 A) a gray shaded mixed type coating has been produced on the steel substrate, where the dark particles are diluted in the light shaded metal matrix. Exceptionally, it has also detected that for using 20% CaF_2, at 80 and 100 A current, the coating was not deposited on the substrate; instead, a large size crater formed at the center of the track and the coating material disseminated non-uniformly nearby region. The images revealed that the variation in the coating structure occurred not only due to the change in processing current but also due to the percentage of CaF_2 used in the precursor. This may attribute to the fact that, with the increase in processing current, the heat input in the coating enhances that diluted the coating material in the substrate matrix. Further, as the percentage of CaF_2 increases in the precursor, owing to fluxing effect, the effective heat in the coating zone augmented (Leconte et al., 2007). It is worth pointing out that CaF_2 commonly used in TIG welding as activated flux, which increases the arc energy density due to arc constriction caused by ionized atoms of the flux material. This phenomenon help to increases the weld penetration by modifying the temperature field. The use of CaF_2 as flux also increases the arc voltage during the TIG welding/melting process that increases the overall heat input in the TIG cladding process. Lecont et al. (2007) demonstrated that the activating flux like fluorides supports the densification of electric arc by dissociation and ionization of the flux elements that causes arc constriction and enhances the arc energy density. Howse and Lucas (2000) showed that active flux is useful to increase the weld penetration for plasma arc or TIG arc as a heat source. The constriction of the arc increases the temperature at the anode, owing to the increase in current density and higher arc voltage. Further, Shen et al. (2012) described that along with the arc constriction, that augmenting the weld penetration, CaF_2 also have an influence on the cooling rate during solidification of the melt pool. These combined effects of CaF_2 enhances the dilution of coating material for a higher percentage of CaF_2 at relatively low current. It is postulated that the synergic effect of enhancement in the heat input at high current and a higher percentage of CaF_2 (20% CaF_2, 80 and 100 A current), might cause localized evaporation of the coating material as well as the substrate surface beneath the coating layer. Furthermore, it is also possible that at high heat input condition, the cooling rate of the coating is extremely high. The high cooling rate may induce residual stress in the coating layer and owing to mismatch in the thermo-mechanical properties of the coating (TiC-Ni-CaF_2) and the steel substrate the

produced coating layer delaminated from the substrate surface (Katipelli et al., 2000a). It is established that CaF_2 in the precursor has no significant effect on the melt flow pattern. Thus, the Marangoni convective flow remains similar to that attain without CaF_2 addition in the melt pool (Leconte et al., 2007). However, the addition of CaF_2 in the precursor improves the fluidity of melt pool (Yang et al., 2004) that enhances the weld penetration as well as create a churning effect on the melt pool. Consequently, the pre-deposited coating material mainly TiC, mixed with the steel substrate and yielded a mixed type coating morphology.

In the present investigation, since single line scanning of the arc was carried out to produce the coating, it is imperative to analyze the variation of coating thickness obtained at different processing condition. From cross-sectional SEM images of the coating (Fig. 7.2 to 7.5), maximum coating thickness and width were measured using image analysis software (ImageJ) and plotted against applied current for using 5, 10 and 15 % CaF_2 in the precursor as depicted in Fig.7.6. Owing to the removal of the coating material from the substrate surface, sample processed with 20% CaF_2 was not considered for the analysis of thickness and width of the coating. The plot indicates that maximum thickness of the coating varies between 225 to 1090 µm depending on the CaF_2 content in the precursor and the TIG processing current. It is also evident that for using 5 wt. %, CaF_2 in the TiC-Ni-CaF_2 system, the coating thickness is relatively low i.e. in the range of 225 to 350 µm and with the increase in CaF_2 content, coating thickness increases gradually for almost all current condition. This variation found more prominent for the coating processed at 100 A current. As already discussed, for using a higher percentage of CaF_2 in the precursor, the pre-deposited coating elements were diluted in the steel matrix within a larger depth, and this phenomenon augmented with the increase in processing current. Exceptionally, it is also evident that with processing current of 80 A, the coating thickness reduces for increasing the CaF_2 percentage from 10 to 15%. This is perhaps due to the random selection of the coating cross-section, where owing to localized imperfection relatively less thickness was obtained and considered for the present analysis.

The variation in the coating thickness predominantly depends on the dilution of the preplaced coating material specifically TiC powder with the base material, which is further related to the heat input during the TIG cladding process. The heat input increases with the increase in processing current, as scan speed and other parameters remain constant. The produced TiC-Ni-CaF_2 coating profile depends on the heat supplied during the coating

process i.e. applied current as well as accumulation of the heat due to the fluxing effect of CaF_2. As the distribution of the heat source in TIG arc scanning is the almost Gaussian type, therefore, the melt pool or the coating profile form a relatively larger depth at the center, and the melt pool depth or coating thickness decreases towards the edges (Mridha et al., 2015). It is worth to mention that, at low current range (60 and 80 A) owing to lower arc power, the input heat is not sufficient to melt the preplaced powder properly and found a lack of mixing of the coating material in the melt pool.

7.3.2 XRD analysis

XRD pattern for the coating surface produced by using a different percentage of CaF_2 (5 to 20%) in the precursor and processed at 60, 80 and 100 A current are shown in Fig. 7.7 (a–c) respectively. The XRD patterns of all the samples show almost similar sequence of peaks. Analysis of the peaks revealed the presence of TiC, CaF_2, and steel on the coating surface as major constituents. It may be noted that for using a lower percentage of CaF_2 (5 and 10%) in the precursor, the coating produced at 60 A current, peaks of CaF_2 are not so prominent. However, the presence of CaF_2 was detected in the coating processed at 60 A current through EDS analysis, which has been discussed later in the microstructural analysis section. This is perhaps attributed to the presence of low percentage of CaF_2 and its non-uniform distribution in the coating. In addition to these major phases, some intermetallic of Ni, Ti and Ca like $TiNi_3$, TiNi, $CaNi_3$ and Ca_2Ni_7 were also detected in the coating surface. Careful observation of the XRD patterns clearly indicates that with the increase in CaF_2 percentage in the precursor, the intensity of the CaF_2 peak also increases. Nevertheless, as a matter of fact, it is difficult and inaccurate to quantify the compounds present in the coating surface, due to the presence of number of phases inconsistently in different samples.

Similarly, the XRD pattern of the coating produced at 80 and 100 A current, for using different percentage of CaF_2 in the precursor also illustrate the presence of TiC, CaF_2, and steel in combination with other intermetallic components (Fig. 7.7b-c). It is worth to note that, despite high energy input, peaks of independent CaF_2 phase are present in the coating surface produced with 80 and 100 A current for using 5 and 10 wt.% CaF_2. In addition, due to partial decomposition of CaF_2, presence of intermetallics like $CaNi_3$ and Ca_2Ni_7 observed the coating.

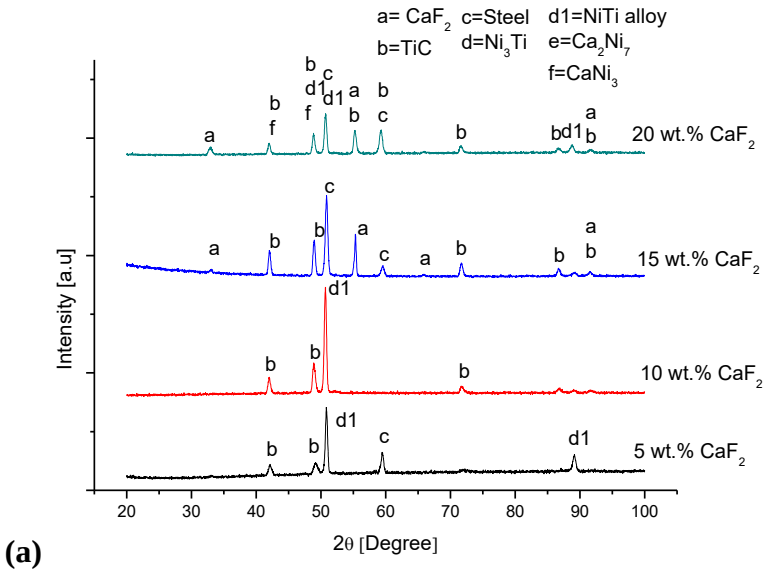

(a)

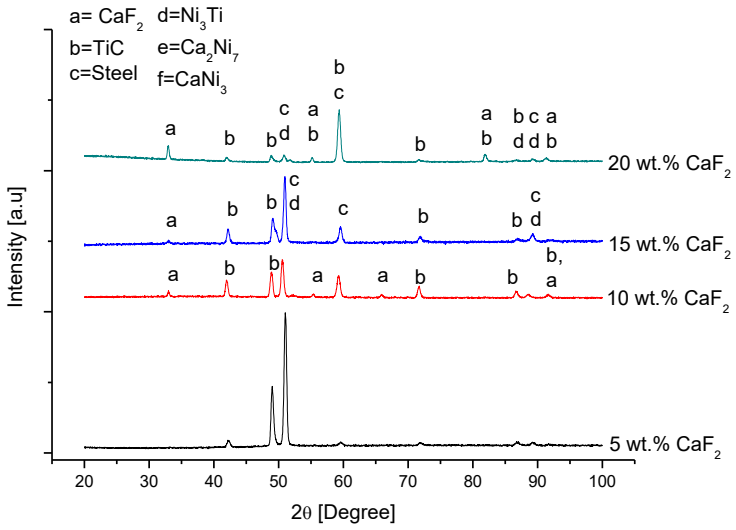

(b)

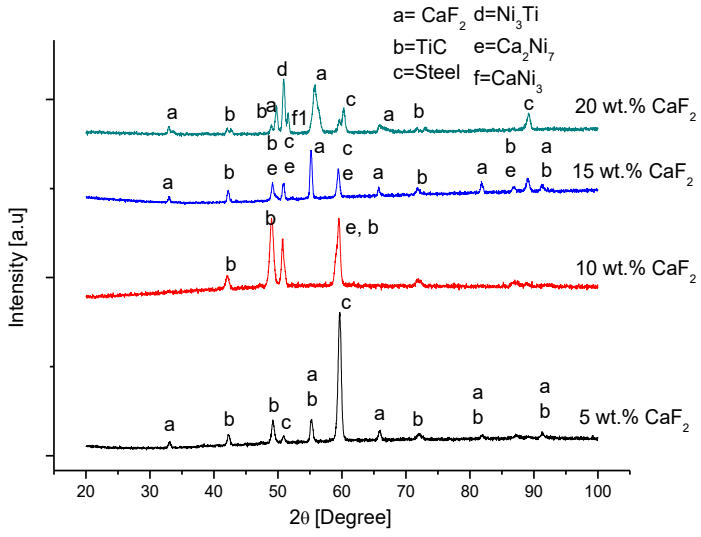

(c)

Fig. 7.7: XRD pattern of TiC-Ni-CaF_2 coating produced with different percentage of CaF_2 in the precursor by TIG cladding process performed at (a) 60 A, (b) 80 A and (c) 100 A current

For sample produced with 20% CaF_2 and higher current (80 and 100 A), as discussed earlier, part of the coating material removed from the center of the coating track. However, at the edge of the track where the intensity of heat is relatively less, highly dense coating material deposited. Therefore, the presence of TiC, CaF_2, and other compounds can be observed from the XRD pattern. Due to high heat input during the TIG cladding process, TiC particles also partially melted in spite of its high melting temperature and reacted with Ni and produces intermetallic like $TiNi_3$, TiNi. CaF_2 as a fluxing material dissociate at high temperature, react with Ni present in the coating system, and consequently produces compounds like $CaNi_3$ and Ca_2Ni_7. However, the percentage of these intermetallic are very less and not effect the performance of the produced coating.

7.3.3 Micro-hardness

Micro-hardness value of TiC-Ni-CaF_2 coating produced at different condition was measured at the cross-section and average micro-hardness value assessed from the ten readings taken randomly from each sample. Fig. 7.8 demonstrate the variation in the average micro-hardness value of the coating produced with different percentage of CaF_2 in the precursor for different current applied during the coating process. It is worth pointing out that owing to non-uniformity and removal of the coating layer, analysis on the micro-hardness value for the samples processed with 20% CaF_2 at 80 and 100 A current has been exempted. It is obvious from the plot that the hardness values of the coatings are reasonably high (above 800 $HV_{0.05}$) for almost all the cases (except for the coating produced with 15 wt.% CaF_2 at 100 A current). The plot also indicates that the hardness value of the coating almost gradually decreasing with the increasing CaF_2 percentage in the precursor for applying different current during TIG cladding process. This variation can be clearly identified for the samples processed at higher current. The analysis also revealed that for using similar composition or similar percentage of CaF_2 in the precursor, the hardness value of the coating gradually reduces with the increase in applied current during the TIG cladding process.

It is worth to note that in the present TiC-Ni-CaF_2 composite coating, TiC act as hard reinforcement, Ni as matrix or binder, whereas CaF_2 act as a solid lubricant and flux. Micro-hardness value of the present coating predominantly governed by the amount of TiC reinforcement and its dissemination in the coated layer. It is also evident that all the coating processed with 60 A current showing almost similar morphology and exhibits uniform hardness value. Nevertheless, careful observation of the plot clearly shows that with the

increase in CaF_2 percentage in the precursor, the average micro-hardness value diminishes marginally. As the heat supplied to the sample during TIG arc scanning is relatively low for 60 A current, dilution of steel substrate in the coating material become extremely low. In contrast, for higher current (80 and 100 A), with the increase in CaF_2 percentage, reduction in the average micro-hardness value can be observed conspicuously. It is worth pointing out that with the increasing current, dilution of relatively soft steel substrate enhances, which leads to a detrimental effect on the coating hardness. Hence, TiC-Ni-CaF_2 composite coatings produced at lower current containing highly dense coating material especially TiC, which exhibits higher hardness value as compared to the coating produced at higher current. Furthermore, with the increasing CaF_2 percentage at relatively higher current, CaF_2 acts as a flux, which enhances the effective heat input, and consequently dilutes the TiC reinforcement in the steel substrate. With a higher percentage of CaF_2, heat absorbed by the coating and substrate surface become higher and a larger melting depth formed, which causes mixing of the coating material with the steel substrate. The high dilution of the TiC reinforced particles ensued reduction in the average micro-hardness value of the coating.

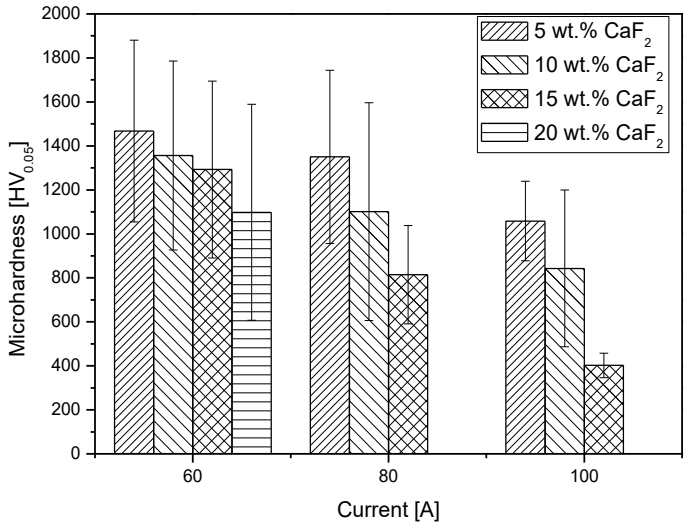

Fig. 7.8: Average micro-hardness value of TiC-Ni-CaF_2 coating produced by TIG cladding process with different current and CaF_2 percentage in the precursor

7.3.4 Microstructural analysis

The magnified SEM images of the cross-section of the TiC-Ni-CaF_2 coating produced with the precursor containing different percentages of CaF_2 and processed at different current are illustrated in Fig. 7.9 to 7.12. Fig. 7.9 shows the images of the coating produced with precursor containing 5 wt. % CaF_2 and current of 60, 80 and 100 A. The images clearly

indicate that a separate layer consisting dark particles deposited on the AISI 304 steel substrate with a minimum dilution of the base material. Although the distribution of dark particles at these layers are highly dense and almost uniform, the thickness of the layers are not uniform throughout the coating width for single line scan. Vigilant observation of the images revealed some cracks at the coating-substrate interface and randomly distributed pores in the coating layer. Careful examination of the SEM images would expose that intensity of pores and cracks in the coating or interface region reduces with the increase in processing current. It is perhaps due to the fact that, the coating-substrate interface cracks mainly appeared near-edge position of the track, owing to relatively low heat intensity. Moreover, the coating produced with 5 wt.% CaF_2 in the precursor containing a relatively higher percentage of TiC, which restricts the heat flow towards the base material and minimizes the melting and subsequent mixing or dilution of the substrate with the coating material. This phenomenon causes a separate layer of TiC-Ni-CaF_2 coating with a high volume percentage of TiC. It may be postulated that during solidification, owing to mismatch in the thermal properties of the coating material (mainly TiC) and steel substrate, the residual stress developed in the coating and produces cracks at the coating-substrate interface. It is accepted that the morphology of reinforced particles in the composite coatings essentially governed by the applied processing current. In the present TiC-Ni-CaF_2 coating produced at lower current, un-melted and partially melted TiC particles appeared in the coating zone. As processing current increased from 60 to 80A, it is evident that TiC particles partially melted and produces small spherical shaped structures as depicted in Fig. 7.9b. It can also be noted from the image (Fig. 7.9c) that with further increase in processing current (100 A), the produced coating exhibited uniformly distributed TiC particles inside the melt pool. This might be attributed to complete melting of TiC particles at higher processing current and subsequent mixing with the steel substrate, which after solidification produces a homogeneously distributed TiC particle reinforced steel composite. It may be postulated that during TIG cladding process, Ni and CaF_2 melted and mixed with the steel matrix and produced a solid solution after solidification. From the XRD analysis, it was revealed that due to the reaction of Ni and CaF_2 some intermetallic like $CaNi_3$, and Ca_2Ni_7 formed, which support the formation of a solid solution containing Ni, Ca and Fe.

The magnified SEM images of the cross-section of TiC-Ni-CaF_2 coating produced with precursor containing 10 wt. % CaF_2 and processed at different current are illustrated in Fig. 7.10. It is interesting to see from the images that a uniformly distributed TiC-Ni-CaF_2

composite coating layer formed on the AISI 304 steel substrate; however, no interfacial crack between the coating and substrate material has been observed. The absence of interfacial gap for using a higher percentage of CaF_2 in the precursor perhaps attributes to better mixing of the coating material with the substrate at the coating-substrate interface. This induces a strong bond between the coating and substrate. A close comparison between the coating produced with 5 and 10 wt.% CaF_2 for similar current condition indicate that the coating produced with 10% CaF_2, exhibit more homogeneous structure than the coating produced with 5% CaF_2.

Similarly, Fig. 7.11 illustrate the SEM images of the cross-section of TiC-Ni-CaF_2 composite coating produced with precursor containing 15 wt.% CaF_2 and processing current of 60, 80 and 100 A. It is relevant to pointing out that the morphology of the coating cross-section is similar to the coating produced with 5 and 10% CaF_2, for using 60 A current; i.e. a uniform and distinguished coating layer formed on the substrate (Fig. 7.11a). However, for applying higher current (80 and 100 A), owing to the combined effect of higher heat input and influence of higher percentage CaF_2 (which act as a flux), the coating material (TiC-Ni-CaF_2) diluted and distributed on the substrate surface (Fig. 7.11b-c). This phenomenon is prominent for the coating produced with 100 A current, where a highly diluted composite layer formed on the steel surface to a larger depth. Careful investigation of Fig.7.11c revealed the formation of a thin dark layer over the substrate surface. A separate EDS analysis for this selected region confirms that, this dark layer containing a higher percentage of CaF_2. It is postulated that for using a higher percentage of CaF_2 in the precursor, due to its low density, the undissolved CaF_2 drifted in the melt pool and after solidification produces a very thin and dark layer.

Finally, the cross-sectional SEM images of the coating produced with 20 wt% CaF_2 and at different current settings are represented in Fig.7.12. From the images, it is evident that, for applying relatively low current (60 A) a uniform coating layer deposited on the substrate surface. From the earlier discussion (section 7.3.1), it is worth to mention that, for using 20 wt. % CaF_2 and higher current (80 and 100 A) the coating layer formed on the substrate are found broken or irregular. Thus, further analysis of these samples was not considered in the present study.

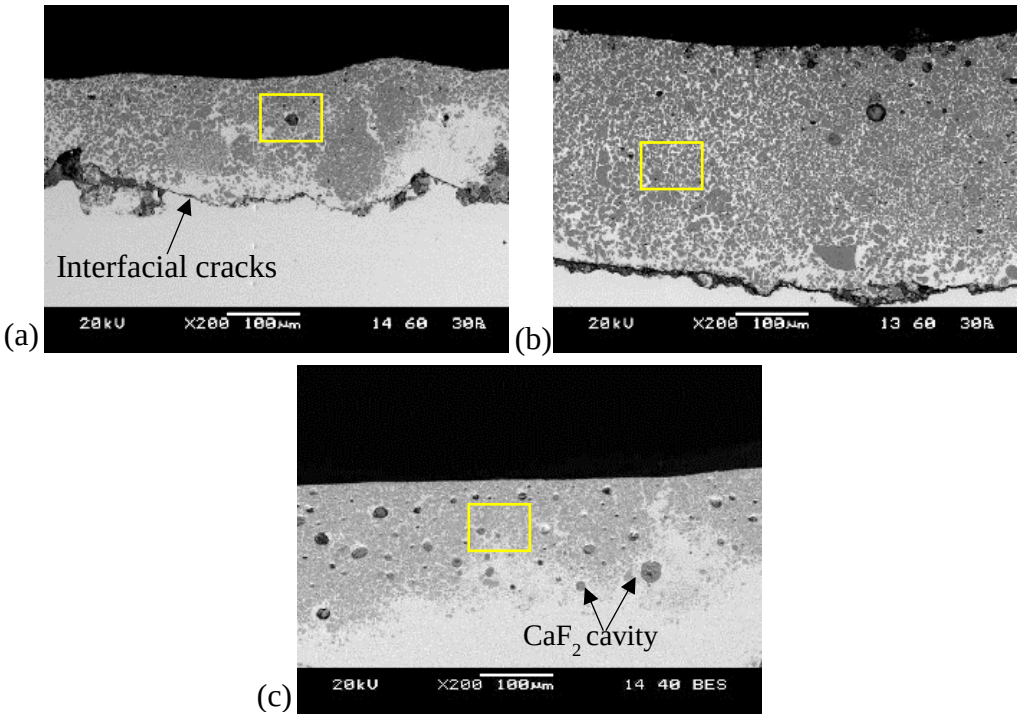

Fig. 7.9: Magnification SEM image correspond to Fig 7.2 of TiC-Ni-CaF_2 produced with precursor coating 5wt.% CaF_2 and processing current of (a) 60 A, (b) 80 A, (c) 100 A

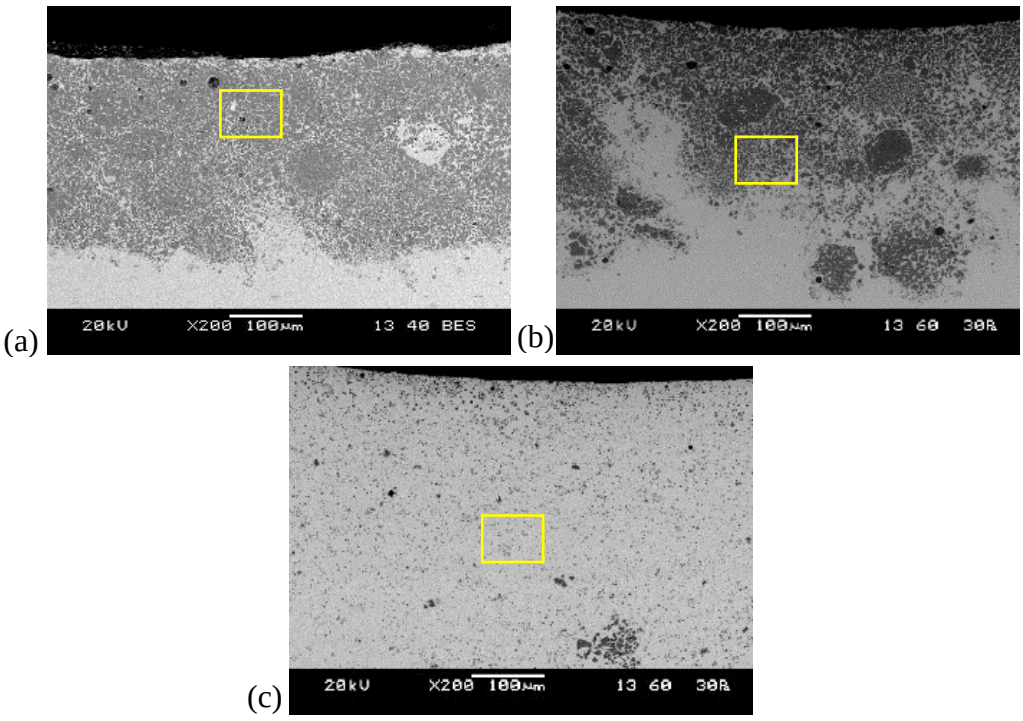

Fig. 7.10: Magnification SEM image correspond to Fig 7.3 of TiC-Ni-CaF_2 produced with precursor coating 10 wt.% CaF_2 and processing current of (a) 60 A, (b) 80 A, (c) 100 A

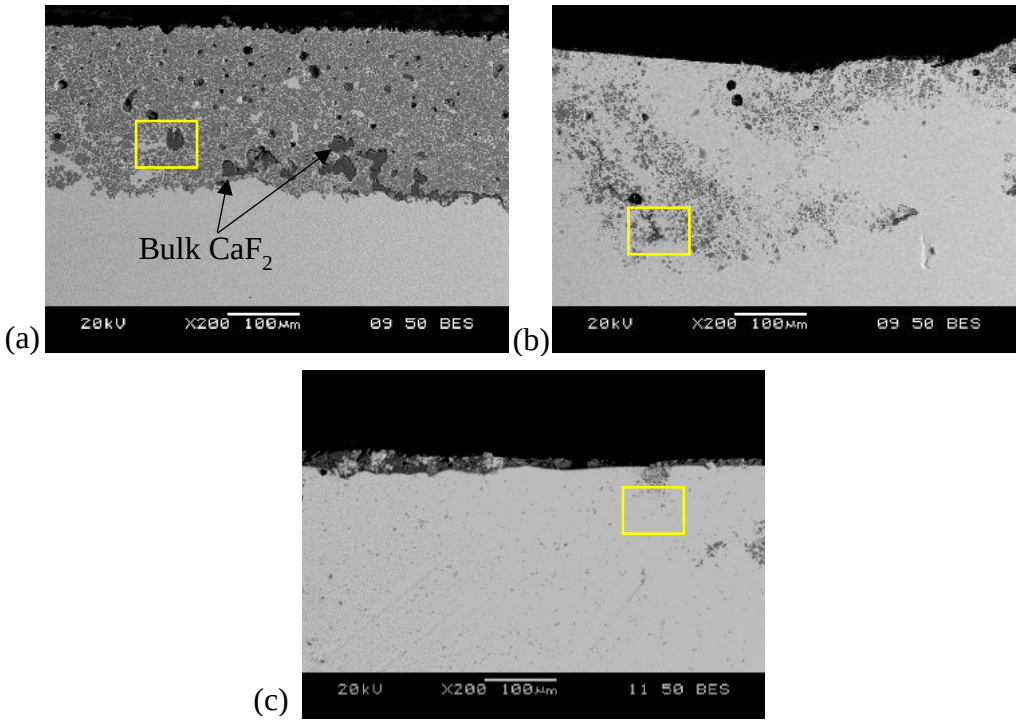

Fig. 7.11: Magnification SEM image correspond to Fig. 7.4 of TiC-Ni-CaF_2 produced with precursor coating 15wt.% CaF_2 and processing current of (a) 60 A, (b) 80 A, (c) 100 A

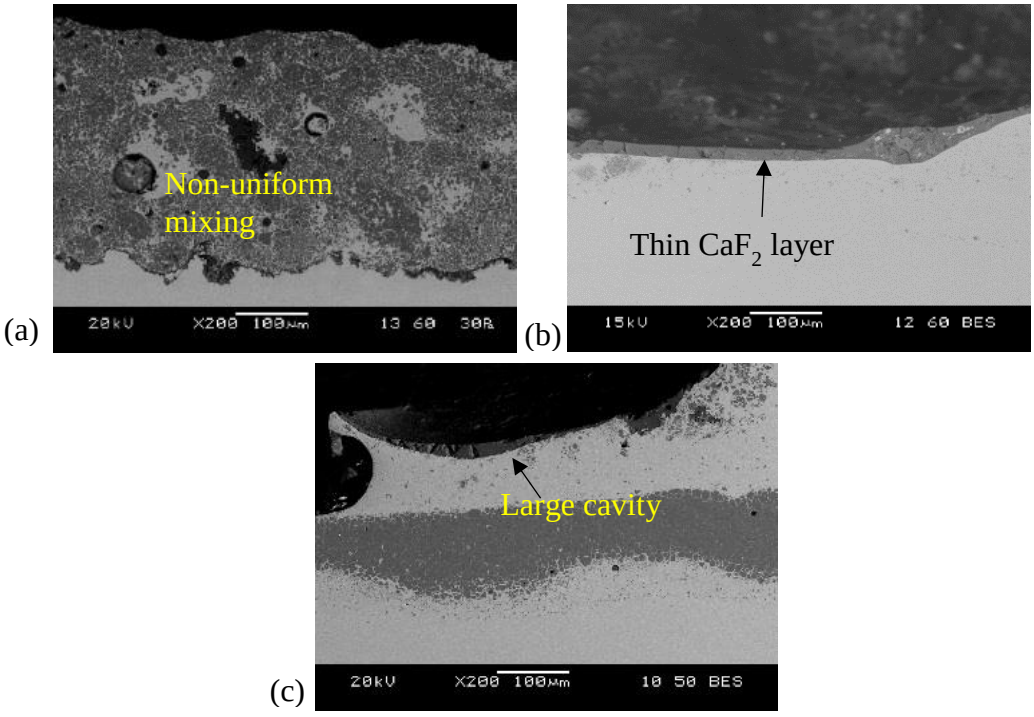

Fig. 7.12: Magnification SEM image correspond to Fig. 7.5 of TiC-Ni-CaF_2 produced with precursor coating 20wt.% CaF_2 and processing current of (a) 60 A, (b) 80 A, (c) 100 A

In order to further characterize the structural features of the produced coatings, high-magnified SEM images from the selected area of Fig. 7.9–7.11 (as marked) are considered and represented in Fig. 7.13–7.15. It is evident from the microstructure (Fig. 7.13–7.15)

that for using low current (60 A) and different percentage of CaF_2 (5, 10 and 15%) in the precursor, globular shaped dark shaded particles are embedded in the lighter shaded matrix. Almost similar structure can also be observed for the coating produced at 80 A current for using 5 and 10% CaF_2 in the precursor. In TIG cladding process, scanning of arc over the pre-deposited TiC/Ni/CaF_2 precursor resulted in complete melting of the Ni powder and surface of the steel substrate. Since the melting temperature of TiC is extremely high (~3000 ^oC), it is postulated that at relatively lower heat input, instead of complete melting, the sharp edges of larger size TiC particles melted and shaped into the spherical structure. The molten part of TiC particles mixed in the matrix and after solidification forms smaller spherical shaped structure. This behavior of melting and solidification of TiC inside a metal matrix supported by earlier research work of laser melting (Gu et al., 2009).

It is obvious from the SEM images that at lower current (60 A), CaF_2 powder appeared in the coating as a black pocket-like structure within the TiC-Ni coated layer. As mixing of the precursor powder was carried out through manual stirring, it is possible that CaF_2 powder not mixed uniformly with TiC and Ni powder in the precursor. At relatively high heat input (synergic effect of high current and a higher percentage of CaF_2 in the precursor), the coating morphology consists small size dark particles reinforced in the relatively larger percentage of light shaded matrix. This might be attributed to complete melting of TiC particles in conjunction with the other constituents and dilution within the molten steel surface and subsequent solidification of the melt pool.

In order to identify the different shaded structure in the produced composite coating, a detailed EDS analysis was performed for the selected samples. High-magnified SEM image and corresponding EDS mapping of the TiC-Ni-CaF_2 coating produced at 60 A current for using 10% CaF_2 in the precursor is shown in Fig. 7.16. It is worth to pointing out that the coating predominantly consisting dark gray shaded particles reinforced in the white shaded matrix. The EDS elemental mapping revealed that these dark shaded particles are essentially containing Ti and C. Thus, it can be inferred that these dark shaded particles are TiC, which reinforced in the light shaded matrix zone. The EDS elemental mapping also revealed that reasonable amount Fe, Ni and Cr are present in the light shaded matrix region, whereas a bulk amount of Ca and F identified in the pore-like structure. The traceable quantity of uniformly distributed Ca and F also detected in the matrix zone.

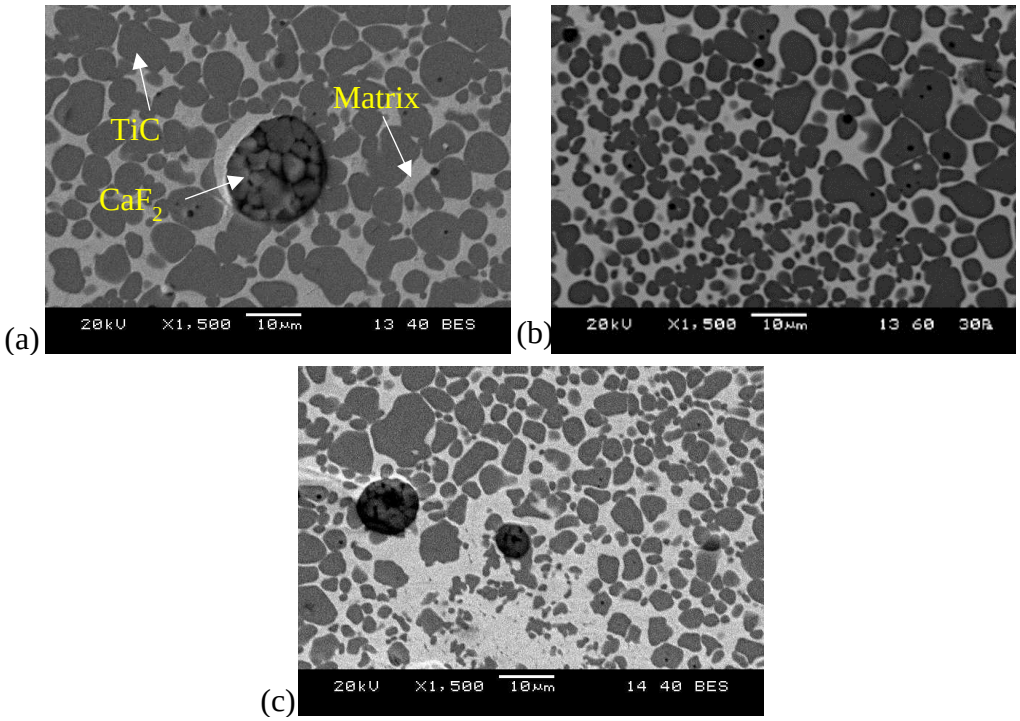

Fig. 7.13: Microstructure of TiC-Ni-CaF_2 produced with precursor coating 5wt.% CaF_2 and processing current of (a) 60 A, (b) 80 A, (c) 100 A

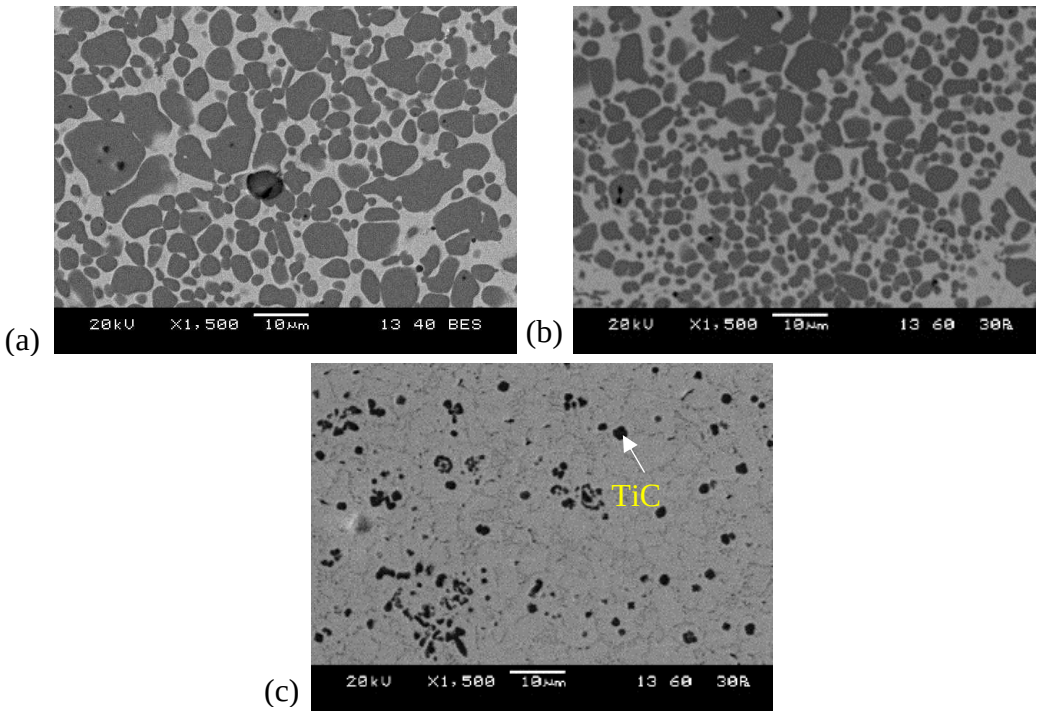

Fig. 7.14: Microstructure of TiC-Ni-CaF_2 produced with precursor coating 10wt.% CaF_2 and processing current of (a) 60 A, (b) 80 A, (c) 100 A

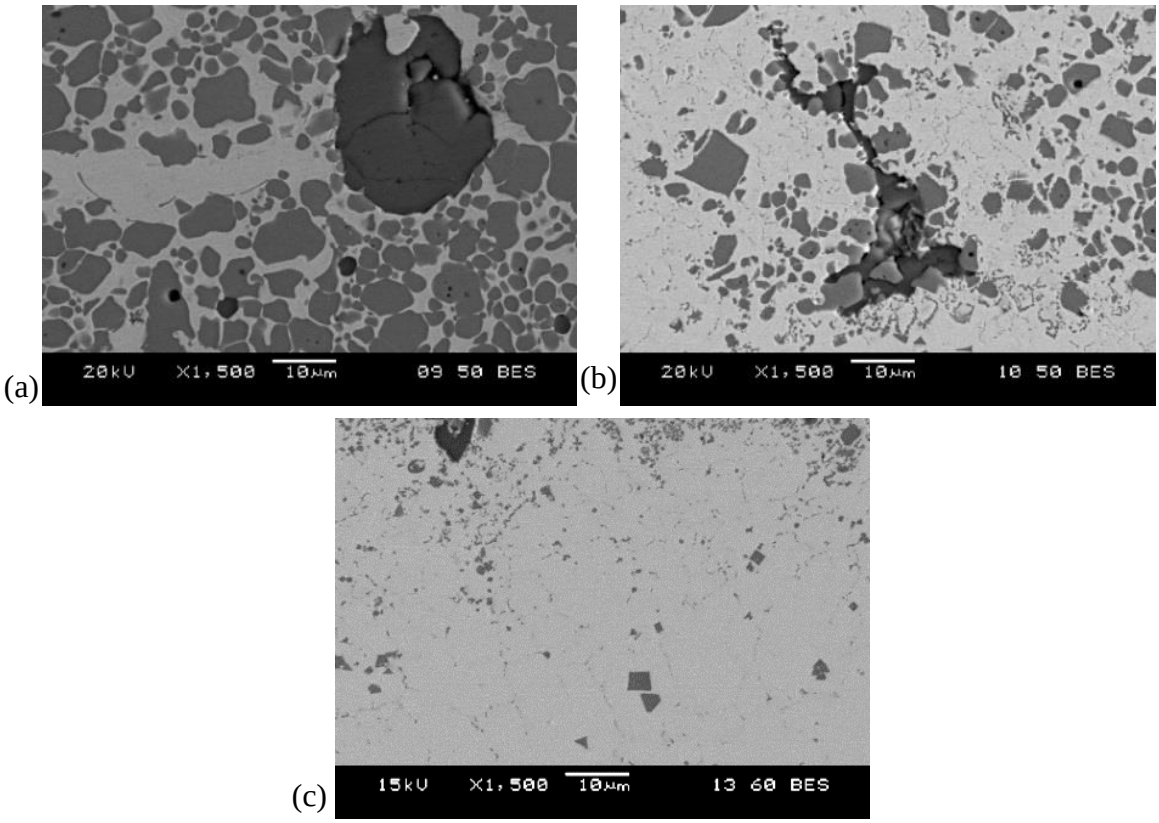

Fig. 7.15: Microstructure of TiC-Ni-CaF_2 produced with precursor coating 15wt.% CaF_2 and processing current of (a) 60 A, (b) 80 A, (c) 100 A

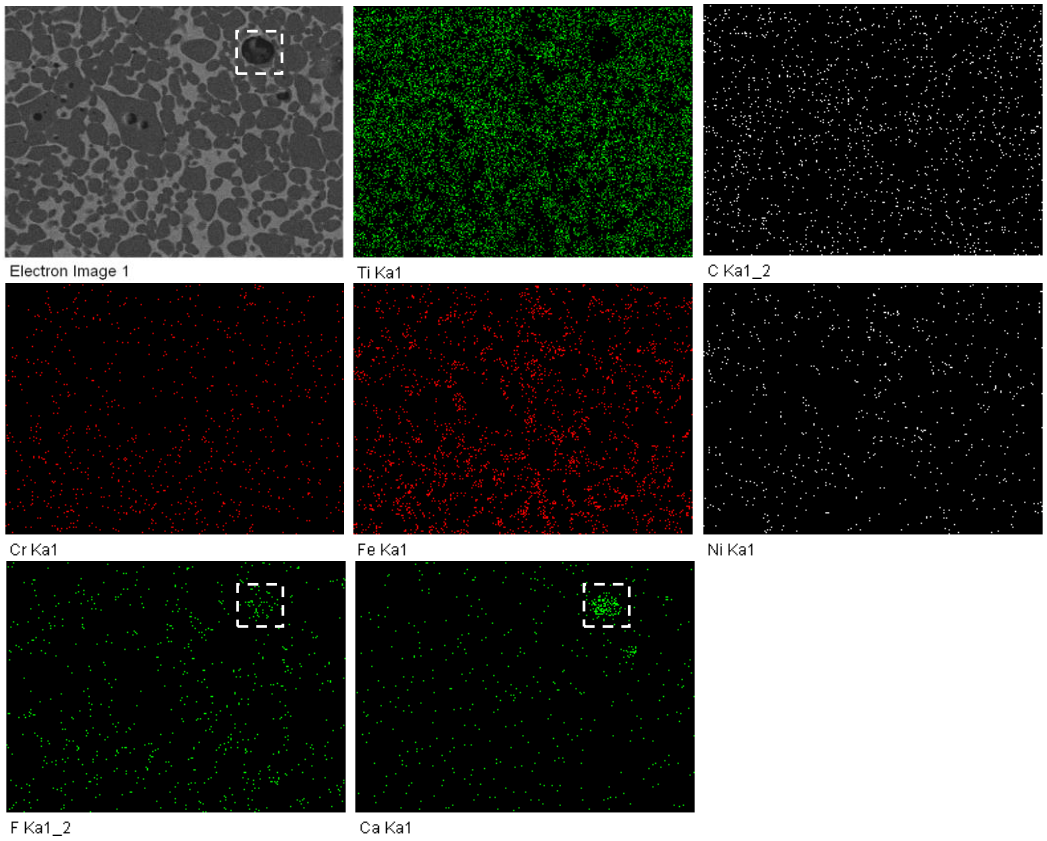

Fig. 7.16: EDS mapping of coating formed using 10 wt.% CaF_2 powder system processed using 60 A current

To confirm the presence of unreacted CaF_2 in the pocket-like structure in the coating, EDS analysis was performed on the selected area as shown in Fig. 7.17. Table 7.4 illustrate the weight percentage of elements detected through EDS analysis at different position of the coating as marked in Fig. 7.17a. The analysis revealed that zone S1 or pore-like structure, where some agglomerated particles are trapped containing nearly 40% Ca and 60 % F, which confirm that these trapped particles are CaF_2. The entrapment of CaF_2 particles in the coating perhaps attributed to inadequate mixing of large size agglomerated CaF_2 with the initial TiC and Ni powder. The high-magnified image of the marked portion as illustrated in Fig. 7.17b unveil the agglomerated CaF_2 particles inside the coating layer. Most notably, the dark particle type structure in the coating as marked S2 found containing predominantly Ti and C and the light shaded matrix zone marked as S3 comprising Fe, Ni, Ti, C, Cr. In this context, it is worth pointing out that similar type porous structure filled with CaF_2 particles also appear in the coated layer for the sample treated with a higher percentage of CaF_2 in the precursor.

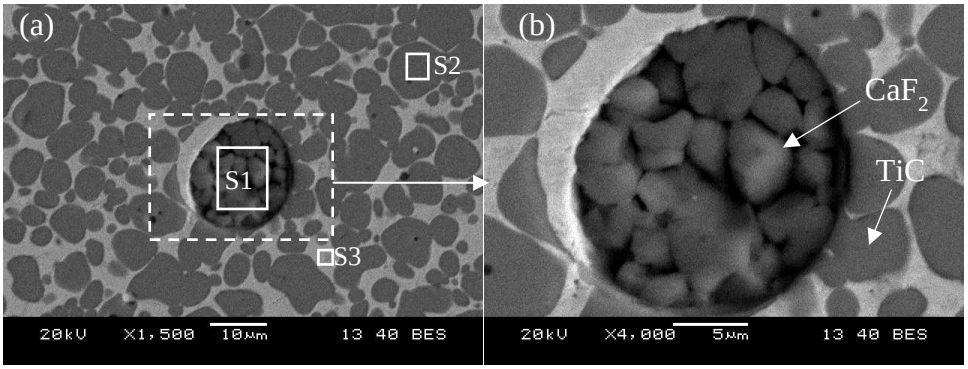

Fig. 7.17: High magnification image of coating for 5wt.% CaF_2 system produced using 60 A current

Table 7.4: EDS elemental analysis of marked position corresponding to Fig. 7.17

Elements	C	F	Ca	Ti	Cr	Fe	Ni
Position	(wt.%)						
S1		60.26	39.74				
S2	25.64			74.36			
S3	11.54			20.67	6.45	37.85	23.49

In order to study the effect of processing current on the used CaF_2 particles inside the coating, a detailed EDS analysis was carried out on the magnified images of the coating produced with 15% CaF_2 in the precursor, and different current condition. Fig. 7.18a & b show the SEM photomicrographs and corresponding EDS analysis performed on different

shaded structure (as marked S1, S2 and S3) for TiC-Ni-CaF_2 coating produced with 15% CaF_2 in the precursor and processing current of 60 and 80 A respectively.

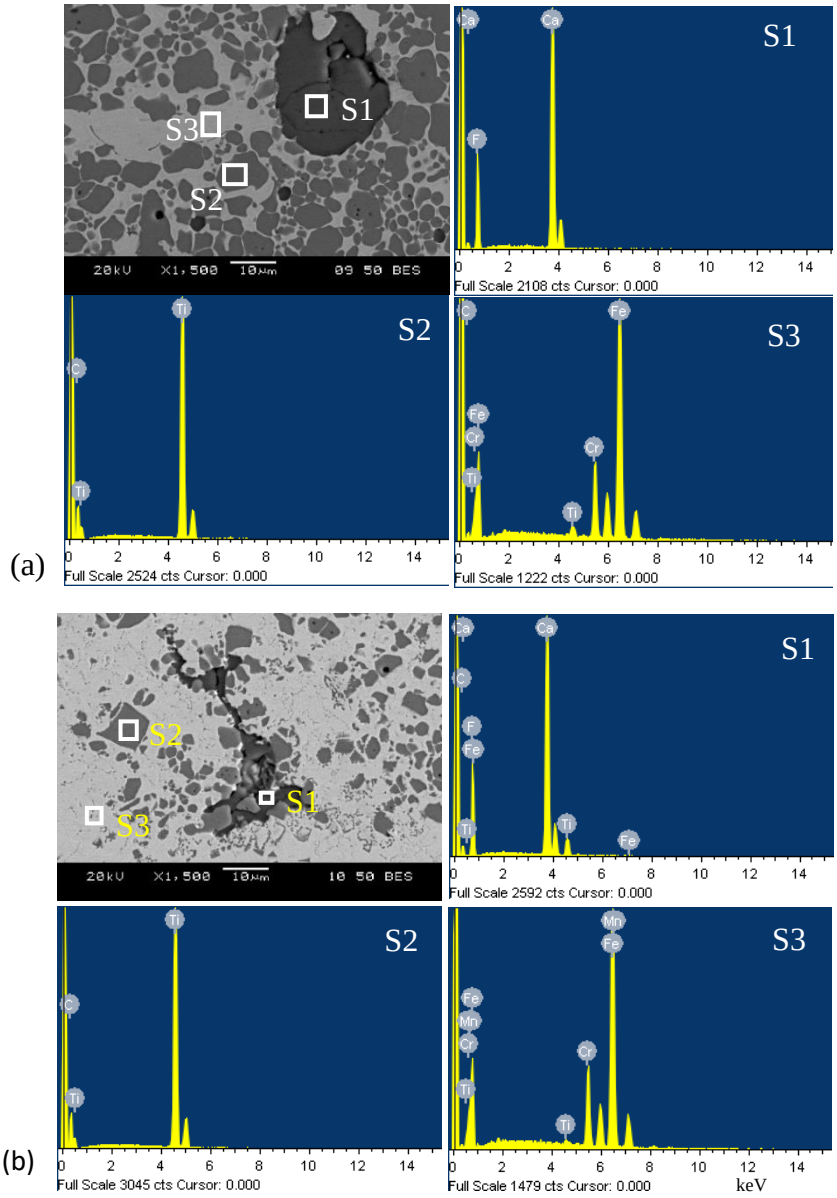

Fig. 7.18: EDS elemental analysis of the microstructure of the coating produced with 15 wt.% CaF_2 in the precursor and current of (a) 60 A and (b) 80A

Table 7.5: EDS analysis of TiC-Ni-CaF_2 coating produced with 15wt.% CaF_2 in the precursor and current of 60 and 80 A, as marked in Fig. 7.18

	Elements	**Ca**	**F**	**Ti**	**C**	**Fe**	**Cr**	**Mn**
	Position	**Wt.%**						
Fig. 7.18a (60 A)	S1	41.42	58.58					
	S2			75.72	24.28			
	S3			1.58	5.86	76.81	15.75	
Fig. 7.18b (80 A)	S1	35.29	54.07	4.32	5.81	0.51		
	S2			76.39	23.61			
	S3			0.61		75.66	14.63	9.10

The percentage of elements present in different zones (as marked S1, S2 and S3) are exemplified in Table-5. Similar to the earlier analysis, the dark shaded trapped particles, those are erratically dispersed in the coating (marked as S1) show the presence of highly concentrated Ca and F. Therefore, it can be inferred that these dark particles are unreacted CaF_2 trapped in the coating during solidification. Similarly, the gray shaded particles (marked as S2), and light shaded matrix (marked as S3) zones are detected as TiC and steel matrix with some alloying elements. A close comparison of the micrographs of the coating produced with different current setting revealed that the CaF_2, which is present as large size particles in agglomerated condition for using 60 A current (Fig. 7.18a), become fragmented and distributed in the steel matrix for using 80 A current (Fig. 7.18b).

7.3.5 Sliding abrasive wear

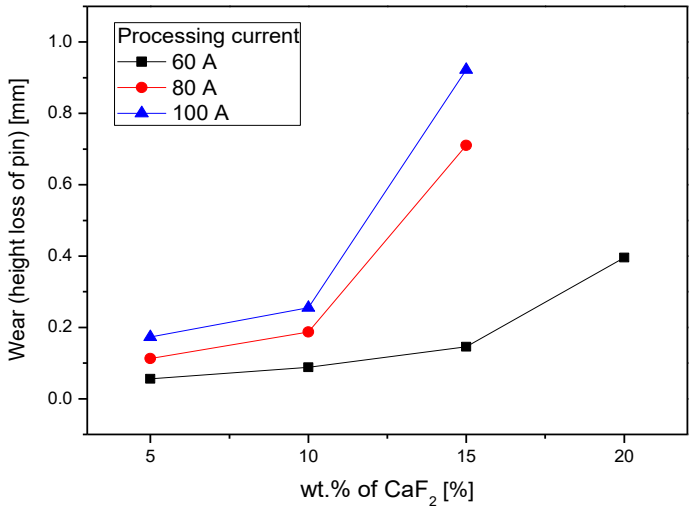

Fig. 7.19: Variation in abrasive wear (height loss) of the TiC-Ni-CaF_2 coated pin for using different percentage of CaF_2 in the precursor processed at different current condition

It is well accepted that the wear characteristics of the composite coating largely govern by the constituent percentage and its microstructure. Hence, it is essential to understand the wear mechanism of the coating produced with precursor containing different percentage of CaF_2 and processed at variable processing current. The present study investigates the detailed wear mechanism as well as comparative evaluation of the wear characteristics of the coated samples under sliding abrasive condition. Rotational sliding wear test of the TiC-Ni-CaF_2 coated pin samples, and as-received AISI 304 steel pin has been performed against alumina abrasive disc in room temperature. The height loss of the pin after the test considered as wear of the coated sample. The wear in terms of height loss for the samples processed at different current plotted against the used CaF_2 percentage in the precursor are

shown in Fig.7.19. From the plot, it is seen that the wear (height loss) of the TiC-Ni-CaF_2 coated pin for 5 and 10 % of CaF_2 are in the range of 0.05 to 0.25 mm, whereas for higher percentage of CaF_2 this value reaches to 0.9 mm. It has been found that these wear values are considerably lower than the wear of as-received AISI 304 steel pin (1.4 mm), after the sliding abrasive wear test performed under similar test condition. It is interesting to note that the wear or height loss of the pin prepared from the samples produced with a lower percentage of CaF_2 (5 and 10 %) are significantly less. However, with the increase in CaF_2 percentage, the wear rate of the coating increases almost gradually. From the graph, it can also be inferred that for the sample produced with a fixed percentage of CaF_2, wear or height loss is significantly low for the sample processed at lower current (60 A) and the wear value gradually increases with the increase in processing current.

The analysis of SEM micrographs and micro-hardness of the TiC-Ni-CaF_2 coating as discussed earlier revealed that with the use of low percentage of CaF_2 in the precursor, the produced coating retained high-intensity TiC reinforcement and exhibited higher hardness value. The high intensity of TiC particles and corresponding high hardness of the coating resulted in low abrasive wear in terms of height loss for the coated pin sample produced with a low percentage of CaF_2 in the precursor. The analysis also elucidated that with the increasing CaF_2 percentage, the hardness value of the coating reduces steadily. From the microstructural analysis of the coating, it was revealed that as CaF_2 acting as an activating flux, effective heat input in the coating zone enhances. Consequently, the coating material (especially hard TiC particles) diluted in the softer Ni-steel matrix. It is obvious that the average distance between the reinforced TiC particles in the TiC-Ni-CaF_2 coating become larger, as the dilution of matrix material is augmented owing to the synergic effect of higher processing current and increased CaF_2 percentage. As the distance between the hard TiC particles increases, degradation of relatively softer matrix material enhanced. Additionally, pull out of undissolved TiC particles through plowing action by the alumina abrasive increases. Thus, overall wear or height loss of the coated pin enriched for a higher percentage of CaF_2 in the coating.

To ascertain the wear behavior of the TiC-Ni-CaF_2 coating produced with different percentage of CaF_2 in the precursor for variable processing current, measurement of height loss was also accomplished through data acquisition system attached to the test rig. Fig. 7.20 (a-c) illustrate the wear behavior of the TiC-Ni-CaF_2 coated steel pin samples in terms of height loss at the time of test measured through data acquisition system.

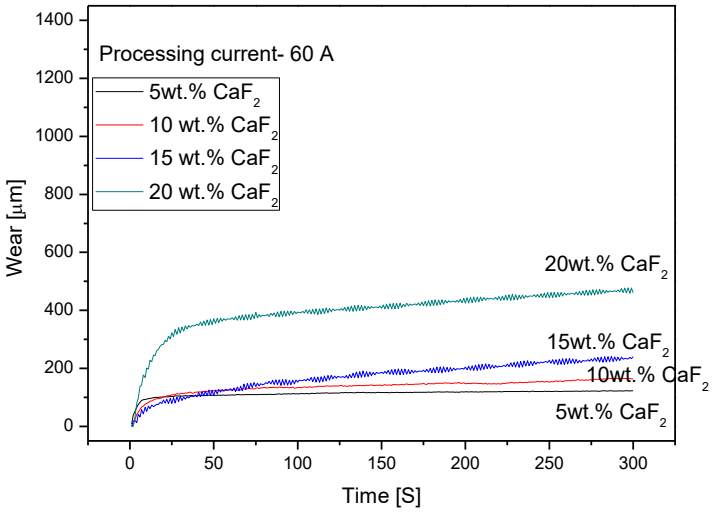

(a)

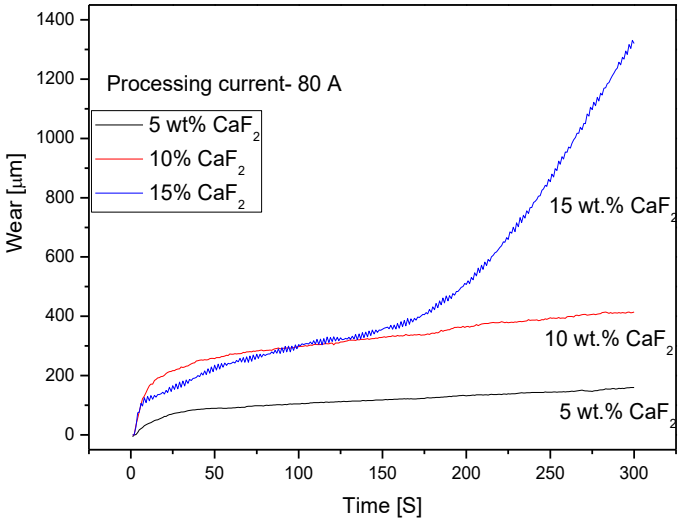

(b)

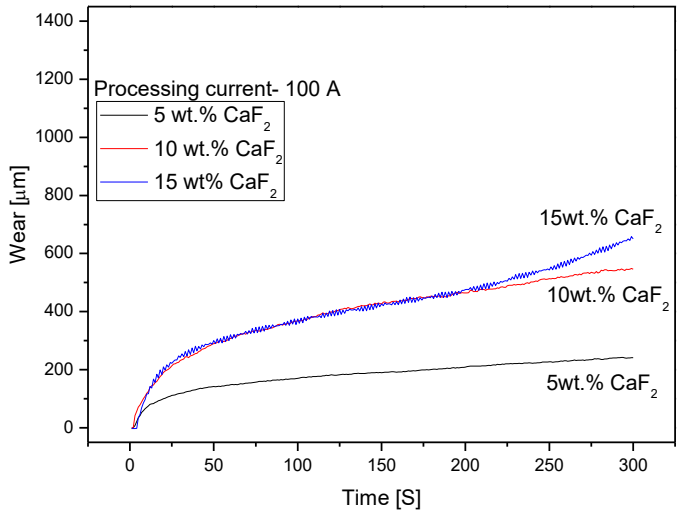

(c)

Fig. 7.20: Variation in wear behavior of TiC-Ni-CaF_2 coated pin produced with different percentage of CaF_2 in the precursor and current of (a) 60 A, (b) 80 A and (c) 100 A

It is interesting to comprehend from the plots that the height loss or wear of the coated pins gradually increases with time, although the gradient or rate of height loss is varying effectively, subjected to the processing condition i.e. the percentage of CaF_2 in the precursor and processing current. Fig. 7.20a clearly indicate that the wear or height loss at the end of the test for the coatings processed with 60 A current and different percentage of CaF_2 (5–15 % CaF_2) are in the range of 122 to 240 μm. It is evident from the plot that the wear rate of the coating produced with 5, 10 and 15 wt.% CaF_2 are significantly low. However, careful analysis of the plot clearly indicates that with the increase in CaF_2 percentage, the wear rate of the coated pin gradually increases, which is consistent with the results obtained through the measurement of height loss for the coated pins using Vernier caliper as illustrated in Fig. 7.19. Almost similar trend in the wear behavior also observed for the coating produced with 80 and 100 A current for using 5, 10 and 15 wt.% CaF_2 in the precursor as illustrated in Fig. 7.20b and 7.20c respectively. It is interesting to note that wear rate of the coating produced with 15 % CaF_2 and 80 A current surprisingly amplified after a certain period of test (170 S). This undesirable behavior in the wear rate of the coating perhaps explained from the morphology of the respective coating. As understood from Fig.7.11b and 7.15b, the density of hard TiC particle is very less and distributed non-uniformly in the produced coating. Thus, it may be postulated that after a period of test, the hard particles removed from the coating zone, and due enrichment of softer matrix, the wear rate of the coated pin drastically enhanced.

7.3.6 Morphology of worn surface

The SEM images of the worn out coating surface (produced with 60 A current and different percentage of CaF_2 in the precursor) after the sliding abrasive wear test against alumina abrasive disc are illustrated in Fig.7.21. From the SEM images, it is reveal that for using 5% CaF_2 in the coating and processed with 60A current, the worn out surface is almost smooth and no major delamination or peeled out region observed on the surface. However, the magnified image (Fig.7.21b) shows the presence of pores and very low intense scratches on the worn out surface after the sliding abrasive wear test. Moreover, no trace of lamellar wear debris was observed, which is a common phenomenon occurred because of plastic deformation or oxidation of the worn surface during sliding wear test of ductile materials (Rasool and Stack, 2014). On the contrary, it is interesting to note that for using a higher percentage of CaF_2 (10 and 15 %), the worn surface of the coating partially removed along with some crack formation at the surface. Magnified image of the selected region revealed

that the worn out surface consisting some wear debris, which perhaps formed because of plastic deformation and oxidation of the coated surface.

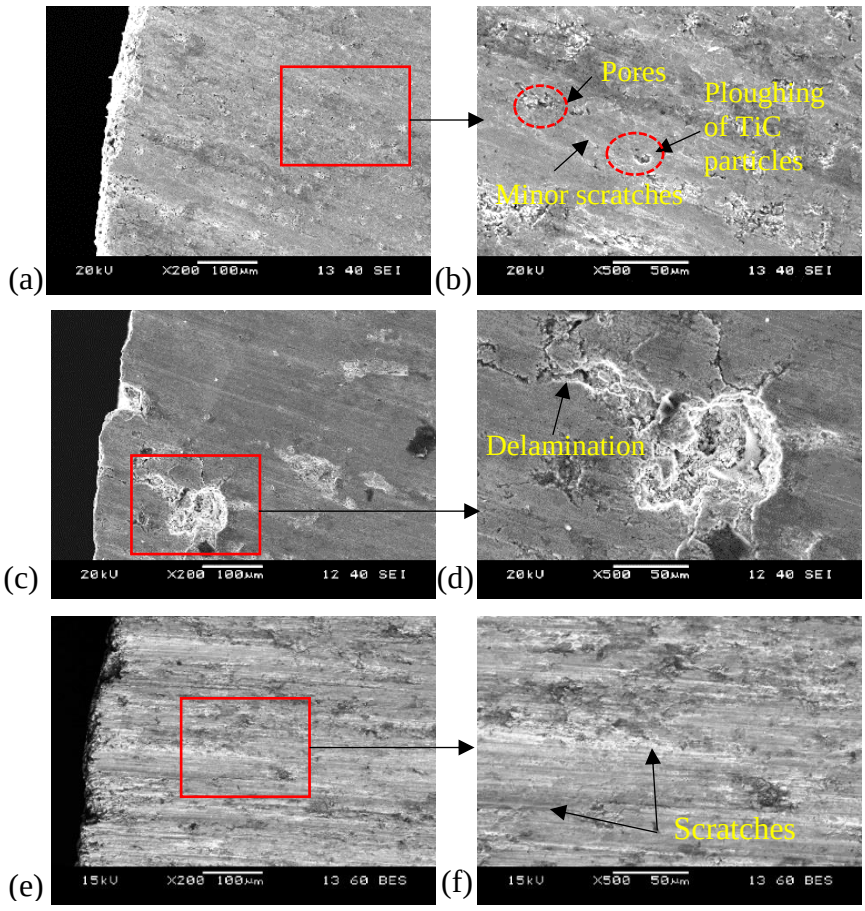

Fig. 7.21: SEM images (at different magnification) of the worn out TiC-Ni-CaF_2 composite coating surface (after sliding abrasive wear test) produced at 60 A current, for using (a–b) 5wt.% (c–d) 10wt.% and (e-f) 15wt.% CaF_2 in the precursor

Due to high concentration of TiC reinforcement, coating produced with 5 wt.% CaF_2 precursor exhibits high resistance to abrasive wear against alumina disc. Consequently, the removal of TiC layer become restricted with negligible scratch induces in the coated surface. With the increasing CaF_2 content in the precursor, a hard coating layer formed on the substrate surface. However, it is evident that some portion of the coating surface peeled off during the wear test (as depicted in Fig. 7.21c-d). This may be attributed to the dilution of the softer matrix, which makes the coating less resistive to plastic deformation. Therefore, TiC-Ni-CaF_2 coating produced with a higher percentage of CaF_2 (10 and 15%) exhibited higher abrasive wear compared to the coating produced with 5% CaF_2 processed with similar processing current.

Fig. 7.22 show the SEM micrographs of the worn surface of the TiC-Ni-CaF_2 coating produced with 80 A current for using different percentage of CaF_2 in the precursor. Similar

to the samples produced at 60 A current, the effect of CaF_2 percentage, can be observed from the worn out surface. It is also evident that the appearance of scratch and pores due to delamination of the coating is less for the coating produced with precursor contained a lower percentage of CaF_2. In contrast, high intense scratch or delaminated layer witnessed on the worn surface of the coating produced with a higher percentage of CaF_2.

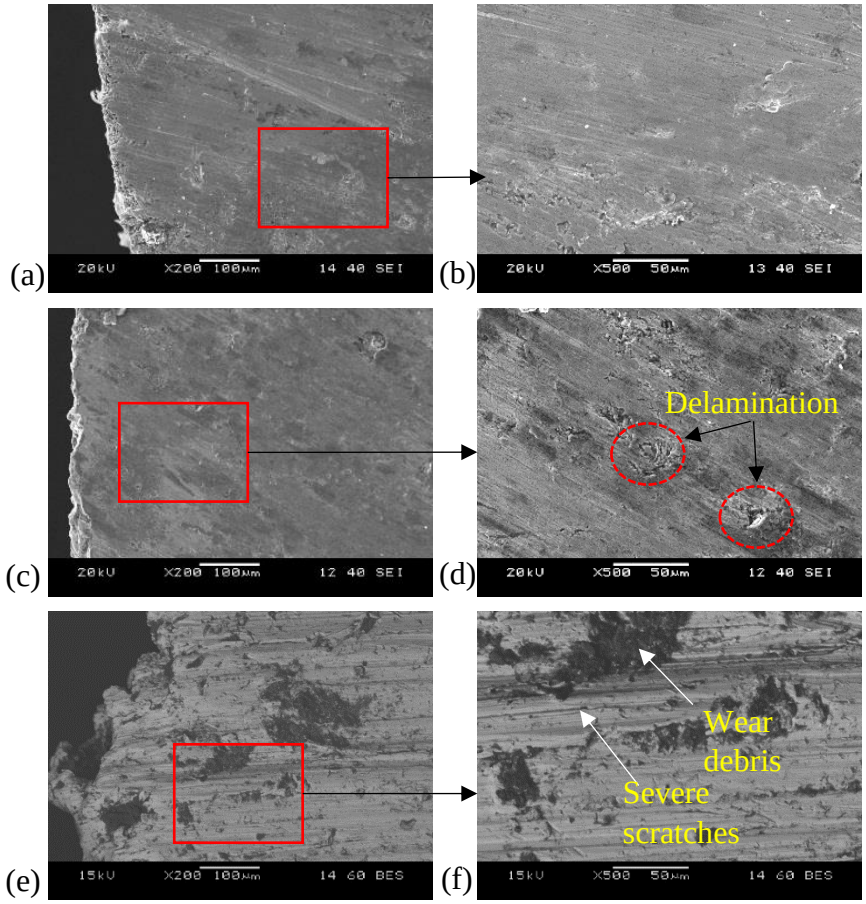

Fig. 7.22: SEM micrographs (at different magnification) of the worn out TiC-Ni-CaF_2 composite coating surface (after sliding abrasive wear test) produced at 80 A current, for using (a–b) 5wt.% (c–d) 10wt.% and (e-f) 15wt.% CaF_2 in the precursor

Fig. 7.23 (a-b) illustrate the magnified SEM image of the worn out surface and corresponding EDS analysis of the selected region (as marked S1 and S2) for the coating produced with 80A current and precursor containing 5 and 15% CaF_2 respectively. The elements present at zone S1 and S2 are illustrated in Table-7.6. The micrograph of the worn surface for coating produced with 5% CaF_2 (Fig. 7.23a) clearly indicate that the dark shaded TiC particles (marked as S1) are still present in the coating after the sliding abrasive wear test. However, due to sliding against alumina abrasive disc, some TiC particle removed out from the coating surface and produces cavity on the surface. EDS analysis of zone S2 revealed that this dark zone consists high percentage of Al, O, C in consort with the elements

of steel matrix. It is expected that during sliding abrasive wear test, loosely bonded Al_2O_3 abrasive grits removed out from the disc and mixed with the debris emerging from the coating surface and embedded on the surface again due to continuous sliding. In contrast, for the sample processed with 15% CaF_2 in the precursor (Fig. 7.23b) the SEM image and corresponding EDS analysis revealed that the white shaded zone S1 consists high percentage of Fe, Cr, and Mn with negligible amount of Ti, Ca and F. Therefore, it may be inferred that after the sliding wear test TiC layer together with CaF_2 removed from the coating layer and exposed the steel substrate. The absence of TiC particles on the worn surface, processed with 80 A current for using a higher percentage of CaF_2 (15%), attribute to dilution of the TiC hard phase owing to the synergic effect of CaF_2 and higher current. Similar to the earlier analysis, it is found that the dark scattered region in the image (marked as S2) consists higher percentage of Al, O, and C. As already described, it is perhaps due to embedding of debris that contains alumina particles removed from the counter-disc, and removed oxide and carbide from the coating surface.

Fig. 7.24 (a–f) show the worn surface of coating processed with 100 A current and different percentage of CaF_2 in the precursor. The microstructure of the coatings produced with 100 A current for different percentage of CaF_2 as described earlier, revealed the formation of diluted TiC reinforced layer. Consequently, during sliding abrasive wear test, the removal of the coating layer augmented significantly, which can be differentiated from the scratches appeared on the worn surfaces produced with different percentage of CaF_2. Careful observation of the images further revealed that the intensity of the scratches appeared on the worn surfaces of the TiC-Ni-CaF_2 coating produced with a lower percentage of CaF_2 (5%) is relatively less than the coating produced with a higher percentage of CaF_2 in the precursor. The images clearly revealed that for using 15% CaF_2, removal of coating material during sliding abrasive wear test causes catastrophic scratches. It is perhaps due to the characteristic of abrasive wear of the present TiC reinforced composite coating, which predominantly depends on the morphology of TiC reinforcement in the matrix and hardness value of the coating. Due to relatively lower hardness value of the coating produced with a higher percentage of CaF_2, resistance to abrasive wear of the coating surface drastically reduces. Therefore, intense scratches and catastrophic delamination of the coating layer occurred, and consequently enriched wear or height loss obtained as compared to the coating produced with a lower percentage of CaF_2.

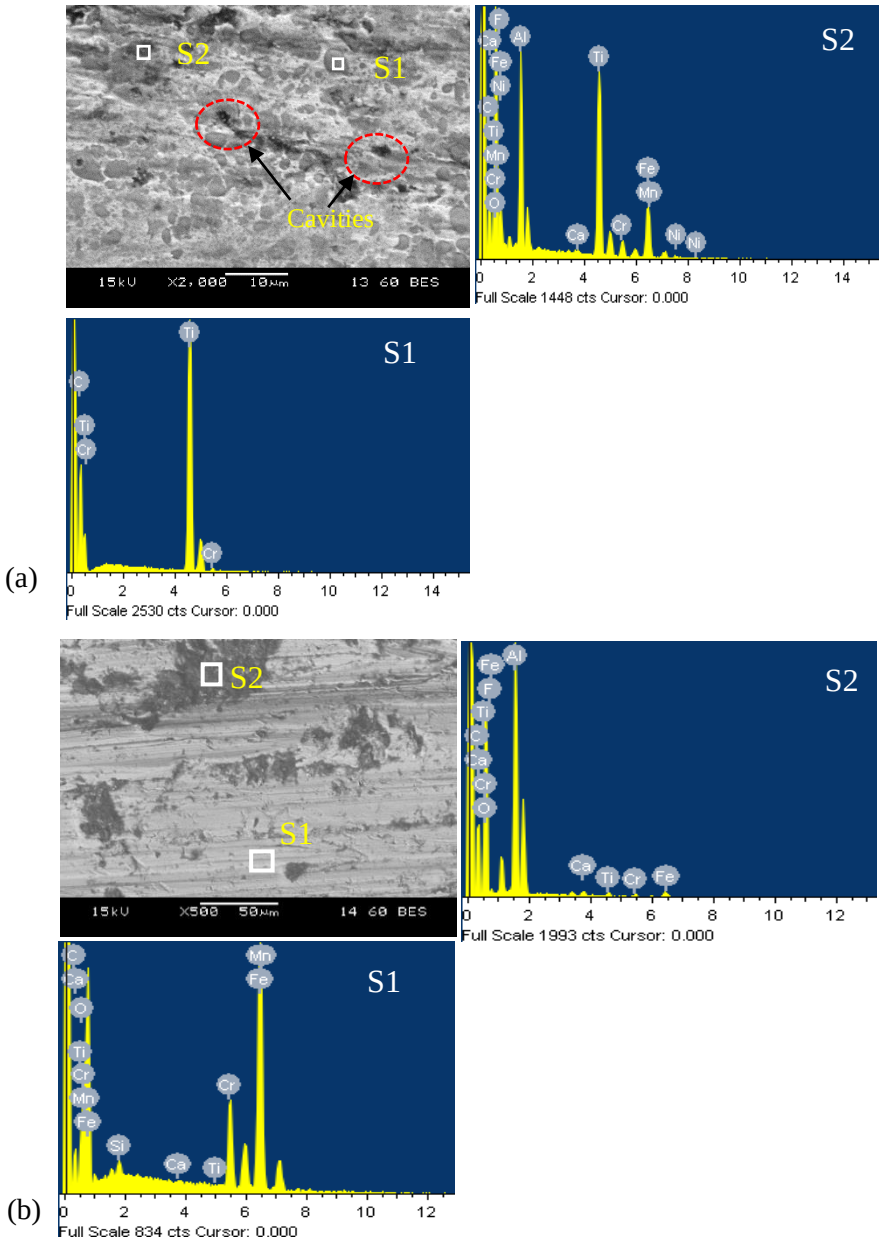

Fig. 7.23: SEM image and corresponding EDS analysis of the worn out surface for the coating produced with 80A current and precursor containing (a) 5% CaF_2 (b) 15% CaF_2

Table 7.6: EDS analysis of the marked region corresponding to Fig. 7.23

	Elements	C	O	F	Al	Ca	Ti	Cr	Fe	Si	Mn
	Position	(Wt.%)									
Fig. 7.23a (5% CaF_2)	S1	9.85	37.92	0.61	8.07	0.2	23.15	3.14	14.91	0.75	1.4
	S2	27.52					71.49	0.99			
Fig. 7.23b (15% CaF_2)	S1	28.36	46.94	1.12	18.73	0.69	0.65	0.7	2.82		
	S2	9.01	2.51			0.11	0.1	13.53	66.25	0.7	7.79

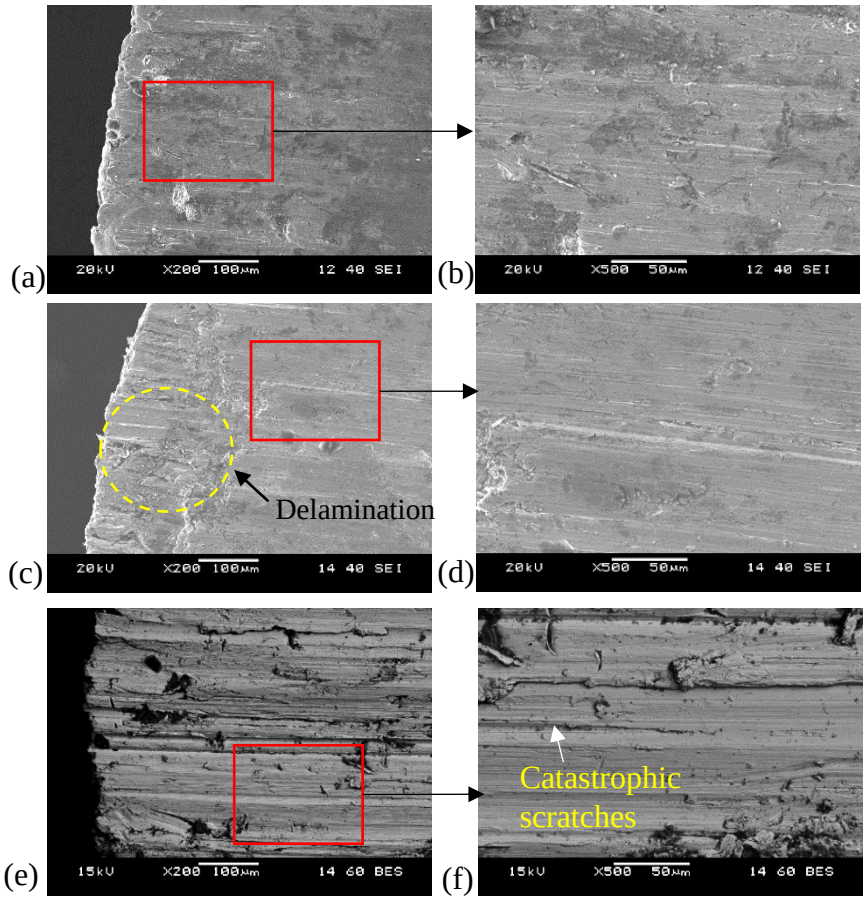

Fig. 7.24: SEM micrographs (at different magnification) of the worn out TiC-Ni-CaF_2 composite coating surface (after sliding abrasive wear test) produced at 100 A current, for using (a–b) 5wt.% (c–d) 10wt.% and (e-f) 15wt.% CaF_2 in the precursor

7.3.7 Coefficient of friction

To assess the coefficient of friction (COF) value of the produced TiC-Ni-CaF_2 coating, sliding wear test of the coated pin samples was carried out against a rotating hardened steel (HRC 58) disc, under 30 N normal load and sliding speed of 314 mm/s. To evaluate the effect of CaF_2 percentage on the COF value, the coatings produced with 60 and 100 A current for using precursor containing different percentage of CaF_2 were considered in the present test. Fig. 7.25 (a, b) shows the variation of COF against the time of test for the coating produced at 60 and 100 A current and different percentage of CaF_2 in the precursor. The plot (Fig. 7.25a) indicated that for using a lower percentage of CaF_2 in the coating, the average COF value is reasonably higher and for increasing the CaF_2 content in the composite coating, steady state COF value reduces gradually. The plot also indicated that for using lower percentage of CaF_2 (5%) in the precursor, the steady state COF value of the coating found approximately in the range of 0.65. However, COF value of the coating

produced with 20% CaF_2 appeared in the range of 0.3 at the initiation of the test, and increased to 0.4 at steady state condition. In this regard, it is relevant to mention that, COF value of produced TiC-Ni-CaF_2 composite coating produced at different processing condition are significantly lower than the COF value obtained for as-received AISI 304 steel (0.85) under similar test condition as described in Chapter-4.

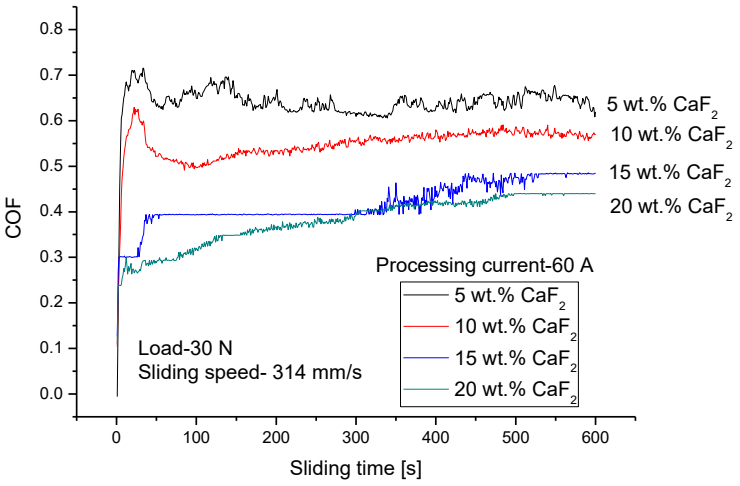

(a)

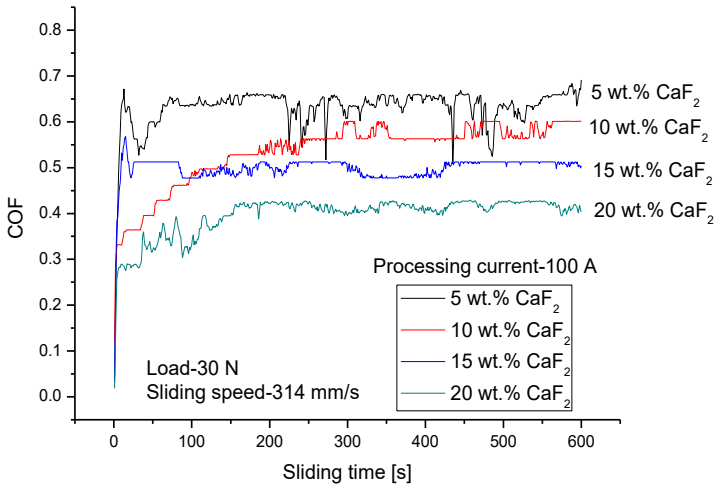

(b)

Fig. 7.25: Variation in coefficient of friction (against hardened steel, HRC 58) of TiC-Ni-CaF_2 coating produced at (a) 60 A and (b) 100 A current for using different percentage of CaF_2 in the precursor

A similar trend in the variation of COF can also be observed for the coatings produced with 100 A current and different percentages of CaF_2 in the precursor as depicted in Fig. 7.25b. From the earlier deliberation, it can be stated that, at higher current, attribute to high heat induction, reinforced TiC particles were diluted in the coating zone. Thus, the volume percentage of softer steel matrix increases, and owing to plastic deformation of the matrix material, the tendency of adhesion wear encouraged, that resulted in higher COF

value against hardened steel. Furthermore, it postulated that at higher temperature, CaF_2, react with Ni matrix and produces some intermetallic of relatively higher COF value. On the contrary, at lower processing current relative intensity of TiC reinforcement in the coating found significantly higher, that restrict the exposure of the steel matrix to counterpart and a relatively lower COF value for the coating obtained.

7.4 Outcomes

Hard and self-lubricant based TiC-Ni-CaF_2 composite coating consisting different percentage of CaF_2 have been effectively fabricated on AISI 304 stainless steel substrate by TIG cladding process. With the incorporation of CaF_2 in the TiC-Ni system, owing to self-fluxing effect of CaF_2, effective heat input in the melt pool enhances during TIG cladding process, and consequently dilution of hard phase namely TiC augmented.

From the experimental result, it is revealed that the morphology of the TiC-Ni-CaF_2 composite coating essentially depends on the processing current and percentage of CaF_2 in the precursor, that consequently effect the mechanical properties of the coating. The analysis of SEM micrographs and micro-hardness of the TiC-Ni-CaF_2 coating exposed that with the use of low percentage of CaF_2 in the precursor, the produced coating retained high-intensity TiC reinforcement and exhibited higher hardness value. The high intensity of TiC particles and corresponding high hardness of the coating resulted in low sliding abrasive wear in terms of height loss for the coated pin sample produced with a low percentage of CaF_2 in the precursor.

The hardness values of almost all the produced TiC-Ni-CaF_2 coatings are reasonably high (above 800 $HV_{0.05}$), but gradually decreasing with the increasing CaF_2 percentage during TIG cladding process. Furthermore, for using a similar percentage of CaF_2 in the precursor, the hardness value of the coating reduces with the increase in applied current, owing to dilution of the relatively soft steel substrate.

The experimental results revealed that for using a lower percentage of CaF_2 (5%) in the precursor, the steady state COF value of the TiC-Ni-CaF_2 coating against hardened steel disc found approximately in the range of 0.65 and with the increasing CaF_2 percentage in the precursor, the steady state COF value of the coating reduced to 0.4.

Chapter 8

Conclusions

8.1 Major conclusions

From the analysis of the results obtained during various phase of this study, following conclusions can be made:

A hard layer of TiC deposited or reinforced on AISI 304 steel substrate after laser irradiation over TiC preplaced steel surface using a pulsed Nd:YAG laser, depending on the laser processing parameters.

Analysis of the results indicates that the pulse laser parameters i.e. peak power and overlapping factor have great influence on the formation of TiC-steel composite layer. The increase in overlapping factor from 60 to 80% during laser processing, enhances the distribution of TiC particles inside steel substrate and increases the laser processed composite layer depth and width.

At lower range of peak power (1-1.5 kW), TiC composite coating deposited on steel substrate with a relatively low composite layer depth and width. In contrast, at higher peak power range (2 kW and above), TiC particles partially melted and distributed inside the surface of the steel substrate. At high peak power and higher overlapping condition, homogeneous structure of TiC-steel metal matrix composite coating formed due to melting and re-solidification of the preplaced TiC powder. Higher pulse duration improves the TiC distribution inside the steel surface and increases the composite layer depth.

The average surface hardness value of the AISI 304 steel substrate (220 $HV_{0.05}$) enhanced in the range of 400-1200 $HV_{0.05}$ depending on the laser processing parameters after laser surface coating with TiC. The average micro-hardness value of the composite layer is considerably high with low uniformity for using lower peak power. However, at higher peak power, uniform but relatively low hardness value obtained.

From the 2^{nd} phase of the experiment it can be concluded that TiC or TiC–steel composite coating has been successfully deposited on AISI 304 steel by using TIG cladding process with suitable processing parameters. Depending on the applied processing current and scan speed, TiC either deposited on the steel substrate as a dense layer with a very low

dilution of steel or form a TiC particle reinforced steel matrix composite layer on the substrate surface.

From the coating layer geometry, it can be concluded that the melt pool depth and width decreases with the reduction of heat input during the arc scanning. At low current (60 A) and high scan speed (6.5 mm/s), owing to low heat input, partially melted dense TiC layer produced over the steel substrate. In contrast at high current (100 A), TiC powder melted and diffused into the steel substrate due to the sturdy convective flow of the molten pool. This leads TiC to mix uniformly and dispersed at the upper layer of steel substrate during solidification. At lower current and higher speed combination, the heat input become insufficient for mixing the TiC powder inside the steel substrate and confining the convective flow of molten metal. Hence, a mix type structure consisting dense TiC layer and TiC-steel MMC structure formed. Furthermore, due to inadequate heating, the convective flow of molten metal may restrict and trapped the blown Ar gas used for shielding the arc, which leads to the formation of large voids specifically at the coating-substrate interface.

The micro-hardness value of the TiC coating produced with lower current (60 A) and high scan speed extended up to 1600 $HV_{0.05}$. Nevertheless, for the sample processed with high current and slow scan speed, due to dilution of TiC in the steel matrix, a reduced hardness value observed. Additionally, because of non-uniform coating morphology, the variation in hardness value found larger for the coating comprising an inhomogeneous structure.

Sliding abrasive wear test of the TIG coated TiC coating exhibited five to fifty times improvement in the wear resistance than the as received AISI 304 steel substrate. Owing to the high concentration of TiC and corresponding high hardness, abrasive wear of the coating produced with low current and high scan speed combination found very low. Conversely, coating processed with high heat input (high current and low scan speed combination), abrasive wear becomes inordinate due to the removal of softer steel matrix at a higher rate by SiC abrasive paper.

In the 3rd phase of the experiment, a hard and wear resistance TiC-Ni composite coating has been successfully deposited on AISI 304 stainless steel substrate by TIG cladding process.

Analysis of the results from this phase of experiments indicates that TiC-Ni metal matrix composite layer made a strong interfacial bond between the coating and substrate surface owing to the incorporation of Ni with TiC preplaced powder.

The experimental results revealed that TiC-Ni coating is possible to produce at relatively lower heat input (lower current) which exhibits comparatively higher hardness value than pure TiC coating. As the thermal and electrical conductivity of Ni is superior to TiC powder, incorporation of Ni in the preplaced powder mixture alter the electrical conductivity of the preplaced layer, that resulted in a continuous and smooth arc. Furthermore, the addition of Ni diminishes the total heat requirement for the melting of preplaced TiC-Ni layer.

The average micro-hardness value of TiC-Ni coating improved up to 1300 $HV_{0.05}$. The hardness value of TiC coating found superior to TiC-Ni coating deposited under similar processing condition; however, the enhanced bonding between the TiC particles with steel-Ni matrix compared to the bonding between TiC and steel matrix leads to a higher abrasive wear resistance in TiC-Ni coating than TiC coating.

Abrasive wear resistance of TiC-Ni coating has improved up to 70 times than the as received AISI 304 steel substrate and significantly higher than the TiC coating. High abrasive wear resistance observed in the low diluted coating, and the wear resistance decreases with the dilution of TiC reinforcement in the steel-Ni matrix.

TiC morphology in the TiC-Ni coating essentially depends on the TIG processing parameters i.e. current and scan speed that consequently effect the mechanical properties of the coating.

In the final phase of experiment, a hard and self-lubricant based TiC-Ni-CaF_2 composite coating consisting different percentage of CaF_2 have been effectively fabricated on AISI 304 stainless steel substrate by TIG cladding process.

With the incorporation of CaF_2 in the TiC-Ni system, owing to self-fluxing effect of CaF_2, effective heat input in the melt pool enhances during TIG cladding process, and consequently dilution of hard phase namely TiC augmented.

The morphology of the TiC-Ni-CaF_2 composite coating essentially depends on the TIG processing current and percentage of CaF_2 in the precursor, that consequently influence the mechanical properties of the coating.

SEM micrographs and micro-hardness of the TiC-Ni-CaF_2 coating exposed that with the use of low percentage of CaF_2 in the precursor, the produced coating retain high-intensity TiC reinforcement and exhibited higher hardness value. The high intensity of TiC particles and corresponding high hardness of the coating resulted in low sliding abrasive wear in terms of height loss for the coated pin sample produced with a low percentage of CaF_2 in the precursor.

The hardness values of almost all the produced TiC-Ni-CaF_2 coatings are reasonably high (above 800 $HV_{0.05}$), but gradually decreasing with the increasing CaF_2 percentage in the precursor during TIG cladding process. Furthermore, for using a similar percentage of CaF_2 in the precursor, the hardness value of the coating reduces with the increase in applied current, owing to dilution of the relatively soft steel substrate.

For using a lower percentage of CaF_2 (5%) in the precursor, the steady state COF value of the TiC-Ni-CaF_2 coating against hardened die-steel found approximately in the range of 0.7 and with the increase in CaF_2 percentage in the precursor, steady state COF value of the coating reduced down to 0.4.

8.2 Major contributions

A hard and wear resistance TiC/TiC-steel reinforced composite coating have deposited on AISI 304 steel by a pulsed laser and TIG cladding process. In addition, TiC-Ni composite coating with an improved bonding characteristic with the substrate, and TiC-Ni-CaF_2 composite coating with self-lubricating property have been successfully deposited on the AISI 304 steel substrate by TIG cladding process. The adopted TIG cladding method found an economical alternative of the expensive laser cladding process.

The developed coatings are found reasonably hard and have the potential to work as abrasive wear resistance coating. Sliding abrasive wear behavior of the developed coatings evaluated through pin-on-disc test revealed that the produced coating has high abrasive resistance. With the addition of Ni, owing to better bonding between TiC particles and the steel substrate, the effective wear resistance of the coating improved significantly. Furthermore, with the incorporation of CaF_2 in the coating, due to self-lubrication effect tribological property of the coating also enriched. The knowledge and the information engendered from the present study have not only academic importance but also be useful for the industrial personal involved in the manufacturing of hard, wear-resistant coatings for engineering applications.

8.3 Future scope of the present work

1. With the prospect of the superior performance of the produced different graded coatings (TiC/TiC-steel, TiC-Ni, and TiC-Ni-CaF_2), further experimentation can be performed by altering the ratio of the pre-placed powder constituents.

   Any change in the ratio of the constituents of the precursor leads to an alteration in the microstructural morphology which could enhance the mechanical and tribological properties of the coating. This may enhance the ability to tailor the properties of a coating according to the requirements.
2. The TIG processing parameters can be optimized for maximum mechanical and tribological performances of the produced composite coatings.

   In the present study, the effect of various parameters has been analyzed on the performance of the produced coating with a different composition. However, in order to apply the coating method as well as a particular coating composition, it is essential to adopt the coating condition which gives the best performance. Thus an optimization technique can be implemented to select the best-suited parameters for optimum performance within the operating range.
3. The produced TiC/TiC-steel, TiC-Ni, and TiC-Ni-CaF_2 coating can be deposited on a larger area by overlapping the single line scan of TIG cladding process and tested for real life applications.

   In the present work, to study the feasibility of the proposed coatings experimentation have been performed by single line scan of TIG arc. However, for actual employment of the coating, a larger area should be processed by overlapping of each scan and the effect of overlapped track on the performance of the coating can be analyzed.
4. The experiment can be accomplished with a high power laser system to attain TiC-Ni-CaF_2 coating either on AISI 304 steel or other structural materials to improve their surface properties more precisely.

   It is globally accepted that performance of laser coating is much superior to the TIG cladding process. Thus, it is justified to fabricate the proposed coatings especially self-lubricating TiC-Ni-CaF_2 composite coating with high power laser coating method.

References

Abdolahi, B., Shahverdi, H.R., Torkamany, M.J., Emami, M., 2011. Improvement of the corrosion behavior of low carbon steel by laser surface alloying. Appl. Surf. Sci. **257**, 9921–9924. doi:10.1016/j.apsusc.2011.06.108

Adebiyi, D.I., Popoola, A. P.I., Pityana, S.L., 2014. Microstructural evolution at the overlap zones of 12Cr martensitic stainless steel laser alloyed with TiC. Opt. Laser Technol. **61**, 15–23. doi:10.1016/j.optlastec.2014.01.014

Agarwal, A., Dahotre, N.B., 1999. Laser surface engineering of steel for hard refractory ceramic composite coating. Int. J. Refract. Met. Hard Mater. **17**, 283–293. doi:10.1016/S0263-4368(98)00063-8

Akhtar, F., Guo, S.J., 2008. Microstructure, mechanical and fretting wear properties of TiC-stainless steel composites. Mater. Charact. **59**, 84–90. doi:10.1016/j.matchar.2006.10.021

Amirsadeghi, A., Sohi, M.H., 2008. Comparison of the influence of molybdenum and chromium TIG surface alloying on the microstructure, hardness and wear resistance of ADI. J. Mater. Process. Technol. **201**, 673–677. doi:10.1016/j.jmatprotec.2007.11.157

Arabi Jeshvaghani, R., Jaberzadeh, M., Zohdi, H., Shamanian, M., 2014. Microstructural study and wear behavior of ductile iron surface alloyed by Inconel 617. Mater. Des. **54**, 491–497. doi:10.1016/j.matdes.2013.08.059

Ariely, S., Shen, J., Bamberger, M., Dausiger, F., Hugel, H., 1991. Laser surface alloying of steel with TiC. Surf. Coatings Technol. **45**, 403–408.

Axén, N., Zum Gahr, K.-H., 1992. Abrasive wear of TiC-steel composite clad layers on tool steel. wear **157**, 189–201.

Ayers, J.D., 1984. Wear behavior of carbide-injected Titanium and Aluminum alloys. Wear **97**, 249–266.

Ayers, J.D., Tucker, T.R., 1980. Particulate-TiC-Hardened steel surfaces by laser melt injection. Thin Solid Films **73**, 201–207.

Ayers, J.D., Tucker, T.R., Bowers, R.C., 1980. A reduction in the coefficient of friction for Ti-6Al-4V. Scr. Metall. **14**, 549–550.

Berger, L.M., 2015. Application of hard metals as thermal spray coatings. Int. J. Refract. Met. Hard Mater. **49**, 350–364. doi:10.1016/j.ijrmhm.2014.09.029

Buytoz, S., 2006a. Microstructural properties of M7C3 eutectic carbides in a Fe-Cr-C alloy. Mater. Lett. **60**, 605–608. doi:10.1016/j.matlet.2005.09.046

Buytoz, S., 2006b. Microstructural properties of SiC based hardfacing on low alloy steel. Surf. Coatings Technol. **200**, 3734–3742. doi:10.1016/j.surfcoat.2005.01.106

Buytoz, S., Ulutan, M., 2006. In situ synthesis of SiC reinforced MMC surface on AISI 304 stainless steel by TIG surface alloying. Surf. Coatings Technol. **200**, 3698–3704. doi:10.1016/j.surfcoat.2005.02.178

Buytoz, S., Ulutan, M., Yildirim, M.M., 2005a. Dry sliding wear behavior of TIG welding clad WC composite coatings. Appl. Surf. Sci. **252**, 1313–1323. doi:10.1016/j.apsusc.2005.02.088

Buytoz, S., Yildirim, M.M., Eren, H., 2005b. Microstructural and microhardness characteristics of gas tungsten arc synthesized Fe-Cr-C coating on AISI 4340. Mater. Lett. **59**, 607–614. doi:10.1016/j.matlet.2004.08.038

Cai, B., Tan, Y., He, L., Tan, H., Wang, X., 2013. Tribological behavior and mechanisms of graphite / CaF_2 / TiC / Ni-base alloy composite coatings. Trans. Nonferrous Met. Soc. China **23**, 392–399. doi:10.1016/S1003-6326(13)62475-9

Candel, J.J., Amigó, V., Ramos, J.A., Busquets, D., 2010. Sliding wear resistance of TiCp reinforced titanium composite coating produced by laser cladding. Surf. Coatings Technol. **204**, 3161–3166. doi:10.1016/j.surfcoat.2010.02.070

Candel, J.J., Jimenez, J.A., Franconetti, P., Amigó, V., 2014. Effect of laser irradiation on failure mechanism of TiCp reinforced titanium composite coating produced by laser cladding. J. Mater. Process. Technol. **214**, 2325–2332. doi:10.1016/j.jmatprotec.2014.04.035

Çelik, O.N., Ulutan, M., Gaşan, H., Er, Ü., Buytoz, S., 2011. Effects of graphite content on the microstructure and wear properties of an AISI 8620 steel surface modified by Tungsten Inert Gas (TIG). Surf. Coatings Technol. **206**, 1423–1429. doi:10.1016/j.surfcoat.2011.09.009

Cetegen, B.M., Basu, S., 2009. Review of modeling of liquid precursor droplets and particles injected into plasmas and high-velocity oxy-fuel (HVOF) flame jets for thermal spray deposition applications. J. Therm. Spray Technol. **18**, 769–793. doi:10.1007/s11666-009-9365-7

Chakraborty, G., Kumar, N., Das, C.R., Albert, S.K., Bhaduri, A. K., Dash, S., Tyagi, A. K., 2014. Study on microstructure and wear properties of different nickel base hardfacing alloys deposited on austenitic stainless steel. Surf. Coatings Technol. **244**, 180–188. doi:10.1016/j.surfcoat.2014.02.013

Chang, C.-M., Lin, C.-M., Hsieh, C.-C., Chen, J.-H., Wu, W., 2009. Micro-structural characteristics of Fe–40wt%Cr–xC hardfacing alloys with [1.0–4.0wt%] carbon content. J. Alloys Compd. **487**, 83–89. doi:10.1016/j.jallcom.2009.07.134

Chehrghani, A., Torkamany, M.J., Hamedi, M.J., Sabbaghzadeh, J., 2012. Numerical modeling and experimental investigation of TiC formation on titanium surface pre-coated by graphite under pulsed laser irradiation. Appl. Surf. Sci. **258**, 2068–2076. doi:10.1016/j.apsusc.2011.04.064

Chen, D., Liu, D., Liu, Y., Wang, H., Huang, Z., 2014. Microstructure and fretting wear resistance of γ/TiC composite coating in situ fabricated by plasma transferred arc cladding. Surf. Coatings Technol. **239**, 28–33. doi:10.1016/j.surfcoat.2013.11.012

Chen, J.H., Chen, P.N., Lin, C.M., Chang, C.M., Chang, Y.Y., Wu, W., 2009a. Microstructure and wear properties of multicomponent alloy cladding formed by Gas Tungsten Arc Welding (GTAW). Surf. Coatings Technol. **203**, 3231–3234. doi:10.1016/j.surfcoat.2009.03.058

Chen, J.H., Chen, P.N., Lin, C.M., Chang, C.M., Chang, Y.Y., Wu, W., 2009b. Characterization of multi-element alloy claddings manufactured by the Tungsten Inert Gas process. Surf. Coatings Technol. **203**, 2983–2988. doi:10.1016/j.surfcoat.2009.02.138

Chen, J.H., Hua, P.H., Chen, P.N., Chang, C.M., Chen, M.C., Wu, W., 2008. Characteristics of multi-element alloy cladding produced by TIG process. Mater. Lett. **62**, 2490–2492. doi:10.1016/j.matlet.2007.12.038

Chen, Y., Wang, H.M., 2003. Growth morphologies and mechanism of TiC in the laser surface alloyed coating on the substrate of TiAl intermetallics. J. Alloys Compd. **351**, 304–308. doi:10.1016/S0925-8388(02)01077-0

Cheng, F., Kwok, C., Man, H., 2001. Laser surfacing of S31603 stainless steel with engineering ceramics for cavitation erosion resistance. Surf. Coatings Technol. **139**, 14–24. doi:10.1016/S0257-8972(00)01103-8

Cheng, F.T., Lo, K.H., Man, H.C., 2003a. NiTi cladding on stainless steel by TIG surfacing process Part I. Cavitation erosion behavior. Surf. Coatings Technol. **172**, 316–321. doi:10.1016/S0257-8972(03)00346-3

Cheng, F.T., Lo, K.H., Man, H.C., 2003b. NiTi cladding on stainless steel by TIG surfacing process Part II. Corrosion behavior. Surf. Coatings Technol. **172**, 316–321. doi:10.1016/S0257-8972(03)00346-3

Chong, P.H., Man, H.C., Yue, T.M., 2002. Laser fabrication of Mo-TiC MMC on AA6061 aluminum alloy surface. Surf. Coatings Technol. **154**, 268–275.

Courant, B., Hantzpergue, J.J., Avril, L., Benayoun, S., 2005. Structure and hardness of titanium surfaces carburized by pulsed laser melting with graphite addition. J. Mater. Process. Technol. **160**, 374–381. doi:10.1016/j.jmatprotec.2004.06.025

Courant, B., Hantzpergue, J.J., Benayoun, S., 1999. Surface treatment of titanium by laser irradiation to improve resistance to dry-sliding friction. Wear **236**, 39–46. doi:10.1016/S0043-1648(99)00254-9

Covelli, L., Pierdominici, F., Smurov, I., Tosto, S., 1996. Surface microstructure of titanium irradiated by Nd:YAG pulsed laser in presence of carbon and nitrogen. Surf. Coatings Technol. **78**, 196–204.

Cui, C., Guo, Z., Wang, H., Hu, J., 2007. In situ TiC particles reinforced grey cast iron composite fabricated by laser cladding of Ni–Ti–C system. J. Mater. Process. Technol. **183**, 380–385. doi:10.1016/j.jmatprotec.2006.10.031

Das, D.K., Prasad, K.S., Paradkar, A.G., 1994. Evolution of microstructure in laser surface alloying of aluminum with nickel. Mater. Sci. Eng. A **174**, 75–84.

Desale, G.R., Paul, C.P., Gandhi, B.K., Jain, S.C., 2009. Erosion wear behavior of laser clad surfaces of low carbon austenitic steel. Wear **266**, 975–987. doi:10.1016/j.wear.2008.12.043

Dong, C., Wu, A., Hao, S., Zou, J., Liu, Z., Zhong, P., Zhang, A., Xu, T., Chen, J., Xu, J., Liu, Q., Zhou, Z., 2003. Surface treatment by high current pulsed electron beam. Surf. Coatings Technol. **163–164**, 620–624. doi:10.1016/S0257-8972(02)00657-6

Dong, Y.J., Wang, H.M., 2009. Microstructure and dry sliding wear resistance of laser clad TiC reinforced Ti–Ni–Si intermetallic composite coating. Surf. Coatings Technol. **204**, 731–735. doi:10.1016/j.surfcoat.2009.09.024

Doubenskaia, M., Smurov, I., Grigoriev, S., Pavlov, M., 2013. Complex analysis of elaboration of steel–TiC composites by direct metal deposition. J. Laser Appl. **25**, 042009. doi:10.2351/1.4807624

Du, B., Samant, A.N., Paital, S.R., Dahotre, N.B., 2008. Pulsed laser synthesis of ceramic-metal composite coating on steel. Appl. Surf. Sci. **255**, 3188–3194. doi:10.1016/j.apsusc.2008.09.010

Du, B., Wang, X., Zou, Z., 2011. Microstructure and tribological behavior of laser in situ synthesized TiC-reinforced Fe-based composite coatings. Tribol. Lett. **43**, 295–301. doi:10.1007/s11249-011-9808-4

Duraiselvam, M., Galun, R., Siegmann, S., Wesling, V., Mordike, B.L., 2007. Investigation of hydroabrasive erosion of laser alloyed Nickel and Titanium based intermetallic matrix composites with TiC reinforcement. Surf. Eng. **23**, 425–430. doi:10.1179/174329407X260609

Duraiselvam, M., Galun, R., Siegmann, S., Wesling, V., Mordike, B.L., 2005. Particle-Laden liquid impact erosion characteristics of laser clad Ni-based intermetallic matrix composites with TiC and WC reinforcements. Lasers Eng. 15, 355–373.

Duraiselvam, M., Galun, R., Wesling, V., Mordike, B.L., Reiter, R., Oligmüller, J., 2006. Cavitation erosion resistance of AISI 420 martensitic stainless steel laser-clad with nickel aluminide intermetallic composites and matrix composites with TiC reinforcement. Surf. Coatings Technol. **201**, 1289–1295. doi:10.1016/j.surfcoat.2006.01.054

Eghlimi, A., Shamanian, M., Raeissi, K., 2014. Effect of current type on microstructure and corrosion resistance of super duplex stainless steel claddings produced by the gas tungsten arc welding process. Surf. Coatings Technol. **244**, 45–51. doi:10.1016/j.surfcoat.2014.01.047

Emamian, A., Alimardani, M., Khajepour, A., 2012a. Correlation between temperature distribution and in situ formed microstructure of Fe–TiC deposited on carbon steel using laser cladding. Appl. Surf. Sci. **258**, 9025–9031. doi:10.1016/j.apsusc.2012.05.143

Emamian, A., Corbin, S.F., Khajepour, A., 2010. Effect of laser cladding process parameters on clad quality and in-situ formed microstructure of Fe–TiC composite coatings. Surf. Coatings Technol. **205**, 2007–2015. doi:10.1016/j.surfcoat.2010.08.087

Emamian, A., Corbin, S.F., Khajepour, A., 2011. The influence of combined laser parameters on in-situ formed TiC morphology during laser cladding. Surf. Coatings Technol. **206**, 124–131. doi:10.1016/j.surfcoat.2011.06.062

Emamian, A., Corbin, S.F., Khajepour, A., 2012b. Tribology characteristics of in-situ laser deposition of Fe-TiC. Surf. Coatings Technol. **206**, 4495–4501. doi:10.1016/j.surfcoat.2012.01.051

Eroğlu, M., Özdemir, N., 2002. Tungsten-inert gas surface alloying of a low carbon steel. Surf. Coatings Technol. **154**, 209–217. doi:10.1016/S0257-8972(01)01712-1

Ettaqi, S., Hays, V., Hantzpergue, J.J., Saindrenan, G., Remy, J.C., 1998. Mechanical, structural and tribological properties of Titanium nitrided by a pulsed laser. Surf. Coatings Technol. **100–101**, 428–432.

Farnia, A., Malek Ghaini, F., Ocelík, V., Hosson, J.T.M., 2013a. Microstructural characterization of Co-based coating deposited by low power pulse laser cladding. J. Mater. Sci. **48**, 2714–2723. doi:10.1007/s10853-012-7069-8

Farnia, A., Malek Ghaini, F., Rao, J.C.C., Ocelík, V., De Hosson, J.T.M.T.M., 2012. Effect of Ta on the microstructure and hardness of Stellite 6 coating deposited by low power pulse laser treatments. Surf. Coatings Technol. **213**, 278–284. doi:10.1016/j.surfcoat.2012.10.065

Farnia, A., Malek Ghaini, F., Sabbaghzadeh, J., 2013b. Effects of pulse duration and overlapping factor on melting ratio in preplaced pulsed Nd:YAG laser cladding. Opt. Lasers Eng. **51**, 69–76. doi:10.1016/j.optlaseng.2012.07.015

Fouilland-Paille, L., Ettaqi, S., Benayoun, S., Hantzpergue, J.J., 1997. Structural and mechanical characterization of Ti/TiC cermet coatings synthesized by laser melting. Surf. Coatings Technol. **88**, 204–211. doi:10.1016/S0257-8972(96)02925-8

Fu, Y., Batchelor, A.W., Gu, Y., Khor, K.A., Xing, H., 1998. Laser alloying of aluminum alloy AA 6061 with Ni and Cr. Part 1. Optimization of processing parameters by X-ray imaging. Surf. Coatings Technol. **99**, 287–294.

Gåård, A., Krakhmalev, P., Bergström, J., 2006. Microstructural characterization and wear behavior of (Fe,Ni)–TiC MMC prepared by DMLS. J. Alloys Compd. **421**, 166–171. doi:10.1016/j.jallcom.2005.09.084

Ghadami, F., Heydarzadeh Sohi, M., Ghadami, S., 2015. Effect of TIG surface melting on structure and wear properties of air plasma-sprayed WC–Co coatings. Surf. Coatings Technol. **261**, 108–113. doi:10.1016/j.surfcoat.2014.11.050

Ghaini, F.M., Hamedi, M., Torkamany, M., Sabbaghzadeh, J., 2007. Weld metal microstructural characteristics in pulsed Nd: YAG laser welding. Scr. Mater. **56**, 955–958. doi:10.1016/j.scriptamat.2007.02.019

Gopagoni, S., Hwang, J.Y., Singh, A.R.P., Mensah, B.A., Bunce, N., Tiley, J., Scharf, T.W., Banerjee, R., 2011. Microstructural evolution in laser deposited Nickel–Titanium–Carbon in situ metal matrix composites. J. Alloys Compd. **509**, 1255–1260. doi:10.1016/j.jallcom.2010.09.208

Gordani, G.R., ShojaRazavi, R., Hashemi, S.H., Isfahani, A.R.N., 2008. Laser surface alloying of an electroless Ni–P coating with Al-356 substrate. Opt. Lasers Eng. **46**, 550–557. doi:10.1016/j.optlaseng.2008.02.002

Goswami, G.L., Kumar, D., Pappachan, A. L., Grover, A. K., Sridhar, K., 1995. Characterization of chromium bearing surface alloys produced by laser alloying on low carbon steel substrates. J. Laser Appl. **7**, 153–161. doi:10.2351/1.4745389

Groover, M.P., 2007. Fundamentals of modern manufacturing: materials processes, and systems. John Wiley & Sons.

Gu, D., Hagedorn, Y.-C., Meiners, W., Wissenbach, K., Poprawe, R., 2011. Selective Laser Melting of in-situ TiC/Ti5Si3 composites with novel reinforcement architecture and elevated performance. Surf. Coatings Technol. **205**, 3285–3292. doi:10.1016/j.surfcoat.2010.11.051

Gu, D., Shen, Y., Meng, G., 2009. Growth morphologies and mechanisms of TiC grains during Selective Laser Melting of Ti-Al-C composite powder. Mater. Lett. **63**, 2536–2538. doi:10.1016/j.matlet.2009.08.043

Hajihashemi, M., Shamanian, M., Azimi, G., 2015. Physical, Mechanical, and Dry sliding wear properties of Fe-Cr-W-C hardfacing alloys under different Tungsten addition. Metall. Mater. Trans. B **46**, 919–927. doi:10.1007/s11663-014-0230-9

Hamedi, M.J.J., Torkamany, M.J.J., Sabbaghzadeh, J., 2011. Effect of pulsed laser parameters on in-situ TiC synthesis in laser surface treatment. Opt. Lasers Eng. **49**, 557–563. doi:10.1016/j.optlaseng.2010.12.002

Hong, C., Gu, D., Dai, D., Alkhayat, M., Urban, W., Yuan, P., Cao, S., Gasser, A., Weisheit, A., Kelbassa, I., Zhong, M., Poprawe, R., 2015. Laser additive manufacturing of ultrafine TiC particle reinforced Inconel 625 based composite parts: Tailored microstructures and enhanced performance. Mater. Sci. Eng. A **635**, 118–128. doi:10.1016/j.msea.2015.03.043

Hong, C., Gu, D., Dai, D., Cao, S., Alkhayat, M., Jia, Q., Gasser, A., Weisheit, A., Kelbassa, I., Zhong, M., Poprawe, R., 2015. High-temperature oxidation performance and its mechanism of TiC/Inconel 625 composites prepared by laser metal deposition additive manufacturing. J. Laser Appl. **27**, S17005. doi:10.2351/1.4898647

Howse, D.S., Lucas, W., 2000. An Investigation into arc constriction by active fluxes for tungsten inert gas welding. Sci. Technol. Weld. Join. **5**, 189–193. doi:10.1179/136217100101538191

Hsieh, C.-C., Liu, Y.-C., Wang, J.-S., Wu, W., 2014. Microstructural evolution with various Ti contents in Fe-based hardfacing alloys using a GTAW technique. Met. Mater. Int. **20**, 701–712. doi:10.1007/s12540-014-4015-0

Hu, Y., Yao, Z., 2008. Overlapping rate effect on laser shock processing of 1045 steel by small spots with Nd:YAG pulsed laser. Surf. Coatings Technol. **202**, 1517–1525. doi:10.1016/j.surfcoat.2007.07.008

Huang, S.W., Nolan, D., Brandt, M., 2003. Pre-placed WC/Ni clad layers produced with a pulsed Nd:YAG laser via optical fibres. Surf. Coatings Technol. **165**, 26–34.

Ion, J.C., 2005. Cladding, in: Laser processing of engineering materials. Elsevier Butterworth-Heinemann, pp. 296–326.

Isalgue, A., Fernandez, J., Cinca, N., Villa, M., Guilemany, J.M., 2013. Mechanical and nanoindentation behavior of TiC-NiTi thermal spray coatings. J. Alloys Compd. **577**, S277–S281. doi:10.1016/j.jallcom.2012.05.033

Islak, S., Buytoz, S., Karagöz, M., 2012. Microstructural development on AISI 1060 steel by FeW /B_4C composite coating produced by using tungsten inert gas (TIG) process. Indian J. Eng. Mater. Sci. **19**, 253–259.

Islak, S., Eski, Ö., Buytoz, S., 2011. Microstructure and wear properties of FeW-SiC based composite coating produced with tungsten inert gas (TIG) surfacing method. Optoelectron. Adv. Mater. Rapid Commun. **5**, 665–672.

Jankauskas, V., Antonov, M., Varnauskas, V., Skirkus, R., Goljandin, D., 2015. Effect of WC grain size and content on low stress abrasive wear of manual arc welded hardfacings with low-carbon or stainless steel matrix. Wear **328–329**, 378–390. doi:10.1016/j.wear.2015.02.063

Jeng, M.-C., Soong, Y.-L., 1993. Wear behaviour of solid lubricants Ag and BaF_2-CaF_2 obtained by laser surface cladding. Surf. Coatings Technol. **57**, 145–150. doi:10.1016/0257-8972(93)90031-I

Jiang, W., Molian, P., 2001. Nanocrystalline TiC powder alloying and glazing of H13 steel using a CO_2 laser for improved life of die-casting dies. Surf. Coatings Technol. **135**, 139–149.

Jianxin, D., Lili, L., Xuefeng, Y., Jianhua, L., Junlong, S., Jinlong, Z., 2007. Self-lubrication of Al_2O_3/TiC/CaF_2 ceramic composites in sliding wear tests and in machining processes. Mater. Des. **28**, 757–764. doi:10.1016/j.matdes.2005.12.003

Jianxin, D., Tongkun, C., Xuefeng, Y., Jianhua, L., 2006. Self-lubrication of sintered ceramic tools with CaF_2 additions in dry cutting. Int. J. Mach. Tools Manuf. **46**, 957–963. doi:10.1016/j.ijmachtools.2005.07.047

Jin, Y., Kato, K., Umehara, N., 1999. Further investigation on the tribological behavior of Al_2O_3–20Ag20CaF_2 composite at 650 ◦C. Tribol. Lett. **6**, 225–232.

Kathuria, Y.P., 2001. Nd-YAG laser cladding of Cr_3C_2 and TiC cermets. Surf. Coatings Technol. **140**, 195–199.

Katipelli, L.R., Agarwal, A., Dahotre, N.B., 2000a. Laser surface engineered TiC coating on 6061 Al alloy: microstructure and wear. Appl. Surf. Sci. **153**, 65–78. doi:10.1016/S0169-4332(99)00368-2

Katipelli, L.R., Agarwal, A., Dahotre, N.B., 2000b. Interfacial strength of laser surface engineered TiC coating on 6061 Al using four-point bend test. Mater. Sci. Eng. A **289**, 34–40. doi:10.1016/S0921-5093(00)00920-5

Kim, J.M., Lee, S.G., Park, J.S., Kim, H.G., 2014. Laser surface modification of Ti and TiC coatings on magnesium alloy. Phys. Met. Metallogr. **115**, 1389–1394. doi:10.1134/S0031918X14130122

Lapsanska, H., Chmelickova, H., Hrabovsky, M., 2010. Effect of beam energy on weld geometric characteristics in Nd:YAG Laser overlapping spot welding of thin AISI 304 stainless steel sheets. Metall. Mater. Trans. B **41**, 1108–1115. doi:10.1007/s11663-010-9399-8

Laroudie, F., Tassin, C., Pons, M., 1995. Hardening of 316L stainless steel by laser surface alloying. J. Mater. Sci. **30**, 3652–3657.

Leconte, S., Paillard, P., Chapelle, P., Henrion, G., Saindrenan, J., 2007. Effects of flux containing fluorides on TIG welding process. Sci. Technol. Weld. Join. **12**, 120–126. doi:10.1179/174329307X159810

Li, G.J., Li, J., Luo, X., 2015. Effects of post-heat treatment on microstructure and properties of laser cladded composite coatings on Titanium alloy substrate. Opt. Laser Technol. **65**, 66–75. doi:10.1016/j.optlastec.2014.07.003

Li, J., Chen, C., Squartini, T., He, Q., 2010. A study on wear resistance and microcrack of the Ti_3Al/TiAl+TiC ceramic layer deposited by laser cladding on Ti–6Al–4V alloy. Appl. Surf. Sci. **257**, 1550–1555. doi:10.1016/j.apsusc.2010.08.094

Li, Q.H., Savalani, M.M., Zhang, Q.M., Huo, L., 2014. High temperature wear characteristics of TiC composite coatings formed by laser cladding with CNT additives. Surf. Coatings Technol. **239**, 206–211. doi:10.1016/j.surfcoat.2013.11.043

Li, Y., Bai, P., Wang, Y., Hu, J., Guo, Z., 2009. Effect of TiC content on Ni/TiC composites by direct laser fabrication. Mater. Des. **30**, 1409–1412. doi:10.1016/j.matdes.2008.06.046

Li, Y., Gao, Y., Xiao, B., Min, T., Yang, Y., Ma, S., Yi, D., 2011. The electronic, mechanical properties and theoretical hardness of chromium carbides by first-principles calculations. J. Alloys Compd. **509**, 5242–5249. doi:10.1016/j.jallcom.2011.02.009

Lin, Y.C., Chen, H.M., Chen, Y.C., 2013. Analysis of microstructure and wear performance of SiC clad layer on SKD61 die steel after gas tungsten arc welding. Mater. Des. **47**, 828–835. doi:10.1016/j.matdes.2013.01.007

Lin, Y.C., Chen, H.M., Chen, Y.C., 2014. The effect of different methods to add nitrogen to titanium alloys on the properties of titanium nitride clad layers. Mater. Des. **54**, 222–229. doi:10.1016/j.matdes.2013.08.069

Lin, Y.C., Cho, Y.H., 2008. Elucidating the microstructure and wear behavior for multicomponent alloy clad layers by in situ synthesis. Surf. Coatings Technol. **202**, 4666–4672. doi:10.1016/j.surfcoat.2008.03.033

Lin, Y.C., Cho, Y.H., 2009. Elucidating the microstructural and tribological characteristics of NiCrAlCoCu and NiCrAlCoMo multicomponent alloy clad layers synthesized in situ. Surf. Coatings Technol. **203**, 1694–1701. doi:10.1016/j.surfcoat.2009.01.004

Liu, W.-G., Liu, X.-B., Zhang, Z.-G., Guo, J., 2009. Development and characterization of composite Ni–Cr–C–CaF2 laser cladding on γ-TiAl intermetallic alloy. J. Alloys Compd. **470**, L25–L28. doi:10.1016/j.jallcom.2008.03.020

Liu, X.-B., Liu, H.-Q., Liu, Y.-F., He, X.-M., Sun, C.-F., Wang, M.-D., Yang, H.-B., Qi, L.-H., 2013. Effects of temperature and normal load on tribological behavior of nickel-based high temperature self-lubricating wear-resistant composite coating. Compos. Part B Eng. **53**, 347–354. doi:10.1016/j.compositesb.2013.05.032

Liu, X.-B., Shi, S.-H., Guo, J., Fu, G.-Y., Wang, M.-D., 2009. Microstructure and wear behavior of γ/Al4C3/TiC/CaF2 composite coating on γ-TiAl intermetallic alloy prepared by Nd:YAG laser cladding. Appl. Surf. Sci. **255**, 5662–5668. doi:10.1016/j.apsusc.2008.11.023

Liu, Y.H., Guo, Z.X., Yang, Y., Wang, H.Y., Hu, J.D., Li, Y.X., Chumakov, A. N., Bosak, N. A., 2006. Laser (a pulsed Nd:YAG) cladding of AZ91D magnesium alloy with Al and Al2O3 powders. Appl. Surf. Sci. **253**, 1722–1728. doi:10.1016/j.apsusc.2006.03.003

Liu, Y.H., Li, J., Xuan, F.Z., 2012. Fabrication of TiC reinforced Ni based coating by laser cladding. Surf. Eng. **28**, 560–563. doi:10.1179/1743294412Y.0000000026

Lu, L., Fuh, J.Y.H., Chen, Z.D., Leong, C.C., Wong, Y.S., 2000. In situ formation of TiC composite using selective laser melting. Mater. Res. Bull. **35**, 1555–1561. doi:10.1016/S0025-5408(00)00339-1

Madadi, F., Ashrafizadeh, F., Shamanian, M., 2012. Optimization of pulsed TIG cladding process of stellite alloy on carbon steel using RSM. J. Alloys Compd. **510**, 71–77. doi:10.1016/j.jallcom.2011.08.073

Majumdar, J.D., Manna, I., 1999. Laser surface alloying of AISI 304-stainless steel with molybdenum for improvement in pitting and erosion–corrosion resistance. Mater. Sci. Eng. A **267**, 50–59. doi:10.1016/S0921-5093(99)00053-2

Majumdar, J.D., Ramesh Chandra, B., Manna, I., 2007. Laser composite surfacing of AISI 304 stainless steel with titanium boride for improved wear resistance. Tribol. Int. **40**, 146–152. doi:10.1016/j.triboint.2006.04.006

Man, H., Zhang, S., Cheng, F., Yue, T., 2002. In situ synthesis of TiC reinforced surface MMC on Al6061 by laser surface alloying. Scr. Mater. **46**, 229–234. doi:10.1016/S1359-6462(01)01230-1

Masanta, M., Shariff, S.M., Choudhury, A.R., 2011. A comparative study of the tribological performances of laser clad TiB_2–TiC–Al_2O_3 composite coatings on AISI 1020 and AISI 304 substrates. Wear **271**, 1124–1133. doi:10.1016/j.wear.2011.05.009

Mateos, J., Cuetos, J.M., Fernández, E., Vijande, R., 2000. Tribological behaviour of plasma-sprayed WC coatings with and without laser remelting. Wear **239**, 274–281. doi:10.1016/S0043-1648(00)00325-2

McGuire, M.F., 2008. Stainless steels for design engineers. ASM International.

Mridha, S., 2005. Titanium nitride layer formation by TIG surface melting in a reactive environment. J. Mater. Process. Technol. **168**, 471–477. doi:10.1016/j.jmatprotec.2005.02.247

Mridha, S., Baker, T.N., 2015. Overlapping tracks processed by TIG melting TiC preplaced powder on low alloy steel surfaces. Mater. Sci. Technol. **31**, 337–343. doi:10.1179/1743284714Y.0000000530

Mridha, S., Dyuti, S., 2011. Effects of Processing Parameters on Microstructures and Properties of TIG Melted Surface Layer of Steel. Adv. Mater. Res. **264–265**, 1421–1426. doi:10.4028/www.scientific.net/AMR.264-265.1421

Mridha, S., Idriss, A.N.M., Baker, T.N., 2012a. Incorporation of TiC Particulates on AISI 4340 Low Alloy Steel Surfaces via Tungsten Inert Gas Arc Melting. Adv. Mater. Res. **445**, 655–660. doi:10.4028/www.scientific.net/AMR.445.655

Mridha, S., Idriss, A.N.M., Maleque, M.A., Suryanto, Souad, A., 2012b. Effect of voltage on the consolidation of TiC particulates on steel substrate fused by TIG welding arc. Int. J. Mech. Mater. Eng. **7**, 48–53.

Mridha, S., Idriss, A.N.M., Maleque, M.A., Yaacob, I.I., Baker, T.N., 2015. Melting of multipass surface tracks in steel incorporating titanium carbide powders. Mater. Sci. Technol. **31**, 1362–1369. doi:10.1179/1743284714Y.0000000712

Mridha, S., Ng, B.S., 1999. Addition of ceramic particles to TIG melted Titanium surfaces. Surf. Eng. **15**, 210–215.

Mridha, S., Ong, H.S., Poh, L.S., Cheang, P., 2001. Intermetallic coatings produced by TIG surface melting. J. Mater. Process. Technol. **113**, 516–520. doi:10.1016/S0924-0136(01)00609-4

Muthuraja, A., Senthilvelan, S., 2015. Adhesive wear performance of tungsten carbide based solid lubricant material. Int. J. Refract. Met. Hard Mater. **52**, 235–244. doi:10.1016/j.ijrmhm.2015.06.019

Nowotny, S., Berger, L.-M., Spatzier, J., 2014. Coatings by Laser Cladding, in: Sarin, V.., Mari, D., Llanes, L. (Eds.), Comprehensive Hard Materials. Elsevier Ltd, pp. 507–525.

Ouyang, J.H., Li, X., Lei, T.C., 2000. Electron Microscopy Structure Study of Laser-Clad TiC-Ni Particle-Reinforced Coating. J. Mater. Eng. Perform. **9**, 234–246.

Ouyang, J.H., Sasaki, S., Murakami, T., Umeda, K., 2005. Tribological properties of spark-plasma-sintered $ZrO_2(Y_2O_3)$–CaF_2–Ag composites at elevated temperatures. Wear **258**, 1444–1454. doi:10.1016/j.wear.2004.10.007

Ouyang, J.H.U., Sasaki, S., Umeda, K., 2001. Low-pressure plasma-sprayed ZrO_2-CaF_2 composite coating for high temperature tribological applications. Surf. Coatings Technol. **137**, 1–2.

Ouyang, T., Wu, J., Yasir, M., Zhou, T., Fang, X., Wang, Y., Liu, D., Suo, J., 2016. Effect of TiC self-healing coatings on the cyclic oxidation resistance and lifetime of thermal barrier coatings. J. Alloys Compd. **656**, 992–1003. doi:10.1016/j.jallcom.2015.07.271

Paital, S.R., Bunce, N., Nandwana, P., Honrao, C., Nag, S., He, W., Banerjee, R., Dahotre, N.B., 2011. Laser surface modification for synthesis of textured bioactive and biocompatible Ca--P coatings on Ti--6Al--4V. J. Mater. Sci. Mater. Med. **22**, 1393–1406. doi:10.1007/s10856-011-4321-8

Parashivamurthy, K.I., Kumar, R.K., Seetharamu, S., Chandrasekharaiah, M.N., 2001. Review on TiC reinforced steel composites. J. Mater. Sci. **36**, 4519–4530.

Patel, P., Mridha, S., Baker, T.N., 2014. Influence of shielding gases on preheat produced in surface coatings incorporating SiC particulates into microalloy steel using TIG technique. Mater. Sci. Technol. **30**, 1506–1514. doi:10.1179/1743284713Y.0000000481

Paul, C., Alemohammad, H., Toyserkani, E., Khajepour, A., Corbin, S., 2007. Cladding of WC–12 Co on low carbon steel using a pulsed Nd:YAG laser. Mater. Sci. Eng. A **464**, 170–176. doi:10.1016/j.msea.2007.01.132

Pawlowski, L., 1999. Thick Laser Coatings: A Review. J. Therm. Spray Technol. **8**, 279–295.

Pei, Y., Zuo, T., 1998. Gradient microstructure in laser clad TiC-reinforced Ni-alloy composite coating. Mater. Sci. Eng. A **241**, 259–263. doi:10.1016/S0921-5093(97)00501-7

Peng, D.-X., 2012. Optimization of Welding Parameters on Wear Performance of Cladded Layer with TiC Ceramic via a Taguchi Approach. Tribol. Trans. **55**, 122–129. doi:10.1080/10402004.2011.636172

Peng, D.-X., Kang, Y., 2014. Wear behavior of ceramic powder and nano-diamond cladding on carbon steel surface. Ind. Lubr. Tribol. **66**, 272–281. doi:10.1016/S0301-679X(02)00094-4

Peng, D.-X., Kang, Y., 2015. Wear Behavior of Ceramic Powder and Solid Lubricant Cladding on Carbon Steel Surface. Tribol. Trans. **58**, 177–185. doi:10.1080/10402004.2014.951749

Peng, D.-X., Kang, Y., Huang, Y.-J., 2014. Microstructure and tribological properties of gas tungsten arc clad TiC composite coatings on carbon steel. Ind. Lubr. Tribol. **66**, 609–617. doi:10.1108/ILT-09-2011-0071

Peng, D.-X., Kang, Y., Li, Z.-X., Chang, S.-Y., 2013. Wear behavior of ceramic powder cladded on carbon steel surface by gas tungsten arc welding. Ind. Lubr. Tribol. **65**, 129–134. doi:10.1108/00368791311303492

Pfender, E., 1988. Fundamental studies associated with the plasma spray process. Surf. Coatings Technol. **34**, 1–14. doi:10.1016/0257-8972(88)90083-7

Piasecki, A., Kulka, M., Kotkowiak, M., 2016. Tribology International Wear resistance improvement of 100CrMnSi6-4 bearing steel by laser boriding using CaF_2 self-lubricating addition. Tribol. Int. **97**, 173–191.

Pirzada, D., Baburaj, E.G., Govindaraju, R., Froes, F.H., 2000. Laser surface coating of TiC on H13 die steel: effects on corrosion and errosion behaviour. Surf. Eng. **16**, 164–168. doi:10.1179/026708400101516955

Rajabi, A., Ghazali, M.J., Daud, A.R., 2015. Chemical composition, microstructure and sintering temperature modifications on mechanical properties of TiC-based cermet - A review. Mater. Des. **67**, 95–106. doi:10.1016/j.matdes.2014.10.081

Ramírez, G., Jiménez-Piqué, E., Mestra, A., Vilaseca, M., Casellas, D., Llanes, L., 2015. A comparative study of the contact fatigue behavior and associated damage micromechanisms of TiN- and WC:H-coated cold-work tool steel. Tribol. Int. **88**, 263–270. doi:10.1016/j.triboint.2015.03.036

Rasool, G., Mridha, S., Stack, M.M., 2015. Mapping wear mechanisms of TiC/Ti composite coatings. Wear **328–329**, 498–508. doi:10.1016/j.wear.2015.03.022

Rasool, G., Stack, M.M., 2014. Wear maps for TiC composite based coatings deposited on 303 stainless steel. Tribol. Int. **74**, 93–102. doi:10.1016/j.triboint.2014.02.002

Sabbaghzadeh, J., Hamedi, M.J., Ghaini, F.M., Torkamany, M.J., 2008. Effect of process parameters on the melting ratio in overlap pulsed laser welding. Metall. Mater. Trans. B **39**, 340–347. doi:10.1007/s11663-008-9137-7

Sahoo, C.K., Masanta, M., 2015. Effect of pulse laser parameters on TiC reinforced AISI 304 stainless steel composite coating by laser surface engineering process. Opt. Lasers Eng. **67**, 36–48. doi:10.1016/j.optlaseng.2014.10.010

Sahoo, C.K., Sahu, J.K., Masanta, M., 2015. Effect of Pulsed Nd:YAG Laser Parameters in Preplaced TiC Coating on Aluminium Substrate, in: Joshi, S.N., Dixit, U.S. (Eds.), Lasers Based Manufacturing, Topics in Mining, Metallurgy and Materials Engineering. Springer India, pp. 117–137. doi:10.1007/978-81-322-2352-8

Sahoo, C.K., Soni, L., Masanta, M., 2016. Evaluation of microstructure and mechanical properties of TiC/TiC-steel composite coating produced by gas tungsten arc (GTA) coating process. Surf. Coatings Technol. **307**, 17–27. doi:10.1016/j.surfcoat.2016.08.056

Saleh, A.F., Abboud, J.H., Benyounis, K.Y., 2010. Surface carburizing of Ti-6Al-4V alloy by laser melting. Opt. Lasers Eng. **48**, 257–267. doi:10.1016/j.optlaseng.2009.11.001

Samant, A.N., Dahotre, N.B., 2010. Three-dimensional laser machining of structural ceramics. J. Manuf. Process. **12**, 1–7. doi:10.1016/j.jmapro.2010.01.001

Sampedro, J., Pérez, I., Carcel, B., Ramos, J. a., Amigó, V., 2011. Laser Cladding of TiC for Better Titanium Components. Phys. Procedia **12**, 313–322. doi:10.1016/j.phpro.2011.03.040

Savalani, M.M., Ng, C.C., Li, Q.H., Man, H.C., 2012. In situ formation of titanium carbide using titanium and carbon-nanotube powders by laser cladding. Appl. Surf. Sci. **258**, 3173–3177. doi:10.1016/j.apsusc.2011.11.058

Sharifitabar, M., Vahdati Khaki, J., Haddad Sabzevar, M., 2016. Microstructure and wear resistance of in-situ TiC–Al_2O_3 particles reinforced Fe-based coatings produced by gas tungsten arc cladding. Surf. Coatings Technol. **285**, 47–56. doi:10.1016/j.surfcoat.2015.11.019

Shen, J.U.N., Wang, L., Peng, D., Wang, D.A.N., 2012. Effects of CaF_2 Coating on the microstructures and mechanical properties of Tungsten Inert Gas Welded AZ31 Magnesium alloy joints **43**, 4397–4405. doi:10.1007/s11661-012-1204-7

Singh, H., Sidhu, B.S., Puri, D., Prakash, S., 2007. Use of plasma spray technology for deposition of high temperature oxidation/corrosion resistant coatings - A review. Mater. Corros. **58**, 92–102. doi:10.1002/maco.200603985

Singh, R., Kumar, M., Kumar, D., Mishra, S.K., 2012. Erosion and corrosion behavior of laser cladded stainless steels with Tungsten carbide. J. Mater. Eng. Perform. **21**, 2274–2282. doi:10.1007/s11665-012-0170-y

Sohi, M.H., Ebrahimi, M., Ghasemi, H.M., Shahripour, A., 2012. Microstructural study of surface melted and chromium surface alloyed ductile iron. Appl. Surf. Sci. **258**, 7348–7353. doi:10.1016/j.apsusc.2012.04.014

Sun, R., Yang, D., Guo, L., Dong, S., 2001. Laser cladding of Ti-6Al-4V alloy with TiC and TiC+NiCrBSi powders. Surf. Coatings Technol. **135**, 307–312. doi:10.1016/S0257-8972(00)01082-3

Sun, R.L., Lei, Y.W., Niu, W., 2009. Laser clad TiC reinforced NiCrBSi composite coatings on Ti–6Al–4V alloy using a CW CO_2 laser. Surf. Coatings Technol. **203**, 1395–1399. doi:10.1016/j.surfcoat.2008.11.012

Sun, S., Durandet, Y., Brandt, M., 2005. Parametric investigation of pulsed Nd: YAG laser cladding of Stellite 6 on stainless steel. Surf. Coatings Technol. **194**, 225–231. doi:10.1016/j.surfcoat.2004.03.058

Tariq, N.H., Hasan, B.A., Akhter, J.I., 2009. Evolution of microstructure in Zr55Cu30Al10Ni5 bulk amorphous alloy by high power pulsed Nd:YAG laser. J. Alloys Compd. **485**, 212–214. doi:10.1016/j.jallcom.2009.06.008

Tassin, C., Laroudie, F., Pons, M., Lelait, L., 1995. Carbide-reinforced coatings on AISI 316 L stainless steel by laser surface alloying. Surf. Coatings Technol. **76-77**, 450–455.

Thawari, G., Sundar, J.K.S., Sundararajan, G., Joshi, S.V., 2005. Influence of process parameters during pulsed Nd:YAG laser cutting of nickel-base superalloys. J. Mater. Process. Technol. **170**, 229–239. doi:10.1016/j.jmatprotec.2005.05.021

Tian, Y.S., Chen, C.Z., 2007. Microstructures and wear properties of in situ formed composite coatings produced by laser alloying technique. Mater. Lett. **61**, 635–638. doi:10.1016/j.matlet.2006.05.035

Tosun, G., 2014. Ni–WC Coating on AISI 1010 Steel Using TIG: Microstructure and Microhardness. Arab. J. Sci. Eng. **39**, 2097–2106. doi:10.1007/s13369-013-0754-3

Ushashri, K., Masanta, M., 2015. Hard TiC Coating on AISI304 Steel by Laser Surface Engineering Using Pulsed Nd:YAG Laser. Mater. Manuf. Process. **30**, 730–735. doi:10.1080/10426914.2014.973593

Vaziri, S.A., Shahverdi, H.R., Torkamany, M.J., Shabestari, S.G., 2009. Effect of laser parameters on properties of surface-alloyed Al substrate with Ni. Opt. Lasers Eng. **47**, 971–975. doi:10.1016/j.optlaseng.2009.04.007

Verezub, O., Kálazi, Z., Buza, G., Verezub, N.V., Kaptay, G., 2009. In-situ synthesis of a carbide reinforced steel matrix surface nanocomposite by laser melt injection technology and subsequent heat treatment. Surf. Coatings Technol. **203**, 3049–3057. doi:10.1016/j.surfcoat.2009.03.024

Viswanathan, A., Sastikumar, D., Kamachimudali, U., Kumar, H., Nath, A. K., 2007. TiC reinforced composite layer formation on Al–Si alloy by laser processing. Surf. Eng. **23**, 123–128. doi:10.1179/174329407X169458

Viswanathan, A., Sastikumar, D., Kumar, H., Nath, A.K., 2012. Laser processed TiC–Al13Fe4 composite layer formation on Al–Si alloy. Opt. Lasers Eng. **50**, 1321–1329. doi:10.1016/j.optlaseng.2012.02.013

Vora, H.D., Rajamure, R.S., Soundarapandian, S., Srinivasan, S.G., Dahotre, N.B., 2013. Dilution of molybdenum on aluminum during laser surface alloying. J. Alloys Compd. **570**, 133–143. doi:10.1016/j.jallcom.2013.03.115

Wang, H.M., Yu, L.G., Li, X.X., Jiang, P., 2001. Growth morphology and mechanism of MC carbide under quasi-rapid solidificatin conditions. Sci. Technolgy Adv. Mater. **173**, 173–176.

Wang, H.M., Yu, Y.L., Li, S.Q., 2002. Microstructure and tribological properties of laser clad CaF_2/Al_2O_3 self-lubrication wear-resistant ceramic matrix composite coatings. Scr. Mater. **47**, 57–61.

Wang, J., Song, R.G., Lin, X., Huang, W.D., 2009. Microstructure and properties of laser cladding TiC/TiAl composite coatings on γ-TiAl intermetallic alloy. Surf. Eng. **25**, 196–200. doi:10.1179/174329408X326452

Wang, X., Han, F., Liu, X., Qu, S., Zou, Z., 2008. Microstructure and wear properties of the Fe-Ti-V-Mo-C hardfacing alloy. Wear **265**, 583–589. doi:10.1016/j.wear.2007.12.001

Wang, X.H., Song, S.L., Qu, S.Y., Zou, Z.D., 2007. Characterization of in situ synthesized TiC particle reinforced Fe-based composite coatings produced by multi-pass overlapping GTAW melting process. Surf. Coatings Technol. **201**, 5899–5905. doi:10.1016/j.surfcoat.2006.10.042

Wang, X.H., Song, S.L., Zou, Z.D., Qu, S.Y., 2006b. Fabricating TiC particles reinforced Fe-based composite coatings produced by GTAW multi-layers melting process. Mater. Sci. Eng. A **441**, 60–67. doi:10.1016/j.msea.2006.06.015

Wang, X.H., Zhang, M., Du, B.S., 2011. Fabrication In Situ TiB_2 – TiC – Al_2O_3 Multiple Ceramic Particles Reinforced Fe-Based Composite Coatings by Gas Tungsten Arc Welding. Tribol. Lett. **41**, 171–176. doi:10.1007/s11249-010-9701-6

Wang, X.H., Zhang, M., Liu, X.M., Qu, S.Y., Zou, Z.D., 2008. Microstructure and wear properties of TiC/FeCrBSi surface composite coating prepared by laser cladding. Surf. Coatings Technol. **202**, 3600–3606. doi:10.1016/j.surfcoat.2007.12.039

Wang, X.H., Zhang, M., Zou, Z.D., Song, S.L., Han, F., Qu, S.Y., 2006a. In situ production of Fe-TiC surface composite coatings by tungsten-inert gas heat source. Surf. Coatings Technol. **200**, 6117–6122. doi:10.1016/j.surfcoat.2005.09.021

Weng, F., Chen, C., Yu, H., 2014. Research status of laser cladding on titanium and its alloys: A review. Mater. Des. **58**, 412–425. doi:10.1016/j.matdes.2014.01.077

Wu, X.L., Hong, Y.S., 2000. Microstructure of Zr-alloyed coating using pulsed laser. Surf. Coatings Technol. **132**, 194–197.

Wu, X.L., Hong, Y.S., 2001. Interfacial microstructure and mechanical behaviour in laser clad TiCp/Ni alloy coatings. Mater. Sci. Technol. **17**, 597–600.

Wu, Y., Wang, A.H., Zhang, Z., Xia, H.B., Wang, Y.N., 2014. Wear resistance of in situ synthesized titanium compound coatings produced by laser alloying technique. Surf. Coatings Technol. **258**, 711–715. doi:10.1016/j.surfcoat.2014.08.012

Xiao-feng, Z., Xiang-lin, Z., Ai-hua, W., Zao-wen, H., 2009. Microstructure and properties of HVOF sprayed Ni-based submicron WS_2/CaF_2 self-lubricating composite coating. Trans. Nonferrous Met. Soc. China **19**, 85–92. doi:10.1016/S1003-6326(08)60233-2

Xinhong, W., Zengda, Z., Sili, S., Shiyao, Q., 2006. Microstructure and wear properties of in situ TiC/FeCrBSi composite coating prepared by gas tungsten arc welding. Wear **260**, 705–710. doi:10.1016/j.wear.2005.03.018

Yan, H., Wang, A., Xiong, Z., Xu, K., Huang, Z., 2010a. Microstructure and wear resistance of composite layers on a ductile iron with multicarbide by laser surface alloying. Appl. Surf. Sci. **256**, 7001–7009. doi:10.1016/j.apsusc.2010.05.015

Yan, H., Wang, A., Xu, K., Wang, W., Huang, Z., 2010b. Microstructure and interfacial evaluation of Co-based alloy Microstructure and interfacial evaluation of Co-based alloy coating on copper by pulsed Nd:YAG multilayer laser cladding. J. Alloys Compd. **505**, 645–653. doi:10.1016/j.jallcom.2010.06.099

Yan, H., Zhang, J., Zhang, P., Yu, Z., Li, C., Xu, P., Lu, Y., 2013. Laser cladding of Co-based alloy/TiC/CaF_2 self-lubricating composite coatings on copper for continuous casting mold. Surf. Coatings Technol. **232**, 362–369. doi:10.1016/j.surfcoat.2013.05.036

Yan, H., Zhang, P., Yu, Z., Li, C., Li, R., 2012. Development and characterization of laser surface cladding (Ti,W)C reinforced Ni-30Cu alloy composite coating on copper. Opt. Laser Technol. **44**, 1351–1358. doi:10.1016/j.optlastec.2011.12.031

Yan, H., Zhang, P., Yu, Z., Lu, Q., Yang, S., Li, C., 2012. Microstructure and tribological properties of laser-clad Ni–Cr/TiB_2 composite coatings on copper with the addition of CaF_2. Surf. Coatings Technol. 206, 4046–4053. doi:10.1016/j.surfcoat.2012.03.086

Yang, S., Chen, N., Liu, W., Zhong, M., Wang, Z., Kokawa, H., 2004a. Fabrication of nickel composite coatings reinforced with TiC particles by laser cladding. Surf. Coatings Technol. 183, 254–260. doi:10.1016/j.surfcoat.2003.09.062

Yang, S., Liu, W., Zhong, M., Wang, Z., 2004b. TiC reinforced composite coating produced by powder feeding laser cladding. Mater. Lett. 58, 2958–2962. doi:10.1016/j.matlet.2004.03.051

Yang, S., Zhong, M., Liu, W., 2003. TiC particulate composite coating produced in situ by laser cladding. Mater. Sci. Eng. A **343**, 57–62. doi:10.1016/S0921-5093(02)00361-1

Yang, X., Wang, Z., Song, P., Cheng, J., Gu, J., Ma, T., 2014. Dry sliding wear behavior of Al_2O_3 -TiC ceramic composites added with solid lubricant CaF_2 by Cold Pressing and Sintering. Tribol. Trans. **58**, 231–239. doi:10.1080/10402004.2014.962206

Yi, D., Yu, P., Hu, B., Liu, H., Wang, B., Jiang, Y., 2013. Preparation of nickel-coated titanium carbide particulates and their use in the production of reinforced iron matrix composites. Mater. Des. **52**, 572–579. doi:10.1016/j.matdes.2013.05.097

Zhong, L., Xu, Y., Hojamberdiev, M., Wang, J., Wang, J., 2011. In situ fabrication of titanium carbide particulates-reinforced iron matrix composites. Mater. Des. **32**, 3790–3795. doi:10.1016/j.matdes.2011.03.031

Zikin, A., Badisch, E., Hussainova, I., Tomastik, C., Danninger, H., 2013. Surface & Coatings Technology Characterisation of TiC – NiMo reinforced Ni-based hardfacing. Surf. Coat. Technol. **236**, 36–44. doi:10.1016/j.surfcoat.2013.02.027

Dissemination

Internationally indexed journals (Web of Science, SCI, Scopus, etc.)[1]

1. **Chinmaya Kumar Sahoo**, Manoj Masanta, Effect of pulse laser parameters on TiC reinforced AISI 304 stainless steel composite coating by laser surface engineering process, **Optics and Lasers in Engineering** 67 (2015) 36–48
   DOI: 10.1016/j.optlaseng.2014.10.010 [**Elsevier,** Journal impact factor – **2.319**]
2. Jageshwar Kumar Sahu, **Chinmaya Kumar Sahoo**, Manoj Masanta, In-situ TiB_2-TiC-Al_2O_3 composite coating on Aluminium by laser surface modification, **Materials and Manufacturing Processes** 30 (2015) 736–742
   DOI: 10.1080/10426914.2014.984225 [**Taylor & Francis**, Journal impact factor - **1.629**]
3. **Chinmaya K Sahoo**, Lalit Soni, Manoj Masanta, Evaluation of microstructure and mechanical properties of TiC/TiC steel composite coating produced by gas tungsten arc (GTA) coating process, **Surface & Coatings Technology** 307 (2016) 17–27
   DOI: 10.1016/j.surfcoat.2016.08.056 [Elsevier, Journal impact factor - **2.139**]
4. **Chinmaya K Sahoo**, Manoj Masanta Microstructure and Mechanical Properties of TiC-Ni Coating on AISI304 Steel Produced by TIG Cladding Process, **Journal of Materials Processing Technology** 240 (2017) 126–137
   DOI: 10.1016/j.jmatprotec.2016.09.018 **[Elsevier,** Journal impact factor **- 2.359]**
5. **Chinmaya K Sahoo**, Manoj Masanta, Effect of CaF_2 Content as Solid-lubricant on Microstructure and Tribological Behaviour of TiC-Ni-CaF_2 Composite Coating Produced by TIG Cladding Process, **Journal of Materials Processing Technology** 240 (2017) 126–137
   DOI: 10.1016/j.jmatprotec.2016.09.018 **[Elsevier,** Journal impact factor **- 2.359]**

Other journals and Book chapters[1]

1. **Chinmaya Kumar Sahoo**, Jageshwar Kumar Sahu, Manoj Masanta, 2015. Effect of Pulsed Nd:YAG Laser Parameters in Preplaced TiC Coating on Aluminium Substrate, in: Joshi, S.N., Dixit, U.S. (Eds.), Lasers Based Manufacturing, Topics in Mining, Metallurgy and Materials Engineering. Springer India, pp. 117–137. doi:10.1007/978-81-322-2352-8

Conferences[1]

1. **Chinmaya Kumar Sahoo**, Jageshwar Kumar Sahu, Manoj Masanta, Effect of Pulsed Nd:YAG Laser Parameters in Preplaced TiC Coating on Aluminium Substrate, 5th International 26th AIMTDR Conference, December 12-14, 2014, IIT Guwahati

Article under preparation[2]

1. Sweta Saroj, **Chinmaya K Sahoo**, Manoj Masanta, Microstructure and mechanical performance of TiC-Inconel825 composite coating deposited on AISI 304 steel by TIG cladding process, **Journal of Materials Processing Technology** (Under review)
2. **Chinmaya K Sahoo**, Manoj Masanta, Effect of process parameters on TiC hard coating on aluminium substrate produced by gas tungsten arc coating process (communicated)
3. Sweta Saroj, Manoj Masanta, **Chinmaya K Sahoo**, Sliding abrasive wear behavior of TiC-Inconel825 composite coating produced by TIG cladding process (communicated)

[1] Articles already published, in press, or formally accepted for publication.
[2] Articles under review, communicated, or to be communicated.

Bio-data

CHINMAYA KUMAR SAHOO

Plot no: 3405/6103 (Prachi Vihar, new colony),

P.O.: G.G.P Colony, P.S: Mancheswar, Bhubaneswar-751025.

Email: chinmaya.cks@gmail.com

The author, Chinmaya Kumar Sahoo, born on 21 July 1985, graduated in Mechanical Engineering from College of Engineering, Bhubaneswar, India in the year 2007. He has completed his M.Tech in Mechanical Engineering with specialization in Production Engineering from VSSUT, Burla, India in the year 2010. After completion his master degree he joined as Assistant Professor in the Department of Mechanical Engineering at GHITM, Puri, India and served for about 2.5 years. In the year 2013, he joined National Institute of Technology, Rourkela as a Ph.D. scholar. The author is engaged in the research area concerning the development of TiC based wear resistance composite coating on AISI 304 steel. He has five research papers to his credit, which have been published in various International journals of repute.